# Study of agro-composite hemp/polypropylene : treatment of fibers, morphological and mechanical characterization

Hongchang Han

Thèse
de doctorat
de l'UTT

**Hongchang HAN**

# Study of Agro-composite Hemp/Polypropylene: Treatment of Fibers, Morphological and Mechanical Characterization

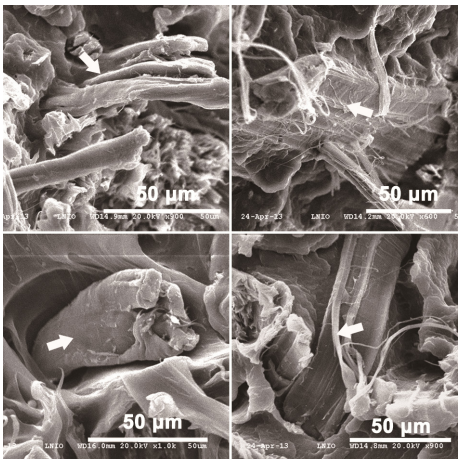


**Spécialité :**
**Systèmes Mécaniques et Matériaux**

**2015TROY0002** **Année 2015**

utt
université de technologie
Troyes

# THESE

*pour l'obtention du grade de*

## DOCTEUR de l'UNIVERSITE DE TECHNOLOGIE DE TROYES

**Spécialité : SYSTEMES MECANIQUES ET MATERIAUX**

*présentée et soutenue par*

**Hongchang HAN**

*le 4 février2015*

# Study of Agro-composite Hemp/Polypropylene: Treatment of Fibers, Morphological and Mechanical Characterization

## JURY

| | | |
|---|---|---|
| M. R. AYAD | PROFESSEUR DES UNIVERSITES | Président |
| M. A. CHEROUAT | PROFESSEUR DES UNIVERSITES | Examinateur |
| M. A. EL HAMI | PROFESSEUR DES UNIVERSITES | Examinateur |
| M. S. FONTAINE | PROFESSEUR DES UNIVERSITES | Rapporteur |
| M. X.-L. GONG | PROFESSEUR DES UNIVERSITES | Directeur de thèse |
| M. M. NAIT ABDELAZIZ | PROFESSEUR DES UNIVERSITES | Rapporteur |
| M. D. ZHANG | PROFESSOR | Examinateur |

# Acknowledgements

Completing this thesis is a great challenging activity for me. The thesis could never be conducted without the assistance, support and encourage of a number persons. I would like to express my gratitude to them and the China Scholarship Council (CSC) for funding my PhD study in such a beautiful place in France.

My first debt gratitude must go to my supervisor, **Mr. GONG X.Lu**, professor of University of Technology of Troyes (UTT), for his guidance and unfailing attention to this research. He patiently provides the encouragements and necessary advices for me throughout the doctoral project and the dissertation. His great passions and rigorous attitude towards scientific research have profound shaped my personality as a junior researcher, but he has always given me a great freedom to conduct the experiments and pursue independent work. I also thank to **Dr. Lama ELIAS BIREMBAUX**, assistance director in the first year of my thesis.

Special thanks to the committee, **Prof. S. FONTAINE** and **Prof. M. NAÏT ABDELAZIZ** for their valuable comments on my thesis. And I would like to thank to **Prof. A.CHEROUAT, Prof. A. EL HAMI, Prof. D. ZHANG**, **Prof. R. AYAD**, , who are so kind to participate in my final defence committee.

The Special thanks should be given to **Bruno LESAGE**. He has given me the assistance in conducting the experiments involved in my thesis, and thanks to **Xavier Gassmann** for his assistance in the utilization of the public chemistry laboratory. Thanks to **Mr. Mustapha ASSARAR** for his help to inject the composites specimens in IUT Troyes. I would like to thanks other technologists, administrators and teachers in Institute Charles Delaunay.

I would also express my thanks to my PhD friends **JIA Kun**, **WANG Tian**, **ZHANG Jie**, **LI YuGang**, **GENG Wei**, **PENG Ying** and many other friends in UTT. I could not complete my work without invaluable friendly assistance of these smart friends.

I wish to thank my parents, my sister and my brother. Their love provided my inspiration and was my driving force. I owe them everything and wish I could show them just how much I love and appreciate them. My specific thanks go to my wife **LI Qiong** for her years of accompanying, encouragement and supports.

HAN HongChang

# Table of contents

**List of figures** ..... **L1**

**List of tables** ..... **L8**

**Abstract** ..... **L9**

**Résumé** ..... **L10**

**General introduction** ..... **1**

**Chapter 1. Planted fiber and reinforced composites** ..... **4**

**1.1. Natural fibers** ..... **6**

**1.1.1. Components and structure** ..... **6**

**1.1.2. Mechanical properties** ..... **7**

**1.1.3. Hydrophilic properties** ..... **9**

**1.2. Treatment of planted fiber** ..... **10**

**1.2.1. Physical treatment** ..... **10**

**1.2.2. Chemical treatment** ..... **11**

*1.2.2.1. Alkali treatment* ..... *12*

*1.2.2.2. Silanization* ..... *14*

*1.2.2.3. Acetylation* ..... *16*

*1.2.2.4. Acrylation* ..... *17*

*1.2.2.5. Isocyanates treatment* ..... *17*

*1.2.2.6. Fatty acid and its derivate treatment* ..... *17*

*1.2.2.7. Benzoylation* ..... *18*

*1.2.2.8. Maleated coupling treatment* ..... *18*

*1.2.2.9. Triazine treatment* ..... *19*

*1.2.2.10. Fungal treatment* ..... *19*

**1.2.3. Other treatments** ..... **19**

**1.3. Reinforced composites** ..... **20**

**1.3.1. Petrochemical plastics** ..... **20**

**1.3.2. Bioplastics** ..... **21**

**1.3.3. All-cellulose composites** ..... **21**

**1.3.4. Hybrid composites** ..... **21**

**1.4. Other applications of planted fiber** ..... **22**

**1.4.1. Sound absorption** ..... **22**

**1.4.2. Fire resistance** ..... **22**

**1.4.3. Dielectric properties** ..... **23**

**1.5. Durability of the reinforced polymer composites** ..... **23**

**1.5.1. Humidity ageing** ..... **23**

**1.5.2. Ultraviolet ageing** ..... **25**

**1.6. Conclusions** ..... **27**

**Chapter 2. Hemp fiber treatments and the reinforced composites ..... 31**

**2.1. Fiber treatment ..... 34**
**2.1.1. Materials ..... 34**
**2.1.2. Fiber treatment ..... 34**
**2.1.3. Characterization methods of hemp fiber ..... 35**
*2.1.3.1. Scanning electron microscopy (SEM) ..... 35*
*2.1.3.2. Fourier transform infrared spectroscopy (FTIR) ..... 36*
*2.1.3.3. Moisture content ..... 36*
*2.1.3.4. Differential scanning calorimetry (DSC) ..... 37*
*2.1.3.5. X-ray diffraction (XRD) ..... 37*
**2.2. Effects of water/alkali treatment on fiber ..... 37**
**2.2.1. Fiber morphology analysis ..... 37**
**2.2.2. Moisture of hemp fiber ..... 38**
**2.2.3. FTIR spectra ..... 39**
**2.2.4. DSC results ..... 41**
**2.2.5. XRD patterns ..... 42**
**2.3. Effects of silane agent modification on fiber ..... 44**
**2.3.1. Fiber morphology analysis ..... 44**
**2.3.2. Moisture of hemp fiber ..... 45**
**2.3.3. FTIR spectra ..... 46**
**2.4. Hemp fiber reinforced polypropylene composites ..... 48**
**2.4.1. Preparation of composites ..... 48**
*2.4.1.1. Materials ..... 48*
*2.4.1.2. Composites processing ..... 48*
**2.4.2. Analytical methods ..... 49**
*2.4.2.1. SEM observations ..... 49*
*2.4.2.2. Tensile tests ..... 49*
**2.5. Effects of PP-g-MAH on the composites ..... 49**
**2.5.1. Mechanical properties ..... 49**
**2.5.2. Fracture sections ..... 51**
**2.5.3. XRD patterns ..... 52**
**2.6. Effects of water/alkali treatment of fiber on the composites ..... 53**
**2.6.1. Mechanical properties ..... 53**
**2.6.2. Fracture sections ..... 55**
**2.7. Effects of silane modifications of fiber on the composites ..... 56**
**2.7.1. Mechanical properties ..... 56**
**2.7.2. Fracture sections ..... 58**
**2.8. Conclusions ..... 59**

**Chapter 3. Humidity ageing and thermal ageing of the reinforced composites . 62**

**3.1. Humidity ageing of composites ..... 64**
**3.1.1. Experimental methods ..... 64**

*3.1.1.1. Humidity ageing* ..... *64*
*3.1.1.2. Water uptake (weight gains)* ..... *64*
*3.1.1.3. Tensile tests* ..... *64*
*3.1.1.4. SEM observations* ..... *65*
**3.1.2. Results and discussion** ..... **65**
*3.1.2.1. Tensile test results* ..... *65*
*3.1.2.2. Water uptake* ..... *67*
*3.1.2.3. Fracture sections analysis* ..... *69*
**3.2. Swelling of hemp fiber and the reinforced composites** ..... **71**
**3.2.1. Calculation methods** ..... **71**
*3.2.1.1. Fiber swelling* ..... *71*
*3.2.1.2. Composites swelling* ..... *72*
**3.2.2. Results and discussion** ..... **74**
*3.2.2.1. Fiber swelling* ..... *74*
*3.2.2.2. Composites swelling* ..... *76*
**3.2.3. Fiber swelling force** ..... **82**
*3.2.3.1. Summarization of theory* ..... *82*
*3.2.3.2. Calculation method* ..... *84*
*3.2.3.3. Fiber swelling force* ..... *85*
**3.3. Thermal ageing of composites** ..... **87**
**3.3.1. Experiments and analysis** ..... **87**
*3.3.1.1. Thermal ageing* ..... *87*
*3.3.1.2. Tensile tests* ..... *87*
**3.3.2. Tensile test results** ..... **88**
**3.4. Conclusions** ..... **90**

**Chapter 4. Ultraviolet ageing of the reinforced composites** ..... **93**

**4.1. Experiments and characterizations** ..... **95**
**4.1.1. UV ageing** ..... **95**
**4.1.2. Characterization methods** ..... **95**
*4.1.2.1. Scanning electron microscopy (SEM)* ..... *95*
*4.1.2.2. Digital microscopy* ..... *95*
*4.1.2.3. Tensile tests* ..... *95*
*4.1.2.4. Fourier transform infrared spectroscopy (FTIR)* ..... *95*
*4.1.2.5. X-ray diffraction (XRD)* ..... *96*
*4.1.2.6. UV-visible spectra* ..... *96*
**4.2. UV ageing of neat PP** ..... **96**
**4.2.1. Micrographic observation** ..... **96**
**4.2.2. SEM images** ..... **97**
**4.2.3. Tensile test results** ..... **98**
**4.2.4. FTIR spectra** ..... **100**
**4.2.5. XRD patterns** ..... **101**
**4.3. Effects of fiber treatment (water/alkali) on UV ageing** ..... **103**

**4.3.1. Composite observations** ..... **103**
**4.3.2. Micrographic images** ..... **104**
**4.3.3. SEM images** ..... **105**
**4.3.4. Tensile test results** ..... **115**
**4.3.5. Carbonyl index** ..... **117**
**4.3.6. XRD patterns** ..... **118**
**4.3.7. UV/visible spectra** ..... **120**
**4.4. Effects of fiber modification (silane agent) on UV ageing** ..... **121**
**4.4.1. Composite photos** ..... **121**
**4.4.2. Micrographic images** ..... **122**
**4.4.3. SEM images** ..... **123**
**4.4.4. Tensile tests** ..... **128**
**4.4.5. Carbonyl index** ..... **129**
**4.4.6. UV/visible spectra of silane agents** ..... **130**
**4.4.7. XRD patterns** ..... **132**
**4.5. Conclusions** ..... **133**

**Chapter 5. Conclusions and perspectives** ..... **136**

**5.1. Conclusions** ..... **137**
**5.2. Perspectives** ..... **139**

**Chapter 6. Résumé en français** ..... **142**

**6.1. Introduction** ..... **143**
**6.2. Traitements des fibres de chanvre et les composites renforcés** ..... **145**
**6.2.1. Traitements des fibres** ..... **145**
**6.2.2. Effets du traitement par l'eau et l'alcali sur les fibres** ..... **146**
*6.2.2.1. Observation par MEB* ..... *146*
*6.2.2.2. L'humidité des fibres traitées par l'alcali et par l'eau* ..... *147*
*6.2.2.3. Spectres de FTIR* ..... *147*
**6.2.3. Effets de la modification de silane sur les fibres** ..... **149**
*6.2.3.1. MEB observation* ..... *149*
*6.2.3.2. Humidité des fibres modifiées par silane* ..... *150*
*6.2.3.3. Spectres de FTIR* ..... *151*
**6.2.4. Composite chanvre/PP** ..... **152**
*6.2.4.1. Préparation des composites* ..... *152*
*6.2.4.2. Essais de traction des composites renforcés par les fibers traitées par l'eau et l'alcali* ..... *153*
*6.2.4.3. Essais de traction des composites renforcés par des fibres modifiées par silane* ..... *155*
**6.3. Vieillissement à humidité et en température des composites** ..... **157**
**6.3.1. Vieillissement à humidité des composites** ..... **157**
*6.3.1.1. Résultats des essais de traction* ..... *157*
*6.3.1.2. Absorption d'eau* ..... *160*

*6.3.1.3. Faciès de la rupture des composites ..... 161*
*6.3.1.4. Gonflement des composites pendant le vieillissement à humidité ..... 162*
**6.3.2. Vieillissement en température des composites ..... 167**
**6.4. Vieillissement aux UV des composites ..... 168**
**6.4.1. Effets de traitement des fibres par l'eau et par l'alcali sous UV ..... 168**
*6.4.1.1. Observations ..... 168*
*6.4.1.2. Observations par MO numérique ..... 169*
*6.4.1.3. Observations par MEB ..... 170*
*6.4.1.4. Spectres d'UV/visible ..... 171*
*6.4.1.5. Résultats des essais de traction après vieillissement UV ..... 172*
**6.4.2. Effets de modification des fibers par silane sous UVs ..... 174**
*6.4.2.1. Résultats des essais de traction ..... 174*
*6.4.2.2. Spectres d'UV/visible des agents de silane ..... 176*
**6.5. Conclusions & perspectives ..... 178**
**Références ..... 181**
**References ..... 185**

# List of figures

Fig. 1-1 Structure of natural fiber cell [8]..... 7

Fig. 1-2 Lignocellulosic fibers in Ashby chart [9]..... 8

Fig. 1-3 Schematic of the fiber constituents that absorb moisture [8]. ..... 9

Fig. 1-4 Typical structure of (i) untreated and (ii) alkalized cellulose fiber [43]. ..... 13

Fig. 1-5 Model of the structure of softwood lignin showing two chromophoric groups (A and B) [116]. ..... 26

Fig. 2-1 Chemical structure of silane agent MPS, PAPS and APS. ..... 34

Fig. 2-2 Schematic of treatment process of hemp fiber and the related sample name. 35

Fig. 2-3 Samples of hemp fiber and its metal holder for SEM observation. ..... 36

Fig. 2-4 Sartorius MA150 Moisture Analyzer, adopted from internet. ..... 37

Fig. 2-5 SEM morphology of hemp fiber (a) untreated fiber; (b) fiber treated with alkali; (c) fiber treated with water. ..... 38

Fig. 2-6 ATR-FTIR spectra of hemp fiber..... 40

Fig. 2-7 DSC results of hemp fiber after different treatments. A close-up of lower temperature spectra were illustrated in the upper-left inset. ..... 42

Fig. 2-8 XRD patterns of untreated hemp fiber, alkali treated and water treated hemp fiber. ..... 43

Fig. 2-9 SEM micrographs of hemp fiber: (a), alkali treated; (b), F-TMPS; (c), F-TPAPS; (d), F-TAPS..... 45

Fig. 2-10 FTIR (3700-500 $cm^{-1}$) spectra of: F-TS; MPS; F-TMPS, PAPS; F-TPAPS; APS; F-TAPS. ..... 47

Fig. 2-11 Mechanical properties of composites (a) Young's modulus; (b) Fracture stress; (c) Fracture strains. ..... 51

Fig. 2-12 SEM micrographs of composites fracture section (a), C-UF; (b), C-UF-MAH. ..... 52

Fig. 2-13 XRD patterns of C-UF, C-UF-MAH, neat PP and PP-MAH (PP blended with PP-g-MAH). ..... 53

Fig. 2-14 Mechanical properties of composites (a) Young's modulus; (b) Fracture stress; (c) Fracture strains. ..... 54

Fig. 2-15 SEM micrographs of composites fracture section (a), C-UF-MAH (untreated fiber); (b), C-FS (alkali treated fiber); (c), C-FW (water treated fiber). ..... 55

Fig. 2-16 Schemes of composites structures: C-UF-MAH (untreated fiber), C-FW (water treated fiber) and C-FS (alkali treated fiber)..... 56

Fig. 2-17 Mechanical properties of C-TS, C-TMPS, C-TPAPS and C-TAPS: (a) Young's modulus; (b) Fracture stress; (c) Fracture strains. ..... 57

Fig. 2-18 Reaction schemes of APS bearing primary amino with maleic anhydride grafted in PP..... 58

Fig. 2-19 SEM micrographs of composites fracture section (a), C-FS; (b), C-FMPS; (c), C-FPAPS; (d), C-FAPS. ..... 59

Fig. 3-1 Tensile test results of composites C-UF, C-UF-MAH, C-FW, C-FS and C-FAPS for 8 weeks humidity ageing: (a), Young's modulus; (b), Fracture stress; (c), Fracture strain. ..... 66

Fig. 3-2 Water uptake of composites C-UF, C-UF-MAH, C-FW, C-FS and C-FAPS. ..... 68

Fig. 3-3 Moisture of hemp fiber F-UT (untreated), F-TW (water treated), F-TS (alkali treated) and F-TAPS (alkali and APS treated)..... 69

Fig. 3-4 SEM micrographs of composite fracture surface after 8 weeks humidity ageing: (a), C-UF; (b), C-UF-MAH; (c), C-FW; (d), C-FS; (e), C-FAPS. ..... 70

Fig. 3-5 Schematic illustration of elementary hemp fiber subjects to swelling. The present study assumes that the fiber only stretched along radial direction. After humidity ageing of time $t$, the fiber radius stretched from $r_0$ to $r(t)$. ..... 71

Fig. 3-6 Schematic illustration of composites specimens subject to swelling. The present study assumes that the fiber orients along the injection direction and swells only in the fiber radial direction. Thus, the composites expands in specimens cross-section with $S_t$ (%) = $[(S_t - S_0) / S_0] \times 100$ %, no expansion in fiber oriented direction. ..... 73

Fig. 3-7 Weight gains (a) and radius swelling (b) of elementary hemp fiber..... 75
Fig. 3-8 A schematic of water swelling of elementary fiber in humidity ageing. The fiber consists of a network of long polymers (cellulose, hemicellulose and lignin) and small water molecules. ..... 76
Fig. 3-9 Weight gains of composites C-UF and the calculated values from weight gains of elementary fiber. ..... 77
Fig. 3-10 Cross-section expansion of composites specimens: C-UF, C-UF-MAH, C-FW, C-FS and C-FAPS..... 79
Fig. 3-11 Swelling ratios of composites specimens, C-UF, C-UF-MAH, C-FW, C-FS and C-FAPS in the direction of width and thickness. ..... 81
Fig. 3-12 Schematic diagrams of composite specimens..... 82
Fig. 3-13 Comparison between the nonlinear theory and the linear poroelasticity for constrained swelling of a hydrogel layer, cited from the reference [155]. Label of y axial $h/h_0$ is the thickness ratio of a thin hydrogel layer, which is normalized by initial thickness $h_0$. Label of x axial $t/\tau_t$ is the swelling time, normalized by a time scale of $\tau_t$. And $\lambda_0$ is the swelling ratio in the initial state. ..... 83
Fig. 3-14 Swelling force of elementary hemp fiber as function of radial stretch: (a), distribution of the number of monomers per polymer chain; (b), distribution of the mixing entropy of water molecule with hemp fiber..... 86
Fig. 3-15 Tensile test results of composites C-UF, C-UF-MAH, C-FW and C-FS: (a), Young's modulus; (b), fracture stress; (c), fracture strain..... 88
Fig. 3-16 Tensile test results of composites C-FS, C-FMPS, C-FPAPS and C-FAPS: (a), Young's modulus; (b), fracture stress; (c), fracture strain. ..... 89
Fig. 4-1 Microscopy photos of neat PP after 8 weeks UV ageing, (a), X 20; (b), X 200. ..... 97
Fig. 4-2 Development of cracks on PP surface during UV ageing: (a), 2 weeks; (b), 4 weeks; (c), 6 weeks; (d), 8 weeks. ..... 98
Fig. 4-3 Tensile test results of PP subject up to 8 weeks UV ageing: (a), Young's modulus; (b), Fracture stress; (c), Fracture strain. ..... 99

Fig. 4-4 FTIR spectra of PP before and after up to 8 weeks UV ageing: (a), FTIR spectra; (b), Carbonyl index.....101
Fig. 4-5 Schematization of the mechanism of oxidized layer growth in the case of auto-accelerated oxidation, times of radiation: t1 < t2 < t3 < t4 [168]. .....101
Fig. 4-6 XRD patterns of PP without and after 8 weeks UV ageing.....102
Fig. 4-7 Photos of composites C-UF, C-UF-MAH, C-FW and C-FS subject UV ageing from 2 to 8 weeks.....104
Fig. 4-8 Micrographic images of specimens' surface of composites C-UF, C-UF-MAH, C-FW and C-FS subject UV radiation from 2 to 8 weeks.....105
Fig. 4-9 SEM images of C-UF surface subject in different UV ageing time: (a, b), 2 weeks; (c, d), 4 weeks; (e, f), 6 weeks; (g, h), 8 weeks.....108
Fig. 4-10 SEM images of C-UF-MAH surface subject in different UV ageing time: (a, b), 2 weeks; (c, d), 4 weeks; (e, f), 6 weeks; (g, h), 8 weeks.....109
Fig. 4-11 SEM images of C-FW surface subject in different UV ageing time: (a, b), 2 weeks; (c, d), 4 weeks; (e, f), 6 weeks; (g, h), 8 weeks.....110
Fig. 4-12 SEM images of C-FS surface subject in different UV ageing time: (a, b), 2 weeks; (c, d), 4 weeks; (e, f), 6 weeks; (g, h), 8 weeks.....111
Fig. 4-13 Cracks concentrated around the fiber, C-UF-MAH after 2 weeks UV ageing. .....112
Fig. 4-14 Surface morphology of composites C-FS subjects 2 weeks UV radiation. 113
Fig. 4-15 Surface cracks of composites (a, b), C-UF-MAH; and (c, d), C-FAPS after 2 weeks UV ageing. .....114
Fig. 4-16 Surface cracks of (a) PP after 4 weeks and (b) C-FAPS after 2 weeks.....115
Fig. 4-17 Mechanical properties of composites C-UF, C-UF-MAH, C-FW and C-FS subject UV ageing: (a), Young's modulus; (b), Fracture stress; (c), Fracture strain. 116
Fig. 4-18 Carbonyl index of composites C-UF, C-UF-MAH, C-FW and C-FS subject up to 8 weeks UV ageing.....118
Fig. 4-19 XRD patterns of composites before and after 8 weeks UV ageing: (a), C-UF; (b), C-UF-MAH; (c), C-FW; (d), C-FS.....119

Fig. 4-20 UV/visible spectra of PP film and C-FS films. The photos of these films are inserted in this figure. ....121
Fig. 4-21 Specimens' photos of composites C-FS, C-FMPS, C-FPAPS and C-FAPS, exposure from 2 to 8 weeks UV ageing. ....122
Fig. 4-22 Microscopy images (magnified by 200 times) of composites C-FS, C-FMPS, C-FPAPS and C-FAPS, exposure from 2 to 8 weeks UV ageing. ....123
Fig. 4-23 SEM images of C-FMPS surface subject in different UV ageing time: (a, b), 2 weeks; (c, d), 4 weeks; (e, f), 6 weeks; (g, h), 8 weeks. ....125
Fig. 4-24 SEM images of C-FPAPS surface subject in different UV ageing time: (a, b), 2 weeks; (c, d), 4 weeks; (e, f), 6 weeks; (g, h), 8 weeks. ....126
Fig. 4-25 SEM images of C-FAPS surface subject in different UV ageing time: (a, b), 2 weeks; (c, d), 4 weeks; (e, f), 6 weeks; (g, h), 8 weeks. ....127
Fig. 4-26 Mechanical properties of composites C-FS, C-FMPS, C-FPAPS and C-FAPS subject up to 8 weeks UV ageing: (a) Young's modulus; (b) Fracture stress; (c) Fracture strains. ....128
Fig. 4-27 Carbonyl index of C-FS, C-FMPS, C-FPAPS and C-FAPS exposed up to 8 weeks UV ageing. ....130
Fig. 4-28 UV/visible spectra of silane agents MPS, PAPS and APS in a concentration of 5 %. ....131
Fig. 4-29 XRD patterns of unexposed composites and exposed up to 8 weeks UV ageing: (a), C-FS; (b), C-FMPS; (c), C-FPAPS and (d), C-FAPS. ....132
Fig. 6-1 Structure chimique de l'agent silane MPS, PAPS et APS ....144
Fig. 6-2 Schéma de processus des traitements des fibres de chanvre ....146
Fig. 6-3 Observation par MEB des fibres de chanvre (a) fibres non traitées; (b) traitées par l'alcali; (c) traitées par l'eau ....147
Fig. 6-4 Spectre FTIR-ATR pour différentes fibres de chanvre ....148
Fig. 6-5 Observation par MEB des fibres de chanvre: (a) fibre traitée par l'alcali; ...150
Fig. 6-6 Spectres FTIR de F-TS (Fibre traitées par l'alcali); MPS; F-TMPS, PAPS; F-TPAPS; APS; F-TAPS (3700-500 $cm^{-1}$) ....152

Fig. 6-7 Propriétés mécaniques des composites (a) Module d'Young; (b) Contrainte à la rupture; (c) Déformation à la rupture .....154
Fig. 6-8: Schémas des structures des composites fibre/PP traitées par l'eau et l'alcali .....155
Fig. 6-9 Propriétés mécaniques de C-TS, C-TMPS, C-TPAPS et C-TAPS: (a) Module d'Young; (b) Contrainte à la rupture; (c) Déformation à la rupture .....156
Fig. 6-10 Schémas de réaction entre l'amino primaire d'APS et l'anhydride maléique greffé au polypropylène (PP-g-MAH) .....157
Fig. 6-11 Résultats des essais de traction des composites C-UF, C-UF-MAH, C-FW, C-FS et C-FAPS: (a), Module d'Young; (b), Contrainte à la rupture; (c), Déformation à la rupture .....158
Fig. 6-12 Variation de masse des composites C-UF, C-UF-MAH, C-FW, C-FS et C-FAPS.....161
Fig. 6-13 Faciès de rupture observés par MEB: (a) C-UF; (b), C-UF-MAH; (c), C-FW; (d), C-FS; (e), C-FAPS.....162
Fig. 6-14 Variation de section des composites: C-UF, C-UF-MAH, C-FW, C-FS et C-FAPS.....164
Fig. 6-15 Taux de gonflement des composites C-UF, C-UF-MAH, C-FW, C-FS et C-FAPS dans la direction de la largeur et de l'épaisseur.....166
Fig. 6-16 Résultats des essais de traction des composites C-UF, C-UF-MAH, C-FW et C-FS: (a), Module d'Young; (b), Contrainte à la rupture; (c), Déformation à la rupture .....167
Fig. 6-17 Variation de couleur des composites C-UF, C-UF-MAH, C-FW et C-FS de 2 à 8 semaines sous UV.....169
Fig. 6-18 Observation par MO numérique de la surface des composites C-UF, C-UF-MAH, C-FW et C-FS de 2 à 8 semaines sous UV.....170
Fig. 6-19 Dégradation du PP autours des fibres, C-UF-MAH après 2 semaines sous UV .....171
Fig. 6-20 Spectres d'UV/visible du film PP et du C-FS pour différentes épaisseurs 172

Fig. 6-21 Propriétés mécaniques des composites en traction pour C-UF, C-UF-MAH, C-C-FW et FS: (a) Module d'Young; (b), Contrainte à la rupture; (c) Déformation à la rupture.....173
Fig. 6-22 Propriétés mécaniques des composites C-FS, C-PAF, C-FPAPS et C-FAP après 8 semaines de vieillissement UV: (a) Module d'Young; (b) Contrainte à la rupture; (c) déformation de rupture.....175
Fig. 6-23 Spectres d'UV/visible des agents de silane MPS, APS et PAPS.....177

# List of tables

Tab. 2-1 Moisture of hemp fiber treated by alkali and water. ..... 38

Tab. 2-2 Main infrared transitions for hemp fiber. ..... 40

Tab. 2-3 Crystallinity index of untreated, water and alkali treated hemp fiber. ..... 43

Tab. 2-4 Moisture of hemp fiber modified by silane. ..... 46

Tab. 2-5 The composites formulations. ..... 48

Tab. 6-1 Humidité des fibres de chanvre traitées par l'alcali et par l'eau .....147

Tab. 6-2 Humidité des fibres de chanvre modifiées par silane .....150

Tab. 6-3 Compositions des composites .....153

# Abstract

Using agro fiber as reinforcement of polymer composites attracts numerous investigations due to the good mechanical properties and environmental benefits. Prior to blend agro fiber with polymer, chemical treatment can be employed to treat agro fiber for the purpose of reducing the hydrophilicity of fiber and improving the interfacial adhesion fiber/polymer matrix. In this thesis, water and alkali are utilized to treat hemp fiber firstly and then three silane agent as 3-(Trimethoxysilyl)propyl methacrylate (MPS), N-[3-(Trimethoxysilyl)propyl]aniline (PAPS) and (3-Aminopropyl)-triethoxysilane (APS) are employed to modify the hemp fiber surface. These treated or modified fibers are blended respectively with polypropylene (PP) to manufacture the hemp fiber/PP composites. The effects of these different treatments on the structure, components and hydrophilicity of fiber, and the mechanical properties of the reinforced PP composites are studied. Moreover, the accelerated ageing experiments including humidity, temperature and ultraviolet of the reinforced PP composites are conducted. The results showed that the fiber treatment of water and alkali has a considerable effect on fiber structure, mechanical properties and durability of the reinforced composites. The silane agent modification of fiber has less influence on the fiber structure but its functional group has great influence on the mechanical properties and ageing resistance of the reinforced composites.

# Résumé

L'utilisation des fibres végétales dans les polymères composites suscite de nombreuses investigations. Avant de mélanger les fibres végétales avec le polymère, un traitement chimique peut être effectué permettant de réduire l'hydrophilicité des fibres et d'améliorer l'adhérence à l'interface fibre/matrice. Dans cette thèse, l'eau et l'alcali sont utilisés d'abord pour traiter les fibres de chanvre, puis trois agents silane : 3-(triméthoxysilyl)propyl méthacrylate (MPS), N-[3- (triméthoxysilyl)propyl] aniline (PAPS) et (3-Aminopropyl)-triéthoxysilane (APS), sont utilisés pour modifier plus ou moins la surface des fibres de chanvre. Ces fibres traitées ou modifiées sont ensuite mélangées avec le polypropylène (PP) pour la fabrication des composites. Les effets de ces différents traitements sur la structure, les composants et l'hydrophilicité des fibres, et les propriétés mécaniques de ces composites sont mis en évidence. Nous avons étudié ensuite l'effet de vieillissement sur leurs comportements mécaniques, notamment l'humidité, la température et le rayonnement ultraviolet. Les résultats ont montré que le traitement de fibres par l'eau et l'alcali a des effets considérables sur la structure de fibres, les propriétés mécaniques et la durabilité des composites renforcés. La modification par l'agent de silane a une influence moins importante sur la structure des fibres, pourtant son groupe fonctionnel a une influence significative sur les propriétés mécaniques et la résistance au vieillissement des composites renforcés.

# General introduction

With the increasing attentions on environment and sustainable development, industries prefer using natural planted fiber as reinforcement of composites due to its good mechanical properties and environmental benefits. Given the importance and ongoing research interests in this field, this thesis mainly focused on the chemical treatment of hemp fiber and the effects of these treatments on both the fiber and the reinforced polypropylene composites.

In the chapter 1, the structure/components, mechanical properties and hydrophilicity of planted fiber are firstly introduced. To overcome the hydrophilicity of planted fiber and improve the interfacial adhesion of fiber/matrix, the generally treatment methods of planted fiber include physical treatments like corona and plasma, and chemical treatments like mercerization, silanization, acetylation, fungi, etc. The reported matrix or composites reinforced by planted fiber including petrochemical matrix, biodegradable matrix, hybrid composites and all-cellulose composites are also introduced. Further, the durability of planted fiber reinforced composites especially the humidity and ultraviolet ageing are introduced.

In the chapter 2, the hemp fiber are treated by water, alkali and three silane agent of 3-(Trimethoxysilyl)propyl methacrylate (MPS), N-[3-(Trimethoxysilyl)propyl] -aniline (PAPS) and (3-Aminopropyl)-triethoxysilane (APS). Then, these treated fibers are blended respectively with polypropylene (PP) to manufacture hemp fiber reinforced composites. Maleic anhydride grafted polypropylene (PP-g-MAH) is used as compatibilizer to improve the interfacial adhesion of hemp fiber with PP matrix. The effects of these treatments on fiber structure/components and the reinforced composites are studied by various technics, such as scanning electron microscopy (SEM), fourier transform infrared spectroscopy (FTIR), moisture analysis, differential scanning calorimetry (DSC), X-ray diffraction (XRD) and tensile tests.

In the chapter 3, the humidity ageing and thermal ageing of hemp fiber reinforced PP composites are performed. The effects of humidity ageing on mechanical properties, weight gains of composites are discussed and their fracture sections after tensile tests

are observed. Then, the swelling behavior including the swelling direction and swelling ratio of elementary hemp fiber and the dimensional stability of the reinforced composites are studied. In addition, according to the free energy function based on the Flory-Rehner theory, the swelling force of elementary hemp fiber is calculated. Finally, the effects of thermal ageing on the mechanical properties of composites are discussed.

In the chapter 4, UV ageing of the hemp fiber reinforced PP composites is conducted. Firstly, the effects of UV ageing on the morphology and mechanical properties of neat PP are discussed. Then, the effects of water/alkali treatment of fiber, PP-g-MAH, and three silanes modification of fiber on the UV resistance of fiber reinforced PP composites are discussed, respectively. The scanning electron microscopy (SEM), digital microscopy, Fourier transform infrared spectroscopy (FTIR), ultraviolet–visible spectroscopy (UV-Vis), X-ray diffraction (XRD) and tensile tests are employed for the characterization of composite degradation.

The chapter 5 presents the main conclusions in this thesis and some perspectives concerning the future work in the planted fiber reinforced composites.

# Chapter 1

# Planted fibers and reinforced composites

# Chapter 1. Planted fiber and reinforced composites


**1.1. Natural fibers** ..... **6**
**1.1.1. Components and structure** ..... **6**
**1.1.2. Mechanical properties** ..... **7**
**1.1.3. Hydrophilic properties** ..... **9**
**1.2. Treatment of planted fiber** ..... **10**
**1.2.1. Physical treatment** ..... **10**
**1.2.2. Chemical treatment** ..... **11**
*1.2.2.1. Alkali treatment* ..... *12*
*1.2.2.2. Silanization* ..... *14*
*1.2.2.3. Acetylation* ..... *16*
*1.2.2.4. Acrylation* ..... *17*
*1.2.2.5. Isocyanates treatment* ..... *17*
*1.2.2.6. Fatty acid and its derivate treatment* ..... *17*
*1.2.2.7. Benzoylation* ..... *18*
*1.2.2.8. Maleated coupling treatment* ..... *18*
*1.2.2.9. Triazine treatment* ..... *19*
*1.2.2.10. Fungal treatment* ..... *19*
**1.2.3. Other treatments** ..... **19**
**1.3. Reinforced composites** ..... **20**
**1.3.1. Petrochemical plastics** ..... **20**
**1.3.2. Bioplastics** ..... **21**
**1.3.3. All-cellulose composites** ..... **21**
**1.3.4. Hybrid composites** ..... **21**
**1.4. Other applications of planted fiber** ..... **22**
**1.4.1. Sound absorption** ..... **22**
**1.4.2. Fire resistance** ..... **22**
**1.4.3. Dielectric properties** ..... **23**
**1.5. Durability of the reinforced polymer composites** ..... **23**
**1.5.1. Humidity ageing** ..... **23**
**1.5.2. Ultraviolet ageing** ..... **25**
**1.6. Conclusions** ..... **27**

Natural planted fiber like hemp, kenaf, jute and sisal reinforced composites attracted lots of attentions in recent years for their good mechanical properties and environmental benefits. Compared with glass fiber, natural planted fiber of low density, can neutralize carbon dioxide in their vegetation process and with no abrasion in the fiber process [1].

However, there are also many challenges in using planted fiber as reinforcing fiber in polymer composites, such as the variability, the natural hydrophilicity of fiber, and the weaker interfacial adhesion of fiber/matrix. The fiber components and properties are variable between fibers, which could be affected by fiber type, planted environment (local climate), retting process, separation methods and fiber treatment. Even in the same bundle, the fiber mechanical properties are variable in different regions [2]. Due to the rich hydroxyl groups, the natural planted fiber shows higher hydrophilic properties, which is incompatible with most hydrophobic plastics [3]. Besides this, the hydrophilicity will also play a role in the dimensional stability of the reinforced composites caused by water uptake behavior. More importantly, the hydrophilicity results in weak interfacial strength of fiber/plastics leading to low mechanical properties of the reinforced composites

Physical/chemical treatment of natural planted fiber is one of the effective methods to decrease its hydrophilicity and improve the interfacial adhesion with the polymer matrix. The physical treatment (corona or plasma) could increase the surface energy without changing the chemical components of hemp fiber. Meanwhile, chemical treatment could decrease the hydrophilic properties by removing hydroxyl groups (hemicellulose) and improve the compatibility with polymer matrix by grafting functional groups onto the fiber surface. In addition, chemical treatments may also have an impact on the thermal and mechanical properties of hemp fiber.

Besides the efforts of improving the mechanical properties of natural planted fiber reinforced plastic composites, the durability of these composites are also important in their final application. In the outdoor applications, the influence could come from humidity, temperature and ultraviolet (UV). The environmental humidity leads to the

planted fiber degradation which would decrease the mechanical properties of composites. And the fiber swelling accelerates the interface degradation by generating shear force in interfacial phase. Moreover, the fiber swelling results in the composites expansion together with the dimensional stability of composites decreased. It's believed that the temperature ageing would accelerate the water absorption behavior during the humidity ageing. The UV radiation enhances both the degradation of plastics matrix and the planted fiber. However, the mechanisms of these ageing are not clearly described or profoundly understood.

In this chapter, we firstly introduce the natural planted fiber, especially its structure and components. Then we summarized the reported treatments used in planted fibers. Afterwards, the different strategies of planted fiber reinforced composites; the humidity and ultraviolet ageing of the composites are discussed.

## *1.1. Natural fibers*

Natural fiber includes planted fiber (jute, hemp, flax, coir, sisal, cotton, etc.), wood fiber, animal fiber (silk, wool), man-made cellulose fiber (rayon fiber) and mineral fiber (asbestos, wollastonite fiber). Except animal fiber, all the others have been reported by using as reinforcing fiber in plastic composites. These reinforcing planted fibers could come from different parts of plant, such as bast, leaf, seed or core. Only planted fiber and its reinforced composites are discussed in the following section of this chapter.

### 1.1.1. Components and structure

The planted fiber generally composes cellulose, hemicellulose, lignin, pectin, wax et al. As the main and basic components of natural fiber, cellulose is generally believed to be a linear condensation polymer with up to 14000 repeating number of anhydrocellobiose unit. Cellulose is resistant to stronger alkali (17.5 %) but is easily hydrolyzed by acid [4]. Unlike cellulose, hemicellulose shows a relatively lower degree of polymerization. It comprises different sugar units in chain branching, which differs from plant to plant. Lignin comprises both aliphatic and aromatic constituents. Due to

this, lignin shows hydrophobic properties and contributes to the rigidity of planted fiber. The lignin could be dissolved by hot alkaline solution, but not hydrolyzed in acid [5]. Pectin consists of polysaccharide acid, which is soluble in water after a partial neutralisation with alkali or ammonium hydroxide. Waxes consist of different alcohols, which is insoluble both in water and acids [6].

The structure of natural fiber is presented in figure 1-1. The planted fiber has the structure of cell wall around the lumen. The cell wall could be divided into primary wall and second wall (layer-S1, S2 and S3), which has different spiral angle and composition [7]. The cell wall could be considered as a composite with the "reinforcement" of oriented semi-crystalline cellulose (microfibrils) embedded in the "matrix" of hemicellulose/lignin. The hemicellulose connects with cellulose by hydrogen bonds. The lignin acts as cementing agent to increase the stiffness of the composites.

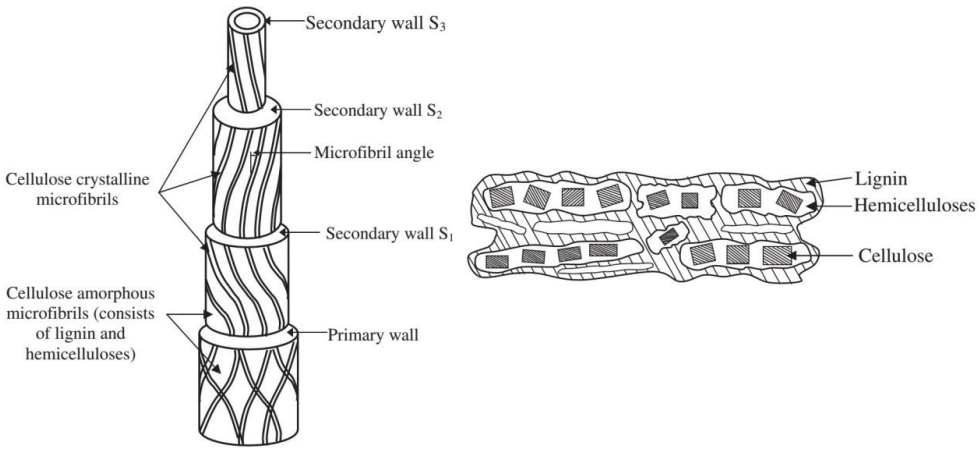


Fig. 1-1 Structure of natural fiber cell [8].

## 1.1.2. Mechanical properties

Planted fiber has good mechanical properties and low density. Figure 1-2 presents the position of lignocellulosic fibers in the Ashby's stress/density charts.

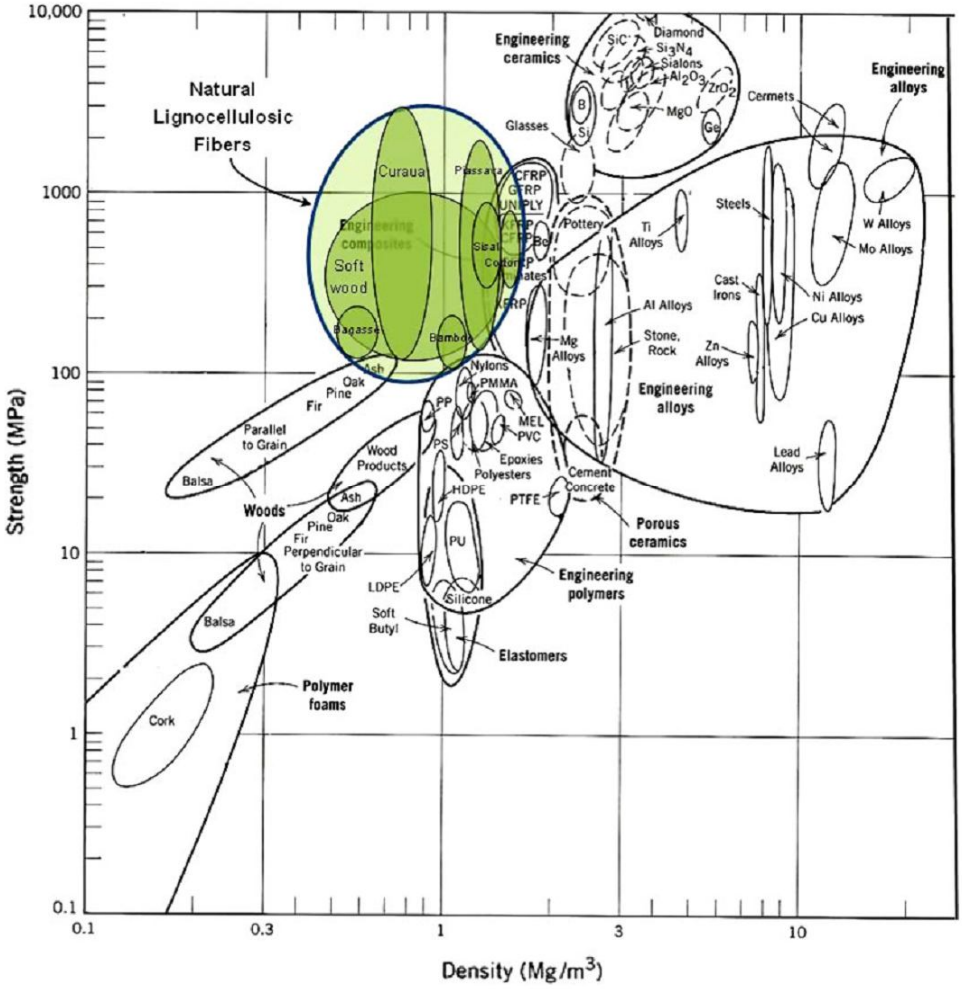


Fig. 1-2 Lignocellulosic fibers in Ashby chart [9].

The mechanical properties of natural fiber are mainly affected by the cellulose content, spiral angle and degree of polymerization. Fiber with a higher cellulose content [10], lower spiral angle and higher polymerization degree generally shows a higher tensile strength and modulus [6]. Well oriented cellulosic fibers like flax have higher Young's modulus than medium orientation fibers like cotton [11].

The tensile strength of fiber differs in the position of stem and fiber diameter. Duval A. et al. [2] found that the fibers from the middle stem exhibit higher tensile strength and ultimate elongation than fibers from top and bottom, but there are no differences in fiber stiffness. And it's observed that the fiber mechanical properties strongly depend on their diameters.

Dislocation is considered as the weakness linkage in planted fiber. Dai D. et al. [12] illustrated that the dislocation decreases fiber mechanical properties due to its

unregulated structure in the dislocation area, indicated by low degree of crystallinity of cellulose and low contents of hemicellulose or lignin.

In addition, the chemical treatment could affect the mechanical properties of planted fiber. For example, the alkali treatment could remove the hemicellulose and lignin in natural fiber and thus remain more crystalline cellulose bringing about the increase of tensile strength of fiber. The drying method also has influence on the mechanical properties of planted fiber [13].

### 1.1.3. Hydrophilic properties

Planted fiber presents hydrophilic properties due to its rich hydroxyl groups on fiber surface (Fig. 1-3). Both cellulose and hemicellulose carry numerous hydroxyl groups, while lignin shows hydrophobic properties. It's generally believed that hemicellulose takes more responsibilities for this hydrophilicity than cellulose [8]. When compared with the amorphous hemicellulose, the regular crystalline structure of cellulose inhibits effectively the water molecule penetration. The absorbed water could occur both on the surface and in the bulk of fiber. And the water absorption trends to reach equilibrium between the environmental humidity and planted fiber determining the quantity of absorbed water.

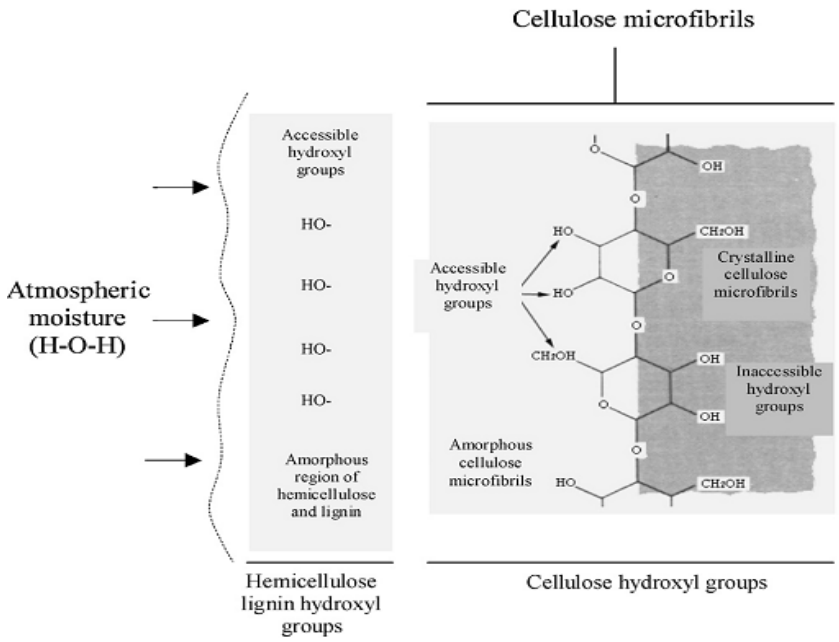


Fig. 1-3 Schematic of the fiber constituents that absorb moisture [8].

## *1.2. Treatment of planted fiber*

The hydrophilicity is one great drawback when using planted fiber as reinforcement in polymer composites. It results in poor interfacial strength with most thermoplastics, lower durability and dimensional stability of the reinforced composites. Many physical and chemical treatments are developed to deal with this drawback.

### 1.2.1. Physical treatment

Physical treatment of planted fiber could be divided into two aspects: Separation of the fiber bundles into filaments; And modification of the fiber for composites applications [14]. The traditional way to separate the fiber is wetting, involving water wetting, dew wetting and enzyme wetting [15]. Dew wetting is still widely utilized in Europe until now. Other alternative methods, such as steam explosion process [16-18] and thermal mechanical process [19, 20] are also developed to separate the fiber bundles in recent years.

The physical modification of fiber surface includes plasma discharge, dielectric barrier technology, laser treatment, vacuum ultraviolet treatment and γ-ray treatment [21-29]. Besides these treatments, soxhlet extractions with a solvent of acetone, ethanol, diethyl ether, or hot/cold water are also usually utilized to remove the aliphatic and aromatic impurities on the fiber surface. Among these treatments, plasma discharge (corona and cold plasma treatment) is considered as an effective and widely used physical treatment in planted fiber [30].

Plasma is generated by high voltage to modify the surface of cellulosic fiber for the purpose of increasing the surface energy or polarity, thus increasing the compatibility with polymer matrix. Ragoubi M. et al. [31] used corona treated hemp fiber and polypropylene. It has been found that the treatment of compounds (fiber or matrix) leads to an increase of tensile strength. The treatment of hemp fiber rather than polypropylene matrix brings about an enhancement of Young's modulus by 30 %. M. N. Belgacem et al. [32] indicated that the enhanced adhesion is ascribed to the dispersive forces in interface of fiber/PP matrix.

Furthermore, plasma treatment could induce novel functional groups or radicals onto fiber surface in order to conduct subsequently grafting reaction. Through decomposition of certain molecules in gas, plasma treatment induces reactive species which could activate or attack on the fiber surface. And they could further react with polymer matrix or coupling agent leading to stronger interfacial strength of fiber/matrix. Sawatari et al. [33] employed corona treatment and found that via washing the whatman #1 filter paper with ethanol/benzene mixture, the carbonyl groups were presented on the paper surface. Sahin, H. T. et al. [34] used carbon tetrafluoride RF-plasma to treat paper and found the covalently bound of $CF_x$ on the paper surface with a content as high as 50 %. It was also indicated that under certain experimental conditions, super-hydrophobic paper could be obtained by combing high surface fluorine atomic concentrations.

The plasma treatment may also improve the interfacial strength by cleaning, ablation or etching fiber surface which can increase its roughness and thus cross linking or branching with polymer matrix [14]. Zhou Z. et al. [35] utilized atmospheric pressure plasma jet treated ramie fiber and found that the increase of surface roughness was due to plasma etching, which is favorable to the mechanical interlock of ramie/PP interface. The interfacial shears strength also increased by 50 % after the plasma treatment due to this roughness and the resulted hydrophobic surface of ramie fiber.

However, both corona and plasma treatment are generally used in the treatment of film or fabrics in printing and textile industry. It is difficult to carry out the treatments on “three-dimensional materials” like disorder accumulated short fiber. In addition, these treatments may cause the decomposition of planted fiber. Gassan, J. et al. [36] observed that the yarn tenacity of jute fiber was decreased when increasing the corona level. Uehara, T. and Sakata I. [37] has found that the chain scission of cellulose during the treatment of beechwood with corona.

### 1.2.2. Chemical treatment

Chemical treatment is frequently employed to treat planted fiber for the purpose of reducing the hydroxyl group contents and inducing functional groups capable of

reactive or compatible with plastic matrix. Various chemical treatments has been reported in literatures, such as alkali treatment, silane treatment, acetylation, benzoylation, peroxide treatment, maleated coupling treatment, sodium chlorite treatment, acrylation or acrylonitrile grafting, isocyanates treatment, stearic acid treatment, permanganate treatment, triazine treatment, fatty acid derivate (oleoyl chloride) treatment and fungal treatment [8, 30, 38-41].

*1.2.2.1. Alkali treatment*

Alkali (NaOH) treatment, also called mercerization, is one frequently used chemical treatment of planted fiber. Alkali treatment mainly concerns the removal of hydrogen bond in the planted fiber (Formula 1-1). As a result, the bundle fiber could be broken down to small fiber because of the removal of hemicellulose and lignin. It's expected that the removal of hemicellulose leaves more free space for the rearrangement of microfibrils along the tensile direction leading to high stress of fiber. With the elimination of rigid lignin, fiber shows better flexibility or plasticity than the untreated fiber. Gassan J. and Bledzki K. [42] used 25 % NaOH to treat jute fiber at 20 ºC for 20 min. They found that the NaOH treated jute yarns gets an increase of tensile strength and modulus by ~120 and 150 %, respectively, owing to the increase of both crystallinity ratio and crystalline orientation.

$$\text{Fiber} - \text{OH} + \text{NaOH} \rightarrow \text{Fiber} - \text{O}^{-}\text{Na}^{+} + \text{H}_2\text{O}$$

Formula 1-1 Alkali treated planted fiber.

Moreover, mercerization enhances the surface roughness and provides more reactive sites favoring the interlocks and wetting with polymer matrix.

The alkali treatment has an effect on the compositions, structure and mechanical properties of planted fiber. The effectiveness of alkali treatment depends on the treatment condition, such as the alkali concentration, reactive temperature and pressure. Even though in the same treatment condition, the effect also differs in various type of planted fiber because of its different compositions and structure. In fact, due to the complex structure, normal mercerization doesn't give rise to the complete fibrillation

of bundle fiber but partly fibrillation by removal of only partial hemicellulose or lignin (Fig. 1-4). It results in lots of defects and damages impairing the mechanical properties of fiber. The composites reinforced with this kind of fiber show low tensile strength compared with untreated fiber.

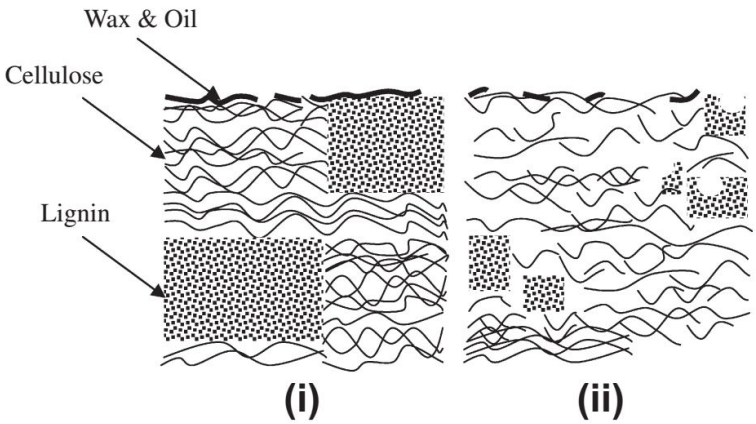


Fig. 1-4 Typical structure of (i) untreated and (ii) alkalized cellulose fiber [43].

Similarly to alkali treatment, it's reported that there are other inorganic solutions used in the treatment of planted fiber like liquid ammonia, sodium chlorite and potassium permanganate.

Liquid ammonia could also cause the rupture of hydrogen bonds in planted fiber, which is considered as an alternative pre-treatment to mercerization. Huang, W. Y. et al. [44] found that liquid ammonia treatment of the scoured/bleached ramie decreased the crystallinity and the cellulose I transformed into cellulose III. The fiber surface becomes smoother than untreated one.

Sodium chlorite ($NaClO_2$) is used in treatment of fiber [45]. After the acidified and oxidation of $NaClO_2$, the obtained chlorine dioxide ($ClO_2$) reacts with lignin constituents and thus remove the lignin. Sodium chlorite reacts with hydroxyl groups of hemicellulose leading to the treated fiber more flexible and with less stiffness than untreated fiber [46].

Potassium permanganate ($KaMnO_4$) is used to treat planted fiber [47]. The formed high reactive permanganate ($Mn^{3+}$) could react with hydroxyl groups in cellulose and form cellulose-manganate (IV). This treatment is also beneficial in improving the chemical interlocking in composites interface and reducing the hydrophilicity of fiber.

*1.2.2.2. Silanization*

Silane or organosilane is recognized as an effective and widely used coupling agent in glass fiber reinforced composites. In the reinforced composites, silane plays a role as a chemical bridge between fiber and matrix to improve the interfacial adhesion of composites. Moreover, for planted fiber reinforced composites, silane treatment also decreases the hydrophilic properties of natural fiber by consuming hydroxyl groups and increases hydrophobic properties by its bearing functional groups.

As shown in formula 1-2, the interaction of silane with planted fiber could be divided into four steps [48]: a) hydrolysis, the silane are hydrolyzed in water or acid/base solution, liberating alcohol and yielding reactive silanol groups; b) self-condensation, the self-condensation of silanol groups occurs during the hydrolytic process. This process should be avoided to leave free silanol groups easily absorbed onto the planted fiber surface; c) adsorption, the reactive silanol monomer or oligomers adsorb onto the fiber surface forming hydrogen bond with hydroxyl groups in fiber; d) chemical grafting, the hydrogen bonds between silanol or oligomers and hydroxyl groups of fiber convert into the covalent bond -O-Si-C- and liberating water.

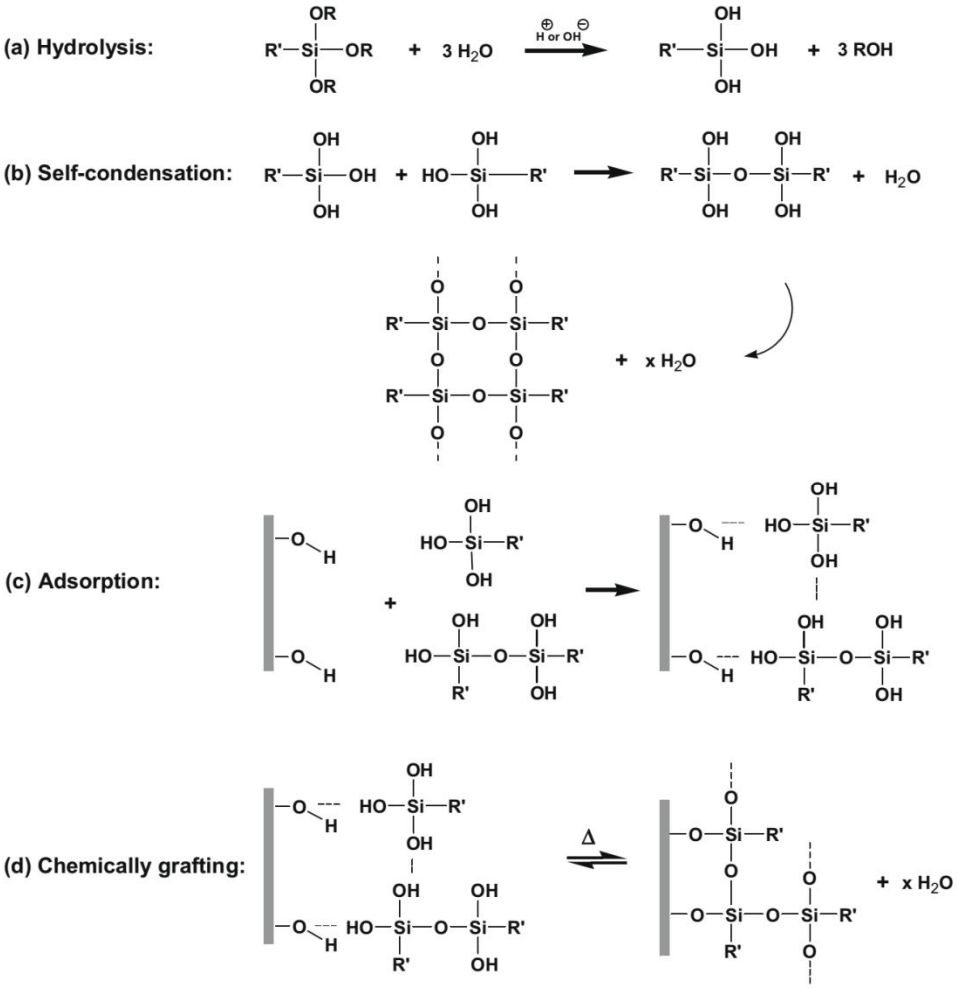


Formula 1-2 Interaction of silane with natural fibers by hydrolysis process [48].

The most used silane agents in the treatment of planted fiber are trialkoxysilanes. The typical functional groups in the other side of silane are amino, mercapto, glycidoxy, vinyl, or methacryloxy groups [48]. The combining force or compatibility of silane with polymer matrix depends on the functional groups of silane and the target polymer. The non-reactive organofunctionality of silane, like alkyl group, may connect with polymer chains by relative weak combination of hydrogen bond; but reactive organofunctionality may form high combination of covalent bond with polymer matrix.

Regardless of the silane type, the efficiency of silane treatment is affected by the treatment condition, such as concentration of silane solution, hydrolytic pH, reaction time, heating condition, and the surface properties of planted fiber. Moreover, the efficiency of silane treatment is high for alkali treated fiber than untreated fiber because

of the former one regenerated more reactive sites and removal “impurities”, remaining more cellulose [30].

*1.2.2.3. Acetylation*

Acetylation is a well-know and effective esterification method (Formula 1-3) in treatment of planted fiber [49]. Acetylation is to introduce acetyl functional groups onto the fiber surface in order to change the fiber surface to hydrophobic. Acetylation reaction generally proceeds in an organic solvent at elevated temperature. It’s believed that the hydroxyls groups, reacted with acetic or propionic anhydride, are those of hemicellulose and lignin, not cellulose [50].

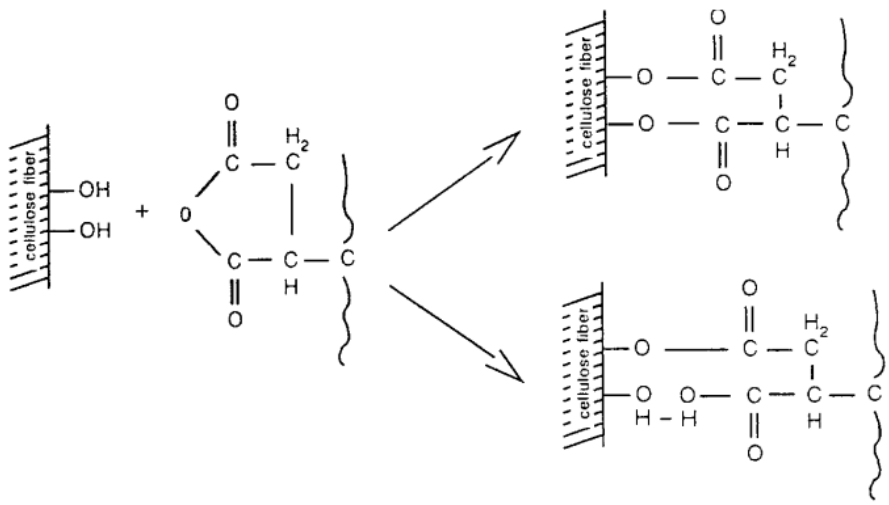


Formula 1-3 Esterification reaction of cellulose fiber [51].

Acetylation could improve the interfacial strength of the reinforced composites. After acetylation process, the fiber surface shows hydrophobic by introducing acetyl groups. It’s beneficial in improving the wettability and compatibility with non-polar polymer matrix [38, 52].

Besides this, acetylation affects the components, moisture of fiber, degree of polymerization and crystallinity. Bledzki A. K. et al. [49] investigated the effects of acetylation on the flax fiber. They found that the cellulose content increased due to the extraction of lignin and then slightly decreased because of the degradation of cellulose. The degree of polymerization of cellulose slowly decreased with increasing the degree

of acetylation until 18 %. And above this acetyl content, the degree of polymerization sharply decreased. Similarly, the degree of crystallinity also increased slightly at low acetyl content, and then decreased with respect of acetylation. It's also observed the thermal stability of fiber improved with increasing acetylation.

Tserki V. et al. [50] compared the effect of acetylation and pripionylation on the flax, hemp and wood fiber. It was indicated that wood fiber obtained the highest extent of esterification reaction due to its higher lignin/hemicellulose content. Both these two treatments induced ester bonds onto the fiber surface and affected the fiber surface morphology by the removal of non-crystalline constituents.

*1.2.2.4. Acrylation*

Acrylic acid is used in treatment of planted fiber to improve the adhesion of fiber and polymer matrix like polypropylene [53, 54]. The carbonyl acid in acrylic acid could react with cellulosic hydroxyl groups forming ester linkage (Formula 1-4). To conduct acrylation, pre-treatment of planted fiber with alkali is generally necessary in order to remove the lignin, hemicellulose and other impurities.

$$\text{Fiber} - \text{OH} + \text{C}_2\text{H}_3\text{COOH} \rightarrow \text{Fiber} - \text{OOC}_2\text{H}_3 + \text{H}_2\text{O}$$

Formula 1-4 Chemical reaction of acrylic acid with cellulosic fiber [38]

*1.2.2.5. Isocyanates treatment*

The isocyanate functional group, with a formula of $\text{R} - \text{N} = \text{C} = \text{O}$ (R could be different chemical group), can react with the hydroxyl groups of cellulose and lignin forming urethane linkages. Moreover, isocyanate reacts with the absorbed water on the fiber surface forming urea, which can further react with the hydroxyl groups of the celluloses. Therefore, the resulted fiber after isocyanates treatment presents high moisture resistance [55-57].

*1.2.2.6. Fatty acid and its derivate treatment*

Fatty acid (stearic acid) and its derivates (Oleoyl chloride) are used to modify the planted fiber [58-61]. The carboxyl groups in fatty acid react with hydroxyl groups

(esterification), which can graft a long aliphatic chain onto the fiber surface to improve water resistance of fiber and interfacial adhesion with polymer matrix. The chemical reaction of stearic acid with cellulosic fiber is shown in formula 1-5.

$$\text{Fiber} - \text{OH} + \text{CH}_3(\text{CH}_2)_{16}\text{COOH} \rightarrow \text{CH}_3(\text{CH}_2)_{16}\text{COO} - \text{O} - \text{Fiber} + \text{H}_2\text{O}$$

Formula 1-5 Chemical reaction of stearic acid with cellulosic fiber [38].

*1.2.2.7. Benzoylation*

In the benzoylation of planted fiber, benzoyl chloride is widely used to treat planted fiber. The grafted benzoyl groups on fiber surface are responsible for improving the hydrophobic properties of fiber. This treatment is also beneficial in improving the thermal stability of fiber. Before benzoylation treatment, it's generally pre-treated planted fiber with alkali to remove the waxes or lignin covering on fiber surface and expose more reactive hydroxyl groups to the following benzoylation reaction [62-64].

Benzoyl peroxide is also reported in the treatment of planted fiber since organic peroxide is easily to decompose to free radical, which could react with hydroxyl groups in fiber [65-67].

*1.2.2.8. Maleated coupling treatment*

Maleic anhydride is one common coupling agent used in improving the interfacial strength of planted fiber and polymer matrix [68-70]. Maleic anhydride reacts with hydroxyl groups in fiber with the formation of long chain brush on fiber surface, and provides covalent bonds with polymer matrix. Additionally, the polymer matrix grafted with maleic anhydride is also widely used to improve the interfacial strength, such as maleic anhydride grafted polypropylene or polyethylene. This process is easily conducted in the extrusion procedure without the pre-treatment of the reinforcing fiber [71-73].

*1.2.2.9. Triazine treatment*

Triazine is used in modification of planted fiber. As one of the triazine derivatives, the reactive chloride in cyanuric chloride, with formula of $(NCCl)_3$, reacts with hydroxyl groups of fiber by esterification and forms covalent bonds with matrix. Owing to this, triazine treatment reduces moisture of fiber and the reinforced composites. In addition, the cross-link by covalent bonds between fiber and matrix inhibits the fiber swelling [38, 74].

*1.2.2.10. Fungal treatment*

In recent years, fungal treatment has been well developed and considered as a promising treatment due to its environmental friendly benefits and efficiency. Fiber components like waxes, hemicellulose or lignin can be selectively removed by choosing suitable enzyme. Gulati D. and Sain M. [75] used a fungus *ophiostoma ulmi* to treat hemp fiber. Pickering K. L. et al. [76] found that by combining alkali and fungal treatment of hemp fiber, the reinforced composites possessed of a tensile strength of 48.3 MPa, an increase of 32 % when compared with the one reinforced with untreated fiber.

Kalia S. et al. [77] carried out a microwave-assisted grafting of methyl methacrylate onto ramie fiber and enzyme-assisted biopolishing of ramie fiber by bacteria *Streptomyces albaduncus*. Recently, they used microwave-assisted grafting of binary and vinyl monomers onto ramie fiber and the fiber pre-treated by another bacteria *Brevibacillus parabrevis* [78].

### 1.2.3. Other treatments

Apart from these treatments aimed at improving the hydrophobic properties of planted fiber, there are also other chemical treatments reported in literatures to obtain additional functions of cellulose based composites. For example, impregnation cellulose fiber in $FeCl_3$ solution or incorporating carbon nanotubes into cellulose to elaborate conductive cellulosic composites [79-81]; and incorporating barium ferrite into a regenerated fiber to fabricate magnetic activities composites [82].

Jonoobi M. et al. [83, 84] fabricated nanofibers from kenaf stem by pulping, bleaching and mechanical grinding. Via the removal of lignin and most of hemicellulose, the obtained nanofibers have diameters within range of 15-25 nm.

Han G. et al. [85] employed microwave-assisted extraction (MAE) to pre-treated hemp fiber. It has been found that MAE is more efficient and environmental in the removal of non-cellulose compounds from hemp bundles when comparing with traditional acid pre-treatment.

There are also many literatures reports using ionic liquid in the treatment of planted fiber [86-89].

## *1.3. Reinforced composites*

With the increasing demand of environmental friendly materials, planted fiber is considered as an alternative candidate to replace synthetic fiber, like glass fiber. Planted fiber has many advantages in reinforcing composites, such as low density, low price, high toughness and biodegradable. The planted fibers are mainly used as reinforcing fiber to improve the mechanical properties of composites. It's reported that planted fiber can be used as reinforcement of petrochemical plastics, bioplastics, cellulosic composites (self-reinforcement) and cements. Planted fibers are also combined with other fibers as glass fiber or carbon fiber to reinforce one or multiple matrix. These reinforced composites have wide applications in automotive interiors, households, buildings, aircraft and packaging [90].

### 1.3.1. Petrochemical plastics

Planted fibers are used in reinforcing petrochemical plastics including thermoplastic, such as polyethylene (PE), high density polyethylene (HDPE) polypropylene (PP), polystyrene (PS), polyvinyl chloride (PVC); and thermosets like polyester, epoxy and phenolic. Most planted fiber degrades at a temperature of 220 ºC and hence the reported polymer matrixes are concentrated in thermosets plastics and thermoplastics with a low processing temperature. PE and PP are two common

petrochemical plastics reinforced by planted fiber because of their broad utilization and recyclability.

### 1.3.2. Bioplastics

Concerning environment, climate change and the limitation reserve of fossil fuel, bioplastics attract more and more attentions in recent decades. Bioplastics are obtained from renewable resources and biodegradable, which are mainly used in short-life application like packaging. The generally used bioplastics are polylactide acid (PLA), polyhydroxybutyrate (PHB) and starch. Using planted fiber to reinforce bioplastics not only improves its mechanical properties but also obtains the completely degradable composites, compared with the partly degradable composites of planted fiber reinforced petrochemical plastics.

### 1.3.3. All-cellulose composites

All-cellulose composites are considered as one kind of monocomponent composites that both the matrix and reinforcing fibers are based on cellulosic materials. Because they have the same chemical compositions and surface morphology, it's expected to form a perfect interfacial adhesion between the matrix and the reinforcing phase. All-cellulose composites are prepared by dissolving cellulosic fiber or its surface following the regeneration of matrix around the cellulosic fiber [91]. The mechanical properties of all-cellulose composites depend on the cellulosic fiber type, dissolution and regeneration condition. Soykeabkaew N. et al. [92] prepared all-cellulose nanocomposites by surface selective dissolution of bacterial cellulose. The obtained nanocomposites have an average Young's modulus of 18 GPa and tensile strength of 411 MPa.

### 1.3.4. Hybrid composites

Planted fiber reinforced hybrid composites generally consist of more than one reinforcing filler or matrix. The reinforcing fillers could be planted fiber/planted fiber, planted fiber/synthetic fiber and planted fiber/nano-fillers. Likewise, the reinforced matrix could also be two or more polymers. Glass fibers and carbon fibers are two

widely used synthetic fibers combining with planted fiber as reinforcement in hybrid composites. Nano-fillers, such as, nanoclay [93-96], layered silicate [97, 98], multiwalls nanotubes [99, 100] are reported to combine with planted fiber to improve the mechanical properties of the reinforced hybrid composites.

## *1.4. Other applications of planted fiber*

### 1.4.1. Sound absorption

Besides the good mechanical properties, natural fiber also has other advantages like sound absorption capacities. Coir fiber is utilized as acoustic materials to act as an effective and wideband absorber in noise control engineering [101]. Nor Mohd Jailani Mohd et al. [102] used coir fiber to fabricate a multilayer of sound absorption materials. They found that the multilayer coconut coir fiber contributed to increase the sound absorption coefficients. Zulkifh, R et al. [103] found that the sound absorption coefficient of multilayer coir fiber is comparable to the commercially used rock wool and synthetic fibers.

### 1.4.2. Fire resistance

The fire resistance of planted fiber is also investigated due to the requirements of industrial, for example, the automobile and building materials require high flame resistance. The flame resistance of natural fiber is related to the contents of the chemical compositions. Generally, with higher cellulose content, the natural fiber shows more flammable [104]. But a relatively higher content of lignin seems to favor the thermal stability of fiber. The decomposition temperature of lignin and hemicellulose is much lower than that of cellulose. With the temperature rising, the decomposition of hemicellulose or lignin, especially lignin, may form a char layer, which could resist the flame of fiber by inhibiting oxygen transmission [105]. The increase of fiber volume fraction could increase the thermal resistance and delay the ignition time [106].

### 1.4.3. Dielectric properties

Zawawi, N. A. et al [107] reports their investigation in dielectric properties of two poly lactic acid (PLA) composites reinforced respectively by kenaf and rice husk. It's prospective to recognize their potential application in electronic communication industries to replace the common printed circuit board.

## *1.5. Durability of the reinforced polymer composites*

Planted fiber reinforced polymer composites are more susceptible to outdoor environment compared with composites reinforced by synthetic fiber. The degradation occurs both in planted fiber and polymer matrix, as well as in the interface of fiber/matrix. It results in the decline of mechanical properties and color changes of composites. Moreover, the fiber swelling weakens the dimensional stability of composites. Therefore, the reinforced composites are greatly limited in their outdoor applications like exposing to atmosphere or contacting with aqueous media, such as windows frames, decking and construction materials [108, 109].

The degradation of planted fiber reinforced composites could be influenced by numerous factors, such as, environmental humidity, temperature, ultraviolet radiation etc… In addition, the compositions and structure of fiber and matrix also affects the degradation rate.

### 1.5.1. Humidity ageing

Humidity ageing of planted fiber reinforced polymer composite is associated with water absorption of planted fiber. This water absorption is driven by hydroxyl groups in planted fiber. Normally, with higher hemicellulose content, it possesses higher water absorption. The voids or defects in the reinforced composites, especially in interfacial region, also facilitate the water absorption owing to the capillary effects. It's observed that the water absorption follows Fick's law where the water goes from high concentration region to low concentration region in the light of a concentration gradient [110]. At room temperature, the water absorption increase linearly at the beginning and then slowly reaches a saturation plateau in certain time.

Along with water absorption, the degradation process occurs in the interface of fiber/matrix and fiber itself. The absorbed water dissolves the water-soluble polysaccharide on the fiber surface causing the debonding of fiber from polymer matrix and the fungi in the water could degrade the cellulosic fiber. In addition, the fiber swells in its radial direction, which develops osmotic pressure on matrix causing the formation of cracks in polymer matrix and generates shear force in interface contributing to the cleavage of fiber/matrix interface. The fiber swelling also causes the composites expansion. Humidity ageing results in the decreased mechanical properties of reinforced composites and the impaired dimensional stability. However, in the initial periods of humidity ageing, the fiber swelling increases the interface pressure with a result of the improved mechanical properties of composites.

Several factors affect the water absorption of planted fiber reinforced composites, such as, temperature, environmental humidity, interfacial adhesion, fiber or matrix type, fiber volume fraction, etc… High temperature and environmental humidity facilitate the water diffusion process. Good interfacial adhesion cuts down water absorption rate and amount. Commonly, with high hemicellulose content, the hydrophilicity of fiber increases, which promotes the water absorption. The chemical component of polymer matrix is pivotal to its hydrophobic or hydrophilic properties. With the increase of fiber volume fraction in composites and the immersion time, the water absorption increases [108]. The absorbed water has great impact on the humidity ageing, for example, ocean water has more influence than fresh water on lowering mechanical properties of the reinforced composites [111].

To overcome the humidity ageing of planted fiber reinforced composites, the common method is to decrease the hydrophilicity of planted fiber and improve the interfacial adhesion strength of fiber/matrix by fiber treatment and/or modification [8, 39, 112, 113], such as using alkali to remove the hydroxyl groups to decrease the moisture of natural fiber itself [114, 115], using silane agents to improve bonding strength with matrix[48], etc..

### 1.5.2. Ultraviolet ageing

Besides the humidity ageing, ultraviolet (UV) radiation also has a great influence on the ageing of planted fiber reinforced composites. Ultraviolet radiation causes surface whitening, cracking and deterioration of mechanical properties. Both planted fiber and polymer matrix degrade under ultraviolet radiation.

In cellulosic fibers, only lignin is responsible for the UV absorption because of those two containing chromophoric groups A and B (as shown in Fig. 1-5). For this reason, lignin absorbs 85-90 % of the light. The mechanism of photodegradation of lignin is complex. It's generally believed that the degradation of lignin leads to the formation of different phenoxy radicals resulting in chain cleavage and yellowing of wood fiber [116].

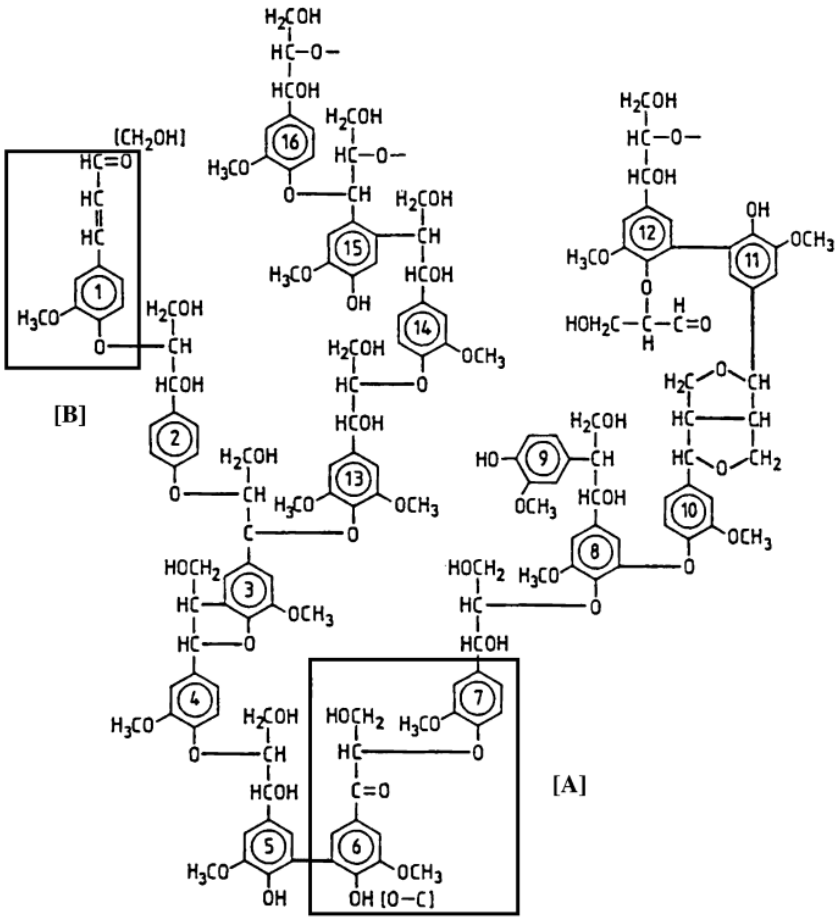


Fig. 1-5 Model of the structure of softwood lignin showing two chromophoric groups (A and B) [116].

The UV radiation leads to polymer matrix degradation of chain cession, cracking and crystallization. The UV radiation boosts the crystalline degree of polymer by the rearrangement of freed segments from amorphous regions into crystalline phase [117], which is mainly responsible for the cracking of polymer degradation. Since the degradation of polymer is photooxidation reaction, the oxygen is exhausted in the surface layer before diffusing into the interior of polymer. Hence the degradation occurs around the surface regions at the beginning. The formed cracks in the surface promote oxygen penetrating into interior inducing the further degradation. The chromophoric groups, introduced in polymer manufacturing, processing and storage, are also favorable to the light absorption and degradation of polymer matrix.

The photodegradation of planted fiber reinforced polymer composites is not just the simple combination of photodegradation of planted fiber and polymer matrix but

more complex. The chromophoric groups produced from lignin of planted fiber could accelerate the degradation of polymers around the fiber. However, the presence of polymer matrix inhibits the oxygen diffusion retarding the photodegradation of planted fiber. Thus, the planted fiber reinforced polymer composites displays faster ageing in the surface layer but lower in interior than the pure polymers. Moreover, the addition of fiber prevents the cracking development of polymer matrix and promotes the interfacial crystallizations of composites [118]. The photodegradation could be affected by several factors including fiber volume fraction, dispersion, processing method, coupling agent, ageing condition (radiation intensity and moisture), and so on.

Many approaches have been developed to improve UV resistance of planted fiber reinforced polymer composites. Adding antioxidant is one common used method to improve the UV resistance of pure polymer. Antioxidants perform as a consumption agent of oxygen to form stable peroxide in order to protect the polymers.

Photostabilizers like UV light absorber (UVA) and HALS (hindered amine light stabilizers) are employed to improve the UV resistance. UVA could absorb some UV radiation and act as shield [119-121]. HALS could capture radicals intermediate produced in photodegradation process [122].

Pigments are added as photo-blocker to block the penetration of UV radiation. Surface coating or dyeing are applied to protect the planted fiber, polymer, or the reinforced composites [123-126].

Coextrusion provides a protection layer on the surface of fiber reinforced composites. By coextrusion, Matuana L. M. et al. [127] prepared a clear HDPE cap layer onto HDPE/wood-flour composites. It was found that the clear hydrophobic HDPE cap layer significantly decreased the discoloration and the interfacial degradation during the weathering process.

## *1.6. Conclusions*

With the increasing attentions on environment and sustainable development, industries prefer biodegradable materials to traditional petrochemical materials. In the domain of fiber reinforced composites, natural planted fiber attracts more attentions as

an alternative in replacing the glass fiber, due to its good mechanical properties and environmental benefits.

However, it's required to overcome some drawbacks in using natural planted fiber as reinforcing fiber. For example, the fiber structure, components and properties are variable in the position of stem, cultivation regions and years. And they can also be affected by the retting process, fiber separation and treatment protocol. The natural hydrophilicity leads to the planted fiber reinforced composites generally have weak interfacial strength and poor dimensional stability. The agglomeration of short planted fiber makes more difficulties of well dispersion in composites by extrusion process. And its relatively low thermostability restricts the processing temperature of polymers matrix under 230 ºC.

Using physical/chemical treatment of natural planted fiber is one effective method to decrease the hydrophilicity and improve the interfacial adhesion with the plastic matrix. The physical treatments increase the surface energy to incorporate with polymer matrix. Chemical treatments remove hemicellulose to improve the moisture resistance and grafting functional groups onto cellulosic fiber to enhance the interfacial strength of fiber/matrix. Fungi treatment is a promising treatment for its environmental friendly benefits and efficiency. Hybrid composites are developed to improve the mechanical properties of composites. All-cellulose composites (both reinforcing fiber and matrix are cellulose) are fabricated to obtain a completely biodegradable and interfacial compatible composites.

The durability of planted reinforced composites is mainly influenced by humidity and ultraviolet. The humidity ageing is associated with water absorption driven by the hydrophilicity of planted fiber and capillary effects of fiber/matrix interface. The absorbed water brings about the degradation of both the fiber and the interface declining the mechanical properties of composites. The water absorption process follows Fick's law. The influence of humidity on composites could be improved by decreasing the hydrophilicity of planted fiber and strengthening the interfacial adhesion.

UV radiation degrades both the planted fiber and the polymer matrix. Moreover, the chromophoric groups degraded from lignin and introduced from polymer manufacturing or processing can accelerate the photooxidation of polymer matrix. The UV degradation of composites is a photooxidation process. Hence, the degradation initially occurs in the surface layer and then expands into interior of composites because of the exhaust of oxygen in the surface. As results of UV ageing, the composites display color changes, surface cracking and mechanical properties deterioration. By adding antioxidant or photostabilizer into polymer matrix, surface coloring or coating of fiber or composites, the UV resistance of planted fiber reinforced composites could be improved.

# Chapter 2

# Hemp fiber treatments and the reinforced composites

# Chapter 2. Hemp fiber treatments and the reinforced composites


**2.1. Fiber treatment** ..... **34**
**2.1.1. Materials** ..... **34**
**2.1.2. Fiber treatment** ..... **34**
**2.1.3. Characterization methods of hemp fiber** ..... **35**
*2.1.3.1. Scanning electron microscopy (SEM)* ..... *35*
*2.1.3.2. Fourier transform infrared spectroscopy (FTIR)* ..... *36*
*2.1.3.3. Moisture content* ..... *36*
*2.1.3.4. Differential scanning calorimetry (DSC)* ..... *37*
*2.1.3.5. X-ray diffraction (XRD)* ..... *37*
**2.2. Effects of water/alkali treatment on fiber** ..... **37**
**2.2.1. Fiber morphology analysis** ..... **37**
**2.2.2. Moisture of hemp fiber** ..... **38**
**2.2.3. FTIR spectra** ..... **39**
**2.2.4. DSC results** ..... **41**
**2.2.5. XRD patterns** ..... **42**
**2.3. Effects of silane agent modification on fiber** ..... **44**
**2.3.1. Fiber morphology analysis** ..... **44**
**2.3.2. Moisture of hemp fiber** ..... **45**
**2.3.3. FTIR spectra** ..... **46**
**2.4. Hemp fiber reinforced polypropylene composites** ..... **48**
**2.4.1. Preparation of composites** ..... **48**
*2.4.1.1. Materials* ..... *48*
*2.4.1.2. Composites processing* ..... *48*
**2.4.2. Analytical methods** ..... **49**
*2.4.2.1. SEM observations* ..... *49*
*2.4.2.2. Tensile tests* ..... *49*
**2.5. Effects of PP-g-MAH on the composites** ..... **49**
**2.5.1. Mechanical properties** ..... **49**
**2.5.2. Fracture sections** ..... **51**
**2.5.3. XRD patterns** ..... **52**
**2.6. Effects of water/alkali treatment of fiber on the composites** ..... **53**
**2.6.1. Mechanical properties** ..... **53**
**2.6.2. Fracture sections** ..... **55**
**2.7. Effects of silane modifications of fiber on the composites** ..... **56**
**2.7.1. Mechanical properties** ..... **56**

**2.7.2. Fracture sections** ..... **58**
**2.8. Conclusions** ..... **59**

To improve the hydrophilic resistance of natural planted fiber, alkali treatment is one of the most popular methods as it could effectively reduce the hydroxyl groups' content in the amorphous matrix of fiber [39, 115, 128-131]. In fact, alkali treatment doesn't lead to complete fibrillation of bundle fiber but only removes partial hemicellulose or lignin. Because of this, alkali treatment results in lots of defects and damages in the treated fiber and hence decreases the mechanical properties of both the fiber and the reinforced composites. In addition, employing alkali (one chemical agent), is in conflicts with environment friendly concept, which is the original intention of using planted fiber instead of artificial fiber. Thus, it's necessary to develop a new economic and green method in fiber treatment.

Silane agents are widely used in glass fiber treatment for its low price, simple modification process and variable structure that have good compatibility with different polymer matrix.

In this chapter, we firstly used water washing as a green method to treat hemp fiber and compared with alkali treatment. In order to obtain optimal interfacial strength and study the effects of different functional groups in silane, three silane agents are selected to modify the hemp fiber in this thesis following the alkali treatment. The employed three silane agents are 3-(Trimethoxysilyl)propyl methacrylate (MPS), N-[3-(Trimethoxysilyl)propyl]aniline (PAPS) and (3-Aminopropyl)-triethoxysilane (APS) (Fig. 2-1). The effects of the fiber treatment (water/alkali) and the fiber modification (MPS, PAPS and APS) on the fiber structure and the reinforced polypropylene composites are evaluated by various technologies, such as scanning electron microscopy (SEM), Fourier transform infrared spectroscopy (FTIR), moisture analysis, differential scanning calorimetry (DSC), X-ray diffraction (XRD) and tensile tests.

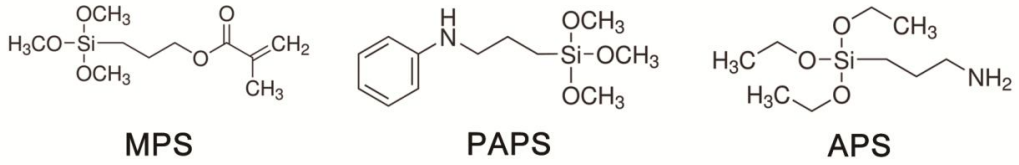


Fig. 2-1 Chemical structure of silane agent MPS, PAPS and APS.

## *2.1. Fiber treatment*

### 2.1.1. Materials

Hemp fibers were kindly supplied by Fiber Research Development FRD®. The fiber arrived in a form of bundles and was cut into short fiber of 2.5 mm. Tap-water was employed directly to wash hemp fiber. Alkali (analysis pure), 3-(Trimethoxysilyl)propyl methacrylate (MPS), N-[3-(Trimethoxysilyl)propyl]aniline (PAPS) and (3-Aminopropyl)-triethoxysilane (APS) were obtained from Sigma-Aldrich.

### 2.1.2. Fiber treatment

To obtain the alkali treated fiber, untreated fiber was washed with water firstly, followed by being immersed in 5 wt. % alkali solution at room temperature for 1 hour. Then, in order to remove the residual sodium hydroxide, the fiber was washed with tap water until the pH reached 7.

The water treated fiber was obtained by washing the untreated fiber with tap water for 3 times, 10 minutes each time. The ratio of fiber/water was 1: 50 (by weight). Finally, the alkali treated fiber and water treated fiber were dried in an oven at 60 °C for 48 hours.

The alkali treated hemp fiber was then modified by the silane agent of MPS, PAPS and APS (75 mmol/L), respectively. The silane agents were all prehydrolyzed for 2 hours initially. The pre-hydrolyzation pH of both MPS and PAPS is 4, but that of APS is 10. The fiber was then immersed in the hydrolyzed solution of silane for 2 hours. The

ratio of fiber/solution was 1: 50 by weight. The fiber was then dried in an oven at 110 °C for 12 hours, followed by washing with tap water to remove the residual silane agents until pH achieved 7. Finally, the silane modified hemp fiber was dried in an oven at 60 °C for 48 hours. The modified fiber is named as F-TMPS, F-TPAPS and F-TAPS, respectively. The fiber treatment procedure is also presented in figure 2-2.

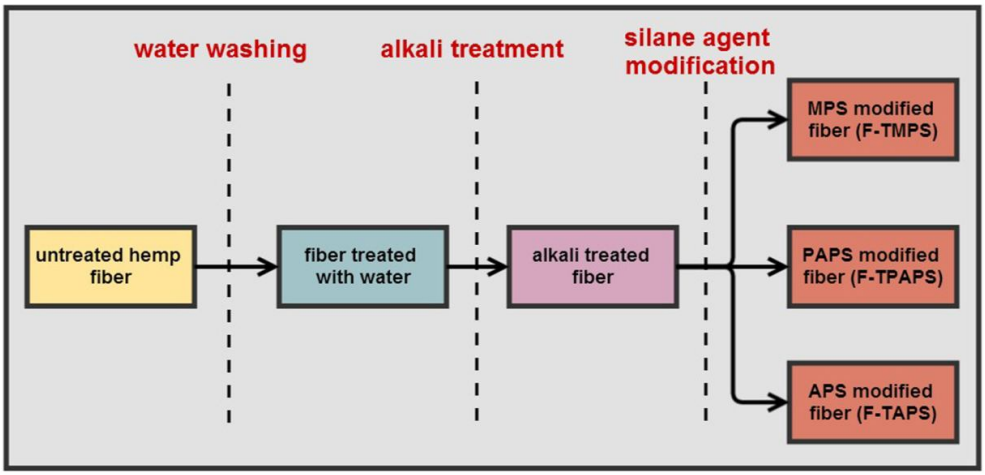


Fig. 2-2 Schematic of treatment process of hemp fiber and the related sample name.

## 2.1.3. Characterization methods of hemp fiber

### *2.1.3.1. Scanning electron microscopy (SEM)*

SEM was employed to observe the fiber surface. To obtain the fiber surface images, hemp fiber was pasted onto a paper firstly, followed by placement onto a metal holder with carbon tape (Fig. 2-3). All samples were coated with carbon by a SEM coater CC7650. The images were captured using a Hitachi S3500N under low magnification.

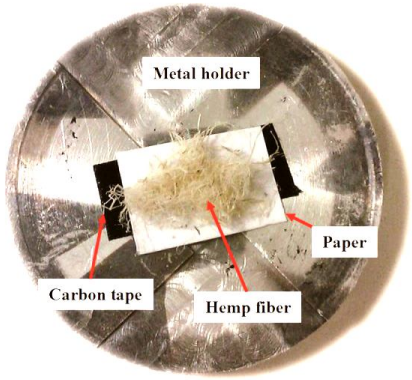


Fig. 2-3 Samples of hemp fiber and its metal holder for SEM observation.

*2.1.3.2. Fourier transform infrared spectroscopy (FTIR)*

FTIR measurements were performed at 400-4000 $cm^{-1}$ in PerkinElmer Spectrum Two with the Universal Attenuated Total Reflectance Accessory (UATR).

*2.1.3.3. Moisture content*

Sartorius MA150 Moisture Analyzer (Fig. 2-4) was employed to analysis the moisture content of fiber. This moisture analyzer use thermogravimetry method which determines the mass loss of fiber from room temperature to 105 °C. The moisture of the fiber was calculated as:

$$\text{Moisture of fiber (\%)} = [(M0-M1)/M0] \times 100\%$$

where M0 is the fiber weight before heating, M1 is the fiber weight after the fiber being heated to 105 °C until no weight losing.

Fig. 2-4 Sartorius MA150 Moisture Analyzer, adopted from internet.

*2.1.3.4. Differential scanning calorimetry (DSC)*

DSC measurements were performed by using a thermal analyzer DSC 131 EVO. In this analysis, approximate 20 mg of fiber sample were heated up at a rate of 10 ºC $min^{-1}$ from 20 to 600 ºC in air.

*2.1.3.5. X-ray diffraction (XRD)*

X-ray diffraction (XRD) measurements were conducted with a Seifert PTS-3000 X-ray diffractometer employing Cu-Kα (0.1540598 nm) radiation and Ni filter, equipped with a Position Sensitive Detector. The XRD patterns were collected from 15 ° to 60 ° (2θ angle) with a step size of 0.05 °.

## *2.2. Effects of water/alkali treatment on fiber*

### 2.2.1. Fiber morphology analysis

Figure 2-5 presents the surface morphology of untreated, alkali treated and water treated hemp fiber, respectively. In figure 2-5a, the surface of untreated fiber is covered with a layer of roughness substance. Lots of small branches have also been found on sides of fiber. After alkali treatment (Fig. 2-5b), fiber surface is cleaner than that of untreated fiber. But the elementary fiber was partly separated at the same time. The surface of water treated fiber (Fig. 2-5c) is cleaner and smoother than untreated fiber.

According to the cellulose fiber structure [38, 132], it is supposed that the treatment of alkali solution removed partial lignin and hemicellulose (amorphous regions of cellulose microfibrils), which are connected with cellulose (crystalline regions of cellulose microfibrils) to form an elementary fiber. Water washing processes could selectively remove water-soluble polysaccharide covering on fiber surface and preserve the integral structure of hemp fiber.

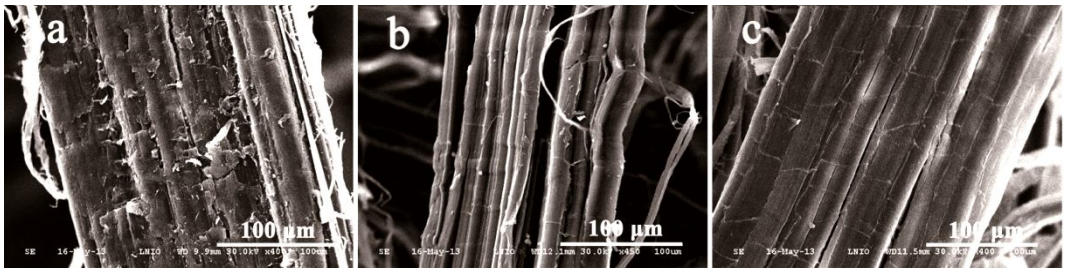


Fig. 2-5 SEM morphology of hemp fiber (a) untreated fiber; (b) fiber treated with alkali; (c) fiber treated with water.

### 2.2.2. Moisture of hemp fiber

The cellulose microfibrils are covered by hemicellulose and lignin which contain lots of hydroxyl groups. Exposure of this layer to air will lead to stronger hydrophilic properties of hemp fiber [8]. Table 2-1 shows the moisture of untreated fiber, alkali treated and water treated fiber.

Tab. 2-1 Moisture of hemp fiber treated by alkali and water.

| Fiber | Untreated fiber | Fiber treated with alkali | Fiber treated with water |
|---|---|---|---|
| Moisture (wt. %) | 6.95 (±0.18) | 5.84 (±0.07) | 7.25 (±0.15) |

After the alkali treatment, with the reductions of higher hydrophilic components, such as hydroxyl groups of hemicellulose in amorphous regions, the moisture decreases from 6.95 wt. % to 5.84 wt. %. In the case of water treated hemp fibers, it seems that the elimination of wax, fats and water-soluble polysaccharide on the fiber surface, more

surface areas of hydroxyl groups and amorphous region are exposed to air (Fig. 2-5c), leading to the fiber moisture increased slightly from 6.95 wt. % to 7.25 wt. %.

### 2.2.3. FTIR spectra

Figure 2-6 displays the ATR-FTIR spectra of hemp fibers after different treatments. The chemical compositions, related functional groups and their corresponding wavenumber are listed in table 2-2 as reference [40, 133]. In the FTIR detection, the Attenuated Total Reflectance (ATR) allows the samples to be examined directly in the solid or liquid state without further preparation.

From table 2-2, the hemicellulose normally shows characteristic peaks at 1732, 1425 and 1162 $cm^{-1}$. Compared with the untreated fiber, the alkali treatment results in the complete disappearance of peak at 1732 $cm^{-1}$ and slight intensity decrease of peaks at 1425 and 1162 $cm^{-1}$, indicating that the alkali treatment only removes partial hemicellulose in the fiber. Similarly, the lignin was also partly removed by alkali. For instance, the two peaks (1241 $cm^{-1}$ and 1505 $cm^{-1}$) of lignin are decreased and disappeared, respectively. The spectrum of untreated fiber and water treated fiber share the similar features. Combining our observations from SEM micrographs and the results of fiber moisture, it's concluded that water treatment cleans the fiber surface without negative effect on the elementary fiber structure. Alkali treatment could remove partial hemicellulose and lignin causing decomposition of elementary fiber structure.

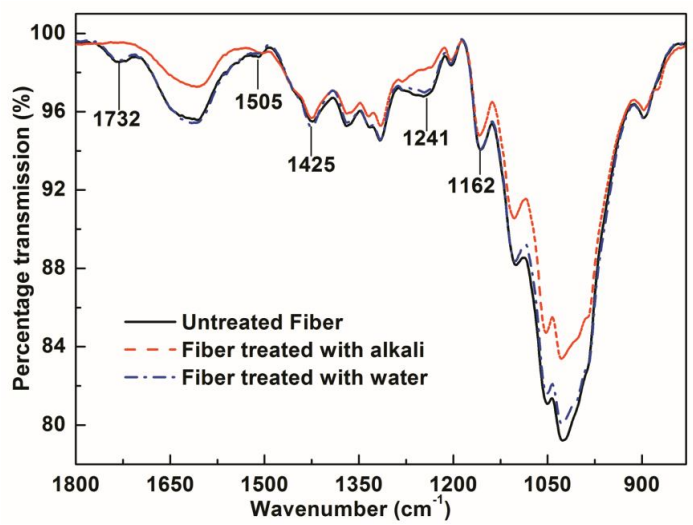


Fig. 2-6 ATR-FTIR spectra of hemp fiber.

Tab. 2-2 Main infrared transitions for hemp fiber.

| Wavenumber($cm^{-1}$) | Vibration | Sources |
|---|---|---|
| 3300 | O–H linked shearing | Polysaccharides |
| 2885 | C–H symmetrical stretching | Polysaccharides |
| 2850 | $CH_2$ symmetrical stretching | Wax |
| 1732 | C=O unconjugated stretching | Xylans (Hemicelluloses) |
| 1650 | -COO | Pectin |
| 1505 | C=C aromatic symmetrical stretching | Lignin |
| 1425 | $CH_2$ symmetric bending C=C stretching aromatic groups | Pectins, lignin, hemicelluloses, |
| 1370 | In-the-plane CH bending | Polysaccharides |
| 1335 | C-O aromatic ring | Cellulose |
| 1240 | C-O aryl group | Lignin |
| 1162 | C-O-C asymmetrical stretching | Cellulose, hemicellulose |
| 895 | Glycosidic bonds symmetric ring-stretching mode | Polysaccharides |
| 670 | C-OH out-of-plane bending | Cellulose |

### 2.2.4. DSC results

Thermal properties of hemp fiber are often analyzed after chemical treatment to evaluate the thermal stability [134]. The decomposition processes of hemp fiber mainly contain two steps: moisture evaporation and degradation of hemicellulose, lignin and cellulose. Evaporation of free and linked water normally occurs below 200 ºC. Generally, the evaporation temperature of linked water is higher than that of the free water (about 100 ºC). The degradation temperature of hemicellulose, lignin and cellulose is 25-290 ºC, 150-420 ºC and 250-350 ºC, respectively [8].

DSC results of hemp fiber after water, alkali treatments and untreated fiber are presented in figure 2-7, including a close-up showing the DSC curves in the lower temperature range. Around 100 ºC, endothermic quantities of alkali treated fiber below 160 ºC is apparently less than those of untreated fiber, indicating that the quantity of free water in alkali treated fiber is less than untreated fiber. The temperature of endothermic peak for water treated fiber (109 ºC) is lower than that of untreated fiber (118 ºC), thus more free water is presented in fiber after water treatment. These results corroborate well with the results of fiber moisture analysis in table 2-1.

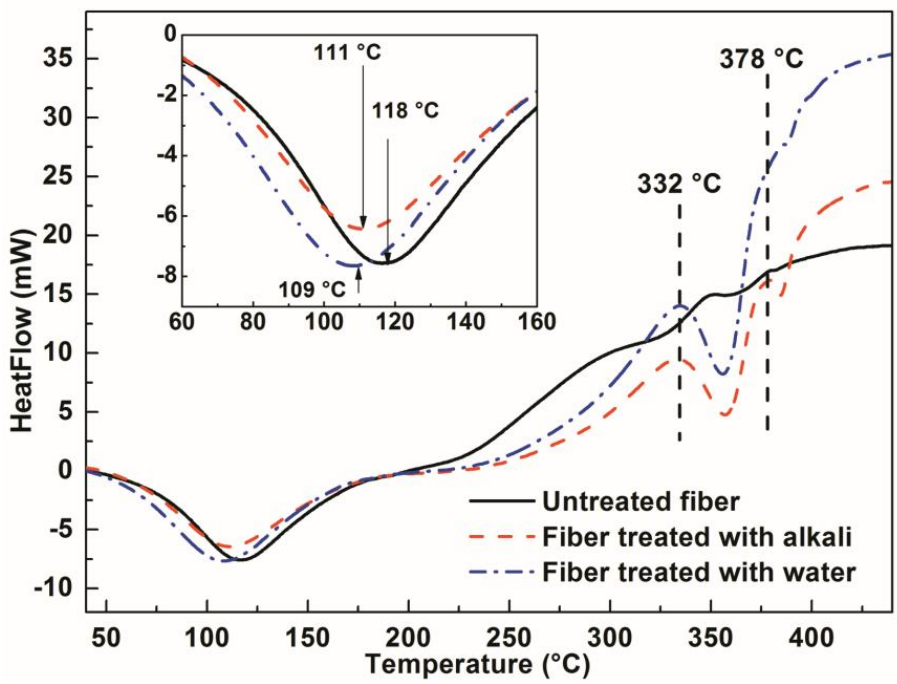


Fig. 2-7 DSC results of hemp fiber after different treatments. A close-up of lower temperature spectra were illustrated in the upper-left inset.

All the three fibers show certain exothermic evolution above 200 ºC, indicating the beginning of fiber decomposition. It is clear that the untreated fiber has the lowest starting temperature in this exothermic region, which should be resulted from the instability of wax, fats and polysaccharide left on the hemp fiber. On the other hand, the two obvious exothermic peaks at 332 ºC and 378 ºC should be attributed to the decompositions of cellulose and lignin, respectively [8]. The much larger exothermic areas of water treated fiber indicate that more fiber elementary compounds are preserved compared to the aggressive alkali treated fiber. Therefore, the water treatment could improve the thermal stability of hemp fiber like alkali treatment.

### 2.2.5. XRD patterns

The XRD patterns of the untreated, alkali and water treated fiber are shown in figure 2-8. In figure 2-8, the patterns of all these three fibers exhibited an intense peak at around 2θ = 22°, assigned to the crystal plane (002) of cellulose I. These results

indicate that both water and alkali treatment did not change the crystal type of hemp fiber.

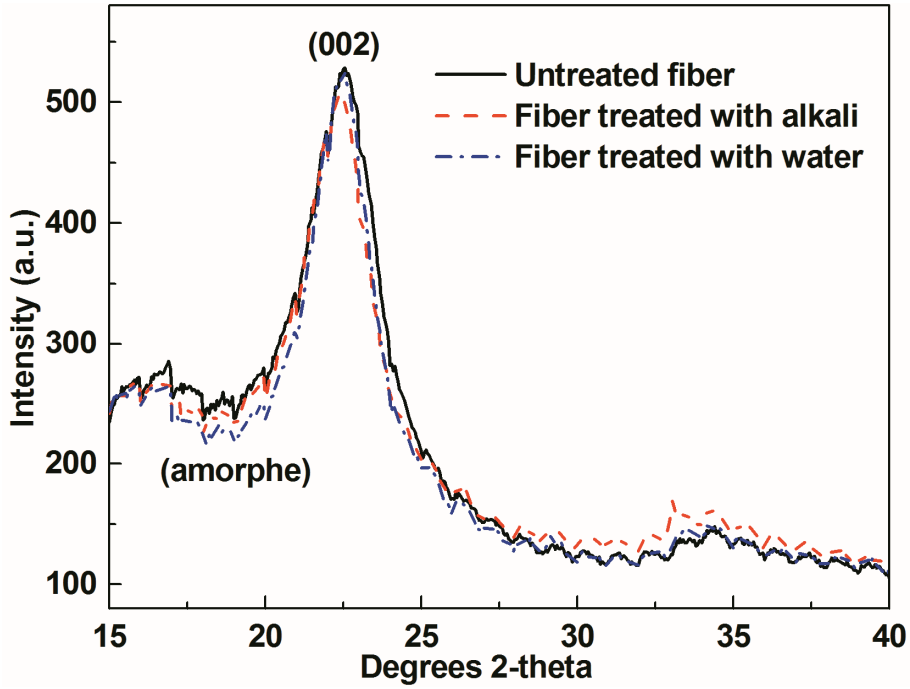


Fig. 2-8 XRD patterns of untreated hemp fiber, alkali treated and water treated hemp fiber.

The crystallinity index (CI) is generally employed to evaluate the crystallinity of natural fiber. It could be calculated according to the following equation [135]:

$$CI(\%) = \frac{I_{002} - I_{am}}{I_{am}} \times 100\% \qquad (2\text{-}1)$$

where $I_{002}$ is the maximum intensity of crystal plane (002) and $I_{am}$ is the intensity of amorphous part of the fiber, which is shown by the valley around 2θ = 18°. The calculated results of CI are shown in table 2-3.

Tab. 2-3 Crystallinity index of untreated, water and alkali treated hemp fiber.

| Fiber | Untreated fiber | Water treated fiber | Alkali treated fiber |
|---|---|---|---|
| Crystallinity index (%) | 55.3 | 55.5 | 58.7 |

The CI of water treated hemp fiber (55.5 %) is nearly unchanged comparing with untreated fiber (55.3 %). After alkali treatment, the CI slightly increased to 58.7 %. The increase in crystallinity index is resulted from the removal of lignin and hemicellulose, facilitating the arrangement of cellulose chains [136].

## *2.3. Effects of silane agent modification on fiber*

### 2.3.1. Fiber morphology analysis

Figure 2-9 presents the morphology of alkali treated fiber, F-TMPS, F-TPAPS and F-TAPS. With the alkali treatment, waxes and pectins covering on the fiber surface are removed and the cleaning surface of elementary fiber is exposed outside (Fig. 2-9a). After the silane modification, a thin silane layer can be observed on the fiber surface (Fig. 2-9b, c and d). The formation of the silane film is attributed to the reaction of silane with hydroxyl groups on the surface of hemp fiber. In the presence of water molecule, silane is hydrolyzed liberating reactive silanol groups. Then these reactive silanol monomers are physically absorbed to hydroxyl groups of nature fiber by hydrogen bonds. Through heating processes, the hydrogen bonds between the silanol and the hydroxyl groups of fibers can be converted into the covalent -Si-O-C- bonds. During the hydrolysis process, there is also the self-condensation of silanol [137].

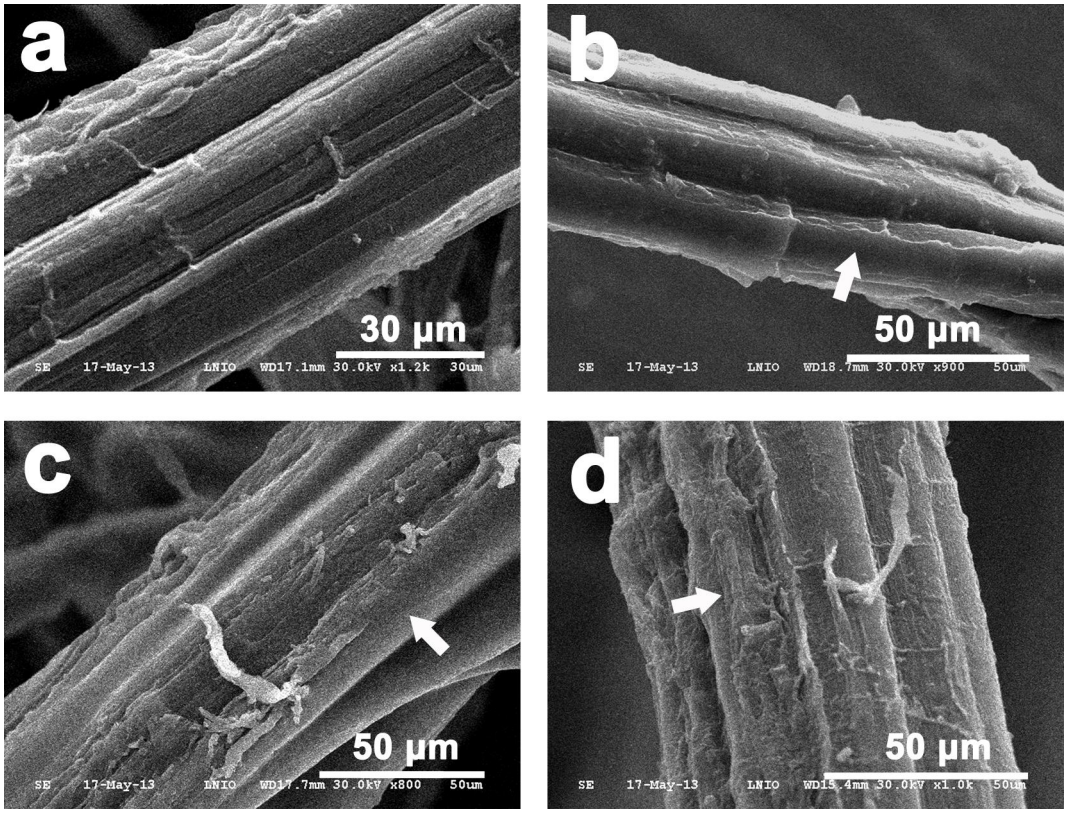


Fig. 2-9 SEM micrographs of hemp fiber: (a), alkali treated; (b), F-TMPS; (c), F-TPAPS; (d), F-TAPS.

### 2.3.2. Moisture of hemp fiber

The moisture of alkali treated hemp fiber, F-TMPS, F-TPAPS and F-TAPS are shown in table 2-4. We can see that the silane agents didn't have great influence on the moisture of hemp fiber. As is known, the water absorption of hemp fiber is mainly ascribed to the hydroxyl groups in the fiber. In other words, it's mainly dependent on the chemical constitutions of hemp fiber. In fact, the modification by silane agents doesn't change the chemical constitutions of fiber. Therefore, the moisture of fiber F-TMPS, F-TPAPS and F-TAPS barely changed when compared with alkali treated fiber.

Tab. 2-4 Moisture of hemp fiber modified by silane.

| Fiber | Alkali treated fiber | F-TMPS | F-TPAPS | F-TAPS |
|---|---|---|---|---|
| Moisture (wt. %) | 5.84 (±0.07) | 5.88 (±0.04) | 5.63(±0.09) | 5.71 (±0.06) |

### 2.3.3. FTIR spectra

In figure 2-10, the FTIR spectrum of hemp fiber before and after the silane modification is compared in order to evaluate the modification. In addition, the FTIR spectrum of the relative silane agent of MPS, PAPS and APS are also presented in Fig. 2-10.

After the modification of MPS, the spectrum of F-TMPS appears two sharp absorption bands in 1639 and 1718 $cm^{-1}$, which are contributed to the C=C stretch vibration and C=O group of methacrylate [131]. In the spectrum of F-TPAPS, C-N stretching vibrations are observed at 1276 $cm^{-1}$. The absorption bands in 1603 and 1507 $cm^{-1}$ are ascribed to the C=C stretching in benzenoid rings and the group -NH bending of PAPS [38]. The asymmetric and symmetric stretching modes of –CH in APS are observed at 2942 and 2839 $cm^{-1}$ in F-TAPS spectrum. The peak appeared at 1657 and 3404 $cm^{-1}$ are attributed to the bending and stretching of -NH, respectively [132]. Overall, the presence of silane peaks in FTIR spectra of the modified fiber confirms the successful surface modification of hemp fiber by saline agents MPS, PAPS and APS.

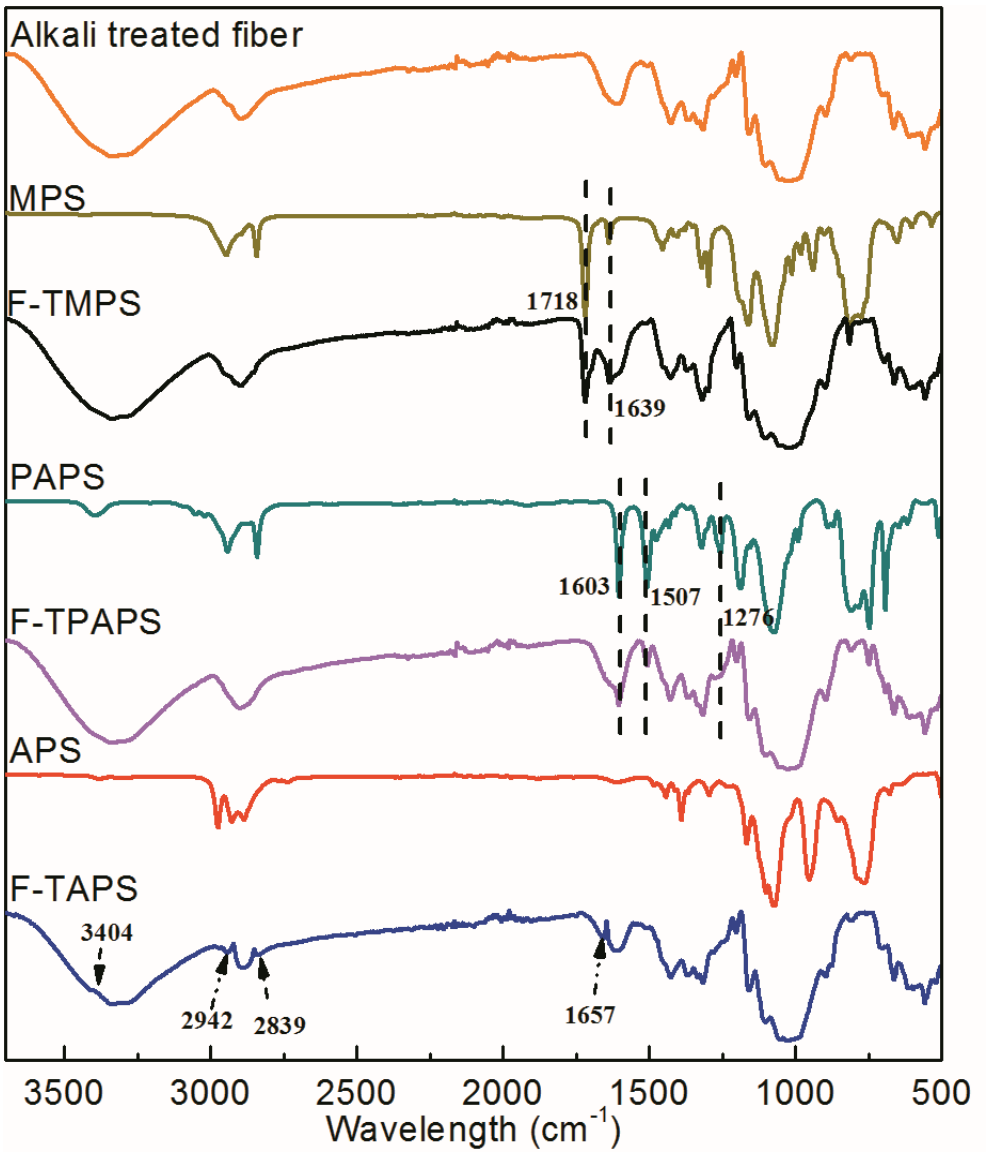


Fig. 2-10 FTIR (3700-500 $cm^{-1}$) spectra of: F-TS; MPS; F-TMPS, PAPS; F-TPAPS; APS; F-TAPS.

In general, to ensure the reaction of silane agent with hydroxyl groups of hemp fiber, the characteristic bands like Si-O-Si (s, 1030 and s, 1100 $cm^{-1}$) and Si-O-C (s, 1080 and s, 1200 $cm^{-1}$) are supposed to be detected from the modified hemp fiber. While because there are several signals of hemp fiber in the range 1700-700 $cm^{-1}$, it's extremely difficult to distinguish the characteristic bands of Si-O-Si and Si-O-C with the original peaks of hemp fiber [137].

## *2.4. Hemp fiber reinforced polypropylene composites*

### 2.4.1. Preparation of composites

*2.4.1.1. Materials*

Polypropylene (PP) was purchased from Dow, France, with density of 0.91 g $cm^{-3}$ and melt index of 8.1 g (10 min)-1 (190 °C, 2.16 kg). Maleic anhydride grafted polypropylene (MAH-g-PP) was also supplied by DOW, France.

*2.4.1.2. Composites processing*

PP, hemp fiber and MAH-g-PP (used as compatibilizer) were mixed in a single screw extruder Brabender KE19 at 170-185 °C. Tensile testing specimens were fabricated by injection moulding Engel Spex Victory 50 at 170-180 °C, 158 MPa (composites specimens 1B, according to standard ISO 527-2), with the help from IUT, Troyes. The composites formulations are listed in table 2-5. The reinforcing rate is 30.0 wt. % for C-FU and 28.6 wt. % for other composites in this thesis.

Tab. 2-5 The composites formulations.

| Samples | PP (phr) | PP-g-MAH (phr) | Hemp fiber(phr) | Notations |
|---|---|---|---|---|
| PP | 100 | 0 | 0 | Neat PP |
| PP-MAH | 100 | 7.14 | 0 | Neat PP blended with PP-g-MAH |
| C-UF | 100 | 0 | 42.86 | Untreated fiber |
| C-UF-MAH | 100 | 7.14 | 42.86 | Untreated fiber |
| C-FW | 100 | 7.14 | 42.86 | Water treated fiber |
| C-FS | 100 | 7.14 | 42.86 | Water and alkali treated fiber |
| C-FMPS | 100 | 7.14 | 42.86 | MPS modified alkali treated fiber |
| C-FPAPS | 100 | 7.14 | 42.86 | PAPS modified alkali treated fiber |
| C-FAPS | 100 | 7.14 | 42.86 | APS modified alkali treated fiber |

### 2.4.2. Analytical methods

*2.4.2.1. SEM observations*

SEM was employed to observe the fracture surface of composites after tensile tests. All samples were coated with carbon by a SEM coater CC7650. The images were captured using a Hitachi S3500N under low magnification.

*2.4.2.2. Tensile tests*

The tensile tests were carried out in a static tension machine Instron 4484 at room temperature. The displacement rate of composite is 2 mm $min^{-1}$ but that of the neat PP and PP-MAH is 20 mm $min^{-1}$. An extensometer with a 12.5 mm initial opening length was placed at the center of specimens to measure the deformation of composites.

## 2.5. *Effects of PP-g-MAH on the composites*

### 2.5.1. Mechanical properties

PP-g-MAH is an efficient coupling agent in improving the interfacial adhesion of the composites. Compared with the complicated of fiber treatment process, PP-g-MAH can be easily blended with polymer in extrusion of the composites. Thus, the effects of PP-g-MAH on the PP matrix (neat PP) and the fiber reinforced composites are studied firstly.

Figure 2-11 shows the mechanical properties of composite C-UF, C-UF-MAH, neat PP and PP blended with PP-g-MAH (PP-MAH). By the addition of compatibilizer PP-g-MAH, the Young's modulus of PP is almost unchanged, but the fracture stress slightly decreased from 21.0 MPa (PP) to 17.3 MPa (PP-MAH). At the same time, it's observed that the fracture strain increased from 367.3 % (PP) to 518.2 % (PP-MAH). PP-g-MAH is one kind of compatibilizer fabricated by grafting a low molecule of maleic anhydride (MAH) to long PP chains. These grafted MAH will decrease the

intermolecular force between PP chains. That's why the fracture stress of PP decreased and the fracture strain increased after the addition of PP-g-MAH.

In contrast, the addition of PP-g-MAH improved considerably both the Young's modulus and fracture stress of PP composites reinforced by untreated hemp fiber, but decreased the fracture strain. Comparing the tensile test results of C-UF with C-UF-MAH (with added the PP-g-MAH), the Young's modulus increased from 3.0 to 3.7 GPa, and the fracture stress increased from 28.6 to 39.8 MPa. The Young's modulus and fracture stress increased by 23.3 and 39.1 %, respectively. In one side of PP-g-MAH structure, MAH could react with hydroxide groups on the natural fiber surface, on the other side, the longer molecule chains of PP could entangle with the chains of PP matrix. As the enhancing of interfacial adhesion strength, the fracture strain decreased because of the restraints of interfacial fracture. That's why the fracture strain decreased from 5.6 % (C-UF) to 3.7 % (C-UF-MAH).

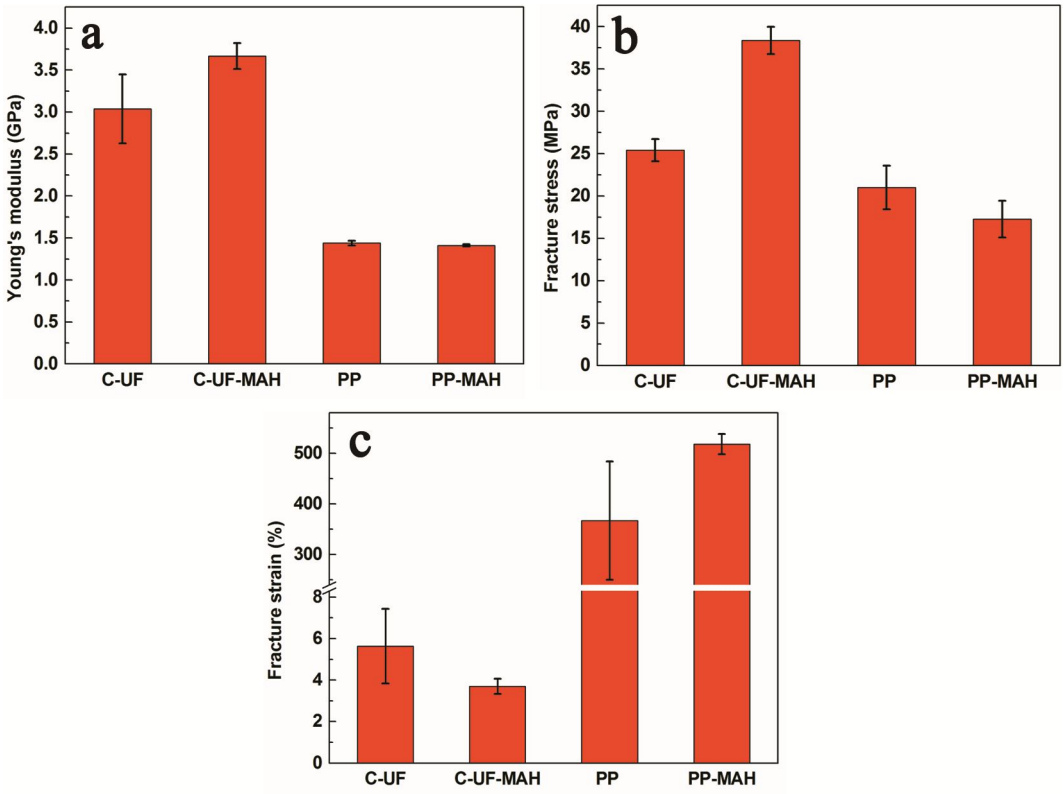


Fig. 2-11 Mechanical properties of composites (a) Young's modulus; (b) Fracture stress; (c) Fracture strains.

### 2.5.2. Fracture sections

Figure 2-12 shows the SEM micrographs of composites fracture section of C-UF and C-UF-MAH. In figure 2-12a, the fiber is completely pulled out from the PP matrix because of the poor interfacial adhesion (point out by white arrows). To the contrary, in figure 2-12b, the fiber is completely fractured (as indicated by white ellipse and arrow). It's indicated that the PP-g-MAH significantly improved the interfacial adhesion strength of hemp fiber/PP matrix. The tensile force could successfully transfers from PP matrix to fiber leading to the improvement of composite mechanical properties.

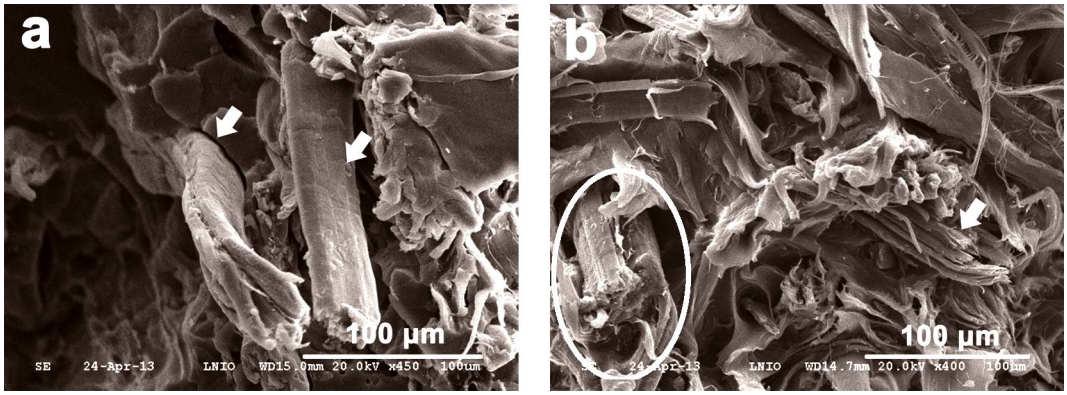


Fig. 2-12 SEM micrographs of composites fracture section (a), C-UF; (b), C-UF-MAH.

### 2.5.3. XRD patterns

The XRD patterns of C-UF, C-UF-MAH, neat PP and PP-MAH are shown in figure 2-13. It's observed that α-form and β-form crystalline appeared in both neat PP and the fiber reinforced composites. As was known, α-form is a dominant crystalline without the addition of special β-nucleants, which is identified by the diffraction plane of (040), (130), (041), (060) and (220). The crystal plane of (300) and (301) are assigned to the β-form of PP [138]. Owing to the shear forces and temperature gradient of the polymer specimens during injection process, the β-form of PP is generally concentrated in the surface of the specimens, but α-form PP is mostly presented in the core region [139]. As shown in figure 2-13, most crystal peaks of PP increased with the addition of PP-g-MAH, indicating that the crystallinity of PP increased. It's because of the maleic anhydride facilitates the chain slippage of PP and thus leads to the rearrangement of PP chain. As a result, the crystallinity of PP increased.

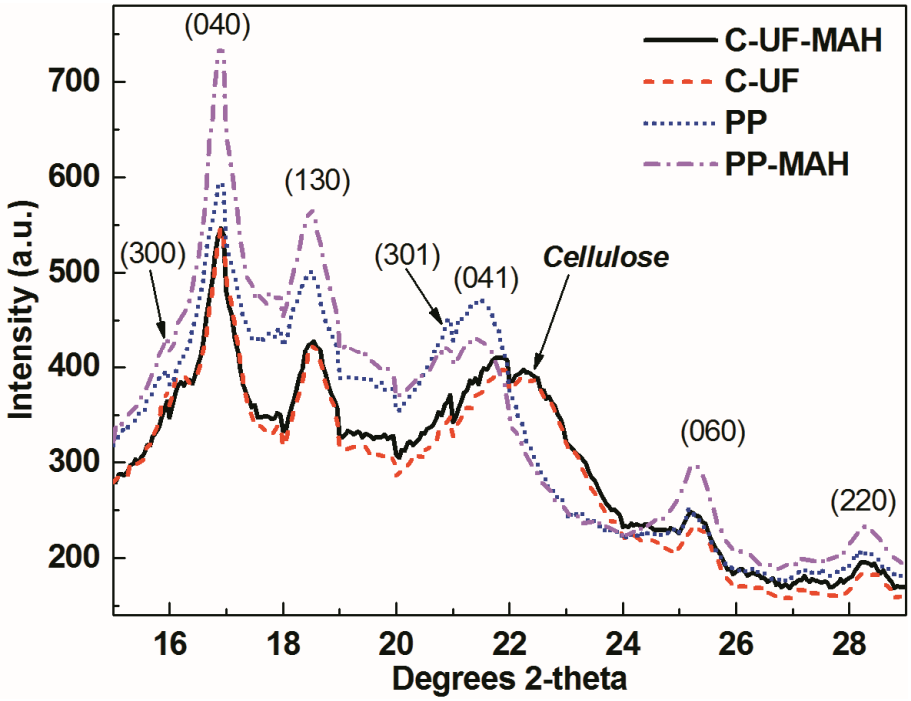


Fig. 2-13 XRD patterns of C-UF, C-UF-MAH, neat PP and PP-MAH (PP blended with PP-g-MAH).

In the XRD patterns of C-UF and C-UF-MAH, the crystal peaks at 2θ = 22.5 ° is assigned to crystal plane of (200) of cellulose I in hemp fiber [140, 141]. And not likely to the neat PP, after the addition of PP-g-MAH, the crystalline peaks of the composites C-UF and C-UF-MAH share the similar intensity. From the tensile test and SEM observation, PP-g-MAH significantly improved the interfacial adhesion of composites. And some researches reported that the good interfacial adhesion could promote the interfacial crystallization [118, 142]. However, it's difficult to observe the corresponding increase of crystallinity in figure 2-13.

## *2.6. Effects of water/alkali treatment of fiber on the composites*

### 2.6.1. Mechanical properties

The tensile test results of the composites reinforced by water or alkali treated fiber are shown in figure 2-14. PP composites reinforced with untreated fiber (C-UF-MAH) was used as the control sample. Overall, the mechanical properties of C-FW are obviously enhanced compared to the other two samples. For the control sample with

untreated fiber (C-UF-MAH), Young's modulus, fracture stress and fracture strain is 3.66 GPa, 39.81 MPa and 3.70 %, respectively. Meanwhile, the fracture stress and fracture strain of C-FS are nearly unchanged, while the Young's modulus is decreased by 7.92 % when compared to the control sample. Interestingly, treating fiber with water obviously improves the composites mechanical properties: Young's modulus, fracture stress and fracture strain increased by 3.66 %, 7.86 % and 14.6 %, respectively, comparing to the control sample of C-UF-MAH (Fig. 2-14a-c).

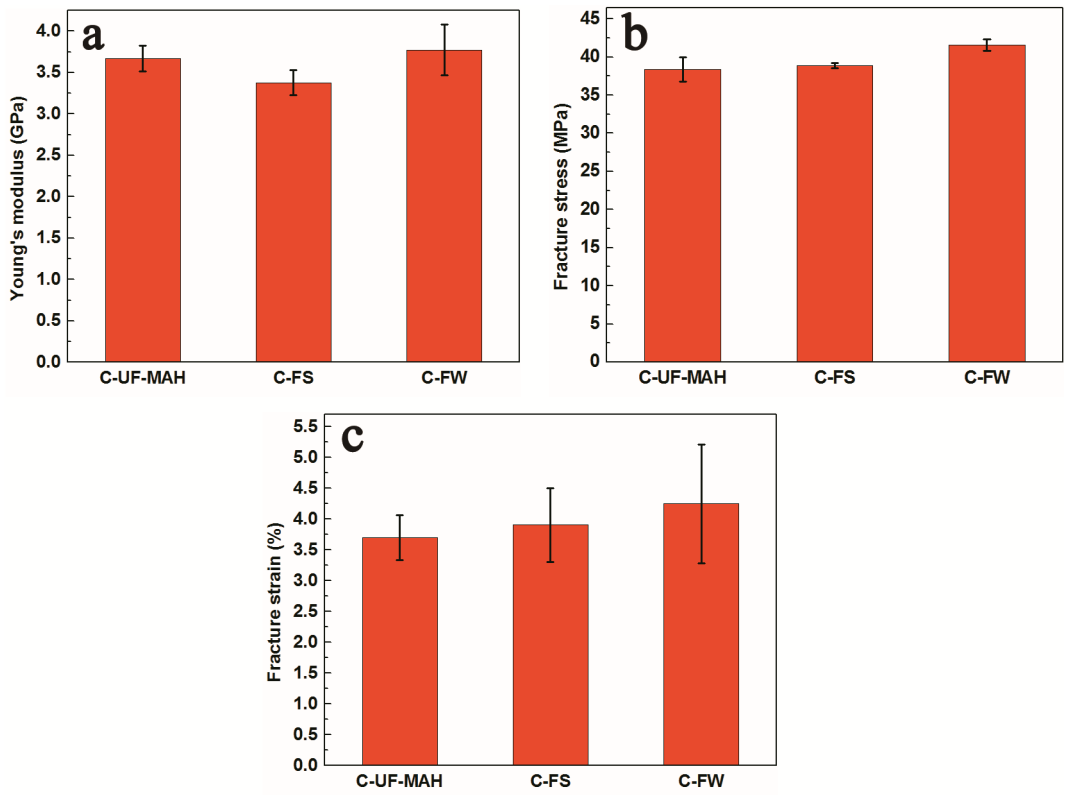


Fig. 2-14 Mechanical properties of composites (a) Young's modulus; (b) Fracture stress; (c) Fracture strains.

It seems that the aggressive alkali treatment would result in the potential degradation of fiber structures leading to the deterioration of mechanical properties of the obtained polymer composites.

### 2.6.2. Fracture sections

Figure 2-15 displays SEM morphology of fracture section of composites. For the composites using untreated fiber (Fig. 2-15a), it could be observed that the pulled out fiber surface is still covered with some substances, which may be the polysaccharide (indicated by white arrow). For the C-FS (Fig. 2-15b, alkali treatment), the elementary fiber structure is partly destroyed (indicated by white arrow). As partial hemicellulose and lignin are removed from the fiber after alkali treatments, the liaison force between the microfibers is greatly reduced. Thus the elementary fiber is separated to lots of microfibrils by strong shearing force during the extrusion and injection process. For C-FW treated fiber (Fig. 2-15c), the fibers are obviously fractured (indicated by white ellipse). And on the fiber surface, there are some microfibrils produced in the tensile processes due to the stronger interfacial adhesion strength (indicated by white arrow).

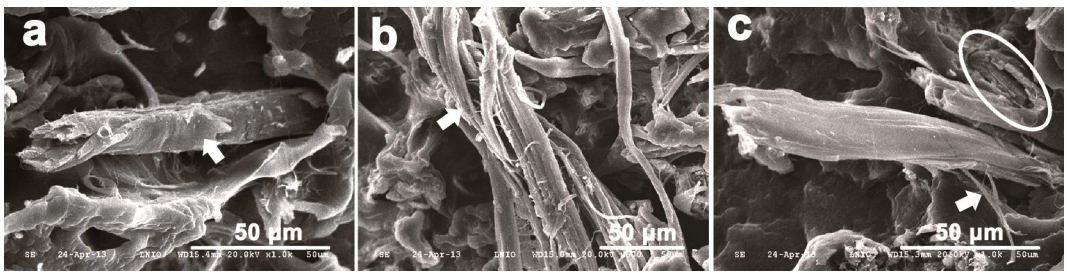


Fig. 2-15 SEM micrographs of composites fracture section (a), C-UF-MAH (untreated fiber); (b), C-FS (alkali treated fiber); (c), C-FW (water treated fiber).

Figure 2-16 presents the schematic diagrams of internal structure of composites reinforced by untreated, water treated and alkali treated hemp fiber. For the C-UF-MAH, the waxes, polysaccharide and others existences on fiber surface prevent the well connection between matrix and fiber, which decreases the interfacial adhesion strength. For the C-FS, the original elementary fiber structure is partly destroyed after aggressive alkali treatment by removing certain constituents of hemicellulose and lignin. For example, the fissures observed in elementary fiber (Fig. 2-5b) may form

defects in composites resulting in lower mechanical properties. Interestingly, for the C-FW, water treatment removes the impurities on fiber surface and conserves the integral structure of fiber resulting in the minimum degradation of fiber but increasing interfacial strength of composites.

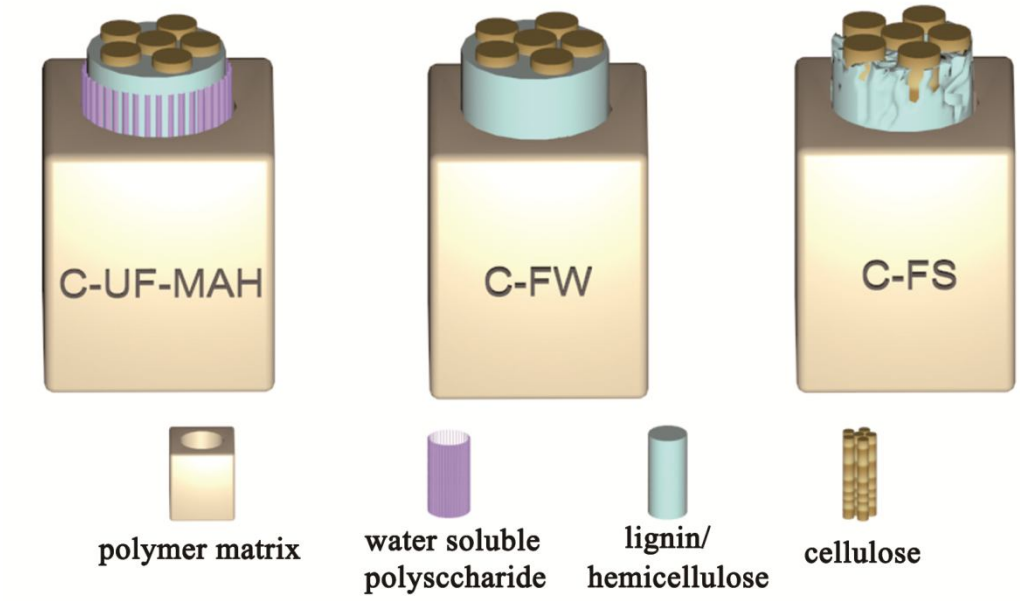


Fig. 2-16 Schemes of composites structures: C-UF-MAH (untreated fiber), C-FW (water treated fiber) and C-FS (alkali treated fiber).

## *2.7. Effects of silane modifications of fiber on the composites*

### 2.7.1. Mechanical properties

The tensile tests results of PP composites reinforced by hemp fiber modified respectively by the silane of MPS, PAPS and APS are shown in figure 2-17. In figure 2-17a, the Young's modulus of composites slightly enhanced with the modification of all these three silane agents. In figure 2-17b, the fracture stress decreased from 38.9 MPa (C-FS) to 37.3 MPa (C-TPAPS) after the modification of PAPS. While, after the modification of APS, the fracture stress increased to 41.8 MPa (C-TAPS). It's reported the amino could react with anhydride to form amide covalent bond [143]. The difference is only the primary amino -$NH_2$ of APS can react with maleic

anhydride grafted in PP to form amide covalent bond (Fig. 2-18). Due to this stronger covalent bond, the liaison strength between the fiber and matrix increases effectively and thus the mechanical properties of C-TAPS enhanced. However, the secondary amino -NH bearing in benzene rings of PAPS didn't react with maleic anhydride. In addition, benzene rings in PAPS have worse compatibility with either maleic anhydride or PP. As a result, the fracture stress decreased after the modification of PAPS. To the composite C-TMPS, the existences of ester and vinyl groups in MPS can form hydrogen bonds with PP matrix, which are beneficial to the increase of fracture strain due to the chain slips between MPS and PP. Therefore, the fracture strain increased from 3.90 % (C-FS) to 4.51% (C-TMPS).

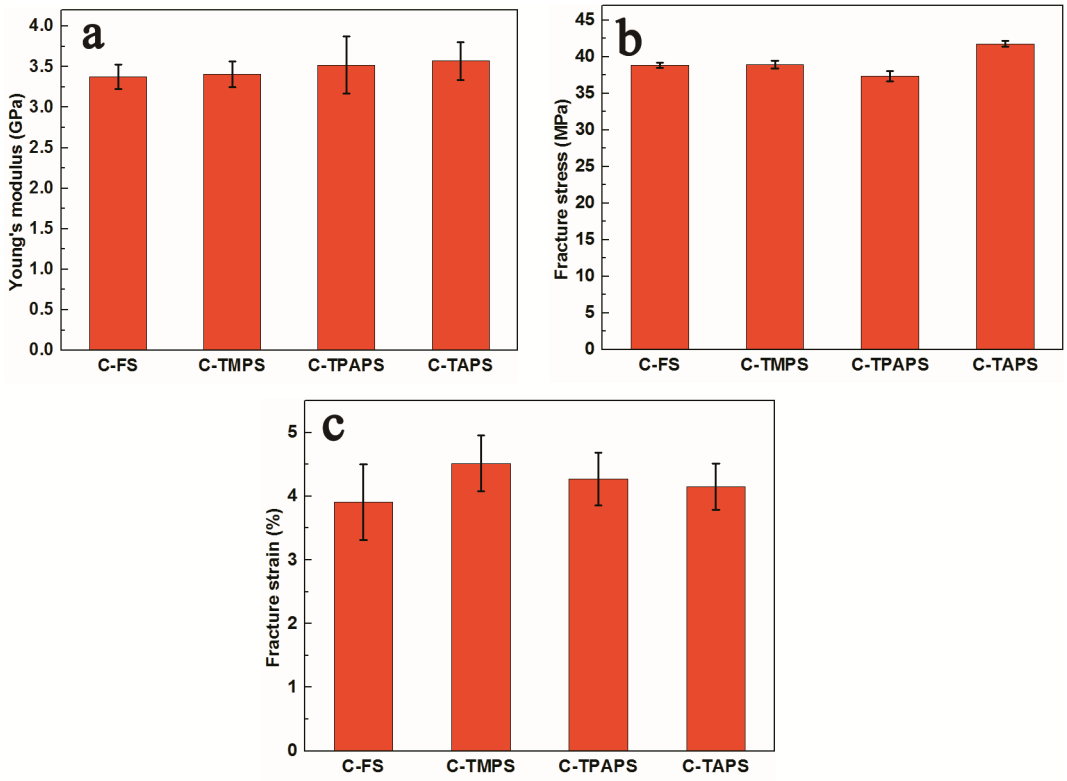


Fig. 2-17 Mechanical properties of C-TS, C-TMPS, C-TPAPS and C-TAPS: (a) Young's modulus; (b) Fracture stress; (c) Fracture strains.

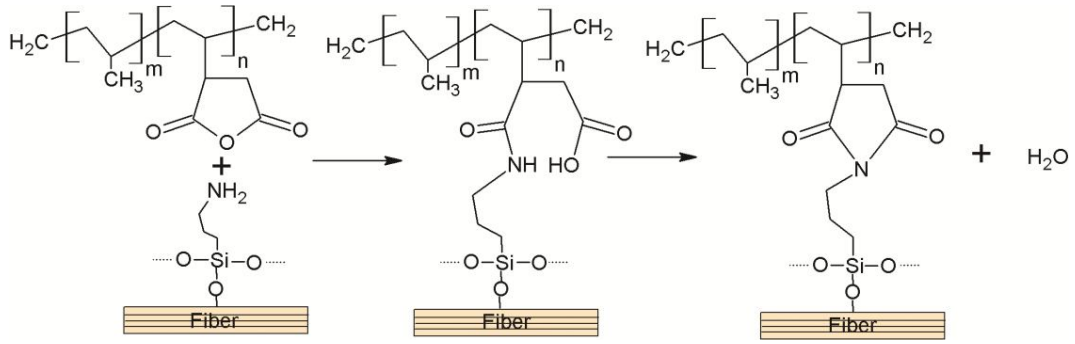


Fig. 2-18 Reaction schemes of APS bearing primary amino with maleic anhydride grafted in PP.

### 2.7.2. Fracture sections

Figure 2-19 shows the SEM micrographs of fracture section of composites C-FS, C-FMPS, C-FPAPS and C-FAPS. In figure 2-19a, the fiber surface is smooth. While in figure 2-19b and d, it's observed the peeled off microfibrils on the fiber surface, which was contributed to the better interfacial strength (indicated by white arrows). But in figure 2-19c, it's found the fiber remaining their complete structure, which should be resulted from the relative poor interfacial adhesion. The SEM observations of composites fracture corresponds well to the tensile test results.

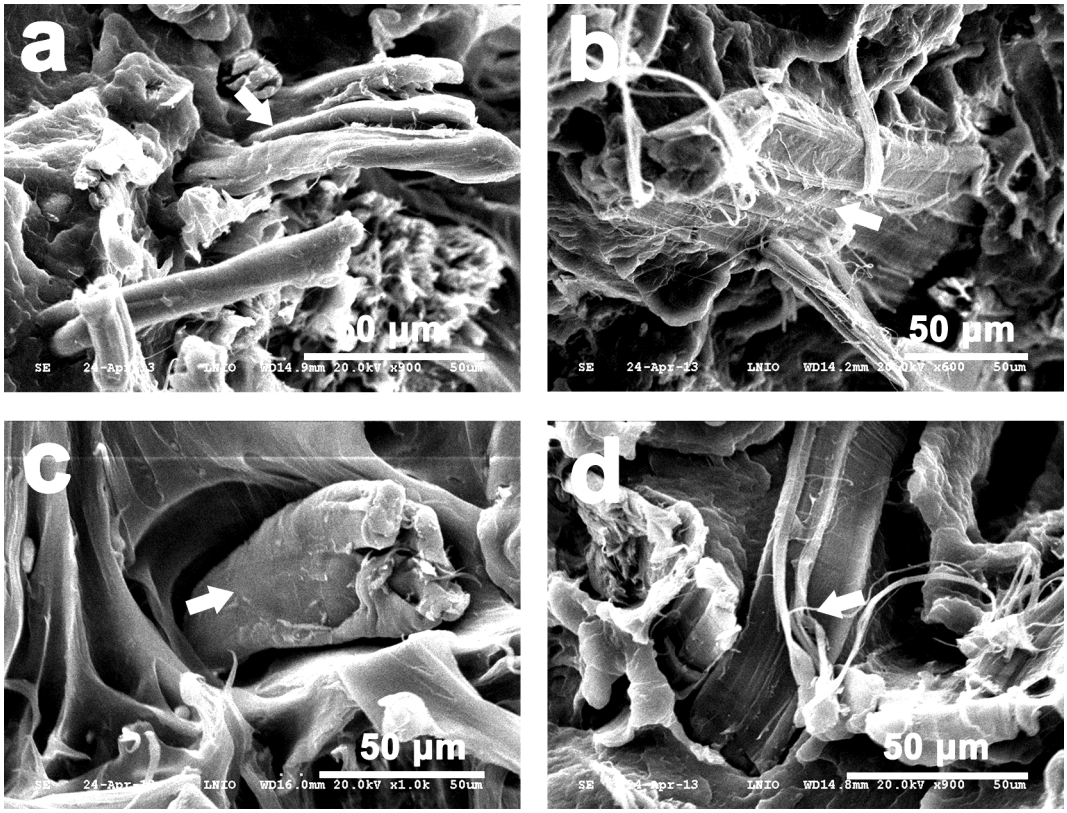


Fig. 2-19 SEM micrographs of composites fracture section (a), C-FS; (b), C-FMPS; (c), C-FPAPS; (d), C-FAPS.

## *2.8. Conclusions*

The SEM micrographics, chemical analysis, moisture of fiber and ATR-FTIR spectra show that alkali treatment not only cleaned the fiber surface but also caused the elementary fiber decomposition by removal of partial hemicellulose and lignin. Water treatments effectively removed water-soluble polysaccharides existing on the surface of hemp fiber, while no obvious damages occurred in elementary fiber. DSC results illustrated that both water and alkali treatment improved the thermal stability of hemp fiber. XRD patterns indicated that alkali and water treatments didn't change the crystal form of hemp fiber. Meanwhile, the crystallinity of hemp fiber was unchanged after water treatment, but slightly increased after alkali treatment.

Due to the smooth surface and integrated elementary fiber structure of water treated fiber, the mechanical properties of PP composite obtained in this case were

enhanced than the composites reinforced with untreated and alkali treated fiber. Thus, water could be considered as an economic and environmental friendly alternative in natural fiber treatment.

The SEM observations and FTIR spectra confirmed the presences of silane agents MPS, PAPS and APS on the surface of hemp fiber. Furthermore, the silane modification has no obvious effects on the hydrophilicity of hemp fiber. To the reinforced composites, even though the existence of PP-g-MAH could cover up the effects of silane agents, we also found some interesting results in the tensile test. The fracture stress of composite reinforced by APS modified hemp fiber is significantly enhanced compared to other composites, since the primary amino of APS could react with maleic anhydride forming amide covalent bond. In contrast, due to the incompatibility of aniline with propylene, PAPS modification decreases the fracture stress of composites. The existences of ester and vinyl groups in MPS are in favor of the increase of composite fracture strain.

In addition, from the tensile test results and SEM observation of the composites, the compatibilizer of PP-g-MAH is proved to be an efficient coupling agent in hemp fiber/PP composites to improve the interfacial adhesion of composites.

# Chapter 3

# Humidity ageing and thermal ageing of the reinforced composites

# Chapter 3. Humidity ageing and thermal ageing of the reinforced composites


**3.1. Humidity ageing of composites..... 64**

**3.1.1. Experimental methods..... 64**

*3.1.1.1. Humidity ageing..... 64*

*3.1.1.2. Water uptake (weight gains)..... 64*

*3.1.1.3. Tensile tests..... 64*

*3.1.1.4. SEM observations..... 65*

**3.1.2. Results and discussion..... 65**

*3.1.2.1. Tensile test results..... 65*

*3.1.2.2. Water uptake..... 67*

*3.1.2.3. Fracture sections analysis..... 69*

**3.2. Swelling of hemp fiber and the reinforced composites..... 71**

**3.2.1. Calculation methods..... 71**

*3.2.1.1. Fiber swelling..... 71*

*3.2.1.2. Composites swelling..... 72*

**3.2.2. Results and discussion..... 74**

*3.2.2.1. Fiber swelling..... 74*

*3.2.2.2. Composites swelling..... 76*

**3.2.3. Fiber swelling force..... 82**

*3.2.3.1. Summarization of theory..... 82*

*3.2.3.2. Calculation method..... 84*

*3.2.3.3. Fiber swelling force..... 85*

**3.3. Thermal ageing of composites..... 87**

**3.3.1. Experiments and analysis..... 87**

*3.3.1.1. Thermal ageing..... 87*

*3.3.1.2. Tensile tests..... 87*

**3.3.2. Tensile test results..... 88**

**3.4. Conclusions..... 90**

The natural hydrophilicity of hemp fiber not only results in poor interfacial adhesion [137], but also leads to the composites are sensitive to environmental humidity [144], which limits the wide applications of agro-composites, like exposing to atmosphere or contacting with aqueous media, for example, windows frames, decking and construction materials [108, 109].

In fact, the humidity ageing studies of planted fiber reinforced composites is mostly focused on the water absorption of composites. With the absorption of water, the interface of fiber/matrix and the fiber may degrade and thus cause the decrease of mechanical properties of composites. The resulted swelling force of fiber may be also responsible for the breaking of the interfacial bonding. For example, the fiber swelling generates shearing force in fiber/matrix interface contributing to the break of fiber/matrix interface. In addition, the absorbed water also gives rise to the weight gains and the volume swelling of composites (swelling ratio, swelling direction).

Based on the obtained results in chapter 2 of this thesis, the water/alkali treatment and silane modification of hemp fiber, and the addition of PP-g-MAH, have more or less influence on the fiber structure or/and the reinforced composites. These treatments may also have great influence on the water absorption of composites.

In this chapter, we mainly studied the humidity ageing and thermal ageing of hemp fiber reinforced PP composites, especially the effects of fiber treatment and interfacial adhesion on the ageing of composites. Firstly, the humidity ageing of composites C-UF, C-UF-MAH, C-FW, C-FS and C-FAPS were performed. The effects of humidity ageing on mechanical properties and weight gains of composites are discussed. And the fracture sections of composites after tensile tests are observed. Then, we studied the swelling behavior including the swelling direction and ratio of both elementary hemp fiber and the reinforced composites. In addition, we calculated the swelling force of elementary hemp fiber by in the light of the free energy function based on the Flory-Rehner theory. Finally, we studied the effects of accelerated thermal ageing on

the mechanical properties of composites C-UF, C-UF-MAH, C-FW, C-FS, C-FAPS C-FS, C-FMPS, C-FPAPS and C-FAPS.

## *3.1. Humidity ageing of composites*

### 3.1.1. Experimental methods

#### *3.1.1.1. Humidity ageing*

Humidity ageing was performed in Atlas suntest XXL for 8 weeks. The ageing condition was: relative humidity 80±5 %, chamber temperature 20±2 ºC, 102 minutes to dry and 18 minutes to water spray according to the standard of ISO 4892-2.

#### *3.1.1.2. Water uptake (weight gains)*

To determine the water uptake, the composite specimens were dried firstly in an oven at 80 ºC for 24 hours to evaporate the residual water in composites and the weight was noted as $M_0$. These dried specimens were then completely immersed in distilled water. For each 5-7 days, specimen's weight was measured after wiping the water on specimen's surface, noted as $M_t$. The weight increase of specimens should equal to the weight of absorbed water $M_{H_2O}$. The water uptake of composites $W_t(\%)$ can be calculated by the following equation:

$$W_t(\%) = \frac{M_t - M_0}{M_0} \times 100\% = \frac{M_{H_2O}}{M_0} \times 100\% \qquad (3\text{-}1)$$

#### *3.1.1.3. Tensile tests*

The tensile tests were carried out in a static tension machine Instron 4484 at room temperature with an imposed displacement rate of 2 mm $min^{-1}$. An extensometer with a 12.5 mm initial opening length was placed at the center of specimens to measure the deformation.

*3.1.1.4. SEM observations*

SEM was employed to observe the fracture surface of composites after tensile tests. All samples were coated with carbon by a SEM coater CC7650. The images were captured using a Hitachi S3500N under low magnification.

## 3.1.2. Results and discussion

*3.1.2.1. Tensile test results*

Tensile test results of composites C-UF, C-UF-MAH, C-FW, C-FS and C-FAPS up to 8 weeks humidity ageing are shown in figure 3-1. The tensile properties of these composites were affected considerably by humidity ageing. Interestingly, it's observed that Young's modulus increased significantly in initial ageing process. In figure 3-1a, Young's modulus increased of 24.3 % (C-UF, 4 weeks), 19.2 % (C-UF-MAH, 6 weeks), 21.7 % (C-FW, 8 weeks), 28.2 % (C-FS, 6 weeks) and 23.5 % (C-FAPS, 6 weeks). The fracture stress also enhanced slightly of 6.5 % (C-UF, 4 weeks), 1.6 % (C-FW, 4 weeks) and 4.1 % (C-FS, 6 weeks). Generally, the tensile strength of elementary hemp fiber decreases directly after humidity ageing [8]. Thus, this increase can be explained like that the swollen fiber due to the water absorption increases the interfacial pressure and thus results in the enhancement of composites mechanical properties. In addition, it seems that stronger interfacial adhesion retards the decrease of Young's modulus, such as the Young's modulus of C-UF and C-UF-MAH began to decrease after 4 weeks and 6 weeks, respectively. However, the Young's modulus of C-FW did not decrease until 8 weeks.

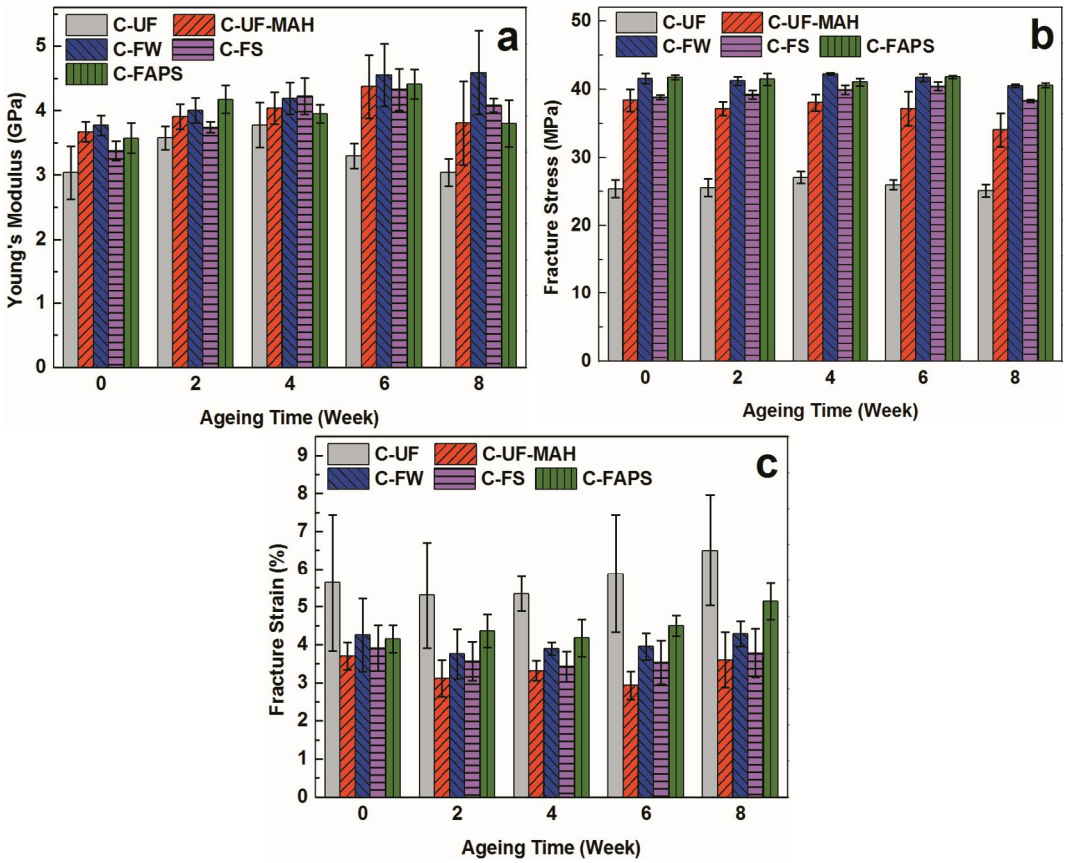


Fig. 3-1 Tensile test results of composites C-UF, C-UF-MAH, C-FW, C-FS and C-FAPS for 8 weeks humidity ageing: (a), Young's modulus; (b), Fracture stress; (c), Fracture strain.

After 8 weeks humidity ageing, the fracture stress decreased of 1.1 % (C-UF), 11.3 % (C-UF-MAH), 2.6 % (C-FW), 1.4 % (C-FS) and 2.9 % (C-FAPS). For C-UF, due to the weak interfacial adhesion before ageing, it's not surprised that there are no obvious diminution of fracture stress caused by the interface degradation. For C-UF-MAH, although PP-g-MAH has effectively improved the interfacial adhesion strength, the untreated fiber in C-UF-MAH is covered with a layer of water-soluble polysaccharide, which is sensitive to water. With the water penetrated into the interface of fiber/matrix, this polysaccharide begins to decompose causing the interface debonding and weakening. Therefore, the fracture stress of C-UF-MAH has an evident decrease of 11.3 %. In contrast, after water or alkali treatment of hemp fiber, the water-soluble

polysaccharide was completely removed from fiber surface (Fig. 2-5) resulting in stronger interfacial adhesion fiber/PP matrix. It's suggested this clean fiber surface and stronger interfacial adhesion are favorable to effectively inhibit the water absorption of interface and hence retard the degradation of interface. Therefore, the fracture stress of C-FW and C-FS only slightly decreased after 8 weeks ageing. For the same reason, C-FAPS also decreased slightly after 8 weeks humidity ageing.

For instance, the increase of Young's modulus is accompanied with a decrease of fracture strain. The Young's modulus increased firstly in humidity ageing. As a result, the corresponding fracture strain decreased. For example, the fracture strain of C-UF decreased of 5.1 % for 2 weeks and then increased of 15.3 % for 8 weeks. Except C-FAPS, the similar tendencies are observed in C-UF-MAH, C-FW and C-FS. After 2 weeks ageing, the fracture strain of C-FAPS didn't show clearly decrease but increased slightly of 5.1 %. In addition, after 6 weeks ageing, the Young's modulus of C-FAPS also increased of 23.4 % and the fracture strain increased of 8.2 %. In summary, considering the fracture stress nearly unchanged after 8 weeks ageing, C-FAPS shows the most excellent resistance to humidity ageing in these five composites.

*3.1.2.2. Water uptake*

Figure 3-2 shows the water uptake of composites at room temperature. From figure 3-2, it's found that the weight of each composite increased initially, followed by saturation or an equilibrium state indicated by a plateau region. The higher water uptake is observed in C-UF (3.9 %), which is reinforced with untreated fiber and has a poor interfacial adhesion. With the addition of PP-g-MAH, C-UF-MAH exhibits a lower water absorption value (2.4 %) indicating that the improvement of interfacial adhesion could reduce the amount of water uptake. Furthermore, the water uptake of composites C-FW and C-FS are 1.1 % and 0.9 %, respectively. It illustrates that the water and alkali treatment is further beneficial to reduce the water uptake of composites. Even though alkali treatment shows more effective than water treatment in reducing the moisture of

hemp fiber (Fig. 3-3), it makes neglected contributions in reducing the water uptake of composites. C-FAPS shows nearly the same water uptake curves to C-FS indicating the modification of hemp fiber by APS didn't make more contribution to the water resistance.

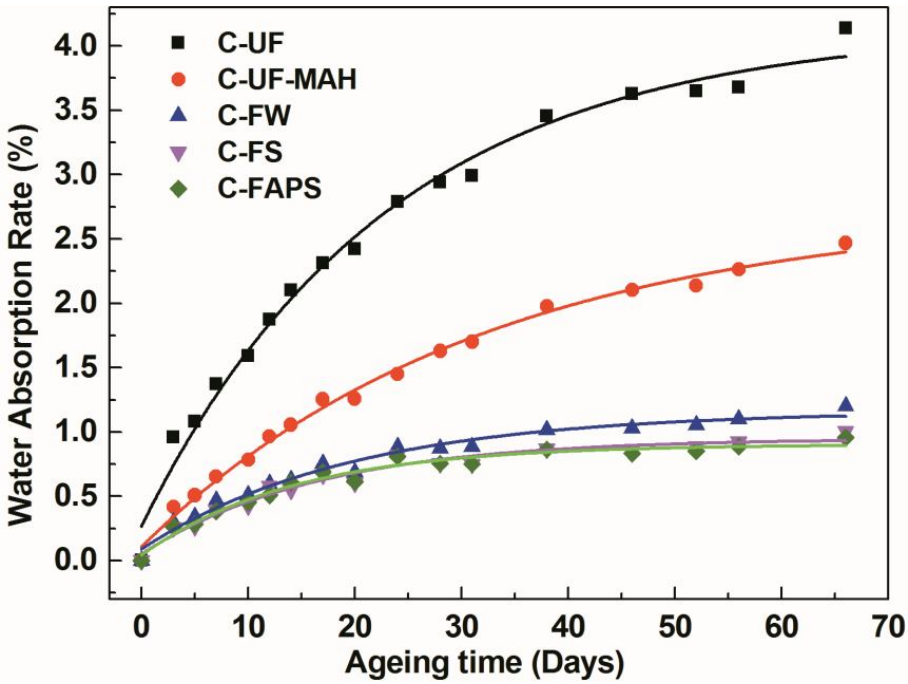


Fig. 3-2 Water uptake of composites C-UF, C-UF-MAH, C-FW, C-FS and C-FAPS.

To the hemp fiber, the level of water uptake is largely dependent on the amount of accessible hydroxyl groups, which can form hydrogen bonds with water molecules. The higher amount of hydroxyl groups, the higher level of water uptake. The moisture of hemp fiber F-UT, F-TW, F-TS and F-TAPS are shown in figure 3-3. Water treated fiber (F-TW) presents nearly the same moisture to the untreated fiber. Alkali treatment could reduce the moisture of hemp fiber from 6.9 to 5.8 %. Using APS to modify alkali treated fiber didn't further reduce the moisture of fiber comparing with alkali treatment (F-TAPS, 5.7 %).

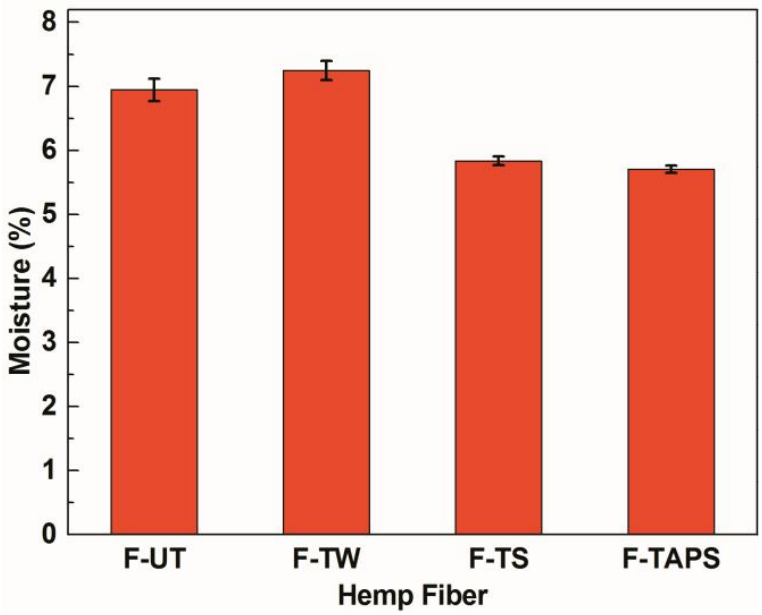


Fig. 3-3 Moisture of hemp fiber F-UT (untreated), F-TW (water treated), F-TS (alkali treated) and F-TAPS (alkali and APS treated).

Overall, PP-g-MAH could effectively decrease the water uptake of composites due to the improvement of interfacial adhesion. Water treatment could further reduce the water uptake of composites because of the removal of water-soluble polysaccharide on fiber surface. Both alkali treatment and the modification of silane agent APS didn't exhibit obvious contribution to the resistance of water uptake. Hence, it's concluded that the water uptake is not just dominated by the amount of hydroxyl groups in hemp fiber, but also the interfacial strength of composites.

*3.1.2.3. Fracture sections analysis*

Figure 3-4 displays SEM images of fracture surface (after tensile tests) of composites after 8 weeks humidity ageing. For the composites reinforced with untreated fiber (Fig. 3-4a), it's observed that the hemp fiber was pulled out directly because of the poor fiber/matrix interfacial adhesion. For other three composites, with adding MAH-g-PP (Fig. 3-4b, c, d and e), the fibers were all broken after tensile tests. In figure 3-4b, it seems that the large gap between fiber and PP was caused by the

degradation of water-soluble polysaccharide on the surface of untreated fiber. In figure 3-4c, d and e, because water or alkali treatment eliminated this water-soluble polysaccharide; there was no obvious degradation of fiber/matrix interface. Therefore, the fiber and PP were still connected very well after tensile tests.

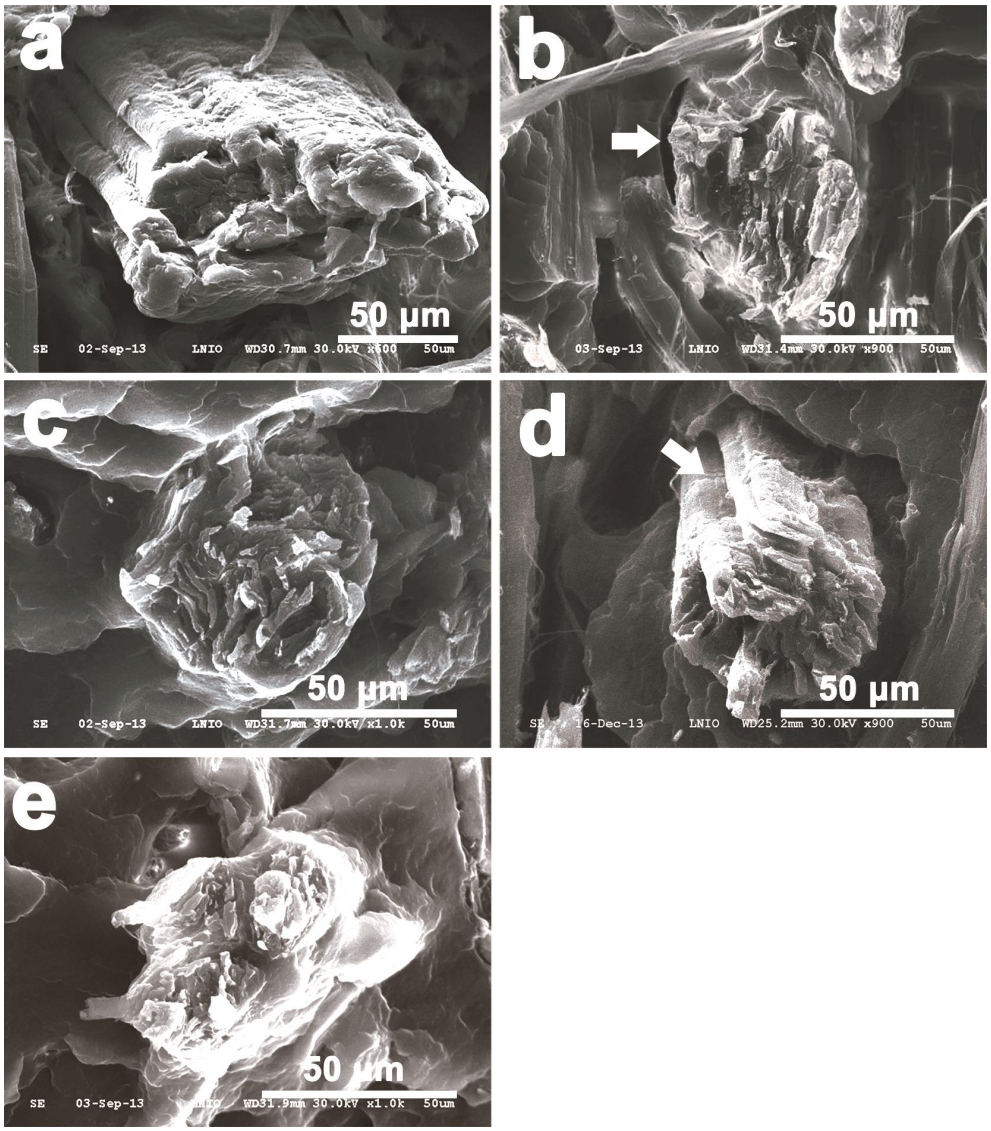


Fig. 3-4 SEM micrographs of composite fracture surface after 8 weeks humidity ageing: (a), C-UF; (b), C-UF-MAH; (c), C-FW; (d), C-FS; (e), C-FAPS.

## *3.2. Swelling of hemp fiber and the reinforced composites*

### 3.2.1. Calculation methods

*3.2.1.1. Fiber swelling*

Figure 3-5 presents the schematic illustration of elementary hemp fiber swelling in humidity ageing. The radial swelling ratio $r_t^f(\%)$ can be obtained from the equation of

$$r_t^f(\%) = \frac{r(t) - r_0}{r_0} \times 100\%, \tag{3-2}$$

where $r_0$ is the initial radius of elementary fiber, $r(t)$ is the radius after humidity ageing of $t$ time.

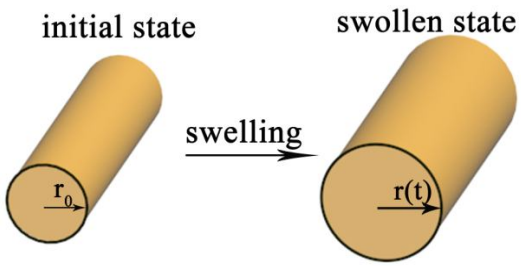


Fig. 3-5 Schematic illustration of elementary hemp fiber subjects to swelling. The present study assumes that the fiber only stretched along radial direction. After humidity ageing of time $t$, the fiber radius stretched from $r_0$ to $r(t)$.

The radial swelling ratio could be calculated from the water absorption of hemp fiber. It's assumed that the hemp fiber only swells in radial direction, no swollen in axial direction. And the increase volume of fiber equals the volume of absorbed water $V_{H_2O}^f$. The increase ratio of fiber volume $v_t^f(\%)$ should be

$$v_t^f(\%) = \frac{V_t^f - V_0^f}{V_0^f} = \frac{V_{H_2O}^f}{V_0^f} \times 100\%. \tag{3-3}$$

where $V_t^f$ is the fiber volume after humidity ageing of time $t$ and $V_0^f$ is the fiber volume before ageing.

The weight gains of elementary fiber $W_t^f(\%)$ can be calculated by the following equation

$$W_t^f(\%) = \frac{M_t^f - M_0^f}{M_0^f} \times 100\% . \quad (3\text{-}4)$$

where $M_0^f$ is the initial weight of bundle hemp fiber, $M_t^f$ is the weight of bundle fiber after humidity ageing of time $t$.

Combining equation (3-3) with equation (3-4), the radius swelling of elementary fiber could be obtained by the following equation:

$$r_t^f(\%) = \frac{\rho_f}{\rho_{H_2O}} \times W_t^f . \quad (3\text{-}5)$$

In equation 3-5, $\rho_f$ (1.07 g·cm$^{-3}$[145]), $\rho_{H_2O}$ (1.00 g·cm$^{-3}$) is the density of hemp fiber and the absorbed water, respectively.

*3.2.1.2. Composites swelling*

Figure 3-6 shows the schematic illustration of composites specimens subject to water swelling. Similarly to the calculation of fiber swelling, the composites swelling could also be calculated from the weight gains of specimens. Based on previous studies, the fiber usually distributes along the injection direction [146] and mainly swells in fiber radial direction [147]. Supposing the composites have no voids, the swelling volume of specimens $V_t^c - V_0^c$ should equals to the volume of absorbed water $V_{H_2O}^c$, where $V_t^c$ is the composite volume after time $t$ and $V_0^c$ is the composite volume

before humidity ageing. Thus, the cross-section area increase of specimens $s_t^c(\%)$ should equal to the increased volume:

$$s_t^c(\%) = v_t^c(\%) = \frac{V_t^c - V_0^c}{V_0^c} = \frac{V_{H_2O}^c}{V_0^c} \times 100\% . \tag{3-6}$$

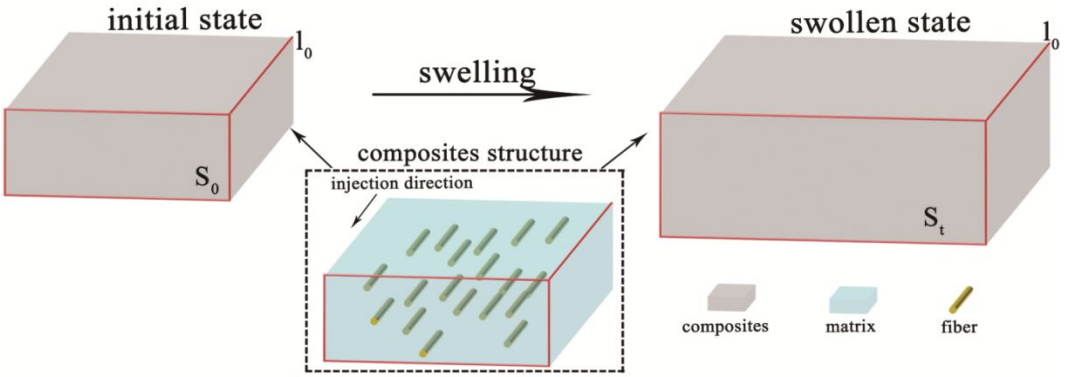


Fig. 3-6 Schematic illustration of composites specimens subject to swelling. The present study assumes that the fiber orients along the injection direction and swells only in the fiber radial direction. Thus, the composites expands in specimens cross-section with $S_t$ (%) = [($S_t$ - $S_0$) / $S_0$] × 100 %, no expansion in fiber oriented direction.

Combining equation (3-6) with equation (3-1), the relationship between composites specimens' weight gains and the area cross-section increase can be found as:

$$s_t^c(\%) = W_t(\%) \times \frac{1}{\rho_{H_2O}} \times \frac{M_0}{V_0}, \tag{3-7}$$

where $\rho_{H_2O}$ is the absorbed water density, $M_0$ is the initial mass of specimens; $V_0$ is the initial volume of specimens. $M_0$ and $V_0$ can be obtained by the following equations:

$$M_0 = m_m + m_f \tag{3-8}$$

$$V_0 = \frac{m_m}{\rho_m} + \frac{m_f}{\rho_f} \tag{3-9}$$

where $m_m$, $m_f$ is the mass of polymer matrix and fiber, respectively; $\rho_m$ and $\rho_f$ is the density of matrix and hemp fiber, respectively.

## 3.2.2. Results and discussion

*3.2.2.1. Fiber swelling*

The experimental data of weight gains and radius swelling ratio of elementary fiber is cited from the thesis of S. JIN [148]. To measure the weight gains and radius swelling ratio of elementary fiber, the author performed humidity ageing of elementary hemp fiber in the same ageing conditions with the composites ageing as in this thesis. To determine the weight gains (Eq. 3-4), the fiber was dried firstly in an oven at 80 ºC for 24 hours to remove the residual water before the ageing experiment. The initial weight of fiber was noted as $M_0^f$. Every 7 days, the fiber was taken out from the chamber and lightly wiped with absorbent paper to remove the water droplet on the fiber surface, the weight was noted as $M_t^f$. At the same time, the author measured the diameter of the elementary fiber to obtain the radial swelling ratio (Eq. 3-2).

Figure 3-7 illustrates the weight gains and radius swelling as function of exposure time of elementary hemp fiber. In figure 3-7a, the weight of hemp fiber increases exponentially with exposure time. After about 21 days, the weight of hemp fiber increased to a saturated stage of around 12.5 %. It's observed that the water absorption follows Fick's law. At room temperature, the water absorption increase linearly at the beginning and then slowly reaches a saturation plateau after certain time [110]. According to the thermodynamics [149], the fiber network swells because the small water molecules mix with the macro molecule of substance in hemp fiber. During this swelling process, the configurational entropy of fiber decreases, while the

configurational entropy of mixture increases. These two kinds of entropy tend to reach an equilibration state, where the swelling ratio of hemp fiber is maximized.

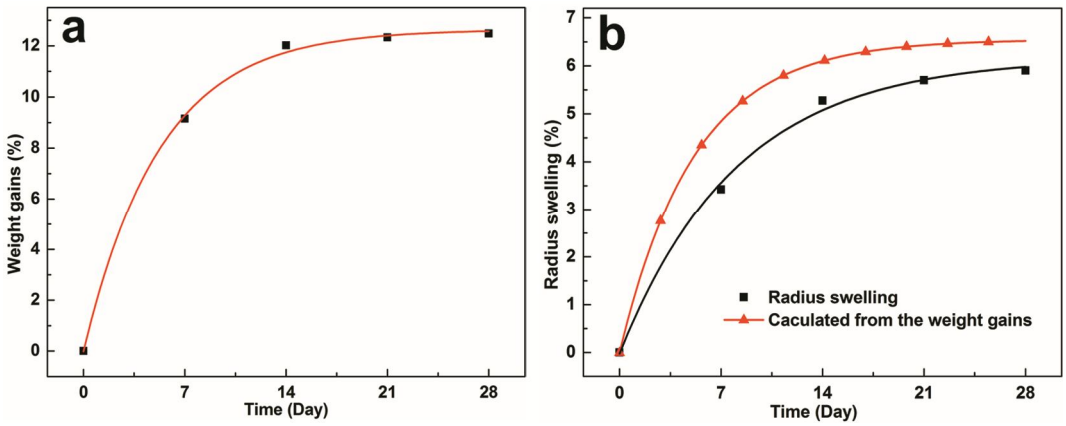


Fig. 3-7 Weight gains (a) and radius swelling (b) of elementary hemp fiber.

In figure 3-7b, the radius swelling of hemp fiber (solid rectangles) presents the same tendency as the weight gains. Fiber radius swells considerably at the beginning of humidity ageing, followed by a plateau region. After 28 days, the radius swells of 5.6 %. The calculated radial swelling ratio (Eq. 3-5) from the weight gains experiment is also presented in figure 3-7b (solid triangles connected by red line). It has been found that the calculated radius swelling is slightly higher than the measured ones during all the ageing process. The highest calculated radius swelling is 6.5 % (28 days ageing), while at the same time, the measured one is 5.9 %. Because the calculation of radius swelling ratio in this case is based on the assumption of the swelling direction of hemp fiber only occurs in the radial direction, no swelling in axial direction, thus, this result indicates that the fiber swells mainly along the radial direction of fiber.

The fiber swelling direction should be determined by its internal network. As shown in figure 3-8, the elementary fiber could be considered as one “composites” of cellulose microfibrils embedded in the “matrix” of hemicellulose/lignin. The microfibrils of cellulose orient along the axial direction of elementary fiber with a spiral angle, and be connected by hemicellulose and lignin to form a network. With humidity ageing, the absorbed water molecules penetrate into the hemicellulose/lignin “matrix”.

Subsequently, water molecules expand greatly the interspaces between cellulose microfibrils towards radial direction and cause a slight stretching of cellulose microfibrils towards axial direction (determined by the spiral angle). That's why the swelling direction of elementary fiber is major in radial direction and minor in axial direction.

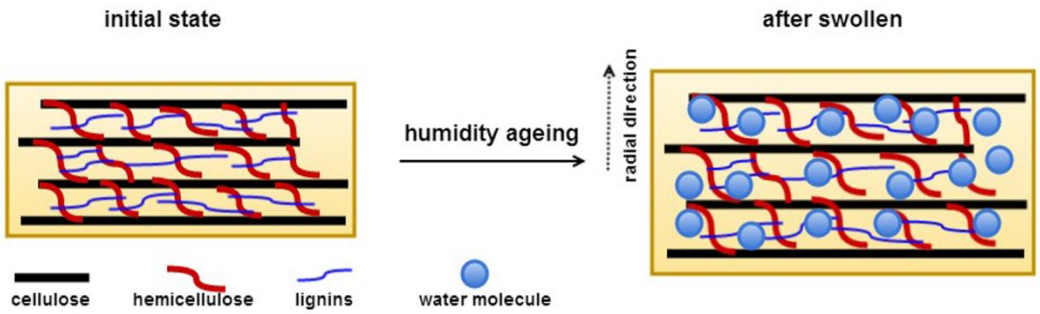


Fig. 3-8 A schematic of water swelling of elementary fiber in humidity ageing. The fiber consists of a network of long polymers (cellulose, hemicellulose and lignin) and small water molecules.

*3.2.2.2. Composites swelling*

Figure 3-9 presents the measured weight gains of composites C-UF (solid rectangles with the best-fit line in red). In addition, to understand the effects of PP matrix on the fiber swelling of fiber, the weight gains of composites is also calculated from the weight gains of elementary fiber (blue solid triangle) according to the equation of

$$w_t^c(\%) = \frac{m_f}{m_m + m_f} \times W_t^f(\%). \qquad (3\text{-}10)$$

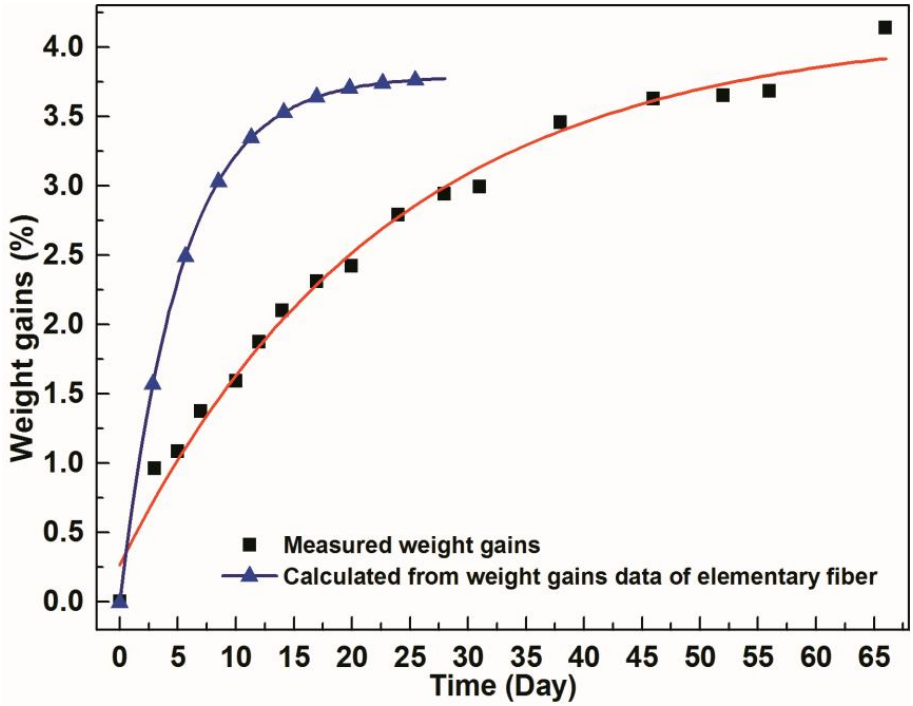


Fig. 3-9 Weight gains of composites C-UF and the calculated values from weight gains of elementary fiber.

In figure 3-9, as increase the exposure time to humidity, both the measured weight gains and the calculated ones reached an equilibrium state of water absorption (about 3.6 %), while the measured values increased much slower than the calculated ones. This suggests that the presence of PP matrix only retards the water absorption without decreasing the quantity of absorbed water of hemp fiber.

The composites swell with the water uptake process of fiber, which has negative effect on the dimensional stability of composites. The composites expansion is normally associated with their water absorption responsible for the weight gains and volume increase. PP doesn't absorb water, so that the water absorption of composites should be ascribed to the hydrophilicity of hemp fiber and the capillary effects of fiber/PP interface. In addition, the voids or defects in composites may also contribute to the weight gains without volume expansion.

For the composites, the expansion direction is as important as the expansion ratio. Combining the results of that hemp fiber mainly swells along the radial direction (section 3.2.2.1) and the assumption of that most fiber distributed in the injection direction, we could find the fiber distribution in composites by constructing the relationship between the cross-section swelling and the weight gains (Eq. 3-7).

Figure 3-10 presents the cross-section swelling of specimens in the humidity ageing (scatter) and the calculated cross-section swelling from the composites weight gains (red line).

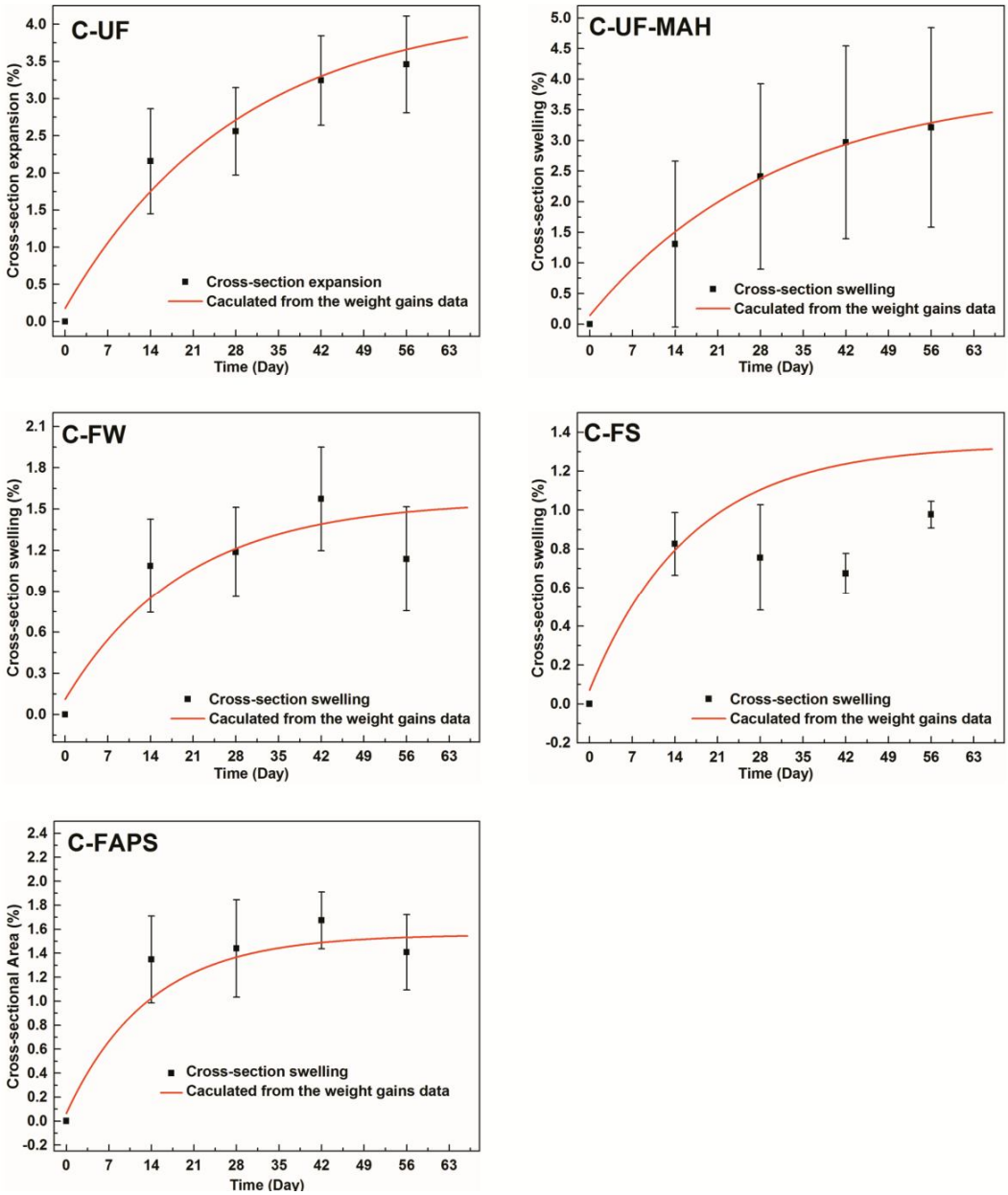


Fig. 3-10 Cross-section expansion of composites specimens: C-UF, C-UF-MAH, C-FW, C-FS and C-FAPS.

As shown in figure 3-10, the cross-section swelling of calculated values matched very well with the determined one, especially in C-UF, C-UF-MAH and C-FW. It proves the assumptions of that fiber in specimens oriented along the injection directions and the fiber mainly swelling in radial direction.

For C-FS, the calculated swelling rate is higher than the experimental determined values after 2 weeks ageing. It's suggested that C-FS absorbed certain quantities of water but its volume didn't increase. As analyzed in previous section, alkali treatment destroyed the fiber structure forming voids or defects in the composites. Due to this, hemp fiber absorbed water and swollen to fill these void and thus the volume of composites apparently didn't swell.

In contrast, C-FAPS shares the similar quantity of weight gains like C-FS in figure 3-2, the cross-section expansions of C-FAPS exhibit the same tendency with the calculated value but is slightly higher than the calculated value during all the humidity ageing. This further proved that C-FAPS shows stronger interfacial adhesion. By comparing C-UF, C-UF-MAH and C-FW, it's concluded that the dimensional stability could be significantly improved by fiber treatment and interfacial adhesion improvement of the composites.

Owing to the cylindrical form, hemp fiber shows isotropic swelling in the radial direction. Not likely to hemp fiber, the cross-section of the reinforced composites is a rectangular form with a width of 10 mm and a thickness of 4 mm. To study the effect of macroscopic dimension on the swelling direction of composites, we measured the swelling ratio of composites in its width direction and thickness direction.

As shown in Fig.3-11, the swelling ratio in thickness direction is much higher (nearly two times) than in the width direction. Take composites C-UF as example, the width increased of 0.7 % (14 days), 0.8 % (28 days) and 1.1 % (42 days). But in the corresponding time, the thickness increased of 1.4 %, 1.8 % and 2.2 %, respectively. Similarly, for C-FW, the width increased to a plateau region of 0.9 % but the thickness increased of 2.0 %. We can observe the similar results in other three composites C-UF-MAH, C-FS and C-FAPS. The swelling ratio of composite specimens in thickness direction is nearly two times of that in width direction.

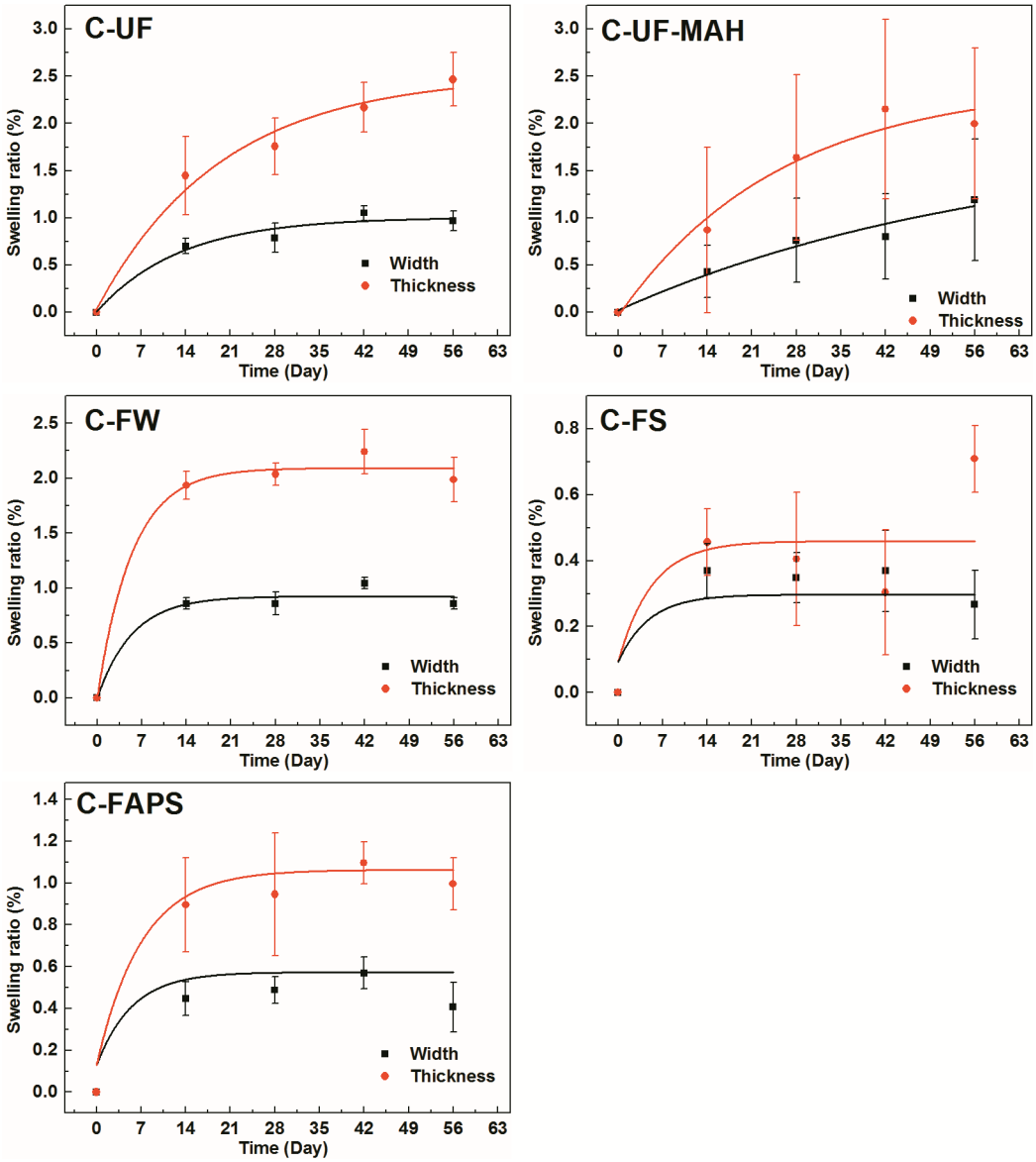


Fig. 3-11 Swelling ratios of composites specimens, C-UF, C-UF-MAH, C-FW, C-FS and C-FAPS in the direction of width and thickness.

It's not surprising to observe the swelling ratio in width and thickness direction like this. As shown in figure 3-12, the fiber shows isotropic swelling, thus the cross-section of composites in the width and thickness direction will show the same swelling quantity. Because of the initial width and thickness is 10 mm and 4 mm, therefore the increase ratio has an inversely proportion to the initial dimension of composites specimens.

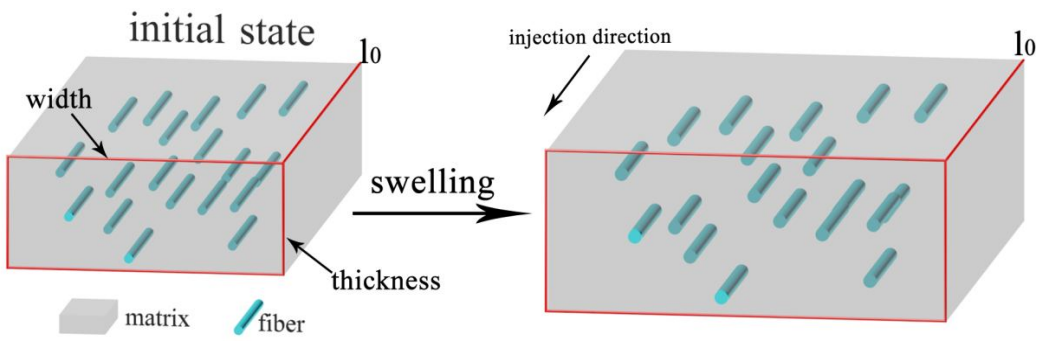


Fig. 3-12 Schematic diagrams of composite specimens.

### 3.2.3. Fiber swelling force

During humidity ageing, the fiber swells and generates the swelling force, which dominates the expansion of PP matrix. Moreover, the swelling force results in break of the interfacial adhesion, followed by the decrease of composite mechanical properties. In this section, we calculated the fiber swelling force according to equations 3-13~15 by using software MATLAB.

#### *3.2.3.1. Summarization of theory*

The hemp fiber can be considered as one kind of a long polymer which is cross-linked into a three-dimensional network (Fig. 3-8). The water, a low molecule, could migrate into the inside of this network due to the hydrophilicity of rich hydroxyl. This migration allows the fiber to change both in shape (especially in the radial direction of hemp fiber as we illustrated in section 3.2.2.1) and volume. This process (Fig. 3-8) is similar to the swelling of polymer gel.

The polymer gel is wildly used in medical devices, drug deliver, tissue engineering and etc…[150], lots of researches have focused in the polymer swelling and numerous theories have been conducted during the past decades [151-154]. Most of them are based on the equilibrium state, which is achieved by a minimum of the Gibbs free energy (thermodynamic and kinetics). The theory used in the gel swelling is generally

divided into nonlinear or linear swelling theory. Both of them have been used to describe or predict the swelling kinetics of polymer gels under various conditions.

Nikolaos Bouklas and Rui Huang[155] compared a nonlinear theory for polymer gels with the classical theory of linear poroelasticity in the swelling kinetics of polymer gel. They establish a relationship between the material properties in the linear theory and those in the nonlinear theory through a linearization procedure. And it has been found that the linear theory agrees with the nonlinear theory at the early stage of swelling. But it is cautioned that the applicability of the linear theory should be limited to relatively small swelling ratios (Fig. 3-13). In the following section 3.2.3.2, we employ a nonlinear theory of polymer gel by Hong et al. [149] to calculate the free swelling stress of elementary hemp fiber.

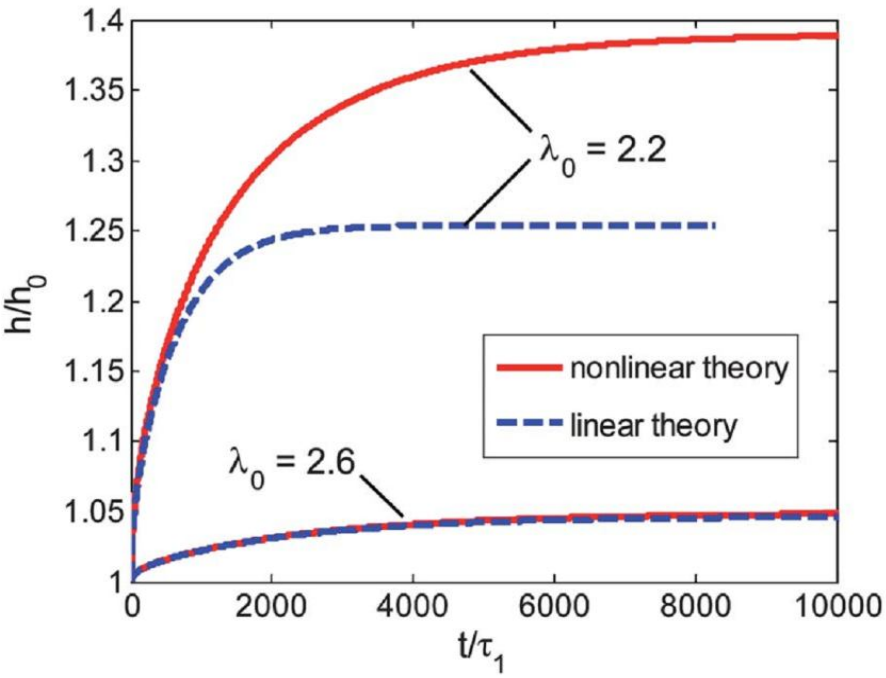


Fig. 3-13 Comparison between the nonlinear theory and the linear poroelasticity for constrained swelling of a hydrogel layer, cited from the reference [155]. Label of y axial $h/h_0$ is the thickness ratio of a thin hydrogel layer, which is normalized by initial thickness $h_0$. Label of x axial $t/\tau_t$ is the swelling time, normalized by a time scale of $\tau_t$. And $\lambda_0$ is the swelling ratio in the initial state.

*3.2.3.2. Calculation method*

Considering the elementary fiber takes the form as cylindrical symmetry, on the fiber surface, the radial stretch $\lambda_r$ and circumferential stretch $\lambda_\theta$ equals

$$\lambda_r = \lambda_\theta = \frac{r(t)}{r_0}. \tag{3-11}$$

The fiber is assumed to deform under the plane-strain conditions (no axial swollen). The axial stretch $\lambda_z$ is

$$\lambda_z = 1. \tag{3-12}$$

The swelling stress of elementary fiber $\sigma_r$ (radial direction), $\sigma_\theta$ (circumferential direction) and $\sigma_z$ (axial direction) could be calculated by using the free energy function based on the Flory-Rehner theory [149, 156, 157], as shown in the following equations

$$\sigma_r = \frac{kT}{nv\lambda_r\lambda_\theta}(\lambda_r^2 - 1) + \frac{kT}{v}\left[\log\left(1 - \frac{1}{\lambda_r\lambda_\theta}\right) + \frac{1}{\lambda_r\lambda_\theta} + \frac{\chi}{(\lambda_r\lambda_\theta)^2}\right] - \frac{\mu}{v}, \tag{3-13}$$

$$\sigma_\theta = \frac{kT}{nv\lambda_r\lambda_\theta}(\lambda_\theta^2 - 1) + \frac{kT}{v}\left[\log\left(1 - \frac{1}{\lambda_r\lambda_\theta}\right) + \frac{1}{\lambda_r\lambda_\theta} + \frac{\chi}{(\lambda_r\lambda_\theta)^2}\right] - \frac{\mu}{v}, \tag{3-14}$$

$$\sigma_z = \frac{kT}{v}\left[\log\left(1 - \frac{1}{\lambda_r\lambda_\theta}\right) + \frac{1}{\lambda_r\lambda_\theta} + \frac{\chi}{(\lambda_r\lambda_\theta)^2}\right] - \frac{\mu}{v}, \tag{3-15}$$

where $n$ is the number of monomers per polymer chain of hemp fiber, $k$ is the Boltzmann constant, $T$ is the absolute temperature, and $\chi$ is a dimensionless measure of the enthalpy of mixing the solvent with polymer, $v$ is the volume per solvent molecule.

*3.2.3.3. Fiber swelling force*

As the fiber only swells in radial planes, the axial stress $\sigma_z$ should be zero. And on the fiber surface, because the swelling ratio in radial direction equals that in circumferential ($\lambda_r = \lambda_\theta$), the swelling stress of $\sigma_r$ should also equal $\sigma_\theta$. Therefore, we only discussed the radial stress $\sigma_r$ in this section.

In equation 3-13, the Boltzmann constant $k$ is $1.3806488 \times 10^{-23}$ $m^2$ kg $s^{-2}$ $K^{-1}$ the humidity ageing temperature of $T$ is 293 K, the volume of one water molecule $v$ equals $3.0 \times 10^{-29}$ $m^3$. $n$ and $\chi$ are the dimensionless materials parameters. Indeed, it's difficult to get the values of $n$ and $\chi$ directly due to the multiple and complicate contents of planted fiber. Take $n$ as example, the planted fiber mainly contains cellulose, hemicellulose and lignin. The degree of polymerization of cellulose ranges from 800 up to 10000 [158]. The hemicellulose are branched polymers of a low weight with a degree of polymerization of 80-200 [159]. Therefore, we discussed the effects of these two parameters on the fiber swelling force when the system of fiber and water achieving equilibrium.

In the equation 3-13, if the fiber contains no solvent, $\lambda_r = 1$, the stress become singular. To avoid this singularity in calculation, we assume that the fiber is already stretched containing a small quantity of water. On the fiber surface, the system of fiber and water approaches a state of equilibrium. The chemical potential of water reaches that of pure water $\mu = 0$. Therefore, we could calculate the radial swelling force as function of radial swelling ratio. Figure 3-14 plots the swelling force of elementary fiber as function of radial stretch.

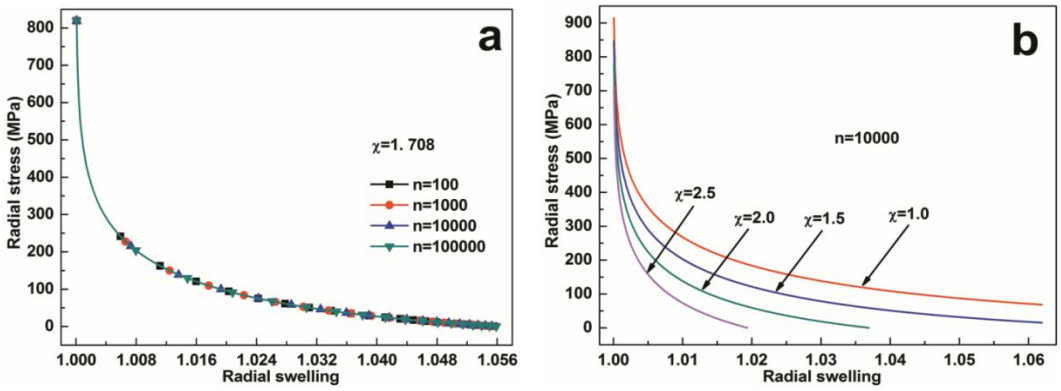


Fig. 3-14 Swelling force of elementary hemp fiber as function of radial stretch: (a), distribution of the number of monomers per polymer chain; (b), distribution of the mixing entropy of water molecule with hemp fiber.

Figure 3-14a shows the effects of numbers of monomers per polymer chain ( $n$ ) on the radial stress. With the increase of $n$ from 100 to 100000, the stress-swelling curves are nearly unchanged. Figure 3-14b plots the distribution of mixture entropy $\chi$. The mixture entropy has distinct effects on the radial stress. With larger mixture entropy value, fiber show lower radial swelling ratio. If we take the value $\chi$ = 1.708, the radial swelling ratio corresponds to the measured swelling ratio (5.6 %) of elementary fiber. The swelling stress is as large as 850 MPa at the beginning, and then decreases as asymptotic curves to zero until achieving the maximum radial swelling ratio.

The treatment of hemp fiber, such as alkali or silane, can decrease the hydrophilicity of hemp fiber. It's indicated that the mixture entropy of fiber with water increased after the alkali treatment. Combining with the results from figure 3-14, with higher mixture entropy, the swelling force decreased much faster, leading to a lower swelling ratio of fiber.

The interfacial adhesion or polymer matrix could limit the swelling of fiber. With the fiber swelling, the matrix or interfacial adhesion produces a constraint force to contend with the swelling force of fiber. The composites will terminate expansion when the swelling force deceases to the magnitude of this constraint force.

The contribution of this constraint force depends on the fiber swelling ratio, the strength of matrix and interfacial adhesion. The larger fiber swelling ratio presents the larger limitation because the swelling force decrease as asymptotic curves to zero at the final swelling process, demonstrating broader range below the constraint stress of matrix or interfacial strength. Besides this, with larger matrix or interfacial adhesion, the swelling force reaches equilibrium earlier with the constraint force.

However, it's difficult to perform the calculation considering the constraint force of matrix or interface for lacking their experimental stress-strain curves at very low strain rate. As presented in figure 3-9, the cross-section of composites only expands 3.5 % for 56 days. In addition, the swelling rate of composites is also variable during all this process.

## *3.3. Thermal ageing of composites*

### 3.3.1. Experiments and analysis

#### *3.3.1.1. Thermal ageing*

Thermal ageing was performed in Atlas suntest XXL for 8 weeks. The ageing condition was: relative humidity 50±5 %, chamber temperature 38±2 °C, no daylight during all the ageing process. The ageing temperature is chosen according to the ISO 4892-2.

#### *3.3.1.2. Tensile tests*

The tensile tests were carried out in a static tension machine Instron 4484 at room temperature with an imposed displacement rate of 2 mm $min^{-1}$. An extensometer with a 12.5 mm initial opening length was placed at the center of specimens to measure the deformation.

### 3.3.2. Tensile test results

The tensile test results of composites C-UF, C-UF-MAH, C-FW and C-FS are shown in figure 3-15 for the purpose of comparing the effects of hemp fiber treatment on the mechanical properties of composites. In figure 3-15a, Young's modulus of composites significantly increased initially (after 2 or 4 weeks) and then decreased, except C-UF-MAH. In figure 3-15b, the fracture stress of all these four composites slightly varied after 8 weeks ageing. The fracture strain decreased initially and then slightly increased with ageing process (Fig. 3-15c).

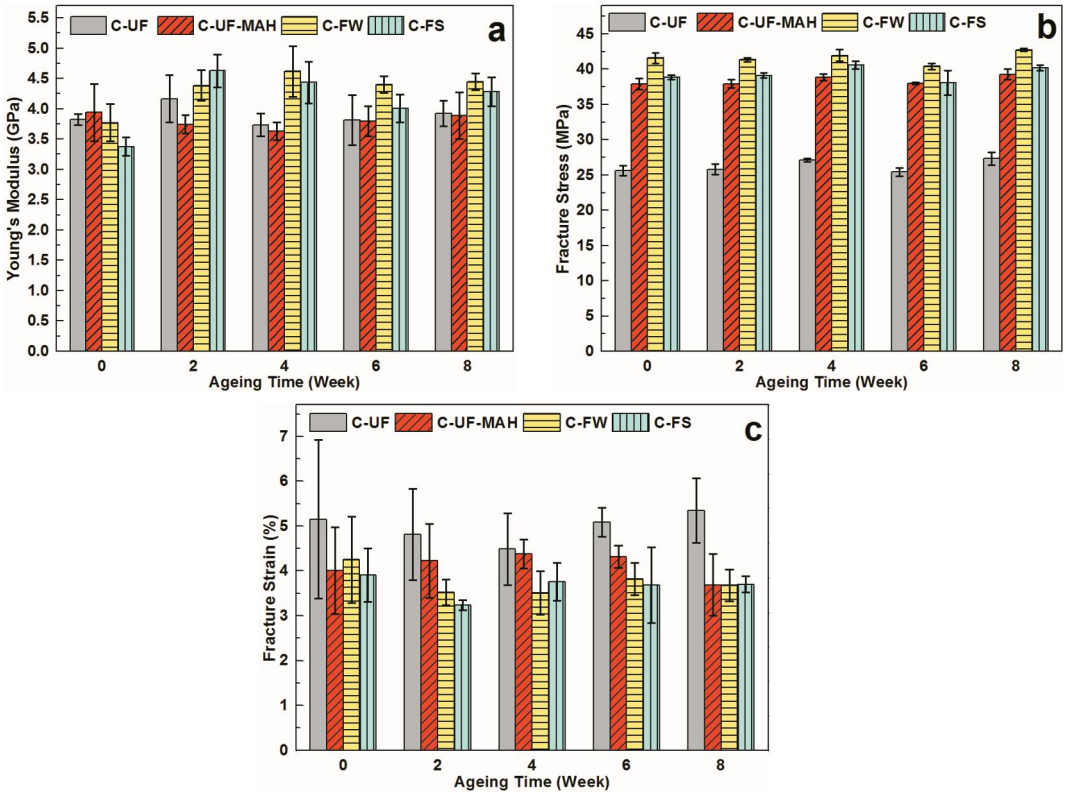


Fig. 3-15 Tensile test results of composites C-UF, C-UF-MAH, C-FW and C-FS: (a), Young's modulus; (b), fracture stress; (c), fracture strain.

The tensile test results of composites reinforced by silane modified fiber (Fig. 3-16) show the same tendency like in figure 3-15. The Young's modulus increased after 2 weeks and then slightly decreased. The fracture stress varies slightly for 8 weeks ageing.

The fracture strain decreased after 2 weeks and then increased a little due to the degradation of composites interface.

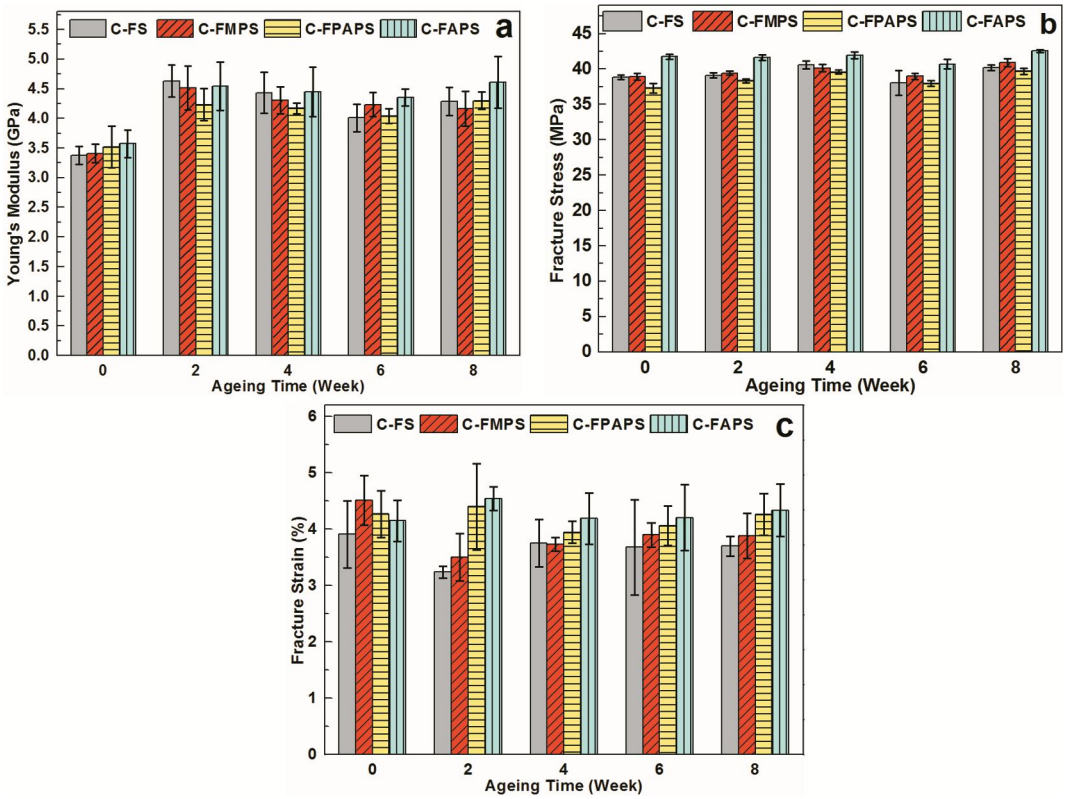


Fig. 3-16 Tensile test results of composites C-FS, C-FMPS, C-FPAPS and C-FAPS: (a), Young's modulus; (b), fracture stress; (c), fracture strain.

These tensile test results after thermal ageing are very similar to that of humidity ageing. As analyzed previously in section 3.1, the water absorption of hemp fiber in composites is one major reason for the increase of Young's modulus in the initial ageing due to enhancement of interfacial pressure. With the penetration of water, the reinforced fiber and interface of composites degraded leading to the fracture stress of composites decreasing and the fracture strain increasing.

However, it's hard to distinguish the effects of temperature with the humidity on the mechanical properties of composites.

By comparing the ageing condition of thermal ageing with humidity ageing in this thesis, the relative humidity decreased from 80±5 to 50±5 %, which may prohibit the

water absorption of composites then retard the deterioration of mechanical properties. However, the ageing temperature increased from 20 to 38 ºC, which may promote the water absorption of composites due to the increased thermal energy for the water molecule penetration. In addition, in the ageing machine, the thermal ageing always performs at a certain relative humidity. Therefore, we couldn't completely eliminate the effect of humidity in thermal ageing. Given this, we separately analyzed the effects of temperature on the PP matrix and hemp fiber in the following paragraph.

The effect of hydrothermal ageing on the neat PP could be neglected. Yuqiu Yang et al. [160] has immersed the neat PP into distilled water at 80 ºC from 3 to 3000 hours, and studied the weight gains and mechanical properties. During all the ageing process, PP absorbed no water and the tensile properties of PP are almost unchanged.

Actually, the effect of temperature on the weight gains of hemp fiber is very negligible [147]. At the relative humidity of 50±5 %, when the ageing temperature increased from 38 to 65 ºC, the weight gains of fiber show almost the same curves as function of ageing time. In contrast, the increase of relative humidity has greater influence on the weight gains of hemp fiber. When the relative humidity increased from 50 to 80 %, the corresponded saturated weight gains increased from 8.5 to 12.0 % after 2 weeks at 20 ºC. Therefore, it's concluded that the increase of temperature doesn't facilitate the water absorption behavior of hemp fiber, but the decrease of relative humidity could reduce water absorption amount of hemp fiber. Therefore, the tensile test results of composites subject to thermal ageing are similar to the humidity ageing but the effect is less remarkable as the humidity ageing.

## *3.4. Conclusions*

The water swelling of hemp fiber can increase the interfacial pressure of composites resulting in the improvement of mechanical properties in the initial periods of humidity ageing. With the process of ageing, the absorbed water causes the degradation of both the interface of fiber/matrix and hemp fiber decreasing the

mechanical properties of composites. The stronger interfacial adhesion of fiber/PP matrix effectively inhibits the water absorption of composites and thus retards the decrease of composite mechanical properties. The addition of PP-g-MAH and water treatment of hemp fiber gives much contribution to the water resistance of composites. However, alkali treatment and silane modification have almost no additional contribution to improve the water resistance of composites.

The fiber achieved saturation with weight gains of 12.5 % and radial swelling ratio of 5.6 %. The fiber swells mainly along the radial direction, which is determined by the microfibrils of cellulose in the fiber network. The presence of PP matrix could retard the water absorption, but fails to decrease the quantity of absorbed water. The composites basically expand in the vertical injection direction due to the fiber distributes along injection direction and swells in the radical direction.

The swelling stress is as large as 850 MPa at the beginning, and then decrease as asymptotic curves to zero until achieving the maximum radial swelling ratio. Comparing with numbers of monomers per polymer chain, the mixture entropy has significant effects on the swelling stress of fiber. With larger mixture entropy value of fiber/water, the fiber swelling force decreased much faster with a lower swelling ratio.

The effect of thermal ageing on the tensile properties of composites is limited. Due to the inertness of PP to the hydrothermal, and the humidity shows more effective than temperature on the water absorption of hemp fiber, the tensile properties of composites subjecting thermal ageing present similar tendencies like humidity ageing but be less affected.

# Chapter 4

# Ultraviolet ageing of the reinforced composites

# Chapter 4. Ultraviolet ageing of the reinforced composites


**4.1. Experiments and characterizations** ..... **95**
**4.1.1. UV ageing** ..... **95**
**4.1.2. Characterization methods** ..... **95**
*4.1.2.1. Scanning electron microscopy (SEM)* ..... *95*
*4.1.2.2. Digital microscopy* ..... *95*
*4.1.2.3. Tensile tests* ..... *95*
*4.1.2.4. Fourier transform infrared spectroscopy (FTIR)* ..... *95*
*4.1.2.5. X-ray diffraction (XRD)* ..... *96*
*4.1.2.6. UV-visible spectra* ..... *96*
**4.2. UV ageing of neat PP** ..... **96**
**4.2.1. Micrographic observation** ..... **96**
**4.2.2. SEM images** ..... **97**
**4.2.3. Tensile test results** ..... **98**
**4.2.4. FTIR spectra** ..... **100**
**4.2.5. XRD patterns** ..... **101**
**4.3. Effects of fiber treatment (water/alkali) on UV ageing** ..... **103**
**4.3.1. Composite photos** ..... **103**
**4.3.2. Micrographic images** ..... **104**
**4.3.3. SEM images** ..... **105**
**4.3.4. Tensile test results** ..... **115**
**4.3.5. Carbonyl index** ..... **117**
**4.3.6. XRD patterns** ..... **118**
**4.3.7. UV/visible spectra** ..... **120**
**4.4. Effects of fiber modification (silane agent) on UV ageing** ..... **121**
**4.4.1. Composites photos** ..... **121**
**4.4.2. Micrographic images** ..... **122**
**4.4.3. SEM images** ..... **123**
**4.4.4. Tensile tests** ..... **128**
**4.4.5. Carbonyl index** ..... **129**
**4.4.6. UV/visible spectra of silane agents** ..... **130**
**4.4.7. XRD patterns** ..... **132**
**4.5. Conclusions** ..... **133**

Besides the humidity ageing, ultraviolet (UV) radiation also has greater influence on the ageing of planted fiber reinforced PP composites. And the UV ageing of planted fiber reinforced polymer composites is much more complex than the degradation of individual fiber or polymer matrix. For example, the chromophoric groups produced from the planted fiber could accelerate the degradation of polymers around the fiber. Conversely, the presence of polymer matrix inhibits the oxygen diffusion and thus retards the photodegradation of planted fiber.

As we known, fiber treatment (water/alkali) or modification (silane agent) has significant influence on the fiber structure and the interfacial adhesion of the reinforced composites. With the decrease of fiber hydrophilicity and the improvement of composites interface, the water absorption of composites can be greatly decreased, which may has great influence on the surface whitening of composites combined with UV radiation [161, 162]. In addition, with better interfacial adhesion, the fiber shows nucleation ability resulting in interfacial crystallization of composites [118, 142]. Moreover, the functional groups of silane could also act as UV stabilizer. For example, the N-[3-(Trimethoxysilyl)propyl]aniline (PAPS) bears a aniline group, showing a broad absorption peak range 245-330 nm.

In this chapter, the UV ageing of neat PP and the PP composites (reinforced fiber treated by water, alkali or silane) were performed. The UV ageing could be considered as a combination of humidity ageing and UV ageing for the presence of relative humidity (50±10 %) and UV radiation. The scanning electron microscopy (SEM), digital microscopy, Fourier transform infrared spectroscopy (FTIR), ultraviolet-visible spectroscopy (UV-Vis) and X-ray diffraction (XRD) are employed for the characterization of composites degradation. UV ageing of neat PP is firstly discussed. Then, the effects of compatibilizer PP-g-MAH and water/alkali treatment of fiber on the UV ageing of the reinforced composites are studied. Finally, the effects of fiber modification by MPS, PAPS and APS on the UV ageing of the reinforced PP composites are investigated.

## *4.1. Experiments and characterizations*

### 4.1.1. UV ageing

UV ageing was performed in Atlas Suntest XXL for 8 weeks, according to the standard ISO 4892-2, method A- Exposures using daylight filters (artificial weathering), cycle 1. The ageing condition are controlled by the following parameter: broadband (300 nm to 400 nm) 60±2 W $m^{-2}$, black-standard temperature 65±3 ºC, relative humidity 50±10 %, chamber temperature 38±3 ºC, 102 minutes dry and 18 minutes water spray.

### 4.1.2. Characterization methods

*4.1.2.1. Scanning electron microscopy (SEM)*

SEM was employed to observe the composites surface. All samples were coated with carbon by a SEM coater CC7650. The images were captured using a Hitachi S3500N.

*4.1.2.2. Digital microscopy*

Visible observations were carried out by a digital microscopy Keyence VHX-1000 with the objective of 20×200.

*4.1.2.3. Tensile tests*

The tensile tests were carried out in a static tension machine Instron 4484 at room temperature with an imposed displacement rate of 2 mm $min^{-1}$ (20 mm·$min^{-1}$ for neat PP). An extensometer with a 12.5 mm initial opening length was placed at the center of specimens to measure the deformation.

*4.1.2.4. Fourier transform infrared spectroscopy (FTIR)*

FTIR measurements were performed at 400-4000 $cm^{-1}$ in PerkinElmer Spectrum Two with the Universal Attenuated Total Reflectance Accessory (UATR). The material

of ATR crystals is diamond. And the penetration depth in the sample is 1.66 μm, indicated by the operation manual of PerkinElmer.

*4.1.2.5. X-ray diffraction (XRD)*

X-ray diffraction (XRD) measurements were conducted with a Seifert PTS-3000 X-ray diffractometer employing Cu-Kα (0.1540598 nm) radiation and Ni filter, equipped with a Position Sensitive Detector. The XRD patterns were collected from 15 to 60 º (2θ) with a step size of 0.05 º.

*4.1.2.6. UV-visible spectra*

The Cary 100 UV-VIS was employed to characterize the UV-visible absorbance of silane agent solution (5.0 %), PP and C-FS film at 200-800 nm. The PP and C-FS film were prepared in a hot-press machine at 185 °C.

## *4.2. UV ageing of neat PP*

### 4.2.1. Micrographic observation

Figure 4-1 illustrates the micrographic photos of neat PP after 8 weeks UV ageing. From figure 4-1, it's observed that numerous cracks appear on PP surface and the direction of these cracks is almost perpendicular to the flow-line (injection direction). The spontaneous cracking of PP is ascribed to the surface densification caused by chemical crystallizations. The patterns and concentration of these cracks generally depend on the processing method and conditions. Regular cracks are often observed perpendicular to the flow-line in injection moulding samples [163]. Whereas in compression PP, the cracks showed random patterns due to no significant flow occurs in compression process [164, 165]. In additional, lower values of A110 (the chain orientation of PP) resulted in lower crack frequency. The molded PP displays more degradation than compressed one due to higher oxygen diffusion resulted from its lower degree of crystallinity [164].

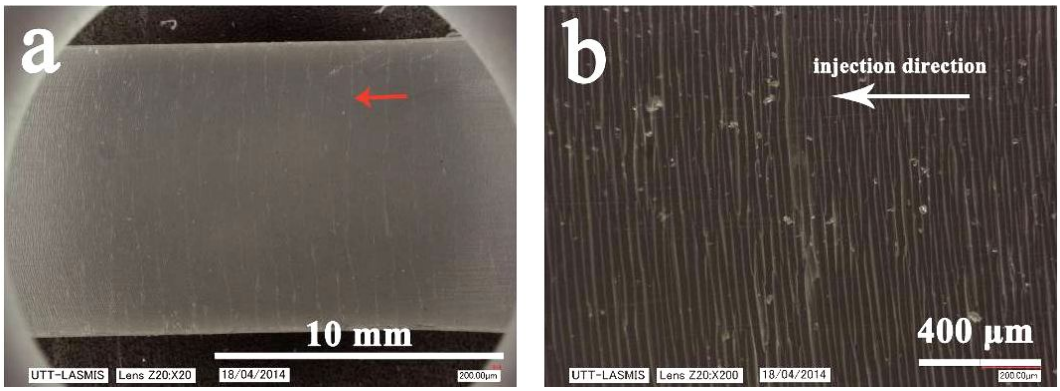


Fig. 4-1 Microscopy photos of neat PP after 8 weeks UV ageing, (a), X 20; (b), X 200.

The cracks direction plays an important role in the mechanical properties of PP. The cracks in perpendicular direction of flow-line have considerable effects on tensile test at the initial process of UV ageing. And the effects of cracks in parallels direction could be negligible [166].

### 4.2.2. SEM images

Figure 4-2 shows the development of cracks on PP surface after UV radiation. Even though after 2 weeks, there are no obvious cracks on PP surface (Fig. 4-2a). While after 4 weeks (Fig. 4-2b), numerous cracks on PP surface are clearly observed. With the process of chemical crystallization, the spontaneous cracks well developed. From figure 4-2c and d, it's found the distance between cracks is significantly increased (indicated by white arrow). The surface cracking is preferential to the photo-oxidation of PP by providing a pathway for the oxygen diffusing deeper into the interior of PP [164].

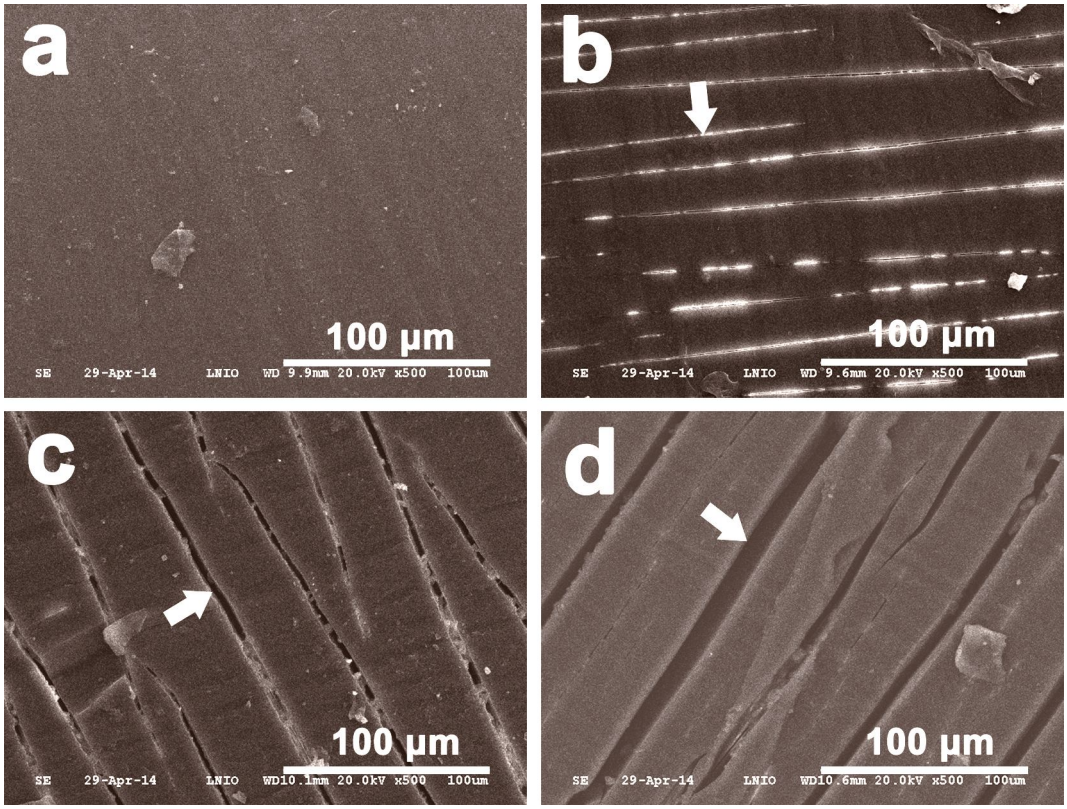


Fig. 4-2 Development of cracks on PP surface during UV ageing: (a), 2 weeks; (b), 4 weeks; (c), 6 weeks; (d), 8 weeks.

The photo-oxidized PP is often concentrated in a thin layer on the surface. For homopolymer PP, the thickness of this layer is 500 µm at utmost [167]. The increase of oxidized layer in thickness is mainly dominated by the pseudo period in PP degradation. And at the end of this period, the cracks shortly formed. Before the appearance of cracks, the thickness of oxidized layer increases with ageing temperature and nearly independent of the light intensity [168].

The development of cracks could be prevented by a ductile zone. M.S. Rabello observed a ductile zone inside the embrittled layer in the fracture surface of PP, which could resist the penetration of cracks reaching the ductile materials in the interior [164].

### 4.2.3. Tensile test results

The tensile test results of PP are shown in figure 4-3. In figure 4-3a and 4-3b, the Young's modulus and fracture stress respectively increased of 10.1 and 42.9 % after 6

weeks UV ageing, and then sharply decreased after 8 weeks. The enhancements of Young's modulus and fracture stress are resulted from the increase of the crystallinity when PP exposed under UV radiation. Owing to the chains scission, the produced small molecules in amorphous phase easily transfer to crystalline phase leading to the degree of crystallinity increase.

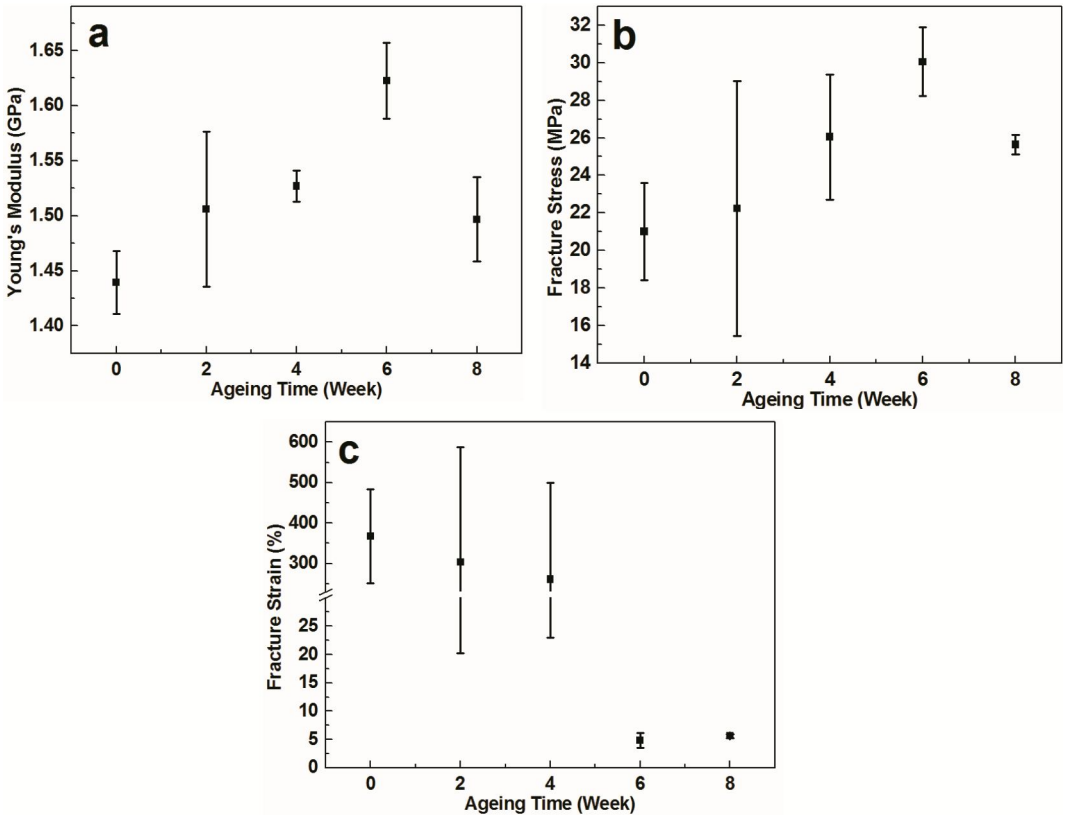


Fig. 4-3 Tensile test results of PP subject up to 8 weeks UV ageing: (a), Young's modulus; (b), Fracture stress; (c), Fracture strain.

The decrease of Young's modulus and fracture stress should be ascribed to the surface cracking and the small independent crystallites produced by chemical crystallization. These two reasons play its role in different period of UV ageing. To separate the influence of surface cracking and chemical ageing on the Young's modulus, Iryna Yakimets et al. [166] utilized the linear elastic fracture mechanics and found that the effects of surface cracking on PP mechanical properties occurs in the period of 5 days to 3 weeks. But in the followed period (3-5 weeks), the small

independent crystallites produced by chemical-crystallization are essentially responsible for the loss of mechanical properties.

As a result of UV ageing, the embitterment of PP leads to the sharply drop of fracture strain (Fig. 4-3c). After 6 weeks, the fracture strain of PP is remarkably reduced from 367.3 to 5.6 %. UV ageing resulted in PP presenting more fragile behavior than ductile behavior.

Besides the surface cracking and crystallites, the loading force could also accelerate or retard the chain scission of PP caused by UV radiation. The tensile stress could accelerate the chain scission due to which favors the diffusion of small radicals, inhibits the nucleation and the growth of micro cracks. To the contrary, the compressive stress retards the chain scission [169].

### 4.2.4. FTIR spectra

Figure 4-4a presents the FTIR spectra of PP before and after up to 8 weeks ageing. In figure 4-4a, a broad absorbance peak at 1700-1800 $cm^{-1}$ has developed with the UV radiation. This peak is usually associated with the presence of carbonyl groups due to the photo-oxidation of PP. In addition, the peak of hydroperoxides, another main production of PP degradation [170], can be also easily observed in the wavelength range of 3300-3600 $cm^{-1}$.

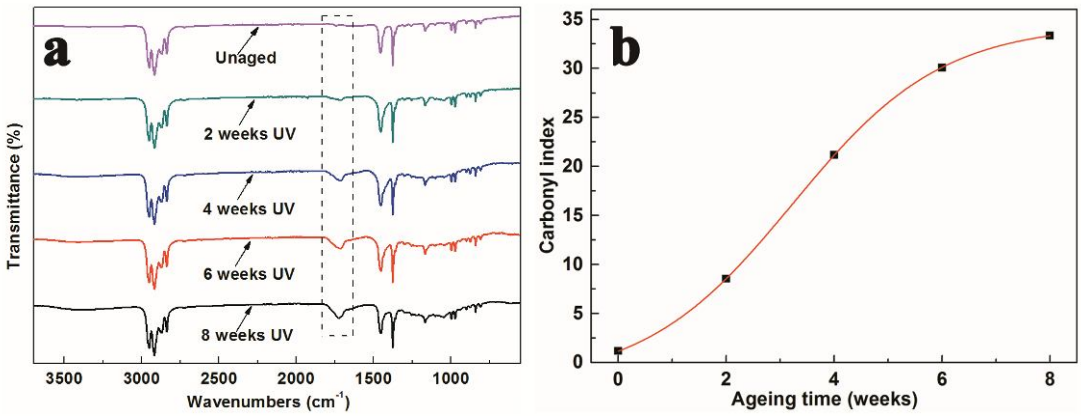


Fig. 4-4 FTIR spectra of PP before and after up to 8 weeks UV ageing: (a), FTIR spectra; (b), Carbonyl index.

The carbonyl index of PP is shown in figure 4-4b. Carbonyl index is taken as the relative areas under the carbonyl peak and a reference peak. To avoid the influence of the degradation and crystallinity of PP, the peak at 2720 $cm^{-1}$ was chosen as the reference peak, which is associated with CH bending and $CH_3$ stretching [164]. In figure 4-4b, the carbonyl index increases progressively from around 0 up to a plateau region of almost 33. Carbonyl index also distributes along the depth of PP sample. The carbonyl index decreases sharply from surface to core. And with the increase of radiation time, it shows a decrease of sequence steps (Fig. 4-5) [168].

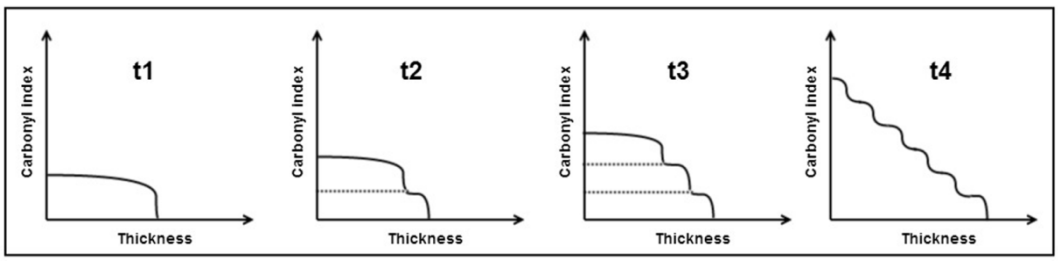


Fig. 4-5 Schematization of the mechanism of oxidized layer growth in the case of auto-accelerated oxidation, times of radiation: t1 < t2 < t3 < t4 [168].

### 4.2.5. XRD patterns

Figure 4-6 shows that the position of the diffraction peak of PP remains the same after UV ageing, however, the height of peak and the amorphous background is varied.

The height of most crystalline peaks increased after 8 weeks ageing signifying the enhancement of crystallinity. The UV degradation of PP is believed to be concentrated in the amorphous region of PP. With UV ageing, the macromolecules of PP break to smaller molecules which allow crystallization easier [166]. Hence, the UV ageing generally accompanied with an enhancement of crystallinity. In addition, L. OGLER reported that the crystallinity increases progressively from the depth to surface [171].

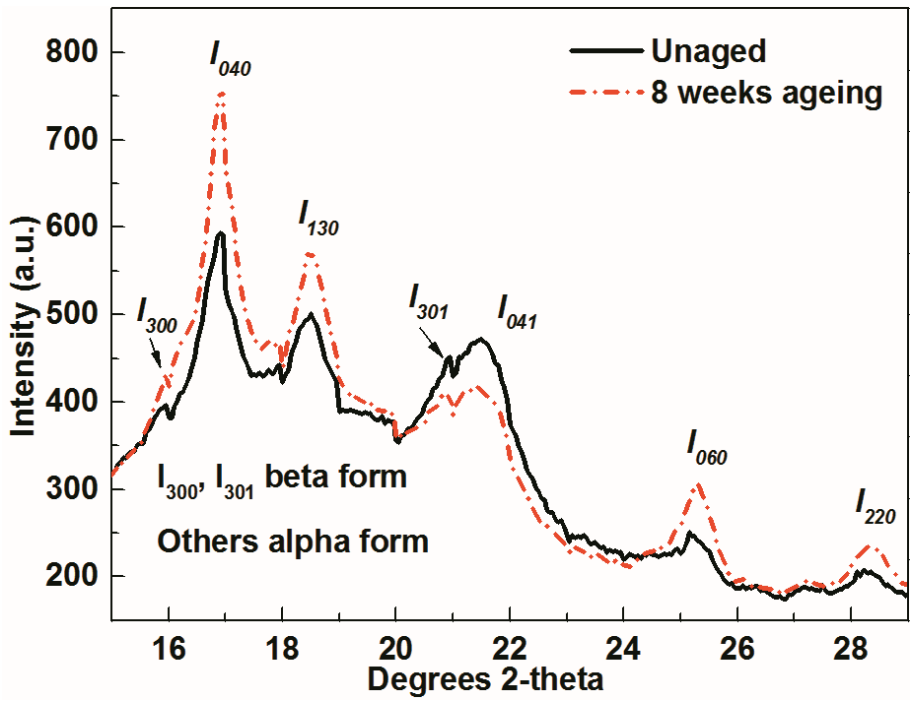


Fig. 4-6 XRD patterns of PP without and after 8 weeks UV ageing.

While, in figure4-6, the diffraction intensity and the full width at half maximum of plane (301) and (041) decreased after ageing. The decrease of full width at half maximum is not correlated with the decrease of average crystalline size but with the formation of new small crystallites [163].

The initial fraction of crystallinity also affects the polymer degradation. Polymers with higher crystallinity generally display less degradation before a longer exposure time (12 weeks or longer). The fraction of crystallinity could be affected by processing condition. For example, when the molded temperature increased from 20 to 60 ºC, the crystallinity increased from 41.3 to 58.2 % [164].

## *4.3. Effects of fiber treatment (water/alkali) on UV ageing*

### 4.3.1. Composite observations

Figure 4-7 displays the photos of composites C-UF, C-UF-MAH, C-FW and C-FS subject UV ageing from 2 to 8 weeks. In figure 4-7, with UV radiation, the color of all these four composites changed from brown to white. The surface whitening is mainly ascribed to the chemicrystalisation of PP matrix. However, these four composites show different whitening rate. For example, after 2 weeks, C-UF appearances larger "white" area than C-UF-MAH. And there are almost absent of "white" on the surface of C-FS. After 4 weeks, the whiteness of composites could be ranged as: C-UF > C-UF-MAH > C-FW > C-FS. After 8 weeks, the surface of all these four composites is nearly completely white. For further observation, the digital microscopy and SEM are performed in the following section.

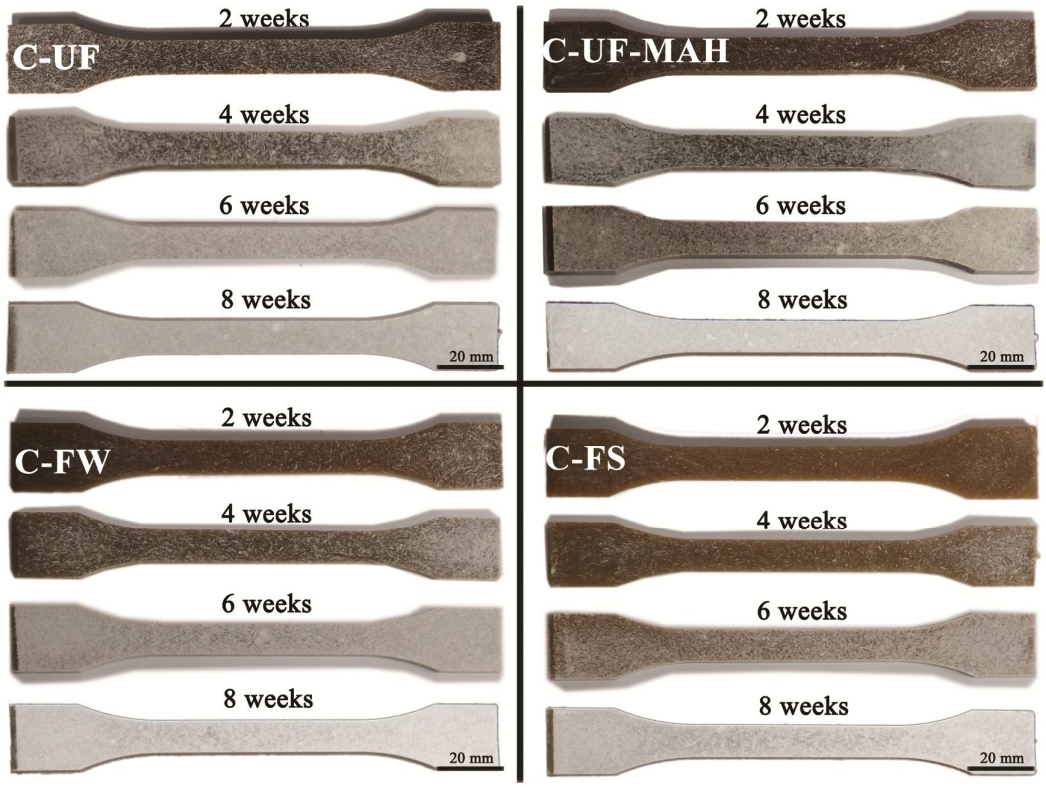


Fig. 4-7 Photos of composites C-UF, C-UF-MAH, C-FW and C-FS subject UV ageing from 2 to 8 weeks.

### 4.3.2. Micrographic images

Figure 4-8 shows the micrographic images of specimens' surface of composites C-UF, C-UF-MAH, C-FW and C-FS subject UV radiation from 2 to 8 weeks. From figure 4-8, it's confirmed that C-UF shows faster but C-FS shows lower whitening rate. In figure 4-8, it's also found that the color of chalky white occurs initially (2 weeks) around the location of fiber (black arrow). It seems that the presence of planted fiber accelerated the degradation of PP around the fiber. It's known that the crystallization of PP could decrease its transparency under UV radiation. Beside this, Nicole M. Stark [172] reported that water spray has great effects on composites whitening when combined with UV radiation.

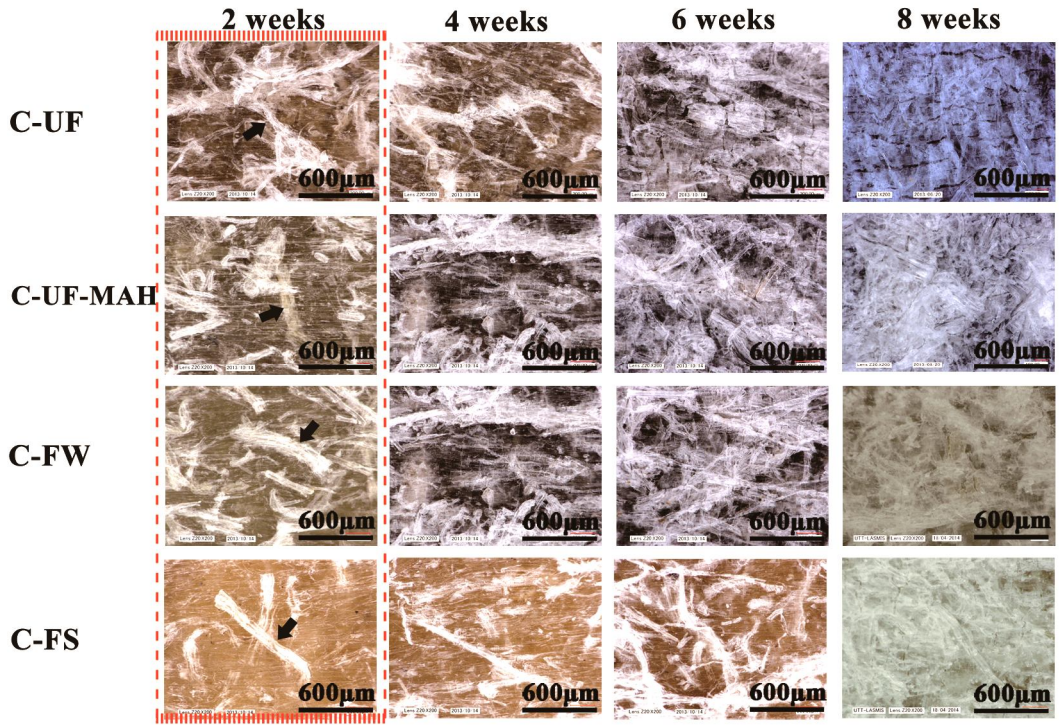


Fig. 4-8 Micrographic images of specimens' surface of composites C-UF, C-UF-MAH, C-FW and C-FS subject UV radiation from 2 to 8 weeks.

### 4.3.3. SEM images

Figure 4-9~12 present the SEM micrographs of composites C-UF, C-UF-MAH, C-FW and C-FS subjected from 2 to 8 weeks UV ageing. In figure 4-9~12, all the composites were presented respectively by a low magnification for "macro" observation and an intermediates magnification to observe the exposed hemp fiber, PP matrix around the fiber and the interfacial state of fiber/matrix.

In figure 4-9a, after 2 weeks UV ageing, the surface of C-UF displays many defects. It's also found that some fibers are already exposed to air, which may be resulted from the degraded PP flakes or powders and which have been washed away by water spray. In figure4-9b, the interface of hemp/PP matrix has degraded and the fiber is completely exposed to air (Fig. 4-9b). This observation is not surprised because the interfacial strength of C-UF is very poor before exposure due to the incompatibility of

fiber and PP matrix. After 4 weeks, it's clearly observed that there are regulation cracks in PP matrix (indicated by white ellipse, Fig. 4-9d). After 6 weeks, the composites surface is approximately fractured in all surface regions (Fig. 4-9e and g). The cracks around the fiber are also gradually developed and smashed to many small flakes (Fig. 4-9f and h).

The development of cracks in composites is similar to that in the neat PP. Nevertheless, the surface cracking occurs earlier in composites (2 weeks) than in PP (4 weeks). The formation of cracks is normally ascribed to the densification of chemicrystalisation and the chain scission of PP. Besides this reason, due to the absorption of water, a swelling force of fiber should also contribute to the surface cracking.

Interestingly, the cracks only present in PP matrix and around the fiber. It's difficult to find the similar cracks on the fiber during the ageing process. One reason should be that the lignin in hemp fiber could absorb 85-90 % of lights. Another reason should be that the covered PP matrix plays as a "protection coating" by preventing the oxygen diffusing into fiber.

From figure 4-10~12, the degradation process of composites C-UF-MAH, C-FW and C-FS is similar like that of C-UF. Besides this, it is observed that the degradation rate of fiber/matrix and PP matrix in C-UF-MAH, C-FW and C-FS is much less than C-UF.

When comparing C-UF (Fig. 4-9a) and C-UF-MAH (Fig. 4-10a), it has been found that the fractured area of C-UF-MAH is smaller than that of C-UF. Moreover, even though after 4 weeks ageing, most regions of the interface of C-UF-MAH still well connected (Fig. 4-10d). However, after 2 weeks radiation, the interface of C-UF is degraded completely. It's because that the addition of PP-g-MAH could significantly improve the interfacial strength of fiber/matrix. The distance between cracks in C-UF-MAH (Fig. 4-10g, h) is also much less than in C-UF (Fig. 4-9g, h) after 8 weeks

ageing. Therefore, it's indicated that the improvement of interfacial strength could retard the formation and growth of cracks in composites surface and the degradation of composite interface in the initial exposure time (especially for 2 weeks).

The water or alkali treatment of fiber could further retard the degradation of composites. Especially for C-FS, composites reinforced with alkali treated fiber, the surface after 6 weeks UV radiation (Fig. 4-12e, f) displays similar fracture pattern like C-UF after 2 weeks ageing. This result agrees well with the digital observation in figure 4-8.

Overall, the improvement of fiber/PP interfacial strength is beneficial to retard the composites surface degradation. In addition, the water/alkali treatment of fiber, especially alkali, could further inhibit the surface degradation.

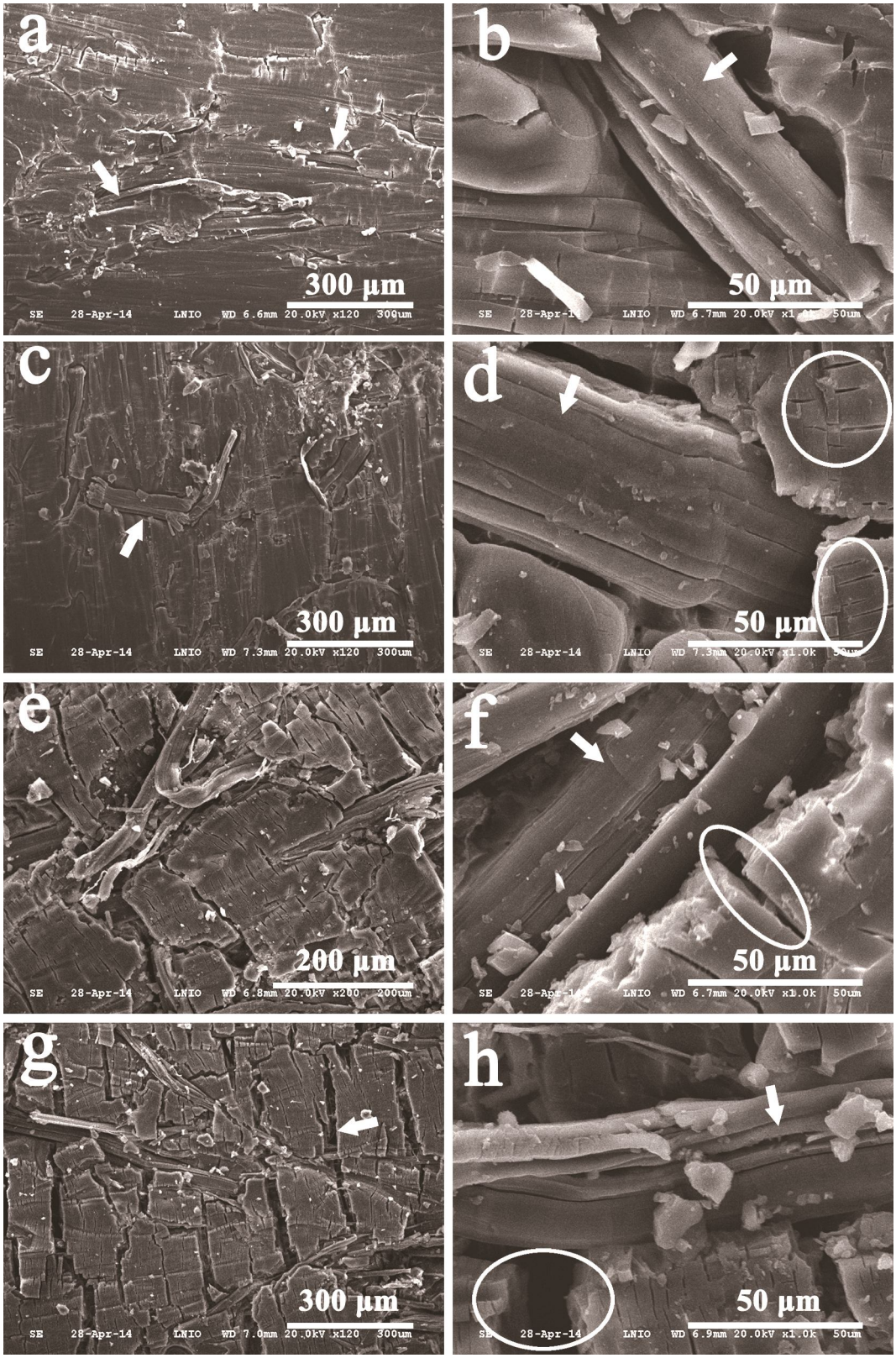


Fig. 4-9 SEM images of C-UF surface subject in different UV ageing time: (a, b), 2 weeks; (c, d), 4 weeks; (e, f), 6 weeks; (g, h), 8 weeks.

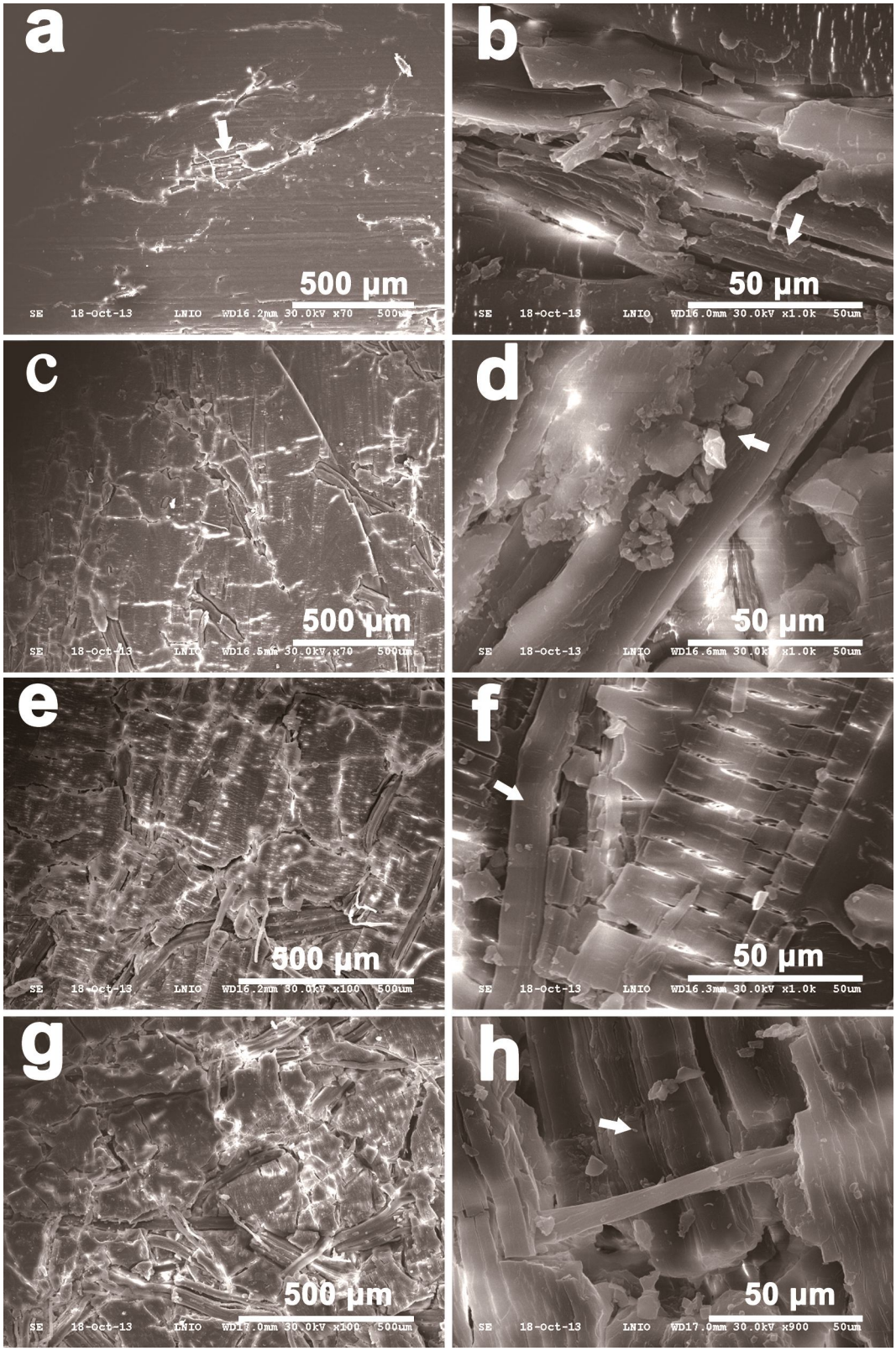


Fig. 4-10 SEM images of C-UF-MAH surface subject in different UV ageing time: (a, b), 2 weeks; (c, d), 4 weeks; (e, f), 6 weeks; (g, h), 8 weeks.

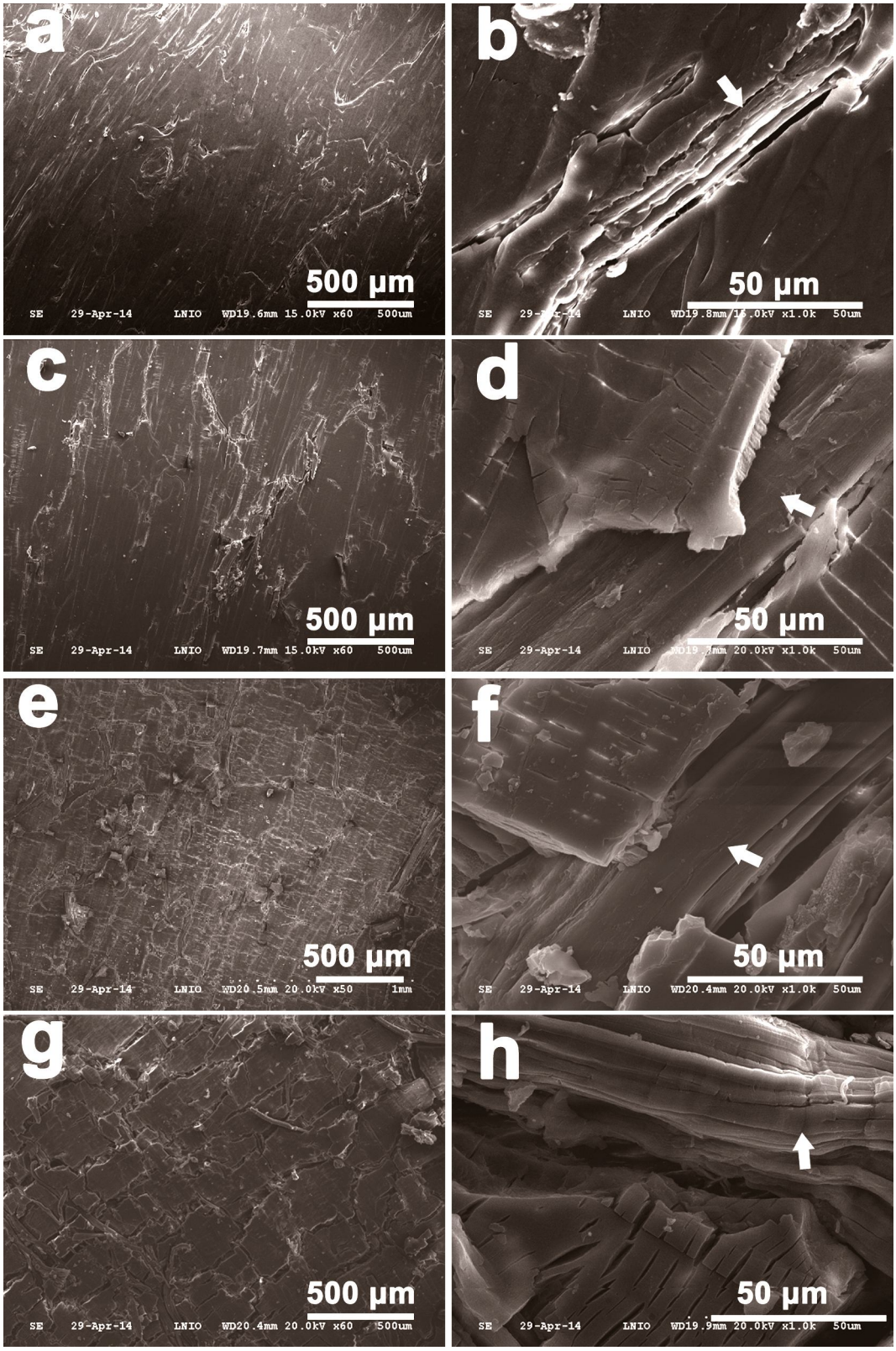


Fig. 4-11 SEM images of C-FW surface subject in different UV ageing time: (a, b), 2 weeks; (c, d), 4 weeks; (e, f), 6 weeks; (g, h), 8 weeks.

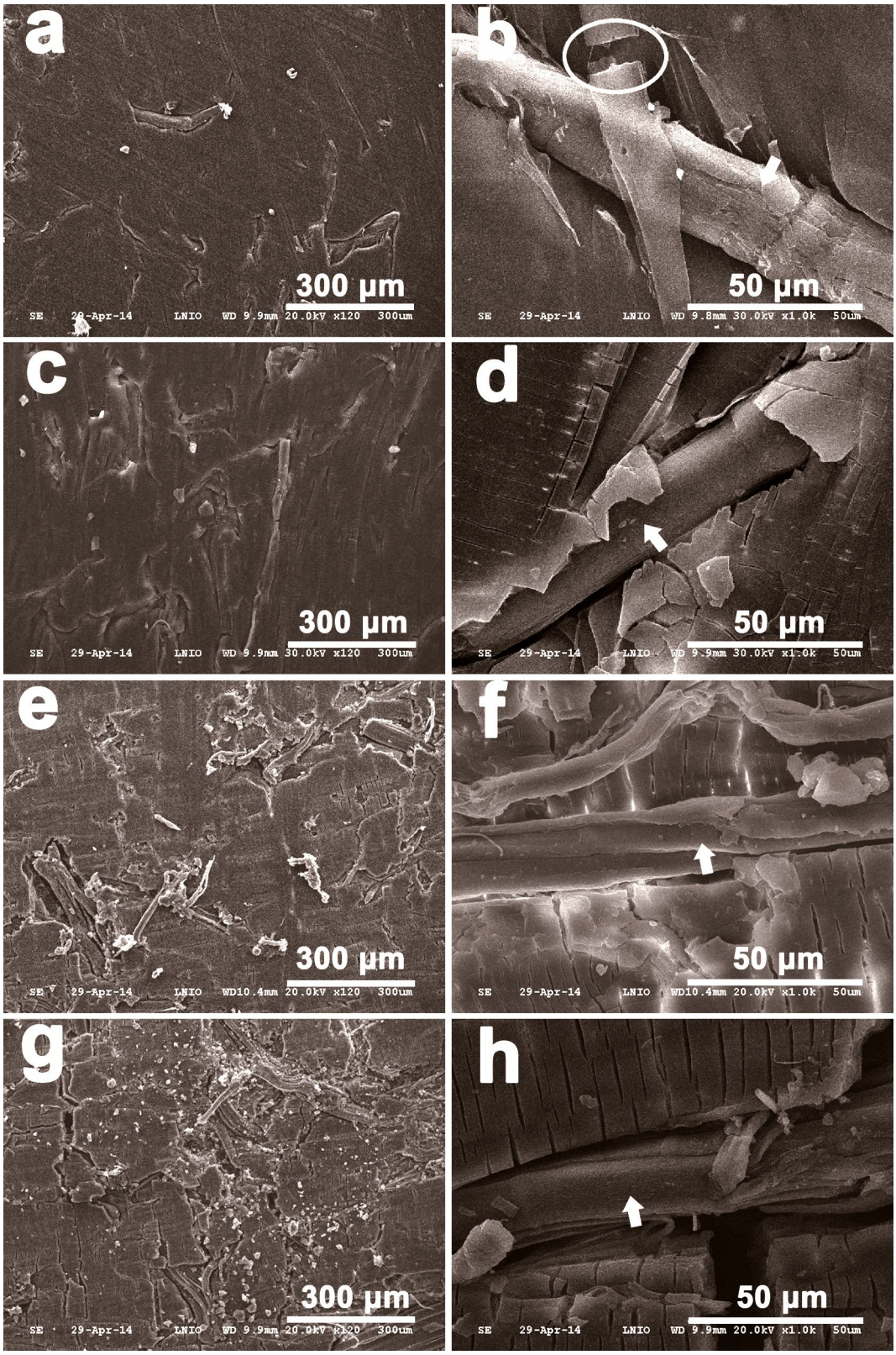


Fig. 4-12 SEM images of C-FS surface subject in different UV ageing time: (a, b), 2 weeks; (c, d), 4 weeks; (e, f), 6 weeks; (g, h), 8 weeks.

Figure 4-13 shows that the degradation of composites firstly occurred around the location of fiber. In other regions, there are no obvious cracks, which are similar to the surface of neat PP after 2 weeks (Fig. 4-2a). This result matches well with our observation in figure 4-8 (micrography images) that the color of chalky white appears initially around the location of fiber.

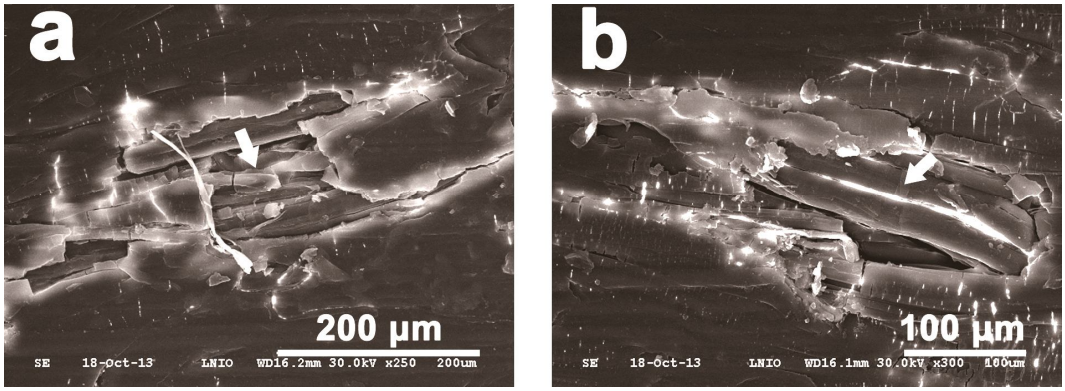


Fig. 4-13 Cracks concentrated around the fiber, C-UF-MAH after 2 weeks UV ageing.

Given to the fact, lignin, as one main constituent of hemp fiber, absorbs stronger in UV/visible region due to the two chromophores groups [116, 173]. And the lignin is normally presented in the fiber surface covering the cellulose microfibrils [43]. Thus, it's suggested that the PP matrix around the hemp fiber may absorb more radiation than other regions. Moreover, the degradation of hemp fiber will generate additional chromophoric groups and promote the degradation of PP [170]. The water swelling of hemp fiber and the absorbed water may also contribute to the degradation of PP around the fiber due to the accelerated oxidation reaction, which facilitated the light penetration and generated swelling force toward the PP matrix [172]. Therefore, it's believed that the degradation of PP occurs initially around the locations of fiber. In other words, the presences of hemp fiber accelerate the photo-degradation of PP. Besides these reasons, the rough surface of composites due to the addition of hemp fiber should also contribute to PP cracking via providing sites for preferential photo-oxidation.

As presented in figure 4-14, the composites surface is not smooth like the neat PP. It's clearly observed that numerous patterns formed on the composites surface. It can be explained that, during the moulding process, the flowability of PP varied considerably due to the addition of hemp fibers. The rough surface of composites also promotes the surface cracking or degradation of PP.

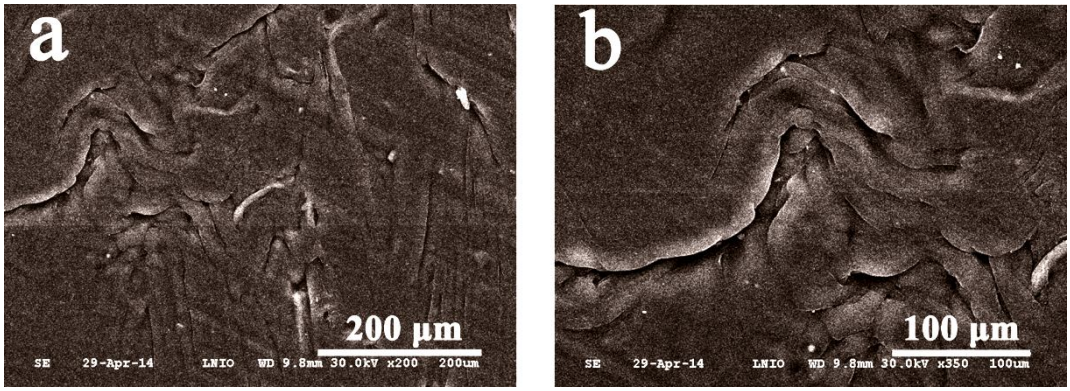


Fig. 4-14 Surface morphology of composites C-FS subjects 2 weeks UV radiation.

Figure 4-15 presents the crack locations in the initial UV ageing (2 weeks). On the composites surface, the cracks could occur in the "smooth" region (indicated by white elliptic in Fig. 4-15a) and in the protruding edges (Fig. 4-15b, c and d). L. Ogier et al. [171] reported that the machine marks (rough surface) provides sites for preferential photo-oxidation in PP leading to the formation of flaws that weaken the PP at low exposure time. And this influence could be reduced by polishing away the machine marks prior to UV exposure or prolonging the exposure time.

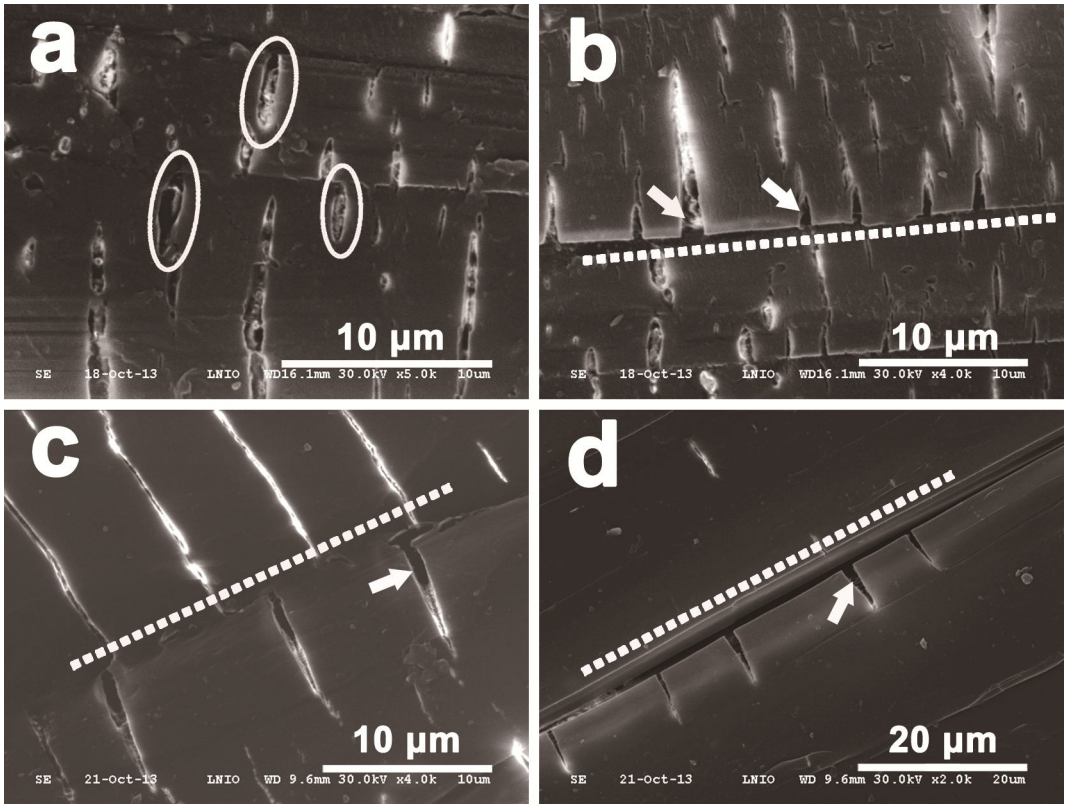


Fig. 4-15 Surface cracks of composites (a, b), C-UF-MAH; and (c, d), C-FAPS after 2 weeks UV ageing.

The cracks in PP surface and in the composites surface are compared in figure 4-16. With the absence of obstacle (hemp fiber), the PP surface degraded uniformly and the cracks could develop more easily. As a result, these cracks are generally straight and longer (Fig. 4-16a). While on the composite surface, owing to the PP around hemp fiber degraded with a relatively faster rate than the PP in other region (without the fiber), the cracks are much shorter than that on neat PP (Fig. 4-16b). Therefore, the neat PP shows uniform UV degradation but the planted fiber reinforced composites show non-uniform UV degradation in the initial UV ageing.

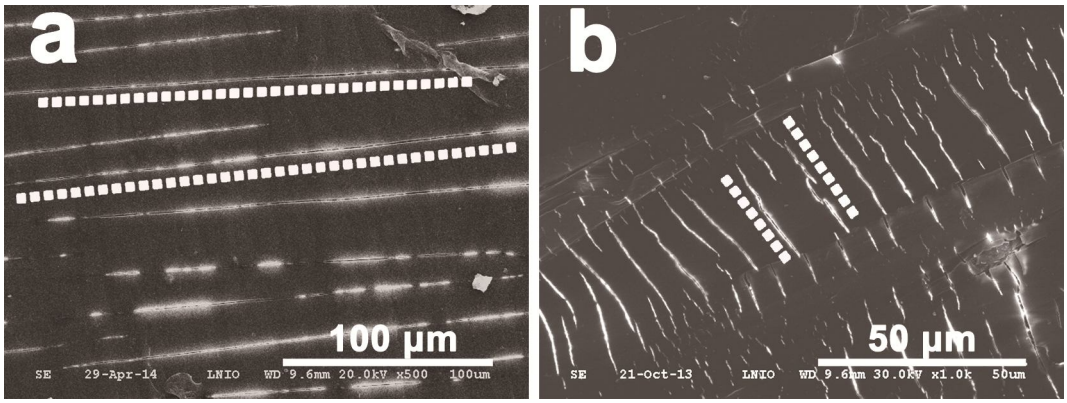


Fig. 4-16 Surface cracks of (a) PP after 4 weeks and (b) C-FAPS after 2 weeks.

### 4.3.4. Tensile test results

Figure 4-17 shows the tensile test results of composites C-UF, C-UF-MAH, C-FW and C-FS subjected to UV ageing up to 8 weeks. From figure 4-17a, we can see that the Young's modulus increased initially and then decreased with UV ageing. For C-UF and C-UF-MAH, the Young's modulus increased respectively of 17.4 and 18.9 % after 4 weeks. And after 8 weeks, it decreased to almost the level before ageing. For C-FW, Young's modulus increased of 14.3 % after 4 weeks and stayed in this level until 8 weeks. C-FS shows the maximum increase of Young's modulus (24.8 % for 2 weeks). Even though for 8 weeks ageing, it also increased of 14.0 % when compared with the unexposed value. One reason for the enhancement of Young's modulus may be the increase of crystallinity. Another reason may be the increase of interfacial pressure due to the fiber swelling, such as we analyzed in humidity ageing (section 3.1.2.1).

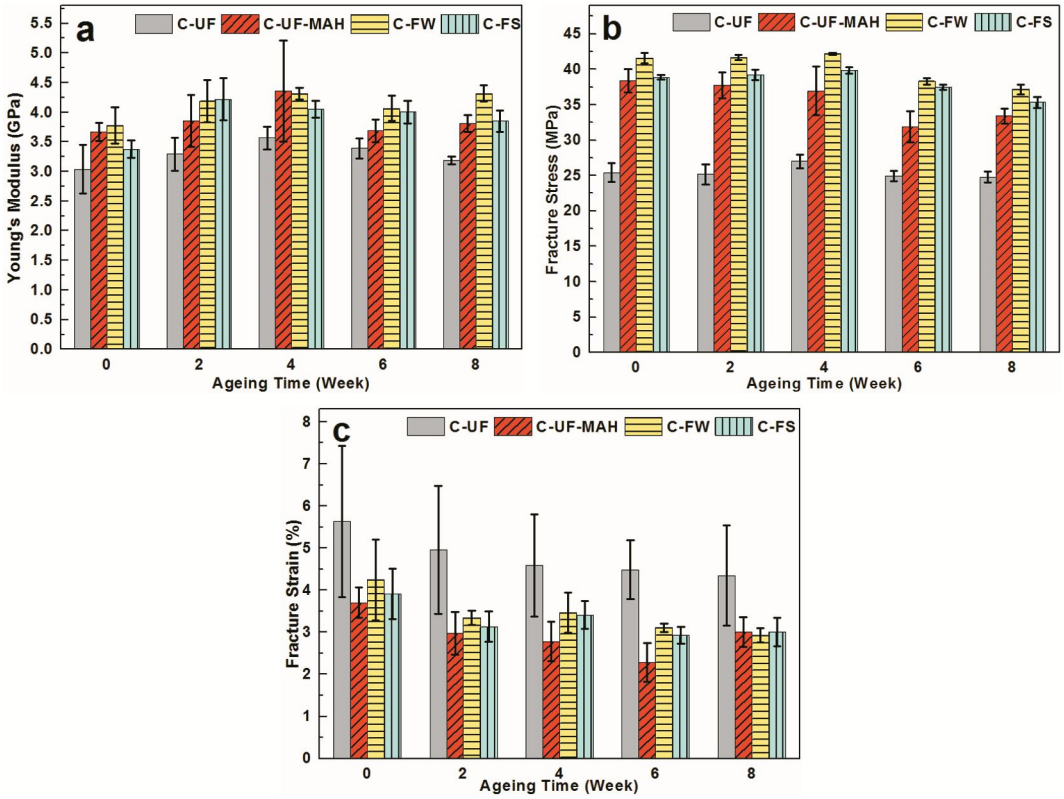


Fig. 4-17 Mechanical properties of composites C-UF, C-UF-MAH, C-FW and C-FS subject UV ageing: (a), Young's modulus; (b), Fracture stress; (c), Fracture strain.

In figure 4-17b, all these four composites display a progressively decrease of fracture stress with the UV ageing except C-UF, which nearly unchanged after 8 weeks ageing. While the fracture stress of C-UF-MAH, C-FW and C-FS decreased respectively of 13.0, 10.6 and 9.1 % after 8 weeks. When comparing the decrease of C-UF and C-UF-MAH, it is found that the degradation of fiber/matrix interface is one major reason for the decline of tensile properties.

In figure 4-17c, after 8 weeks, C-FW shows the greatest deterioration of fracture strain namely 31.2 % in these four composites. For other composites, their fracture strain decreased of 22.8 % (C-UF), 18.8 % (C-UF-MAH) and 23.0 % (FS), respectively.

Overall, the addition of PP-g-MAH and the fiber treatment of water/alkali didn't give obvious contribution to resist the decrease of tensile properties.

In the surface morphological analysis (section 4.3.1~3), the surface of C-UF shows the gravest damages in these four composites and its surface become white faster than others. Only for 2 weeks, the fiber is entirely exposed to air and debonded with PP matrix. But its tensile properties didn't show the greatest decrease. Thus, the surface degradation of composites isn't adequate to indicate the greatest deterioration of tensile properties.

### 4.3.5. Carbonyl index

The carbonyl index is generally employed to characterize the chain scission of the polymer and the composites. In figure 4-18, the carbonyl index of C-FW and C-FS nearly share the same tendency during all UV ageing. While the carbonyl index of C-UF-MAH increases more rapid than C-FW and C-FS but finally reaches the same level with them. It can be explained like that the containing of polysaccharide on the surface of untreated fiber may easily degrade producing more carbonyl groups and further facilitating the degradation of PP to form carbonyl groups.

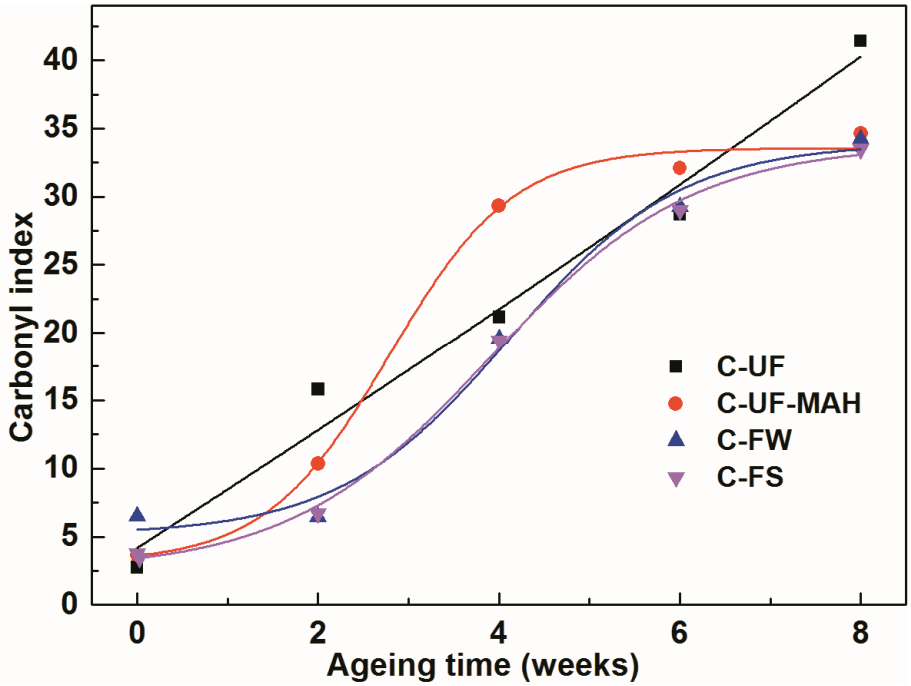


Fig. 4-18 Carbonyl index of composites C-UF, C-UF-MAH, C-FW and C-FS subject up to 8 weeks UV ageing.

It's also found that the carbonyl index of C-UF is much higher than that of other composites for 8 weeks. From the surface morphology analysis (section 4.3.3, Fig. 4-9), the cracks in C-UF surface are formed earlier and the distance of cracks is wider than C-UF-MAH, C-FW and C-FS after 8 weeks ageing. Hence, the oxygen could penetrate deeper than other three composites leading to much serious degradation.

Therefore, it seems that the water or alkali treatment of hemp fiber is favorable in retarding the surface whitening (cracking) and degradation of the reinforced composites.

### 4.3.6. XRD patterns

XRD is normally utilized to characterize the crystallization of polymer composites. From figure 4-19, it's obviously seen that the main difference of the height of crystalline peaks occurring at $2\theta$ = 16.9 ° and 18.5 ° (indicated by dotted elliptic). After 8 weeks UV ageing, the height of these two peaks shows different increase in these four composites. For C-UF, it is found that the height of peaks at 25.3, 28.4 ° are

also significantly increased (Fig. 4-19a). However, it's difficult to conclude that the crystallinity of C-UF increased because the height of amorphous phase of PP matrix in valley near $2\theta = 20$ º (indicated by black arrow) increased at the same time. In contrary, it's clearly observed that the degree of crystallinity increased in composites C-UF-MAH and C-FW (Fig. 4-19 b and c). In addition, the increase of the former one is much larger than the later one.

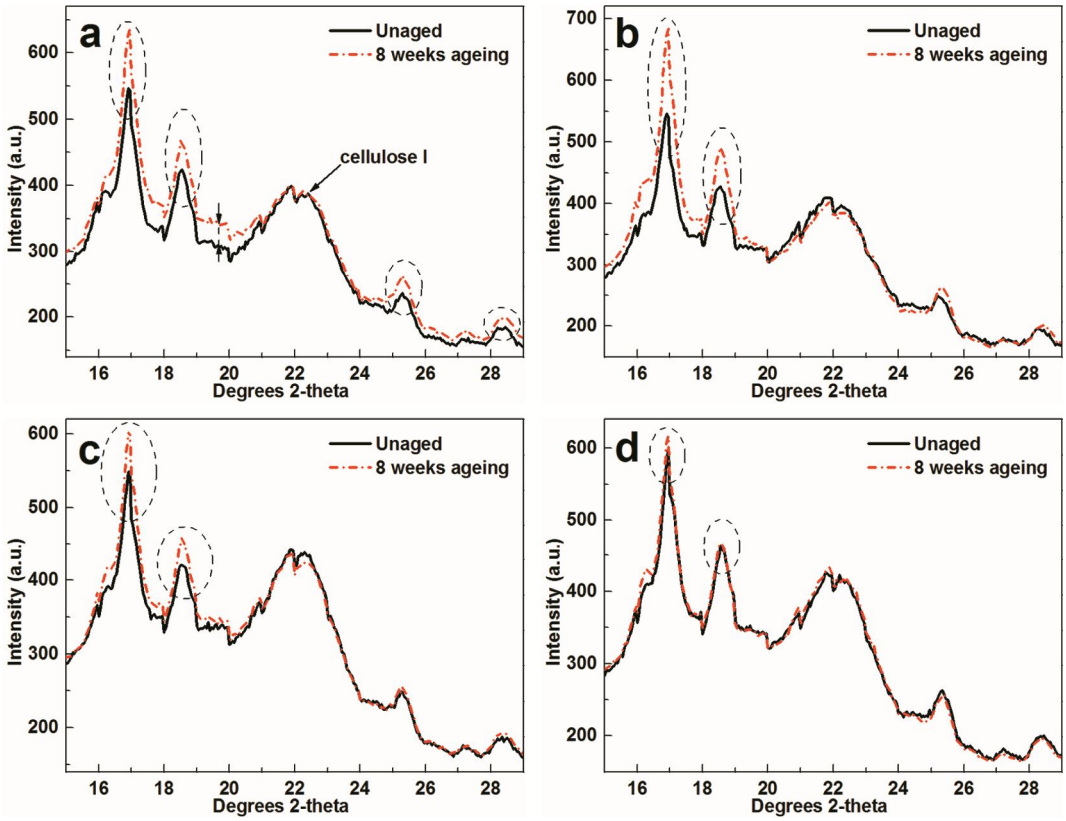


Fig. 4-19 XRD patterns of composites before and after 8 weeks UV ageing: (a), C-UF; (b), C-UF-MAH; (c), C-FW; (d), C-FS.

Indeed, the degree of crystallinity is found to increase through chemicrystalisation, which is caused by the rearrangement of the amorphous segments into crystalline phase during the degradation of PP by chain scission [174]. This result illustrates the composites C-UF-MAH shows greater increase of crystallinity than C-FW. Interestingly, the XRD pattern of C-FS was almost unchanged after 8 weeks ageing signifying UV radiation has less effect on the crystallinity of C-FS than that of C-FW

and C-UF-MAH. But it doesn't mean that the UV radiation has no influence in the C-FS. In fact, the X-ray penetrated depth in polymer is almost 885 μm or larger [139]. But the photo-oxidized of composites is concentrated in a thin layer on the sample surface. Thus, the X-ray penetrated depth may be much larger than the photo-oxidized layer and can cover up the effect of composites degradation. Another explanation may be that the C-FS has a higher degree of crystallinity before UV radiation. As a result, there are few amorphous remained in composites for chemicrystalisation.

In figure 4-19c, the height of crystalline peak of cellulose I slightly decreased. This may be ascribed to the degradation of cellulose. M.S. Islam [174] also found the crystallinity of cellulose peak decreases in aged composites upon accelerated UV ageing.

### 4.3.7. UV/visible spectra

The UV/visible spectra of PP film (thickness, 0.08 mm) and C-FS films (with the thickness from 0.10 to 0.18 mm) are shown in figure 4-20. In figure4-20, the absorption range of neat PP is mainly below 250 nm. While the absorption range of composites is broader than that of neat PP. To the composites C-FS, the larger thickness, the composites film shows stronger absorbance. When the thickness increased to 0.18 mm, the absorbance achieved the maximum in the wavelength of 200 nm. It's suggested the UV radiation couldn't penetrate deeper into the composites interior above this thickness. Therefore, the presence of hemp fiber enhanced the UV absorption and played as a "shield", preventing the penetration of UV radiation into the deep region of composites. And likely neat PP, the UV degradation of composites is concentrated in a thin layer on the surface.

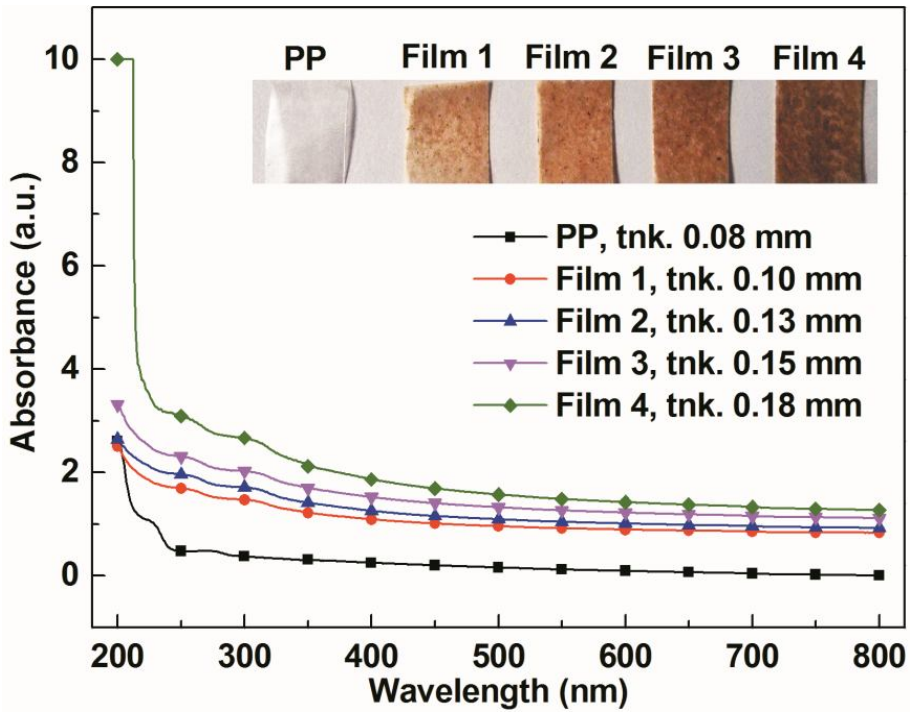


Fig. 4-20 UV/visible spectra of PP film and C-FS films. The photos of these films are inserted in this figure.

## *4.4. Effects of fiber modification (silane agent) on UV ageing*

### 4.4.1. Composite photos

In figure 4-21, specimens' photos of C-FS (without silane modification) are presented here as reference. From figure 4-21, it's observed the surface whitening of C-FMPS is very similar to that of C-FS. While, the great differences are observed in C-FPAPS and C-FAPS aged for 4 and 6 weeks. It's clearly observed that the surface of C-FPAPS shows much faster but C-FAPS shows lower whitening rate than C-FS. By comparing C-FPAPS and C-FAPS after 4 weeks UV ageing, the most surface are of the former one becomes white; while, the later one is still brown. Especially after 6 weeks ageing, most surface area of C-FS, C-FMPS and C-PAPS becomes white except C-FAPS.

Besides this, the color of C-FPAPS displays slightly darker than other composites reinforced by alkali treated fiber. The reason should be that the reinforcing fiber

F-PAPS contains more polysaccharide or hemicellulose than other alkali treated fiber. These contents degraded or carbonated during the extrusion and injection process of composites leading to the similar darkness of the C-FPAPS as that of the composites reinforced with untreated fiber or water treated fiber.

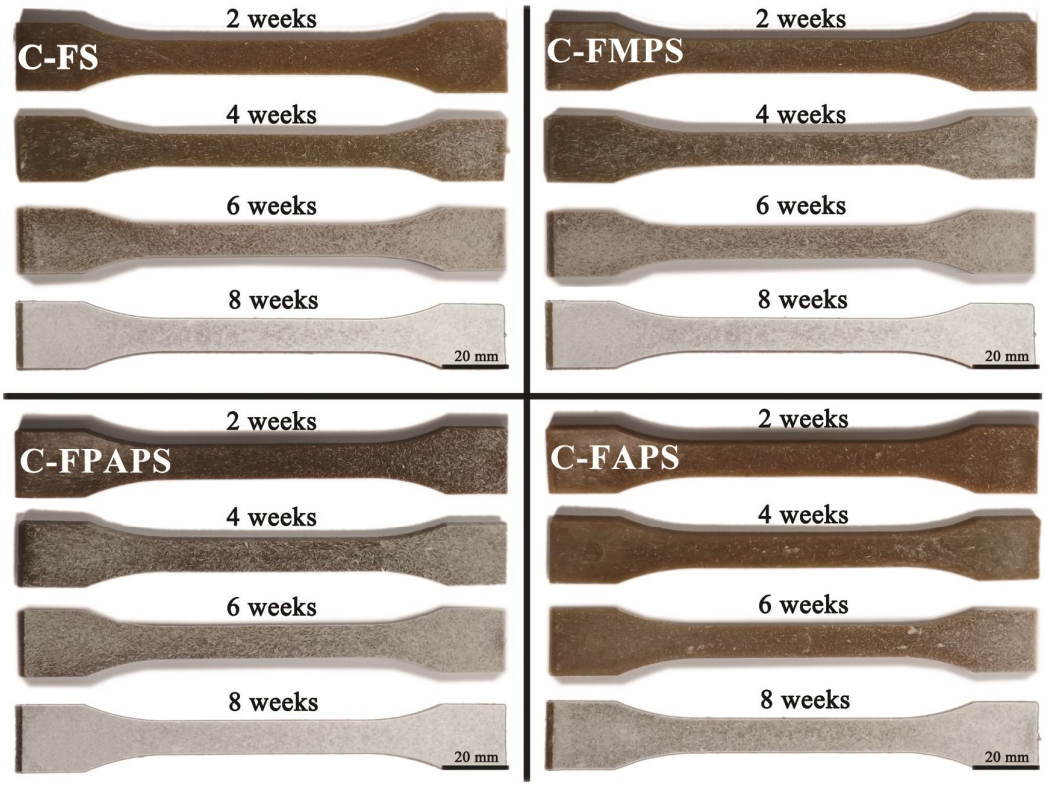


Fig. 4-21 Specimens' photos of composites C-FS, C-FMPS, C-FPAPS and C-FAPS, exposure from 2 to 8 weeks UV ageing.

### 4.4.2. Micrographic images

From figure 4-22, it's also found that the whiteness is initially concentrated around the location of fiber. This result is similar to what we observed in figure 4-8, the presence of hemp fiber accelerated the degradation of PP matrix around it. In addition, the images of C-FPAPS and C-FAPS exposed for 4 and 6 weeks (indicated by dotted frame) confirm that C-FPAPS shows much faster but C-FAPS shows lower whitening rate as we observed in figure 4-21.

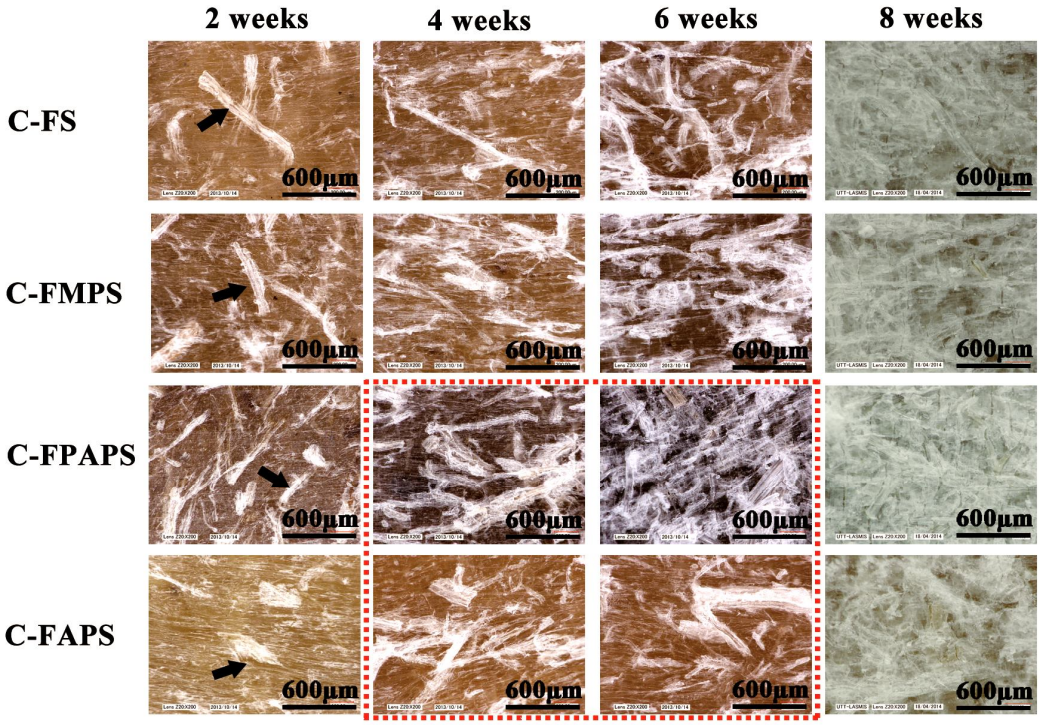


Fig. 4-22 Microscopy images (magnified by 200 times) of composites C-FS, C-FMPS, C-FPAPS and C-FAPS, exposure from 2 to 8 weeks UV ageing.

### 4.4.3. SEM images

Figure 4-23~25 present the SEM micrographs of C-FMPS, C-FPAPS and C-FAPS exposed under UV radiation from 2 to 8 weeks. It's observed similar results as we obtained in figure 4-9~12. Under UV radiation, the cracks spontaneously occur on the surface of composites caused by chemicalcrystallization of PP. With the development of cracks and chain scission, the PP degrades to flakes and powders, which are easily washed away by water spray leading to the fiber exposed to air. The reinforcing fiber accelerated this process by reflection, swelling force and radical groups formed by fiber degradation.

Moreover, it's also found that the surface of C-FPAPS (Fig. 4-23e) is cracking much greater but C-FAPS (Fig. 4-24e) is much lighter than the C-FMPS (Fig. 4-22e). Combining with our observation in figure 4-21, it's indicated that the white regions in

digital photos are related to the surface cracks, larger whiting areas signifying greater cracks. However, for C-FPAPS, it's difficult to conclude that this greater cracking is caused by silane agent of PAPS. Because the more residual polysaccharide or hemicellulose in the reinforcing fiber F-PAPS may also accelerates the cracking of PP. To the contrary, the silane agent of APS seems to be beneficial for retarding the cracking due to it can react with the maleic anhydride grafted in PP forming a stronger interfacial adhesion. With better compatibility of fiber and polymer matrix, the fiber shows nucleation ability and results in interfacial crystallization [118, 142]. The crystalline location may play an important role in the cracking of the composites. From the surface morphology analysis, the C-FMPS shows nearly the same surface whitening or cracking like C-FS. It's indicated that the influence of MPS modification of fiber on the surface cracking could be neglected.

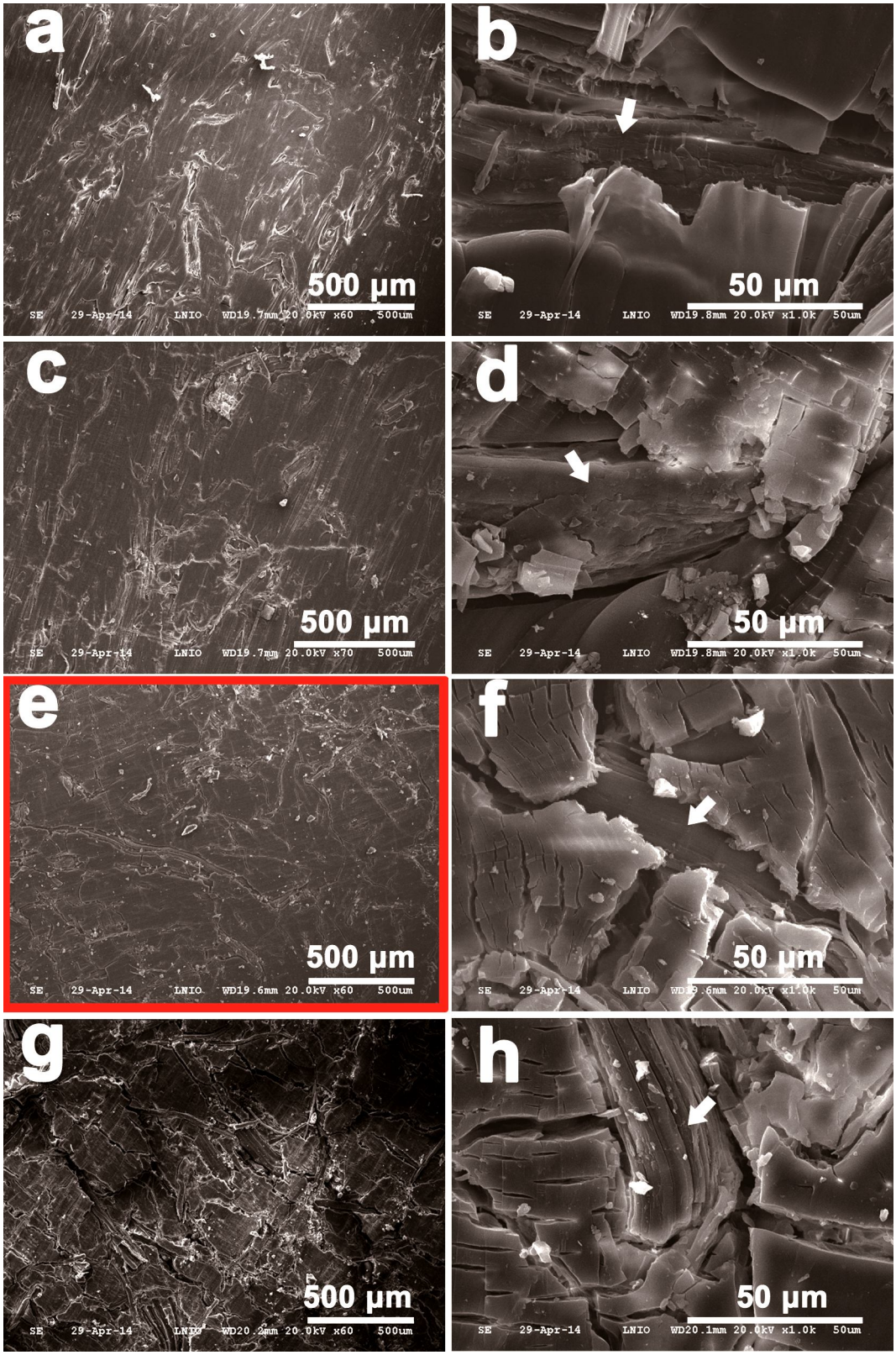


Fig. 4-23 SEM images of C-FMPS surface subject in different UV ageing time: (a, b), 2 weeks; (c, d), 4 weeks; (e, f), 6 weeks; (g, h), 8 weeks.

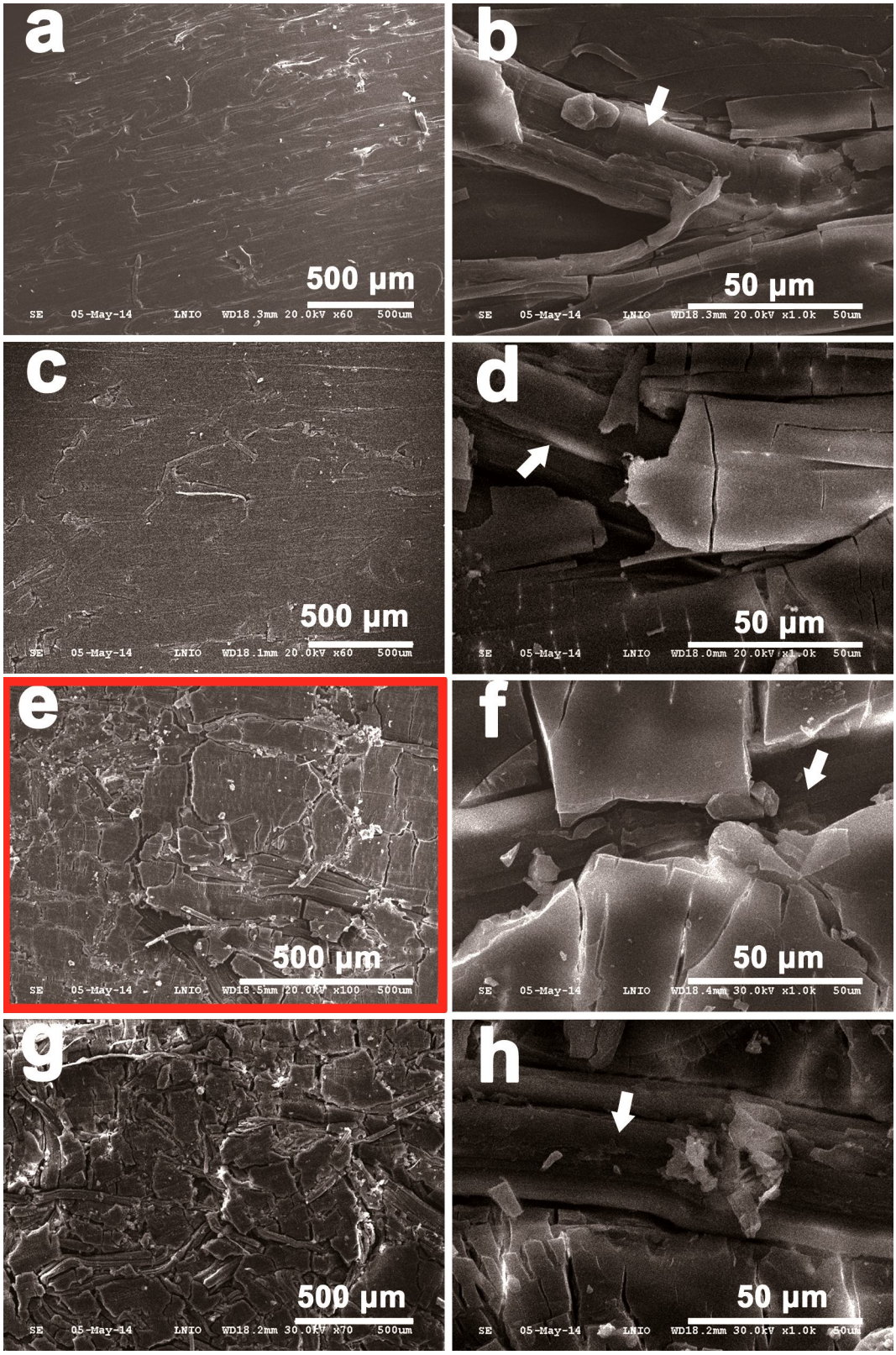


Fig. 4-24 SEM images of C-FPAPS surface subject in different UV ageing time: (a, b), 2 weeks; (c, d), 4 weeks; (e, f), 6 weeks; (g, h), 8 weeks.

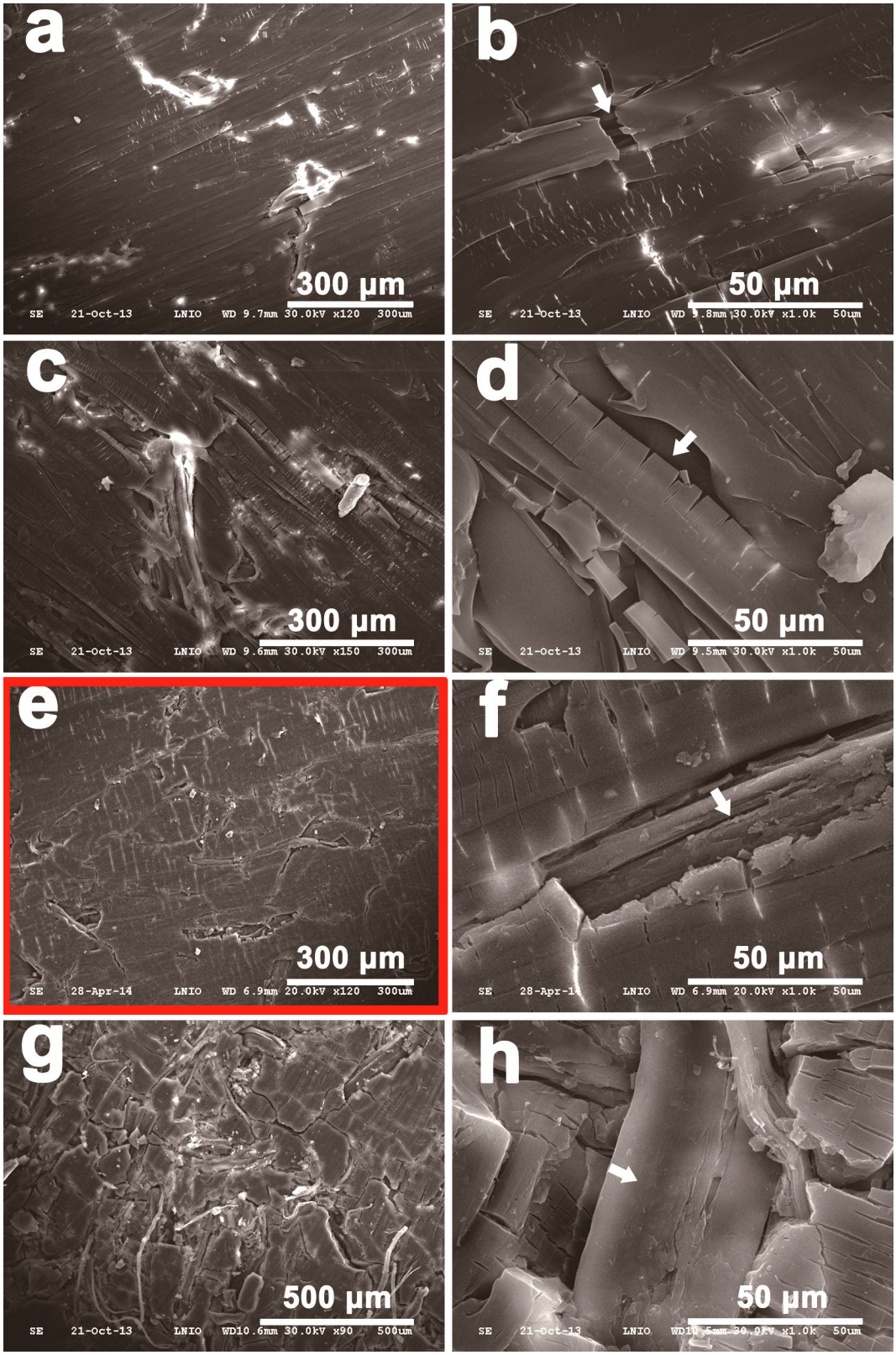


Fig. 4-25 SEM images of C-FAPS surface subject in different UV ageing time: (a, b), 2 weeks; (c, d), 4 weeks; (e, f), 6 weeks; (g, h), 8 weeks.

### 4.4.4. Tensile tests

Figure 4-26 presents the tensile test results of composites C-FS, C-FMPS, C-FPAPS and C-FAPS after UV ageing. From figure 4-26a, we can see the Young's modulus increased initially and then decreased with UV ageing. C-FS achieved the maximum increase of 24.8 % for 2 weeks; while, after 4 weeks, the C-FMPS, C-FPAPS and C-FAPS reached their maximum increase of 21.8 %, 22.1 % and 15.2 %, respectively. It's found C-FAPS shows the lowest increase in these four composites.

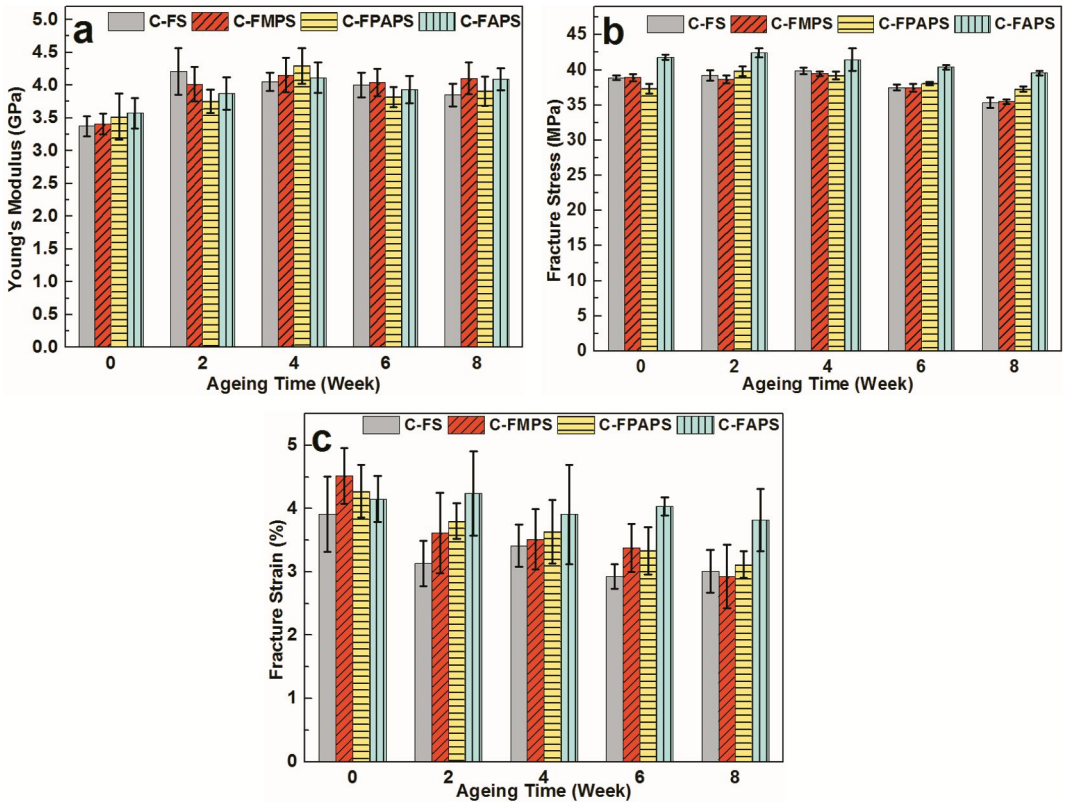


Fig. 4-26 Mechanical properties of composites C-FS, C-FMPS, C-FPAPS and C-FAPS subject up to 8 weeks UV ageing: (a) Young's modulus; (b) Fracture stress; (c) Fracture strains.

The fracture stress of composites is shown in figure 4-26b. After 8 weeks, the fracture stress of C-FAPS decreased of 5.3 %, which is lower than the decrease of C-FS (9.1 %) and C-FMPS (8.8 %). Interestingly, the fracture stress of C-FPAPS increased of 6.8 % after 2 weeks. And then after 8 weeks, it decreased to nearly the value before

ageing. It seems that PAPS acts as an antioxidant. Once it has been consumed, the mechanical properties of composites begin to decline.

Figure 4-26c presents the fracture strain of composites. The fracture strain of composites decreased dramatically except that of C-FAPS. After 8 weeks, the fracture strain of C-FMPS shows greatly decreased of 35.2 %, which is much more than the decrease of C-FS (23.0 %) and C-FPAPS (27.1 %). However, C-FAPS exhibits the lowest decrease of 8.0 %.

Based on these tensile test results, the treatment of fiber by different silane agent has considerable influences on the mechanical properties of PP composites in UV ageing. Overall, C-FMPS shows the greatest decrease of fracture strain of 35.2 % after 8 weeks ageing. The fracture stress of C-FPAPS varied slightly compared with the unaged one after 8 weeks ageing. And C-FAPS exhibits the least influence than other three composites by UV radiation, which is also confirmed by the surface whitening in figure 4-21. In order to elucidate the specific mechanism, further characterizations of composites have been conducted.

### 4.4.5. Carbonyl index

In figure 4-27, the carbonyl index of composites increase from around 2 up to a plateau region of almost 33. C-FS and C-FMPS follow almost the same tendency. While, after 4 weeks ageing, C-FPAPS presents higher carbonyl index than other composites. C-FAPS exhibits the lowest carbonyl index in both 4 and 6 weeks. These results match very well with the visible observations in figure 4-20 and 21. It confirms that the surface of C-FPAPS degraded greater than that of other three composites for 4 weeks, but C-FAPS degraded much less for both 4 and 6 weeks.

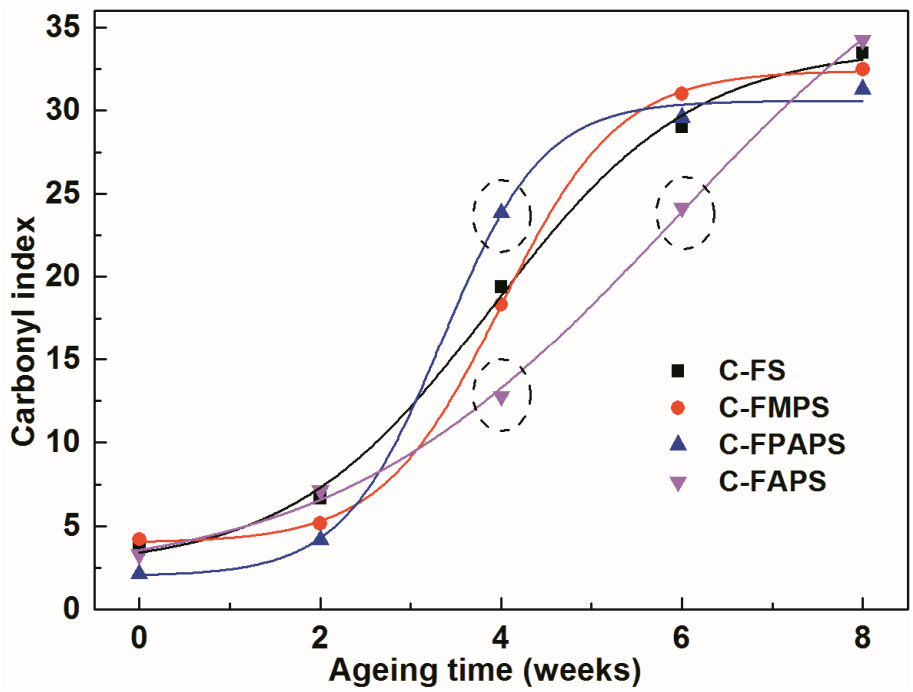


Fig. 4-27 Carbonyl index of C-FS, C-FMPS, C-FPAPS and C-FAPS exposed up to 8 weeks UV ageing.

### 4.4.6. UV/visible spectra of silane agents

Figure 4-28 shows the UV/visible spectra of silane agents MPS, PAPS and APS in a concentration of 5 %. In figure 4-28, PAPS shows a broad absorption peaks range of 245-330 nm. This peak corresponds to the $\pi$-$\pi^*$ transition of benzenoid ring in the aniline monomer of PAPS. Therefore, the PAPS, on fiber surface of C-FPAPS, could absorb most of the UV radiation and thus inhibits the interface degradation of fiber/PP. This could partly explain that the fracture stress of C-FPAPS nearly unchanged after 8 weeks UV weathering even more degradation occurred on its surface layer than other composites.

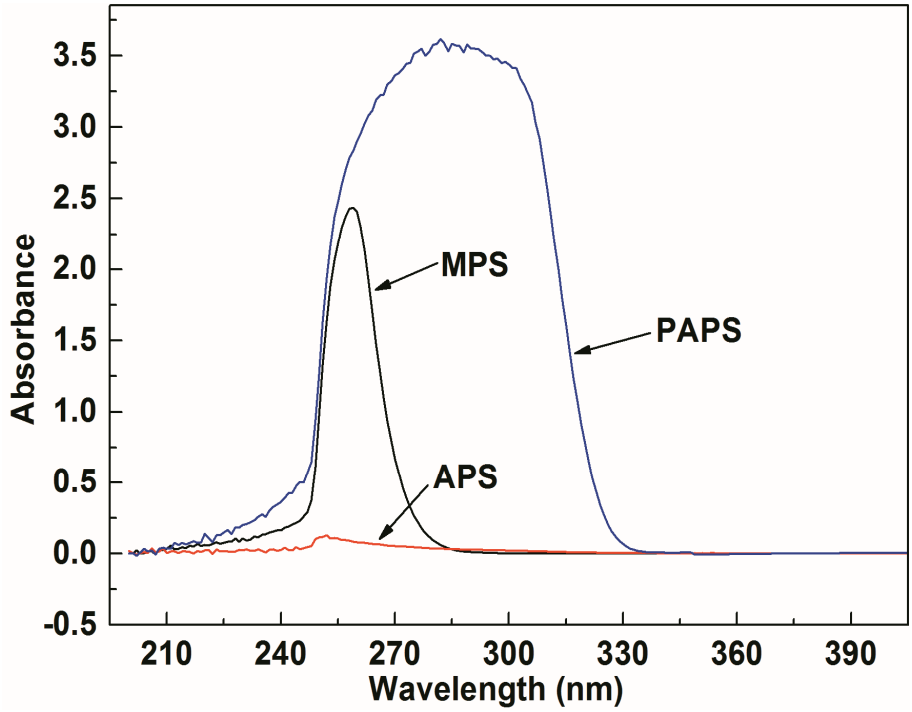


Fig. 4-28 UV/visible spectra of silane agents MPS, PAPS and APS in a concentration of 5 %.

In figure 4-28, the APS shows a small absorption peak of UV radiation. With our previous analysis, the primary amino -$NH_2$ of APS can react with the maleic anhydride, which can be grated onto PP to form a succinimide groups in C-FAPS [175]. Because of this stronger strength of interfacial adhesion, the mechanical properties of C-FAPS are better than those of the other three composites before UV exposure. This good interfacial adhesion may be also favorable to retard the UV ageing by preventing the crack formation in the interface region initially. As a result, the UV ageing has slightest influence on C-FAPS in these four composites.

The MPS solution shows an absorption peak at 256 nm indicating the UV radiation results in the degradation of MPS. And the generated radical groups promoted the degradation of interface and the fiber or PP around the fiber. In addition, the fracture strain of C-FMPS is higher than other three composites before UV ageing due to the ester and vinyl groups in MPS. Consequently, the degradation of MPS leads to the fracture strain of C-FMPS dramatically decreased.

### 4.4.7. XRD patterns

The XRD patterns of C-FS, C-FMPS, C-FPAPS and C-FAPS exposed up to 8 weeks UV ageing are shown in figure 4-29. Similar to the C-FS, all these three silane modification of hemp fiber has no obvious changes in the height of diffraction peaks. It's only observed the peak of cellulose I degraded in C-FMPS and C-FPAPS. It's seemed that the crystallinity almost keeps stable after alkali treated hemp fiber whether in weak (C-FPAPS) or stronger interfacial adhesion (C-FAPS).

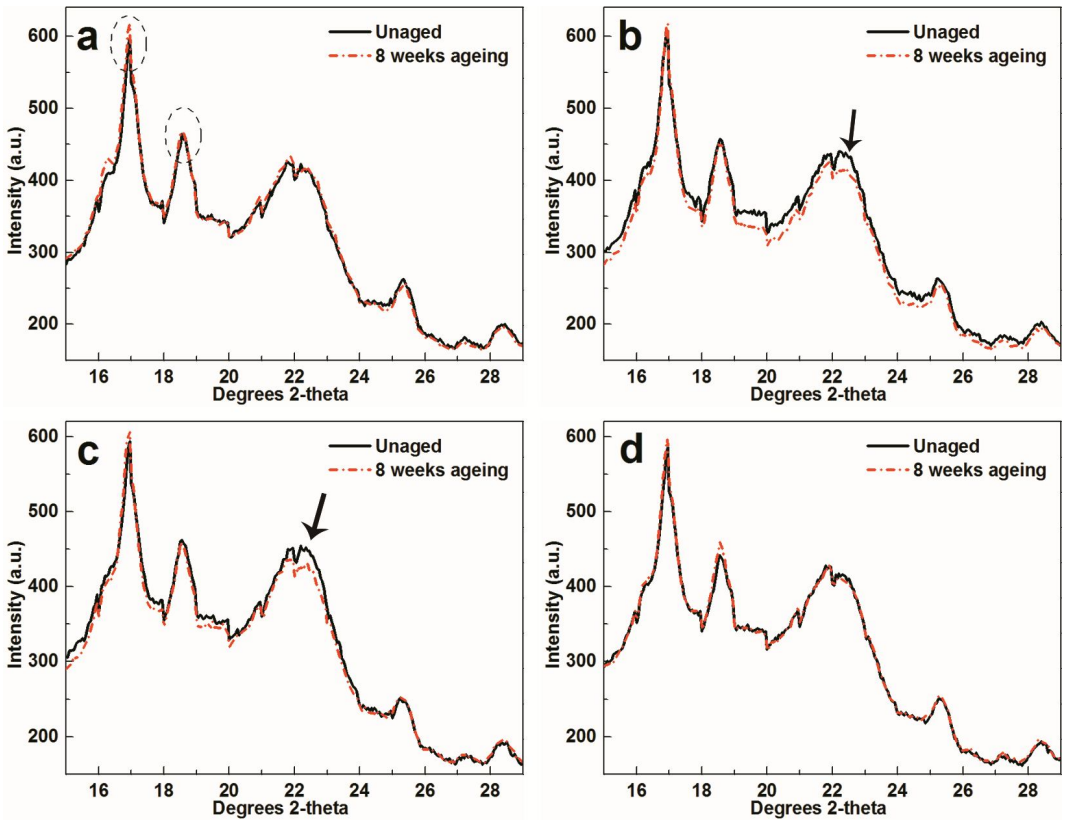


Fig. 4-29 XRD patterns of unexposed composites and exposed up to 8 weeks UV ageing: (a), C-FS; (b), C-FMPS; (c), C-FPAPS and (d), C-FAPS.

Comparing with the effects of fiber treatment (water/alkali) on the crystallization of composites (Fig. 4-18), it can be concluded that the fiber components have greater effect than the silane modification on the crystallization of PP composites in UV ageing.

## *4.5. Conclusions*

In this chapter, the effects of UV ageing on the composites matrix (PP) are investigated firstly. Then the effects of PP-g-MAH and fiber treatment (water or alkali treatment) on the UV ageing of the reinforced PP composites are studied. Finally, the effects of fiber modification (three silane agents MPS, PAPS and APS) are investigated. The main conclusions obtained are listed in the follow.

The PP surface spontaneously cracks after 4 weeks UV ageing due to the surface densification caused by chemicalcrystallization. These cracks are perpendicular to the injection direction and develop both in size and frequency when prolonging the ageing time. The UV radiation leads to the PP chain scission forming carbonyl groups and the increase of crystallinity. The Young's modulus and fracture stress increased for up to 6 weeks UV ageing and then decreased. The fracture strain deceased dramatically after 4 weeks.

To the PP composites reinforced with hemp fiber, the cracks occur initially around the location of hemp fiber on composites surface. The presence of hemp fiber accelerates the degradation of PP around fiber, but prevents the further degradation of penetrated into the composites interior. As a result, the UV ageing of hemp fiber reinforced composites is concentrated in a thin layer on surface.

The improvement of interfacial strength by adding PP-g-MAH prevents the composites degradation for 2 weeks, but accelerated it in the following period. Using water or alkali treated fiber, especially alkali, could further retard the surface ageing (whitening and cracking) of PP composites. The degradation of fiber/matrix interface is one major reason for the decline of tensile properties. However, the fiber treatment didn't give obvious contribution to resist the decrease of tensile properties.

Silane agent has considerable effects on the UV resistance depending on the structure of functional group of silane and its compatibility with composites matrix. Overall, the composites reinforced with APS modified fiber shows slower degradation

than other composites since APS nearly absorbs no UV radiation and its good compatibility with PP matrix leading to stronger interfacial adhesion. The interface degradation of composites is inhibited owing to the great absorption of UV radiation via the aniline monomer in PAPS. The fracture stress of the obtained composites(C-FPAPS) shows no loss after 8 weeks ageing. Because of the degradation of MPS, the composites reinforced with MPS modified fiber exhibits the largest decreasing of fracture strain in these four composites.

# Chapter 5

# Conclusions and perspectives

# Chapter 5. Conclusions and perspectives

**5.1. Conclusions** ..... **137**
**5.2. Perspectives** ..... **139**

## *5.1. Conclusions*

With the increasing attentions on environment and sustainable development, natural planted fiber attracts more attentions as an alternative in replacing the artificial fiber due to its good mechanical properties and environmental benefits. Given the importance and ongoing research interests in this field, this thesis mainly focused on the chemical treatment of hemp fiber and the effects of these treatments on both the fiber and the reinforced PP composites.

In chapter 1, the fiber structure, components and mechanical properties are firstly introduced. To overcome the higher hydrophilicity of planted fiber and improve the interfacial adhesion of fiber/matrix, the generally used fiber treatments like corona, plasma, alkali treatment, silane treatment are then summarized. The reinforced polymer matrix is also presented in this chapter. Finally, the ageing of planted reinforced composites like humidity and ultraviolet ageing are introduced.

In chapter 2, alkali treatment causes the decomposition of hemp fiber by removal of partial hemicellulose and lignin. In contrast, water treatment effectively removes water-soluble polysaccharides on the surface of hemp fiber, while has no obvious damages in fiber structure. Due to the smooth surface and integrated structure of water treated fiber, the mechanical properties of PP composites obtained in this case are enhanced than the composites reinforced with untreated and alkali treated fiber. Thus, water treatment can be considered as an economic and environmental friendly alternative for natural fiber treatment.

Compared with alkali treatment, silane treatment has no significant effects on fiber structure but its functional group has great influence on the mechanical properties of the resulted composites. The fracture stress of composites reinforced by APS modified fiber is enhanced compared to other composites. This is because of the primary amino of APS could react with the maleic anhydride in PP-g-MAH and then form an amide covalent bond in the composite interface. Owing to the incompatibility

of aniline with propylene, PAPS modification of fiber decreases the fracture stress of the composites. The existences of ester and vinyl groups in MPS are beneficial to increase the fracture strain of the composites.

In chapter 3, the humidity ageing and thermal ageing of hemp fiber reinforced PP composites are studied. Interestingly, the mechanical properties increase in the initial periods of humidity ageing due to the fiber swelling increased the interfacial pressure. With the process of ageing, the absorbed water causes the degradation of both the interface of fiber/matrix and hemp fiber, which deteriorate the mechanical properties of the composites. The stronger interfacial adhesion of fiber/PP matrix effectively retards the decrease of the mechanical properties by inhibiting the water absorption of composites.

The fiber mainly swells along the radial direction. The presence of PP matrix can retard the water absorption, but fails to decrease the quantity of absorbed water of hemp fiber. The composites basically expand in the vertical injection direction (fiber distribution direction). The swelling stress is as large as 850 MPa at the beginning, and then decrease gradually to zero until achieving the maximum radial swelling ratio. The tensile properties of composites subjecting thermal ageing present similar tendencies like humidity ageing but be less affected.

In chapter 4, the surface whitening and cracking occur initially around the location of hemp fiber upon UV ageing. The presence of hemp fiber accelerates the degradation of PP around them, but prevents the further degradation of internal composites. Using water or alkali to treat fiber could retard the surface degradation of PP composites. However, these treatments don’t give obvious contribution to resist the decrease of tensile properties.

Silane agent has considerable effects on the resistance of UV degradation depending on the structure of silane and its compatibility with composites matrix. Overall, the composites reinforced with APS modified fiber shows slower degradation

than the one reinforced by MPS or PAPS modified fiber due to the good interfacial strength. The aniline monomer in PAPS absorbs UV radiation greatly, which is favorable to the anti-UV degradation of composites. As a result, the fracture stress of the obtained composites was remains unchanged after 8 weeks ageing. Because of the degradation of MPS, the composites reinforced with MPS modified fiber exhibits the most decrease of fracture strain in these four composites.

## *5.2. Perspectives*

This thesis utilized the water/alkali and three silane agents to treat the fiber, and studied the effects of these treatments on the hemp fiber and the reinforced PP composites, especially on the accelerated ageing of the reinforced composites. There are some works that can be done in the future study following this thesis:

1. The interfacial crystallization of these composites after the water, alkali and silane treatment of hemp fiber should be studied. Especially for the treatment of APS, the reaction of APS with maleic anhydride also needs to give further characterizations and the resulted interfacial crystallization of the composites C-TAPS should be investigated.
2. To calculate the swelling of the plant fibers reinforced composites, it is necessary to develop an analytical model or numerical model according to the mechanics of the interface.
3. The UV degradation of the composites is concentrated on the surface layer at the beginning of UV ageing. The depth of the degradation layer should be studied by surface polishing and XRD. Hence, the degradation depth can be distinguished between the composites reinforced by various fiber treatments in this thesis.
4. The mechanism of UV degradation of the composites should be further studied, like the UV degradation firstly occurs in the fiber or in the matrix? The effects

of water absorption on the UV degradation of the composites? The agent of anti-UV or stabilizer should be added into the fiber or into the polymer matrix?

5. The hydrophilicity of planted fiber is considered as one of the greatest drawback in reinforcing composites. To overcome that, it's required to develop more effective and green protocols in the treatment of fiber for the purpose of improving the hydrophobic properties without degradation of the fiber structure.

# Chapter 6

# Résumé en français

# Chapter 6. Résumé en français

**6.1. Introduction** ..... **143**
**6.2. Traitements des fibres de chanvre et les composites renforcés** ..... **145**
**6.2.1. Traitements des fibres** ..... **145**
**6.2.2. Effets du traitement par l'eau et l'alcali sur les fibres** ..... **146**
*6.2.2.1. Observation par MEB* ..... *146*
*6.2.2.2. L'humidité des fibres traitées par l'alcali et par l'eau* ..... *147*
*6.2.2.3. Spectres de FTIR* ..... *147*
**6.2.3. Effets de la modification de silane sur les fibres** ..... **149**
*6.2.3.1. MEB observation* ..... *149*
*6.2.3.2. Humidité des fibres modifiées par silane* ..... *150*
*6.2.3.3. Spectres de FTIR* ..... *151*
**6.2.4. Composite chanvre/PP** ..... **152**
*6.2.4.1. Préparation des composites* ..... *152*
*6.2.4.2. Essais de traction des composites renforcés par les fibers traitées par l'eau et l'alcali* ..... *153*
*6.2.4.3. Essais de traction des composites renforcés par des fibres modifiées par silane* ..... *155*
**6.3. Vieillissement à humidité et en température des composites** ..... **157**
**6.3.1. Vieillissement à humidité des composites** ..... **157**
*6.3.1.1. Résultats des essais de traction* ..... *157*
*6.3.1.2. Absorption d'eau* ..... *160*
*6.3.1.3. Faciès de la rupture des composites* ..... *161*
*6.3.1.4. Gonflement des composites pendant le vieillissement à humidité* ..... *162*
**6.3.2. Vieillissement en température des composites** ..... **167**
**6.4. Vieillissement aux UV des composites** ..... **168**
**6.4.1. Effets de traitement des fibres par l'eau et par l'alcali sous UV** ..... **168**
*6.4.1.1. Observations* ..... *168*
*6.4.1.2. Observations par MO numérique* ..... *169*
*6.4.1.3. Observations par MEB* ..... *170*
*6.4.1.4. Spectres d'UV/visible* ..... *171*
*6.4.1.5. Résultats des essais de traction après vieillissement UV* ..... *172*
**6.4.2. Effets de modification des fibers par silane sous UVs** ..... **174**
*6.4.2.1. Résultats des essais de traction* ..... *174*
*6.4.2.2. Spectres d'UV/visible des agents de silane* ..... *176*
**6.5. Conclusions & perspectives** ..... **178**
**Références** ..... **181**

## *6.1. Introduction*

De nos jours, les industriels respectent de plus en plus de l'environnement et du développement durable. Les composites renforcés par les fibres végétales (souvent nommées agro-fibres) comme le chanvre, le lin et le jute...etc., attirent de nombreuses attentions en raison de leurs bonnes propriétés mécaniques et de leurs avantages environnementaux. Comparé avec les fibres de verre et de carbone, les fibres végétales ont une faible densité, bonnes propriétés mécaniques et surtout peuvent neutraliser l'anhydride carbonique dans leur processus de végétation [1].

Cependant, il y a également de nombreux défis lorsque ces fibres végétales sont utilisées dans les composites à base de polymère, tels que la variabilité des espèces, le caractère hydrophile, la faible température de décomposition et la faible adhérence à l'interface fibre/matrice. En raison de l'existence des riches groupes d'hydroxyle, les fibres végétales sont souvent incompatibles avec la plupart des polymères hydrophobes [2]. L'hydrophilie affecte également la stabilité dimensionnelle des matériaux composites. En outre, le caractère hydrophile induit une faible adhérence d'interface fibre/matrice et ainsi une baisse importante des propriétés mécaniques des composites renforcés.

Le traitement physique ou chimique des fibres végétales est une méthode très efficace pour diminuer l'hydrophilie des fibres et permet d'améliorer l'adhérence à l'interface fibre/matrice. Le traitement chimique peut réduire les propriétés hydrophiles par élimination des groupes hydroxyles (hémicellulose) et améliorer donc la compatibilité avec la matrice de polymère en greffant des groupes fonctionnels à la surface des fibres. Il existe différents traitements chimiques dans les littératures, on peut citer l'alcali, le silane, l'acétylation et la benzoylation…etc. [3]. Le principe d'amélioration des propriétés des fibres et les effets sur leur structure sont différents, en fonction de l'agent chimique, de la procédure de traitement, de la structure des fibres et

du polymère renforcé. Ces traitements peuvent aussi avoir une grande influence sur la résistance au vieillissement des composites.

Parmi ces traitements chimiques, l'alcali est l'un des agents chimiques le plus populaire car il pourra réduire efficacement des groupes hydroxyles dans la zone amorphe des fibers [4-9]. L'agent de silane a été également largement utilisé dans le traitement des fibres artificielles grâce à son petit prix, à son simple processus de modification et à sa structure variable, ayant une bonne compatibilité avec différentes matrices en polymère.

Dans cette thèse, l'eau et l'alcali sont d'abord choisis pour traiter les fibres de chanvre, puis trois agents silane: 3-(triméthoxysilyl) propyl méthacrylate (MPS), N-[3-(triméthoxysilyl)propyl] aniline (PAPS) et (3-Aminopropyl)-triéthoxysilane (APS) (Fig. 6-1), sont utilisés pour modifier la surface des fibres. Ces fibres traitées ou modifiées sont ensuite mélangées respectivement avec le polypropylène (PP) pour la fabrication de composite. Les effets de ces différents traitements sur la structure des fibres, les compositions, l'hydrophilie des fibres et les propriétés mécaniques des composites sont étudiés. Nous avons également effectué les vieillissements accélérés des composites, notamment à l'humidité, en température et aux ultraviolets afin de pouvoir comparer les propriétés mécaniques avant et après le vieillissement.

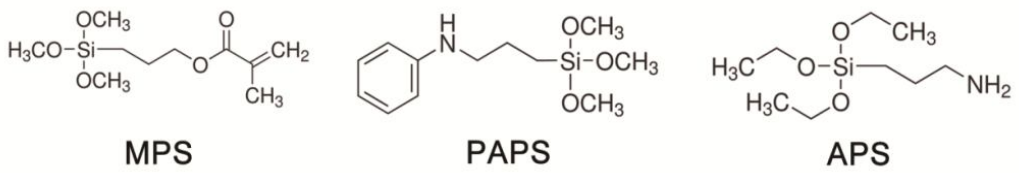


Fig. 6-1 Structure chimique de l'agent silane MPS, PAPS et APS

## *6.2. Traitements des fibres de chanvre et les composites renforcés*

### 6.2.1. Traitements des fibres

Pour les fibres traitées par l'alcali, les fibres non traitées sont d'abord lavées avec de l'eau, suivie par une immersion totale dans la solution alcali ($W_t$=5%) à température ambiante pendant 1 heure. Afin d'éliminer l'hydroxyde de sodium résiduel, les fibres sont ensuite lavées avec de l'eau jusqu'à ce que le pH soit à 7.

Pour les fibres traitées par l'eau, les fibres sont lavées 3 fois directement par l'eau pendant 10 minutes à chaque fois. Le rapport de fibre/eau est de 1: 50 (en masse). Enfin, les fibres traitées par l'alcali et par l'eau sont séchées dans une étuve à 60 ºC pendant 48 heures.

Pour les fibres modifiées par le silane, les fibres déjà traitées par l'alcali sont ensuite modifiées par le silane MPS, PAPS et APS (75 mmol/L). Le silane a été pré-hydrolysé pendant 2 heures avant son utilisation. Le pH de la pré-hydrolysé du MPS et du PAPS est de 4, de l'APS est de 10. Les fibres sont immergées dans la solution hydrolysée de silane pendant 2 heures. Le rapport de fibre/solution est de 1: 50 en masse. Les fibres sont séchées dans une étuve à 110 ºC pendant 12 heures, suivies par un lavage avec de l'eau pour éliminer les agents de silane résiduels jusqu'à ce que le pH soit à 7. Enfin, les fibres modifiées par silane sont séchées dans une étuve à 60 ºC pendant 48 heures.

Ces fibres modifiées sont nommées respectivement F-TMPS, F-TPAPS et F-TAPS. Le schéma de processus de traitement des fibres est présenté sur la figure 6-2.

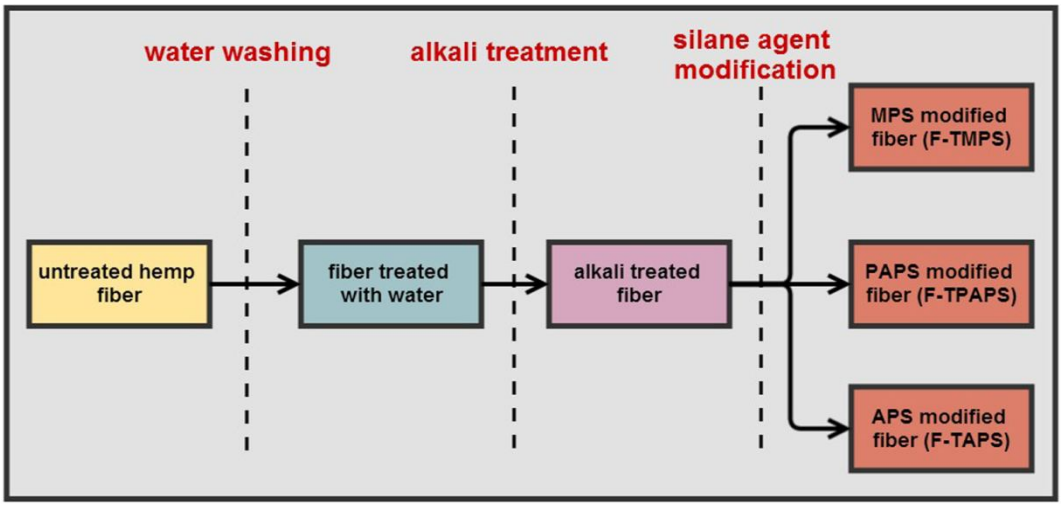


Fig. 6-2 Schéma de processus des traitements des fibres de chanvre

## 6.2.2. Effets du traitement par l'eau et l'alcali sur les fibres

*6.2.2.1. Observation par MEB*

Grâce à l'observation microscopique par MEB, les figures 6-3 montrent la morphologie de surface des fibres non traitées, traitées par l'alcali et par l'eau. Sur la figure 6-3a, la surface de fibre non traitée est recouverte d'une couche de substance dure (cire et polysaccharide). Beaucoup de petites branches sortantes sont constatées sur les côtés et la surface de fibre. Après le traitement de l'alcali (Fig. 6-3b), la surface de fibre devient plus lisse que celle de la fibre non traitée. Cependant, nous avons remarqué que les fibres sont partiellement séparées au long de fibres et donc endommagées. La surface de fibre traitée par l'eau (Fig. 6-3c) est plus propre et plus lisse que la fibre non traitée. En connaissant la structure de cellulose des fibres [10,11], il est supposé que le traitement par l'alcali peut enlever partiellement la lignine et l'hémicellulose, qui sont reliées avec la cellulose. Le lavage à l'eau peut éliminer sélectivement les polysaccharides sur la surface des fibres et ainsi préserver la structure monobloc de fibres.

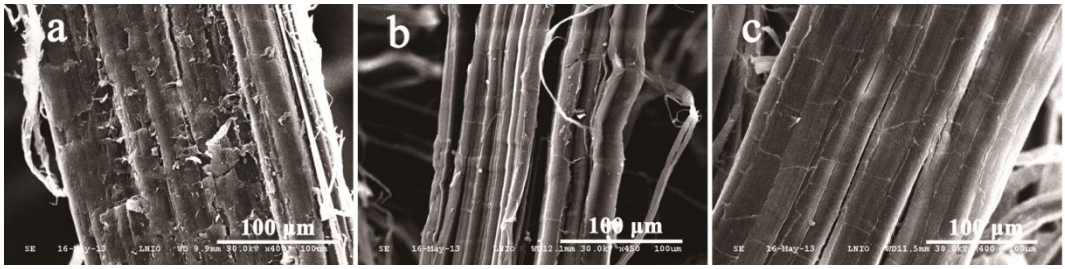


Fig. 6-3 Observation par MEB des fibres de chanvre (a) fibres non traitées; (b) traitées par l'alcali; (c) traitées par l'eau

*6.2.2.2. L'humidité des fibres traitées par l'alcali et par l'eau*

L'humidité des fibres joue un rôle important sur son comportement mécanique surtout pour les fibres végétales. Le tableau 6-1 montre l'humidité en Wt % des fibres non traitées, traitées par l'alcali et par l'eau. Pour les fibres non traitées, l'humidité reste de l'ordre de 6,95%. Après le traitement par l'alcali, les composants hydrophiles sont majoritairement enlevés, tels que les groupes hydroxyle de l'hémicellulose dans la zone amorphe, donc l'humidité diminue à 5,84 %. Dans le cas où les fibres sont traitées par l'eau, une couche mince de cire, de graisse et de polysaccharide (solubles dans l'eau) a été éliminée, une grande zone d'amorphe en surface tels que les groupes hydroxyle est exposée à l'air (Fig. 6-3c) [12], conduisant une légère augmentation de l'humidité des fibres de 6,95 % à 7,25 %.

Tab. 6-1 Humidité des fibres de chanvre traitées par l'alcali et par l'eau

| Fibre | Fibres non traitées | Fibres traitées par l'alcali | Fibres traitées par l'eau |
|---|---|---|---|
| Humidité (wt. %) | 6,95 (±0,18) | 5,84 (±0,07) | 7,25 (±0,15) |

*6.2.2.3. Spectres de FTIR*

Le spectre de FTIR est une méthode d'analyse permettant d'identifier les composants dans la surface de fibres.

La figure 6-4 montre les spectres ATR-FTIR des fibres de chanvre après différents traitements. L'hémicellulose montre souvent des pics caractéristiques à 1732 $cm^{-1}$, 1425 $cm^{-1}$ et 1162 $cm^{-1}$ [13,14]. En comparaison avec les fibres non traitées, le traitement par l'alcali provoque la disparition totale du pic à 1732 $cm^{-1}$ et une légère diminution de l'intensité des pics à 1425 cm-1 et 1162 $cm^{-1}$, ce qui signifie que le traitement par l'alcali supprime uniquement la partie de l'hémicellulose des fibres. De même, les deux pics (1241 $cm^{-1}$ et 1505 $cm^{-1}$) soient disparus soient diminués, ce qui prouvent que la lignine a été partiellement éliminée par l'alcali. Le spectre des fibres non traitées et traitées par l'eau présente des caractéristiques similaires. En comparant avec nos observations par MEB et les résultats de l'humidité des fibres, il est à conclure que l'eau nettoie la surface des fibres, sans effet négatif sur leur structure. Le traitement par l'alcali pourrait éliminer en partie l'hémicellulose et la lignine, provoquant ainsi l'endommagement partiel de la structure de fibres.

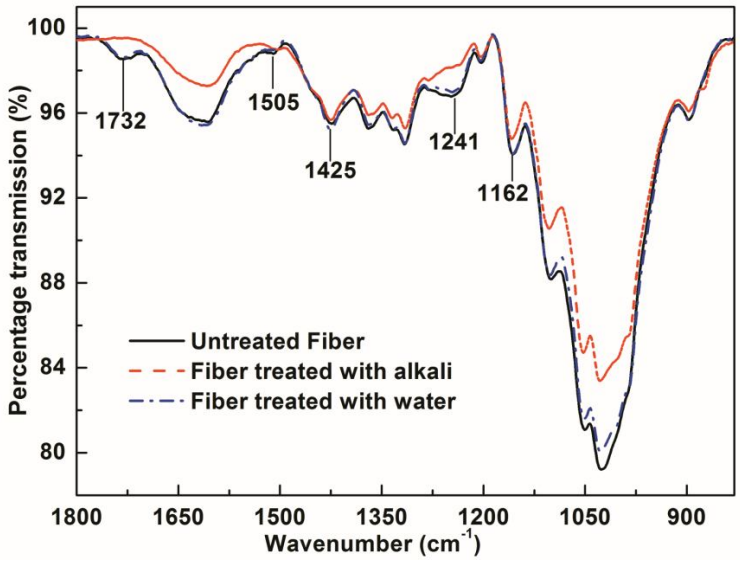


Fig. 6-4 Spectre FTIR-ATR pour différentes fibres de chanvre

### 6.2.3. Effets de la modification de silane sur les fibres

Pour vérifier la réussite de la modification de fibre par silane, nous avons observé la surface des fibres par Microscope Electronique à Balayage (MEB) et analysé la surface des fibres par FTIR dans la partie suivante.

*6.2.3.1. MEB observation*

Les figures 6-5 présentent la morphologie des fibres traitées par l'alcali, et aussi par les post-traitements MPS, PAPS et APS. Après la modification de silane, un film mince de silane peut être observé sur la surface des fibres, indiqué par les flèches sur les figures (6-5b, c et d). La formation de cette couche de silane est due à la réaction de silane avec les groupes hydroxyle sur la surface des fibres. En présence d'une molécule d'eau, le silane est hydrolysé et peut libérer les groupes silanol réactifs. Ensuite, ces monomères silanol réactifs sont absorbés physiquement sur les fibres par des liaisons hydrogène. Lorsque la température monte, les liaisons hydrogène entre les groupes silanol et les groupes hydroxyle peuvent être converties à des liaisons covalentes comme -Si-O-C- [8].

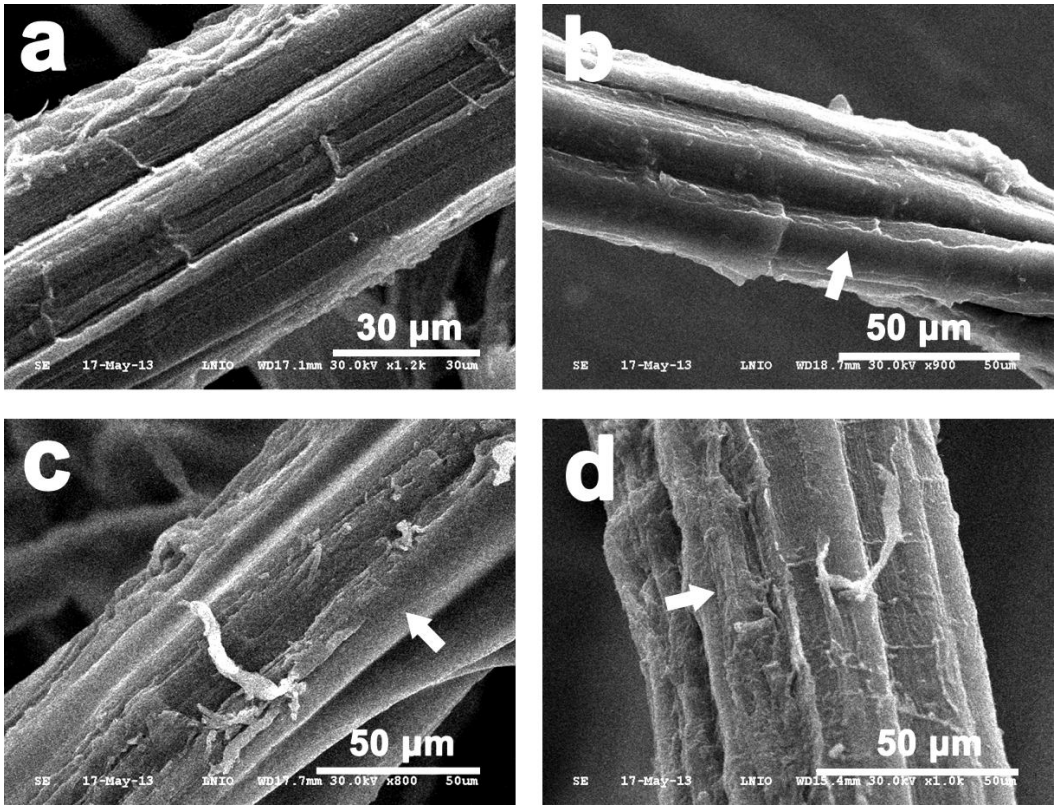


Fig. 6-5 Observation par MEB des fibres de chanvre: (a) fibre traitée par l'alcali; (b) F-TMPS; (c) F-TPAPS; (d), F-TAPS

*6.2.3.2. Humidité des fibres modifiées par silane*

L'humidité des fibres traitées par l'alcali, F-TMPS, F-TPAPS et F-TAPS est présentée dans le tableau 6-2. Nous pouvons constater que toutes les valeurs de l'humidité sont très proches et que le silane n'a pas une influence importante sur l'humidité des fibres. En fait, la modification par le silane ne change pas la constitution chimique des fibres. Par conséquent, les fibres F-TMPS, F-TPAPS et F-TAPS restent quasiment inchangées par rapport aux fibres traitées par l'alcali.

Tab. 6-2 Humidité des fibres de chanvre modifiées par silane

| Fibre | Fibres traitées par l'alcali | F-TMPS | F-TPAPS | F-TAPS |
|---|---|---|---|---|
| Humidité (wt. %) | 5,84 (±0,07) | 5,88 (±0,04) | 5,63 (±0.09) | 5,71 (±0.06) |

*6.2.3.3. Spectres de FTIR*

Nous avons comparé le spectre FTIR des fibres de chanvre, avant (nommées Fibres traitées par l'alcali) et après (nommées avec F-T) la modification de silane (Fig. 6-6). Après la modification de la MPS, le spectre de F-TMPS apparaît deux nettes bandes d'absorption à 1639 et 1718 $cm^{-1}$, qui correspondent à la vibration C = C et à l'étirement C = O de méthacrylate [9]. Dans le spectre de F-TPAPS, la vibration du CN est observée à 1276 $cm^{-1}$. Les bandes d'absorption en 1603 et 1507 $cm^{-1}$ sont attribuées à la C = C étirement dans les anneaux benzéniques et à la flexion de groupe NH du PAPS [10]. Le CH d'APS sous mode d'étirement asymétrique et symétrique est observé à 2942 et à 2839 $cm^{-1}$ dans le spectre F-TAPS. Les pics apparus à 1657 et 3404 $cm^{-1}$ correspondent à la flexion et à l'extension de NH, respectivement [11]. La présence de ces bandes dans les spectres FTIR de fibres confirme le succès de modification de la surface des fibres par des agents silane MPS, PAPS et APS.

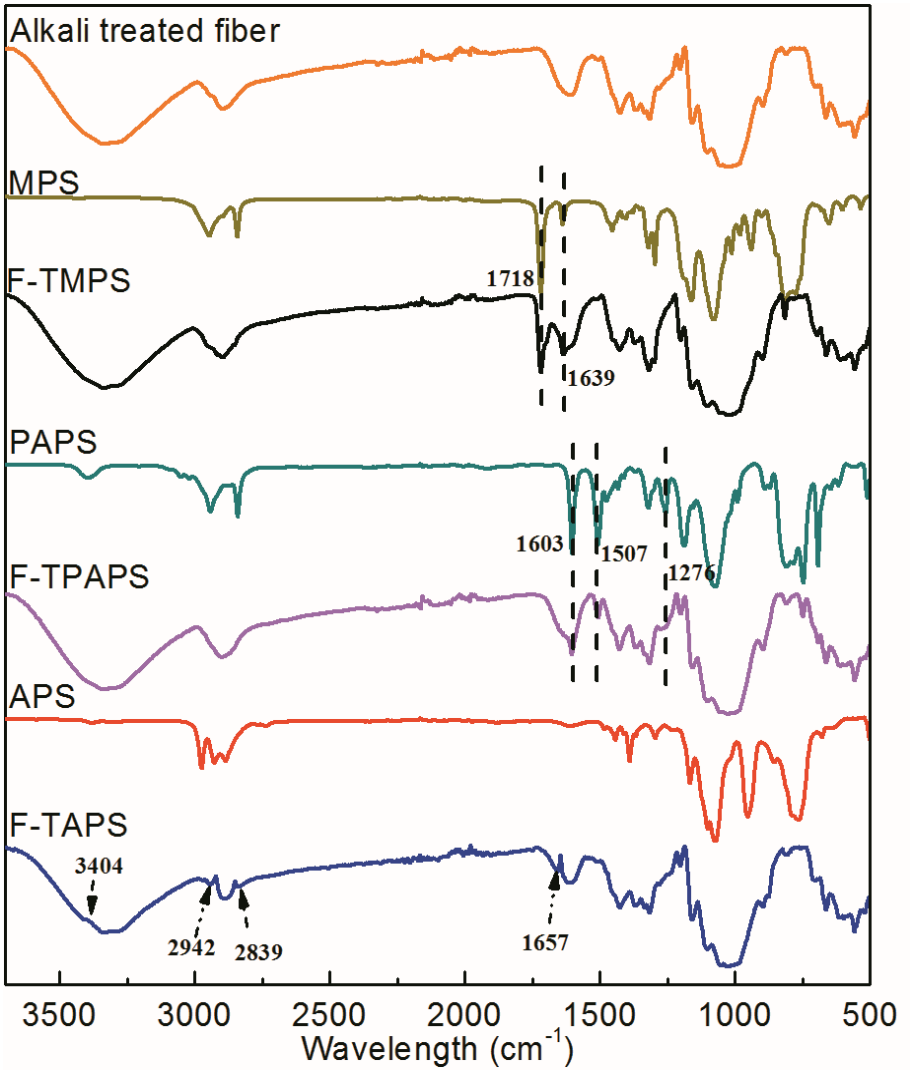


Fig. 6-6 Spectres FTIR de F-TS (Fibre traitées par l'alcali); MPS; F-TMPS, PAPS; F-TPAPS; APS; F-TAPS (3700-500 $cm^{-1}$)

## 6.2.4. Composite chanvre/PP

### *6.2.4.1. Préparation des composites*

Le polypropylène (PP), les fibres de chanvre et le polypropylène greffé anhydride maléique (MAH-g-PP), utilisé comme agent de compatibilité, ont été mélangés et extrudés avec une extrudeuse mono vis Brabender KE19 à 170-185 ºC. Les granulés obtenus sont servis à la fabrication des éprouvettes de traction à l'IUT de Troyes, par une machine à injection Engel Spex Victoire 50 à 170-180 ºC, sous pression à 158 MPa.

(Composites Eprouvettes 1B, conformément à la norme ISO 527-2). Les compositions des éprouvettes sont résumées dans le tableau 6-3. Le taux de renfort est de 30 % en masse pour C-UF et de 28.6 % en masse pour les autres composites dans cette thèse.

Tab. 6-3 Compositions des composites

| Echantillons | PP(phr) | PP-g-MAH(phr) | Fibre chanvre(phr) | Notations |
|---|---|---|---|---|
| C-UF | 100 | 0 | 42,86 | Fibre non traitée |
| C-UF-MAH | 100 | 7,14 | 42,86 | Fibre non traitée + PP-g-MAH |
| C-FW | 100 | 7,14 | 42,86 | Fibre traitée par l'eau |
| C-FS | 100 | 7,14 | 42,86 | Fibre traitée par l'eau et l'alcali |
| C-FMPS | 100 | 7,14 | 42,86 | Fibre traitée par l'alcali et MPS |
| C-FPAPS | 100 | 7,14 | 42,86 | Fibre traitée par l'alcali et PAPS |
| C-FAPS | 100 | 7,14 | 42,86 | Fibre traitée par l'alcali et APS |

*6.2.4.2. Essais de traction des composites renforcés par les fibers traitées par l'eau et l'alcali*

Les résultats des essais de traction des composites PP renforcés par des fibres de chanvre traitées par l'eau ou par l'alcali sont présentés dans les figures 6-7**.**

Pour comparer les résultats, le composite PP renforcé par des fibres non traitées (C-UF-MAH) a été utilisé comme échantillon de référence. Nous avons constaté que les propriétés mécaniques du C-FW sont améliorées par rapport aux autres échantillons. Pour l'échantillon de référence utilisant les fibres non traitées (C-UF-MAH), le module d'Young, la contrainte et la déformation à la rupture sont de 3,66 GPa, 39,81 MPa et 3,70 %, respectivement. Cependant, la contrainte et la déformation à la rupture du C-FS restent inchangées, tandis que le module d'Young est diminué de 7,92% par rapport à l'échantillon de référence. Ce phénomène est très intéressant permettant de conclure

que le traitement des fibres par l'eau améliore nettement les propriétés mécaniques du composite (C-FW). Le module d'Young, la contrainte et la déformation à la rupture ont augmenté de 3,66%, 7,86% et 14,6%, par rapport à l'échantillon de référence C-UF-MAH (voir Figs. 6-7a, b et c).

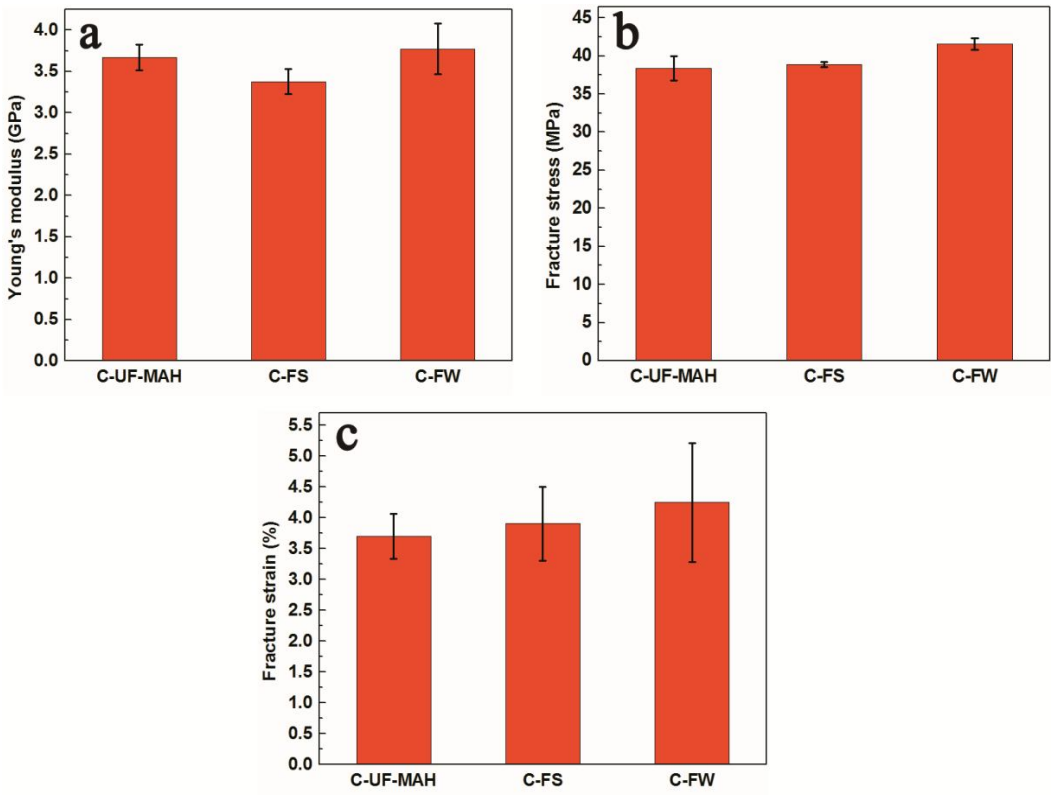


Fig. 6-7 Propriétés mécaniques des composites (a) Module d'Young; (b) Contrainte à la rupture; (c) Déformation à la rupture

Les figures 6-8 schématisent la structure interne des composites renforcés par les fibres non traitées, traitées par l'eau et par l'alcali. Pour le composite non traité C-UF-MAH, la cire, les polysaccharides et les autres composants existent en surface des fibres, diminuent la force d'adhérence à l'interface fibre/matrice, empêchant ainsi la bonne adhésion entre elles. Pour le C-FS, la structure de la fibre élémentaire est en partie endommagée après un traitement agressif de l'alcali, provoquant la suppression de certains constituants de l'hémicellulose et de la lignine. Par exemple, les fissures observées dans les fibres élémentaires (Fig. 6-3b) peuvent former des défauts dans les

composites, induisant la diminution des propriétés mécaniques. Par contre, le traitement par l'eau peut éliminer les impuretés sur la surface des fibres et conserver la structure monobloc de fibres, ça peut aussi diminuer la dégradation des fibres en augmentant la force d'adhésion interface fibre/matrice du composite C-FW.

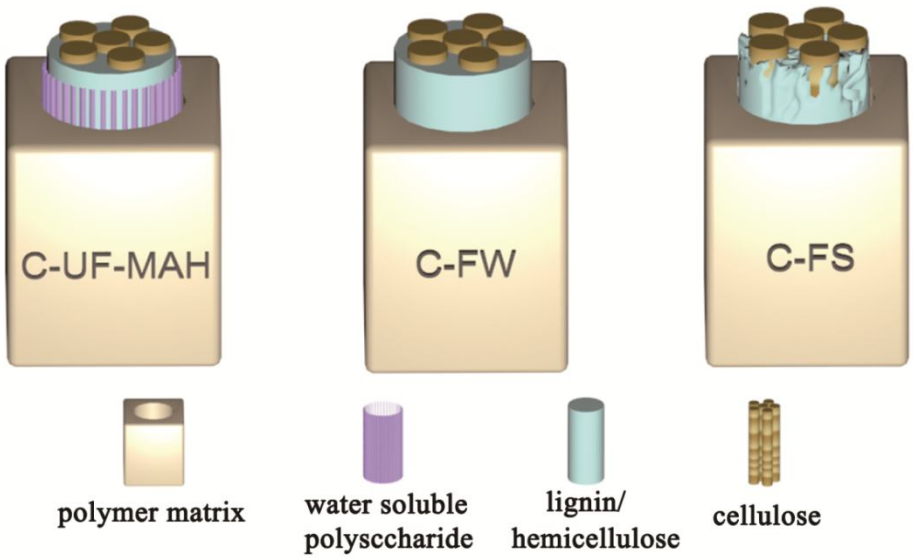


Fig. 6-8: Schémas des structures des composites fibre/PP traitées par l'eau et l'alcali

*6.2.4.3. Essais de traction des composites renforcés par des fibres modifiées par silane*

Les résultats des essais de traction des composites PP renforcés par des fibres non modifiées (traitées uniquement par l'alcali) et des fibres modifiées respectivement par le silane MPS, PAPS et APS, sont présentés dans les figures 6-9.

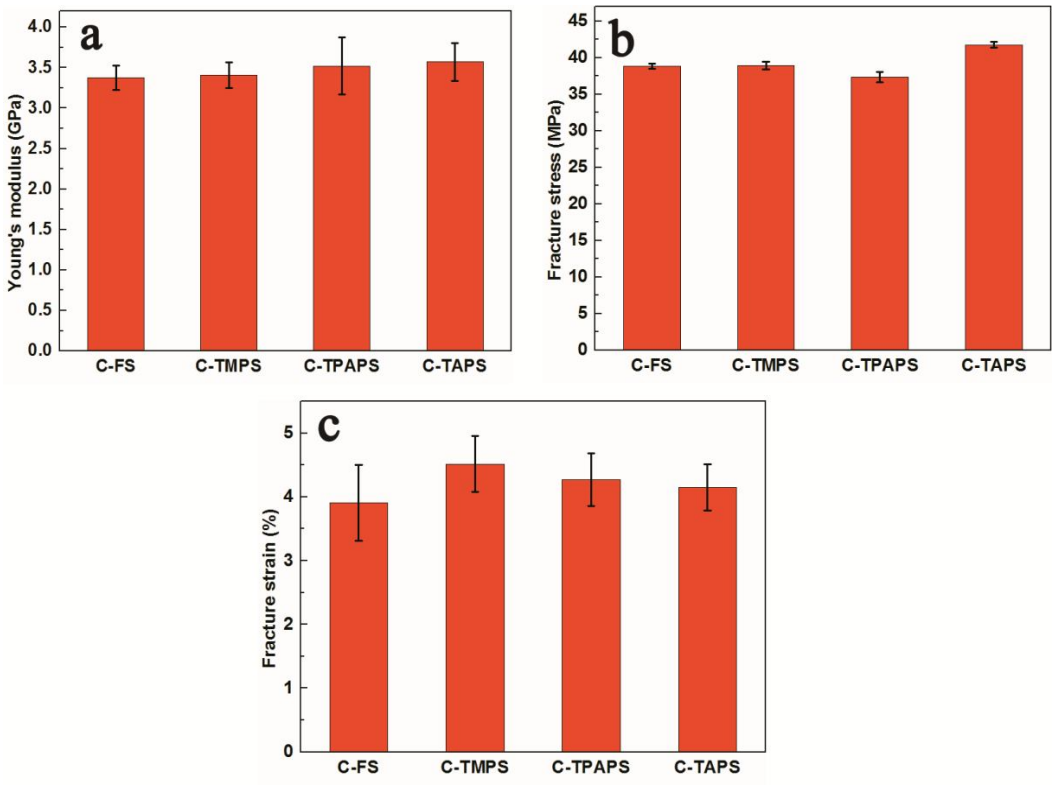


Fig. 6-9 Propriétés mécaniques de C-TS, C-TMPS, C-TPAPS et C-TAPS: (a) Module d'Young; (b) Contrainte à la rupture; (c) Déformation à la rupture

Il est à noter que sur la figure 6-9a, le module d'Young des composites est légèrement amélioré après la modification par ces trois agents de silane. Dans la figure 6-9b, la contrainte à la rupture a diminué légèrement de 38,86 MPa pour le C-TS à 37,32 MPa pour le C-TPAPS; alors qu'elle a augmenté à 41,77 MPa pour le C-TAPS. Ces résultats prouvent que l'amine primaire -$NH_2$ de l'APS peut réagir avec l'anhydride maléique attaché au PP pour former une liaison covalente amide [13] (voir Fig. 6-10), ce qui augmente considérablement la force de liaison d'interface fibre/matrice, permettant d'améliorer les propriétés mécaniques de C-TAPS. Cependant, l'amine secondaire -NH portant en noyaux benzéniques n'a pas réagi avec l'anhydride maléique. En outre, les anneaux du benzène dans les PAPS n'ont pas une bonne compatibilité soit avec l'anhydride maléique soit avec le PP. Par conséquent, la contrainte à la rupture a diminué après la modification du PAPS. Pour le composite C-TMPS, l'existence des groupes ester et du vinyle du MPS, qui forment des liaisons hydrogène avec la matrice

PP, permet une augmentation de la déformation à la rupture en raison des glissements des chaînes entre le MPS et le PP, la déformation à la rupture a augmenté de 3,90% (C-FS) à 4,51% (C-TMPS).

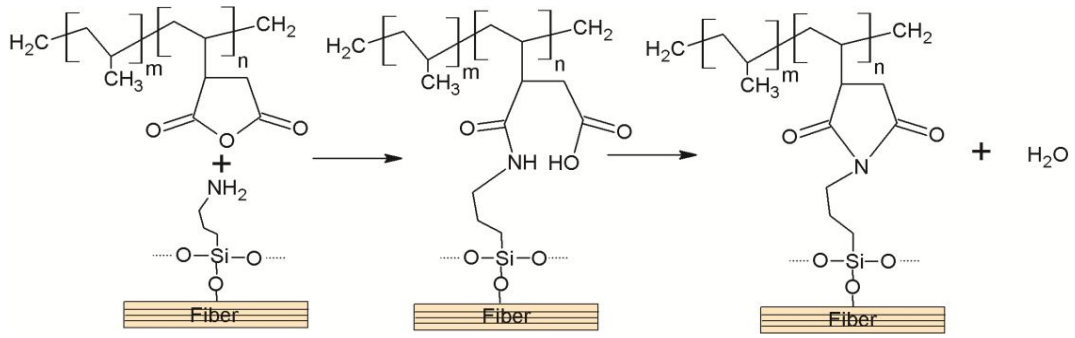


Fig. 6-10 Schémas de réaction entre l'amino primaire d'APS et l'anhydride maléique greffé au polypropylène (PP-g-MAH)

## *6.3. Vieillissement à humidité et en température des composites*

### 6.3.1. Vieillissement à humidité des composites

Le vieillissement à humidité a été effectué grâce à une machine de traitement de vieillissement: Atlas suntest XXL, pendant 8 semaines. Les conditions du vieillissement sont : humidité relative de 80 ± 5%, température de la chambre 20 ± 2ºC, 102 minutes sec et 18 minutes de l'eau pulvérisée en accord avec la norme ISO 4892-2.

*6.3.1.1. Résultats des essais de traction*

Les résultats des essais de traction des composites C-UF, C-UF-MAH, C-FW, C-FS et C-FAP pendant et après 8 semaines de vieillissement par l'humidité sont présentés dans les figures 6-11. Il est intéressant de noter que le module d'Young augmente de façon significative, de 24,3 % pour le C-UF (4 semaines), de 19,2 % pour le C-UF-MAH (6 semaines), de 21,7 % pour le C-FW (8 semaines), de 28,2 % pour le C- FS (6 semaines) et de 23,5 % pour le C-FAPS (6 semaines). La contrainte à la rupture a amélioré de 6,5 % pour le C-UF (4 semaines), de 1,6% pour le C-FW, (4 semaines) et de 4,1% pour le C-FS (6 semaines). Dans le cas général selon la littérature

[15], la résistance de traction des fibres de chanvre doit être diminuée au cours du vieillissement à humidité. Donc, cette augmentation du module d'Young peut s'expliquer par le fait que la modification des fibres renforce l'adhésion à l'interface et que l'enflure des fibres due à l'absorption d'eau augmente la force de pression à l'interface et par conséquent les propriétés mécaniques des composites s'améliorent. En outre, il est probable que la plus forte force d'adhérence à l'interface peut retarder la diminution du module d'Young.

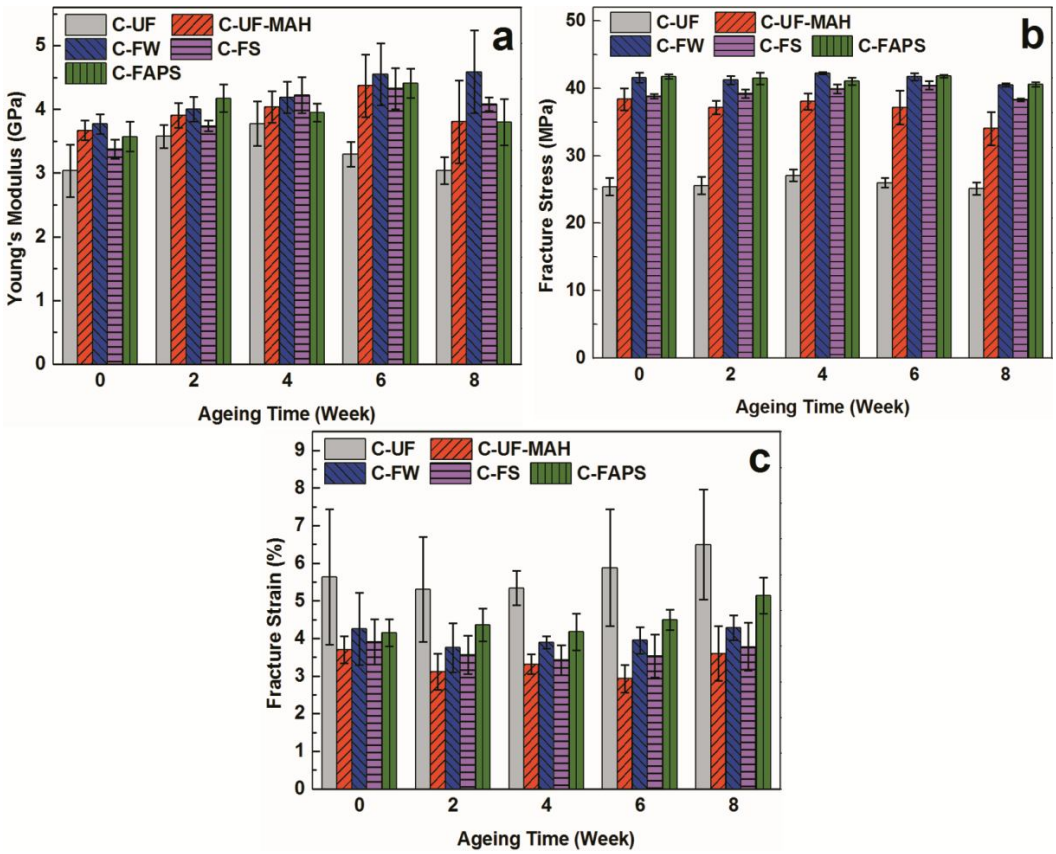


Fig. 6-11 Résultats des essais de traction des composites C-UF, C-UF-MAH, C-FW, C-FS et C-FAPS: (a), Module d'Young; (b), Contrainte à la rupture; (c), Déformation à la rupture

Après 8 semaines, la contrainte à la rupture baisse de 1,1 % pour le C-UF, de 11,3 % pour le C-UF-MAH, de 2,6 % pour le C-FW, de 1,4 % pour C-FS et de 2,9 % pour le C-FAPS. Bien que le PP-g-MAH puisse améliorer la résistance de l'adhérence à

l'interface du C-UF-MAH, les fibres non traitées dans le C-UF-MAH recouvrent toujours une couche de polysaccharide (soluble de l'eau). Après certains temps du vieillissement, l'eau va pénétrer dans l'interface et le polysaccharide commence à se décomposer provoquant ainsi le décollement à l'interface et l'affaiblissement du comportement mécanique. C'est pour cette raison que la diminution évidente de la contrainte à la rupture est bien constatée dans le C-UF-MAH. En revanche, après le traitement à l'alcali ou à l'eau, le polysaccharide a été déjà complètement enlevé, ce qui rend une l'adhésion à l'interface plus forte. Ceci étant dit que la surface de fibre propre et lisse est bénéfique à empêcher efficacement l'absorption d'eau dans l'interface et donc permet de retarder la dégradation à l'interface. La contrainte à la rupture du C-FW, du C-FS et du C-FAPS a légèrement diminué enfin après 8 semaines de vieillissement.

En fait, l'augmentation du module d'Young s'associe toujours avec une diminution de la déformation à la rupture. Comme nous avons cité précédemment, le module d'Young a augmenté jusqu'à 4-6 semaines du vieillissement à humidité, de sorte que la déformation à la rupture correspondante diminue. Par exemple, la déformation à la rupture du C-UF a diminué de 5,1% pendant 2-4 semaines, puis a augmenté de 15,3% jusqu'à 8 semaines. Nous avons également observé les mêmes tendances pour le C-UF-MAH, le C-FW et le C-FS sauf pour le C-FAPS.

Ce qui est important est qu'après 2 semaines de vieillissement, la déformation de rupture de C-FAPS n'a pas clairement diminué, mais a légèrement augmenté de 5,1%. Après 6 semaines, le module d'Young a augmenté de 23,4%, tandis que la déformation à la rupture a également augmenté de 8,2%. En résumé, la résistance à la rupture reste quasiment inchangée après 8 semaines de vieillissement. Parmi les cinq types des composites, le C-FAPS montre une excellente résistance au vieillissement à humidité.

*6.3.1.2. Absorption d'eau*

Comme nous avons montré précédemment, l'absorption d'eau peut affecter considérablement le comportement mécanique des composites. Dans cette partie, nous avons effectué des mesures de l'absorption d'eau sur ces cinq composites.

La figure 6-12 montre le pourcentage d'absorption d'eau des composites à température ambiante. On note que la masse de chaque composite augmente rapidement au début et suivi par un équilibre relatif à cause de la saturation. L'absorption d'eau la plus élevée est observée pour le C-UF (3,9 %), renforcé par des fibres non traitées et sans MAH-g-PP. Avec l'ajout de PP-g-MAH, le composite C-UF-MAH présente une absorption inférieure (2,4 %), indiquant que l'ajout de PP-g-MAH pourrait améliorer l'adhérence de fibre/matrice et réduire la quantité d'absorption d'eau dans les composites. L'absorption finale du C-FW et du C-FS est de 1,1 % et de 0,9 %. Cela signifie que le traitement par l'eau et par l'alcali des fibers est également bénéfique pour réduire l'absorption d'eau des composites. Bien que le traitement par l'alcali soit plus efficace pour la réduction de l'humidité des fibres par rapport au traitement par l'eau (Tabl. 1.6), lorsqu'il s'agit de leurs composites renforcés par ces fibres, son effet reste négligeable. Le composite C-FAPS montre quasiment la même courbe d'absorption d'eau comme dans le cas de C-FS, montrant que la modification des fibres par APS n'a pas de l'effet évident sur l'absorption d'eau du composite par rapport au traitement par l'alcali.

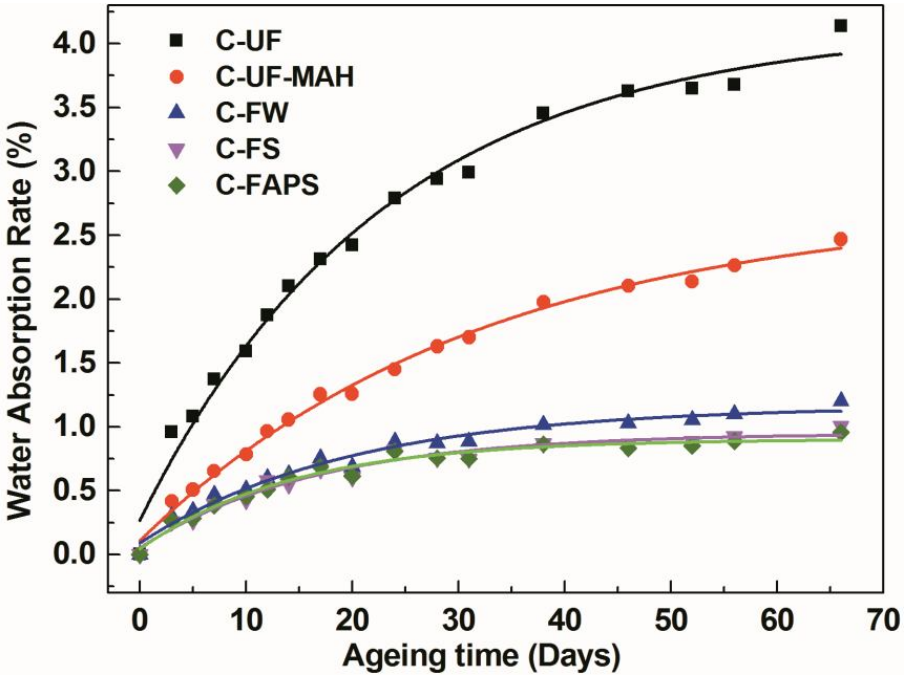


Fig. 6-12 Variation de masse des composites C-UF, C-UF-MAH, C-FW, C-FS et C-FAPS

*6.3.1.3. Faciès de la rupture des composites*

Les figures 6-13 présentent les faciès de rupture en traction des composites observés par MEB après 8 semaines de vieillissement à humidité. Pour le composite C-UF, renforcé par les fibres non traitées (Fig. 6-13a), on peut voir qu'une mèche des fibres est détachée de sa loge à cause de la mauvaise cohésion d'interface. Sur la figure 6-13b, nous avons constaté un décollement entre les fibres et le PP (indiqué par la flèche), provoqué par la dégradation du polysaccharide sur la surface des fibres non traitées. Sur les figures 6-13(c, d et e), après le traitement par l'alcali ou par l'eau, éliminant le polysaccharide soluble, la dégradation à l'interface n'est pas si évidente. Sur la figure 6-13d, la surface des fibres n'est pas lisse à cause du traitement par l'alcali, qui élimine partiellement l'hémicellulose et la lignine, les fibres élémentaires ont été endommagées et les fissures internes ont été formées.

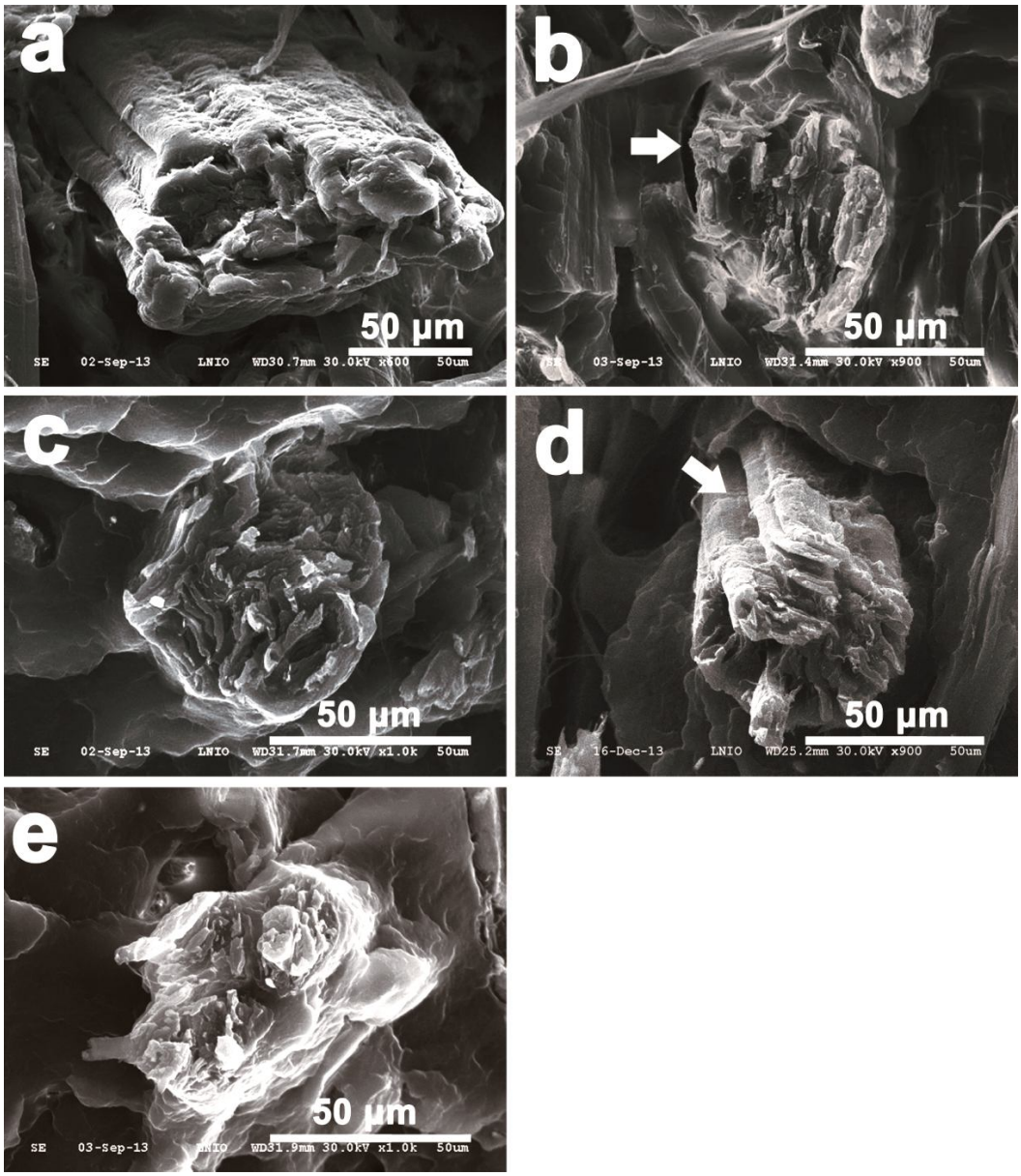


Fig. 6-13 Faciès de rupture observés par MEB: (a) C-UF; (b), C-UF-MAH; (c), C-FW; (d), C-FS; (e), C-FAPS

*6.3.1.4. Gonflement des composites pendant le vieillissement à humidité*

Pendant le vieillissement à humidité, les composites absorbent de l'eau et ne gardent plus ses dimensions originales. Nous avons mesuré la variation de section des éprouvettes pour les cinq composites au cours de leur vieillissement.

Comme la montre les figures 6-14, la section de cinq composites varie en fonction du temps. Nous avons également effectué un calcul théorique permettant de déterminer leurs sections à chaque l'instant selon la formule suivante:

$$s_t^c(\%) = W_t(\%) \times \frac{1}{\rho_{H_2O}} \times \frac{M_0}{V_0} \tag{6-1}$$

où $W_t(\%)$ est la variation de masse du composite mesurée pendant le vieillissement, $M_0$ et $V_0$ correspondent à la masse et au volume du composite avant vieillissement. Cette formule est basée sur la distribution des fibres orientées suivant la direction de l'injection.

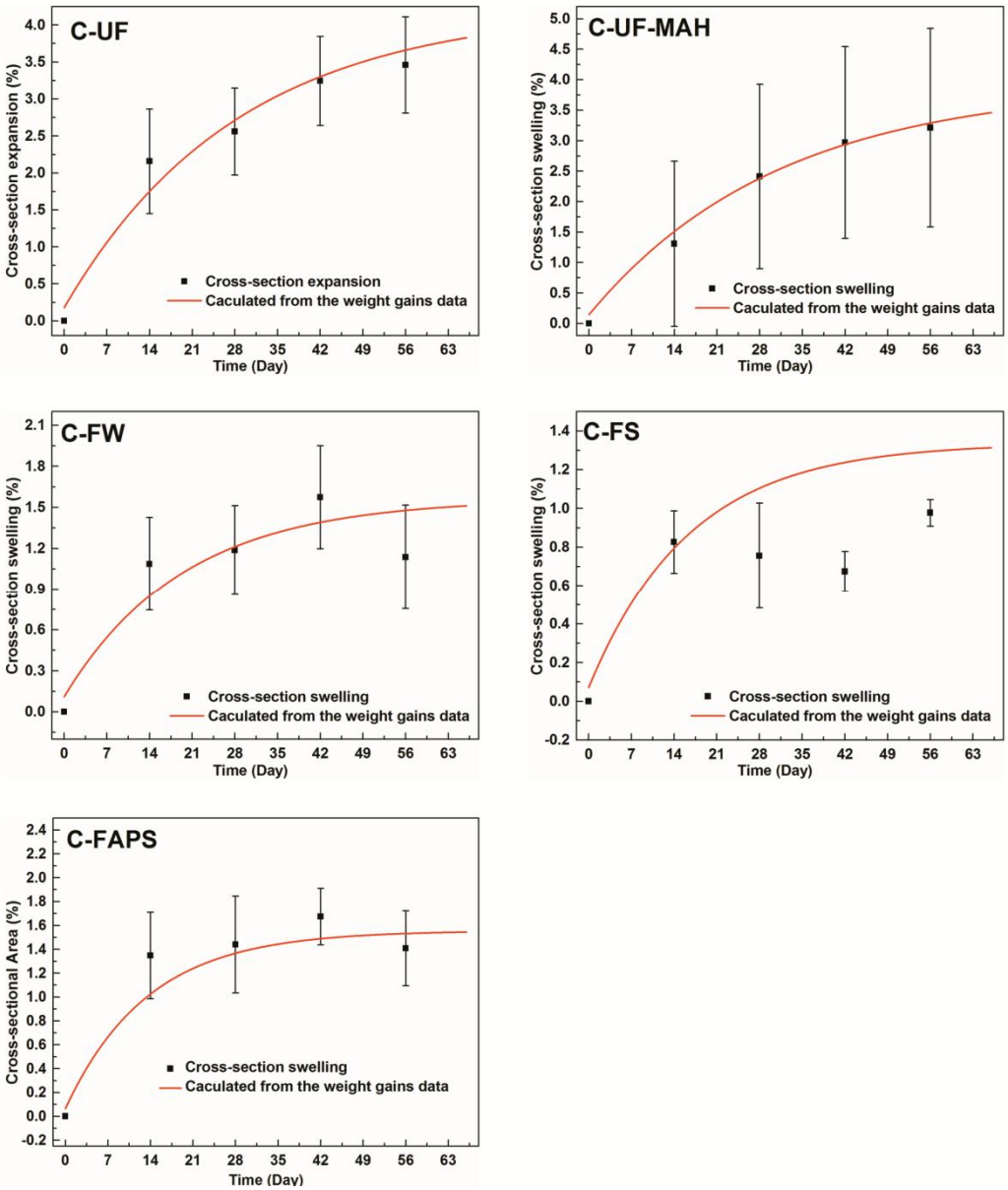


Fig. 6-14 Variation de section des composites: C-UF, C-UF-MAH, C-FW, C-FS et C-FAPS

Les figures 6-14 montrent que les résultats des calculs sont en bonne accord avec les mesures expérimentales, en particulier pour les composites C-UF, C-UF-MAH et C-FW. Cela peut prouver que les hypothèses des calculs (Éq. 6-1), indiquant que les fibres se distribuent au long du composite selon la direction d'injection et que le gonflement des fibres a eu lieu principalement en direction radiale. Pour le composite C-FS, le gonflement calculé est supérieur aux mesures expérimentales après 2 semaines.

Comme il a été analysé précédemment, le traitement par l'alcali dégrade la structure des fibres, formant des lacunes et des défauts dans le composite. Le gonflement des fibres se fait en remplissant ces vides et le volume du composite n'a pas augmenté réellement. Le gonflement du composite est donc inférieur au volume calculé. En comparant avec les C-UF, C-UF-MAH et C-FW, nous pouvons conclure que la stabilité dimensionnelle du composite pourrait être améliorée par l'amélioration de l'adhérence à l'interface.

Après l'étude du gonflement des composites dans la section de l'éprouvette, nous avons aussi effectué de comparaisons du gonflement en direction de la largeur et de l'épaisseur de cette section pour les cinq composites C-UF, C-UF-MAH, C-FW, C-FS et C-FAPS (Figs. 6-15), afin de savoir respectivement la direction du gonflement et l'influence de largeur et d'épaisseur sur le gonflement du composite.

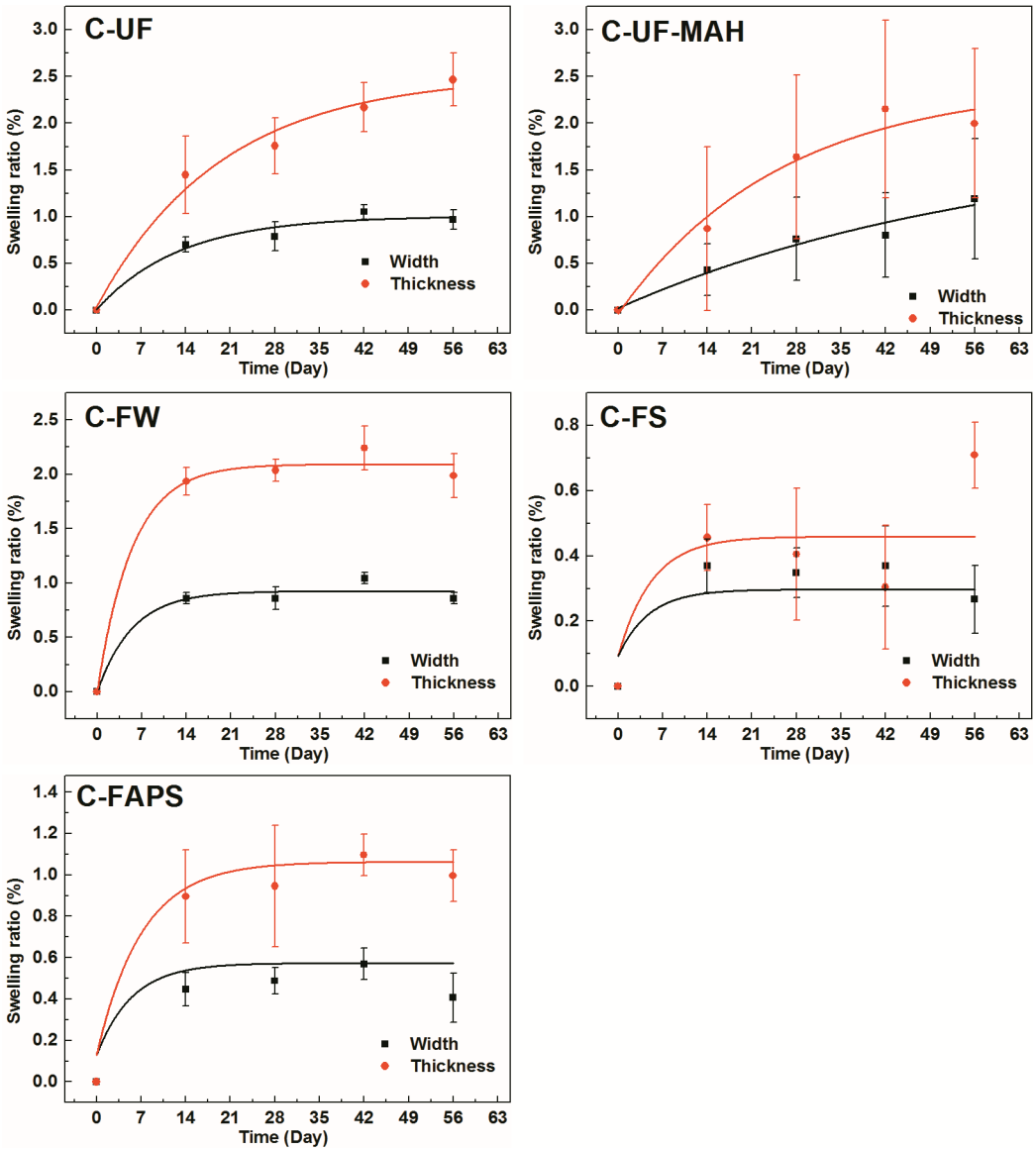


Fig. 6-15 Taux de gonflement des composites C-UF, C-UF-MAH, C-FW, C-FS et C-FAPS dans la direction de la largeur et de l'épaisseur

Il est à noter sur la figure 6-15 que le composite C-UF, comme exemple, la largeur augmente de 0,7 % (14 jours), 0,8 % (28 jours) et 1,1 % (42 jours), aussi que l'épaisseur correspondante augmente de 1,4 %, 1,8 % et 2,2 %. Nous pouvons observer des résultats similaires dans les trois autres composites C-UF-MAH, C-FS et C-FAP. Selon ces résultats, nous avons constaté un rapport de 2 entre le gonflement en épaisseur et largeur.

### 6.3.2. Vieillissement en température des composites

Le vieillissement en température a été réalisé pendant 8 semaines comme dans le cas du vieillissement à humidité. Les conditions du vieillissement sont: humidité relative de 50 ± 5%, température de la chambre 38±2 ºC, sans lumière durant tout processus. La température de vieillissement est choisie selon la norme ISO 4892-2.

Les résultats des essais de traction des composites C-UF, C-UF-MAH, C-C-FW et FS sont présentés sur les figures 6-16 afin de comparer les effets du traitement des fibres sur les propriétés mécaniques des composites.

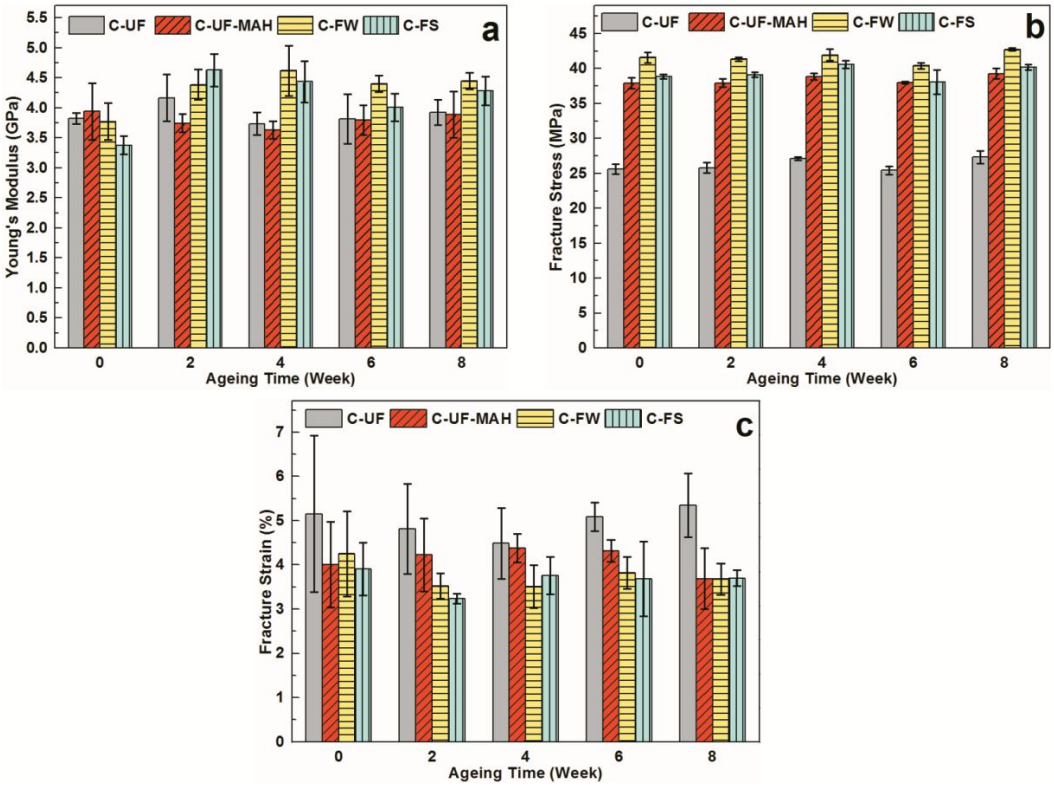


Fig. 6-16 Résultats des essais de traction des composites C-UF, C-UF-MAH, C-FW et C-FS: (a), Module d'Young; (b), Contrainte à la rupture; (c), Déformation à la rupture

Dans la figure 6-16a, le module d'Young augmente de façon significative au début (après 2 ou 4 semaines), puis diminue à partir de 4$^{ième}$ semaine, sauf C-UF-MAH. Sur la figure 6-16b, la contrainte à la rupture reste presque inchangée après 8 semaines. Et la

déformation à la rupture (Fig. 6-16c) diminue après 8 semaines. Ces tendances de variation sont similaires par rapport au vieillissement à humidité sur les propriétés mécaniques des composites.

Cependant, il est difficile de distinguer les effets de la température et de l'humidité sur les propriétés mécaniques des composites. En comparant les conditions du vieillissement en température et à humidité, nous notons que l'humidité relative a diminué de 80±5 % à 50±5 %, ce qui peut ralentir l'absorption d'eau. En revanche, la température a augmenté de 20 ºC à 38 ºC, ce qui peut favoriser l'absorption d'eau dans le composites à cause de la température élevée, fournissant plus d'énergie thermique pour la pénétration des molécules d'eau.

## *6.4. Vieillissement aux UV des composites*

Le vieillissement aux UV a été réalisé dans la même machine Atlas Suntest XXL pendant 8 semaines, selon la norme ISO 4892-2: Méthode A en utilisant les filtres de la lumière du jour (Altération artificielle), cycle 1. Les paramètres du vieillissement sont les suivants: haut débit (300 nm à 400 nm) 60±2 $W \cdot m^{-2}$, température de noir-standard 65±3 ºC, l'humidité relative 50±10 %, la température de la chambre 38±3 ºC, 102 minutes sec et 18 minutes de l'eau pulvérisée.

### 6.4.1. Effets de traitement des fibres par l'eau et par l'alcali sous UV

*6.4.1.1. Observations*

Sur la figure 6-17, nous avons observé la variation de couleur sur les quatre composites C-UF, C-UF-MAH, C-FW et C-FS, ils passent de brun à blanc de 2 à 8 semaines sous UV.

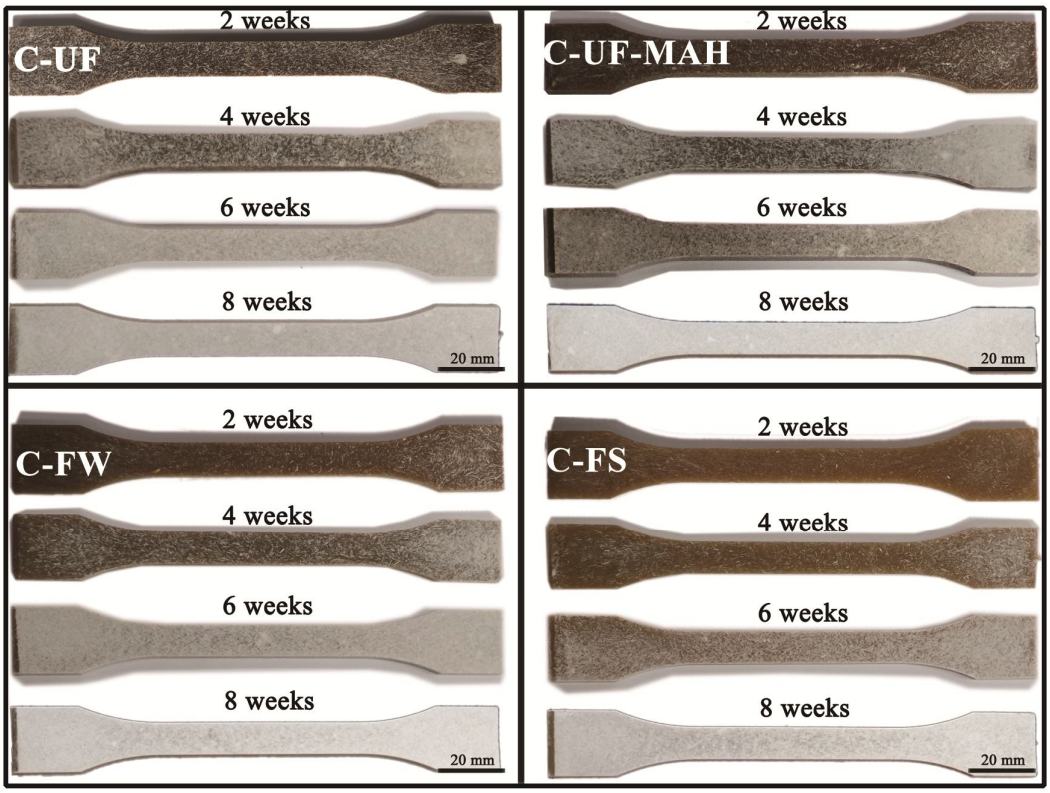


Fig. 6-17 Variation de couleur des composites C-UF, C-UF-MAH, C-FW et C-FS de 2 à 8 semaines sous UV

Toutefois, le taux de blanchiment de ces quatre composites est différent. Après 2 semaines, le C-UF est plus blanc que le C-UF-MAH; pourtant le C-FS change de couleur très légèrement. Après 4 semaines, le taux de blanchiment des composites peut varier comme: C-UF> C-UF-MAH> C-FW> C-FS. Après 8 semaines, la surface des composites est presque complètement blanchie. Pour comprendre ce phénomène, des observations par microscopie optique numérique et MEB sont effectuées.

*6.4.1.2. Observations par MO numérique*

Les figures 6-18 montrent les photos prises par microscopie optique numérique sur la surface des composites C-UF, C-UF-MAH, C-FW et C-FS, de 2 à 8 semaines du vieillissement aux UV. La figure 6-18 confirme que le blanchiment du C-UF est le plus rapide, mais le C-FS est le moins rapide dans ces quatre composites. Nous constatons également que la couleur du blanc crayeux se produit d'abord (deux semaines) autour

des fibres (flèche). Il est connu que la cristallisation du PP sous rayonnement UV peut diminuer sa transparence. Pour ce genre de phénomène, NM. Stark [16] a indiqué que l'eau pulvérisée a des effets importants sur le blanchiment en combinaison avec un rayonnement UV. Il semble que les fibres végétales sont favorables à la dégradation du PP autour d'elles.

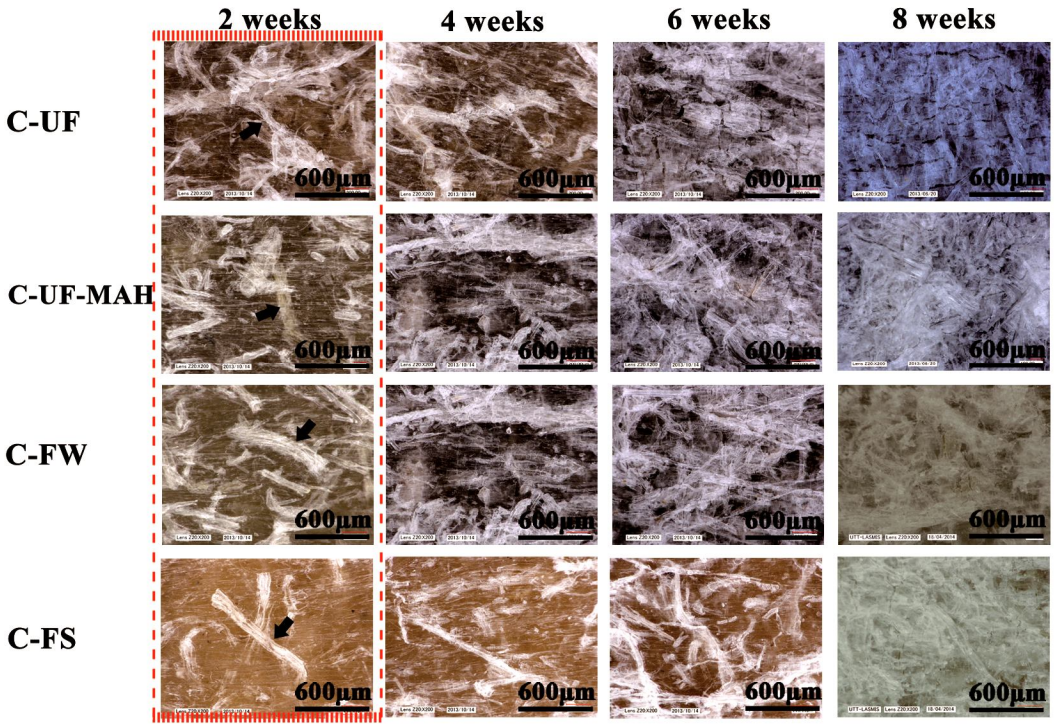


Fig. 6-18 Observation par MO numérique de la surface des composites C-UF, C-UF-MAH, C-FW et C-FS de 2 à 8 semaines sous UV

*6.4.1.3. Observations par MEB*

Les observations par MEB permettent de mieux comprendre cette dégradation par UV. Les figures 6-19 montrent comme exemple les fissures internes des fibres pour C-UF-MAH après 2 semaines sous UV.

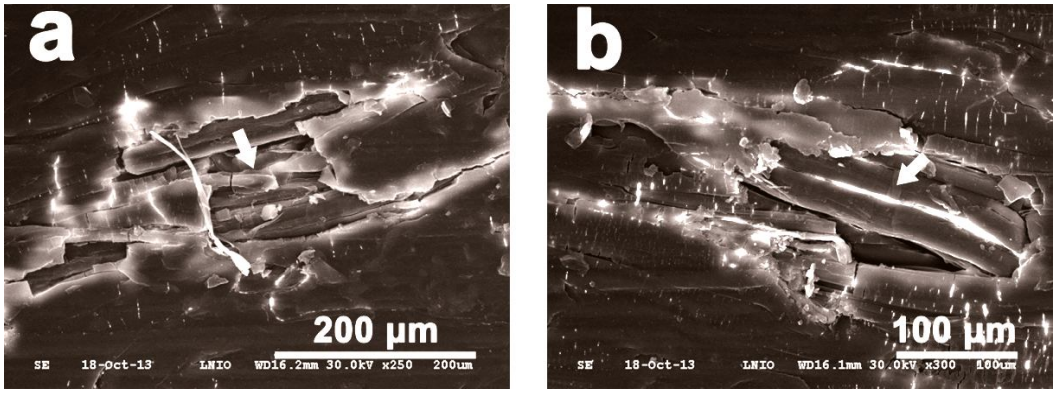


Fig. 6-19 Dégradation du PP autours des fibres, C-UF-MAH après 2 semaines sous UV

Nous pouvons constater sur les figures 6-19 que la dégradation du composite C-UF-MAH a eu lieu d'abord autour des fibres. Ce résultat correspond bien à nos observations dans les figures 6-18, montrant que la couleur du blanc crayeux apparaît d'abord autour des fibres.

La lignine, comme un constituant principal de la fibre de chanvre, absorbe plus UV/visible en raison de l'existence de deux groupes chromophores [17,18]. Elle est principalement sur la surface des fibres, couvrant les micros fibrilles de cellulose [19]. Donc, il est normal que la matrice PP autour des fibres puisse absorber plus de rayonnement que les autres régions. En outre, la dégradation des fibres durant le vieillissement produit des groupes chromophores supplémentaires et favorise donc la dégradation de PP. Le gonflement de fibres et de l'eau absorbée peuvent aussi dégrader les fibres autour de PP en raison de la réaction chimique accélérée par l'oxydation et facilitant la pénétration de la lumière [16]. Par conséquent, nous pensons que la dégradation du PP se produit initialement autour des fibres, la présence de fibres accélère la photo-dégradation du PP.

*6.4.1.4. Spectres d'UV/visible*

Les spectres d'UV/visible du film du PP (épaisseur 0,08 mm) et du C-FS (épaisseur variant de 0,10 à 0,18 mm) sont présentés dans la figure 6-20. La gamme

d'absorption d'UV du PP pur est inférieure à 250 nm. La gamme d'absorption d'UV pour les composites est plus large que celle du PP pur. La plus grande épaisseur du composite (de 0,10 mm à 0,18 mm) a une absorption plus importante. Lorsque l'épaisseur a augmenté à 0,18 mm, l'absorbance atteint au maximum à la longueur d'onde de 200 nm. Cela signifie qu'à partir de cette épaisseur, le rayonnement UV ne peut pas facilement pénétrer plus profondément à l'intérieur des composites. La présence de fibres améliore l'absorption UV et joue un rôle comme un "bouclier", ce qui empêche la pénétration du rayonnement UV à la région profonde des composites.

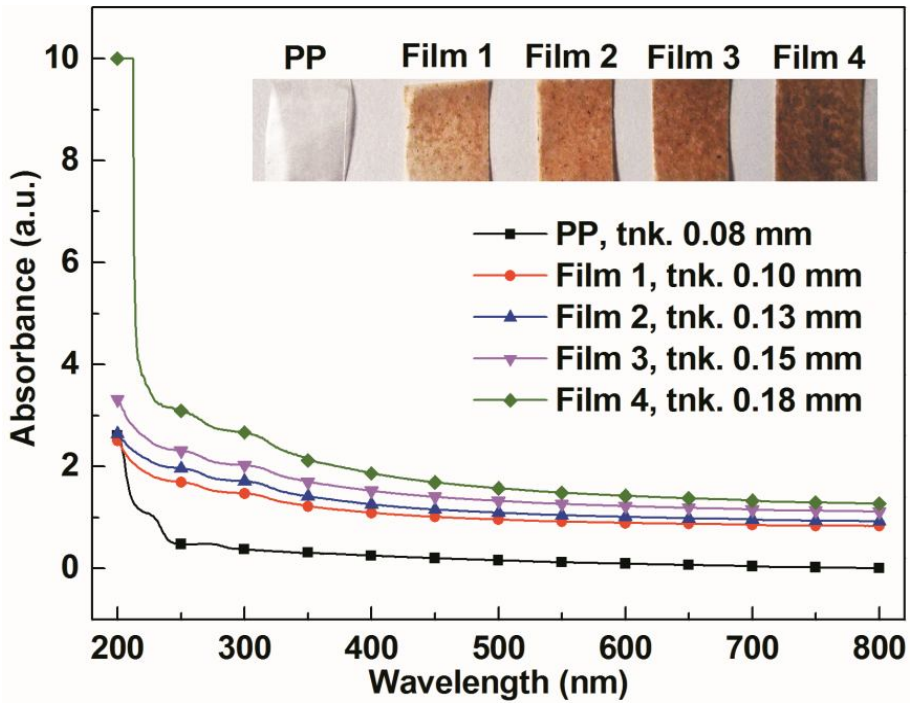


Fig. 6-20 Spectres d'UV/visible du film PP et du C-FS pour différentes épaisseurs

*6.4.1.5. Résultats des essais de traction après vieillissement UV*

Les figures 6-21 résument les résultats des propriétés mécaniques en traction des composites C-UF, C-UF-MAH, C-FW et C-FS après 8 semaines de vieillissement aux UV. Pour le module d'Young (Fig. 6-21a), il augmente jusqu'à 4 semaines et puis diminue jusqu'à 8 semaines. L'amélioration du module d'Young jusqu'à 4 semaines peut s'expliquée par le fait que sous UV, le degré de cristallinité augmente. Une autre

raison de cette diminution peut être due à la forte pression d'interface fibre/matrice grâce au gonflement des fibres. Après 4 semaines, les autres effets interviennent, comme la dégradation à l'interface, la rupture de chaîne du PP et des fibers. Par conséquent, la rigidité totale diminue.

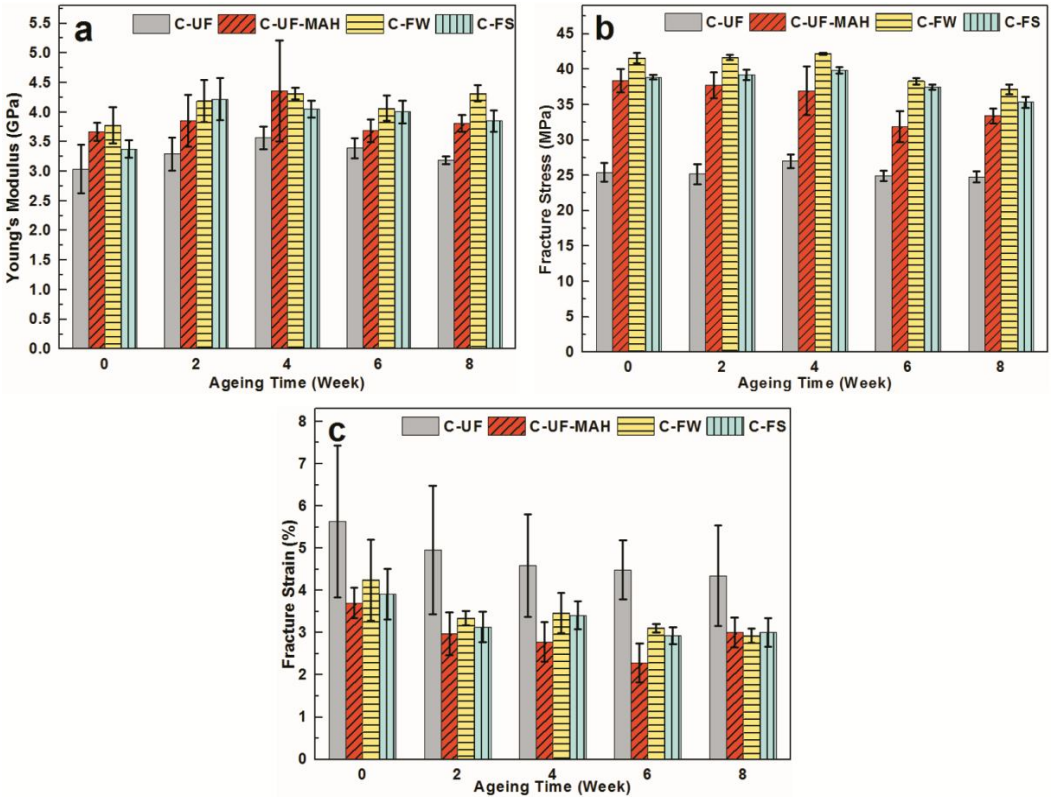


Fig. 6-21 Propriétés mécaniques des composites en traction pour C-UF, C-UF-MAH, C-C-FW et FS: (a) Module d'Young; (b), Contrainte à la rupture; (c) Déformation à la rupture

La contrainte à la rupture des composites (Fig. 6-21b) diminue progressivement en fonction du temps sous UV sauf dans le cas de C-UF, qui reste inchangée après 8 semaines du vieillissement. Lorsque l'on compare la diminution du C-UF et du C-UF-MAH, nous pouvons remarquer que la dégradation à l'interface du C-UF-MAH est une des raisons principales de la baisse des propriétés mécaniques.

Dans la figure 6-21c, après 8 semaines sous UV, le C-FW montre la plus grande perte de déformation à la rupture (31,2%). Pour les autres composites, la déformation à

la rupture diminue de 22,8 % pour le C-UF, de 18,8 % pour C-UF-MAH et de 23,0 % pour FS.

Pour conclure, l'addition de PP-g-MAH et le traitement de fibres par l'eau et par l'alcali n'ont pas une contribution évidente sur le comportement mécanique en traction lorsque ces composites sont soumis au traitement aux UV.

## 6.4.2. Effets de modification des fibers par silane sous UVs

*6.4.2.1. Résultats des essais de traction*

Les résultats de l'essai de traction sur des composites C-FS, C-PAF, C-FPAPS et C-FAPS après 8 semaines de vieillissement aux UV sont présentés dans les figures 6-22, où le composite C-FS est une référence de comparaison par rapport à trois autres composites (C-TMPS, C-FPAPS et C-FAPS) renforcés par les fibres modifiées par silane. Dans la figure 6-22a, nous pouvons voir que le module d'Young du C-FS augmente de 24,8 % pendant 2 semaines; tandis qu'au bout de 4 semaines, ce module pour le C-FMPS, C-FPAPS et C-FAPS a une augmentation maximale de 21,8 %, 22,1 % et 15,2 %, respectivement.

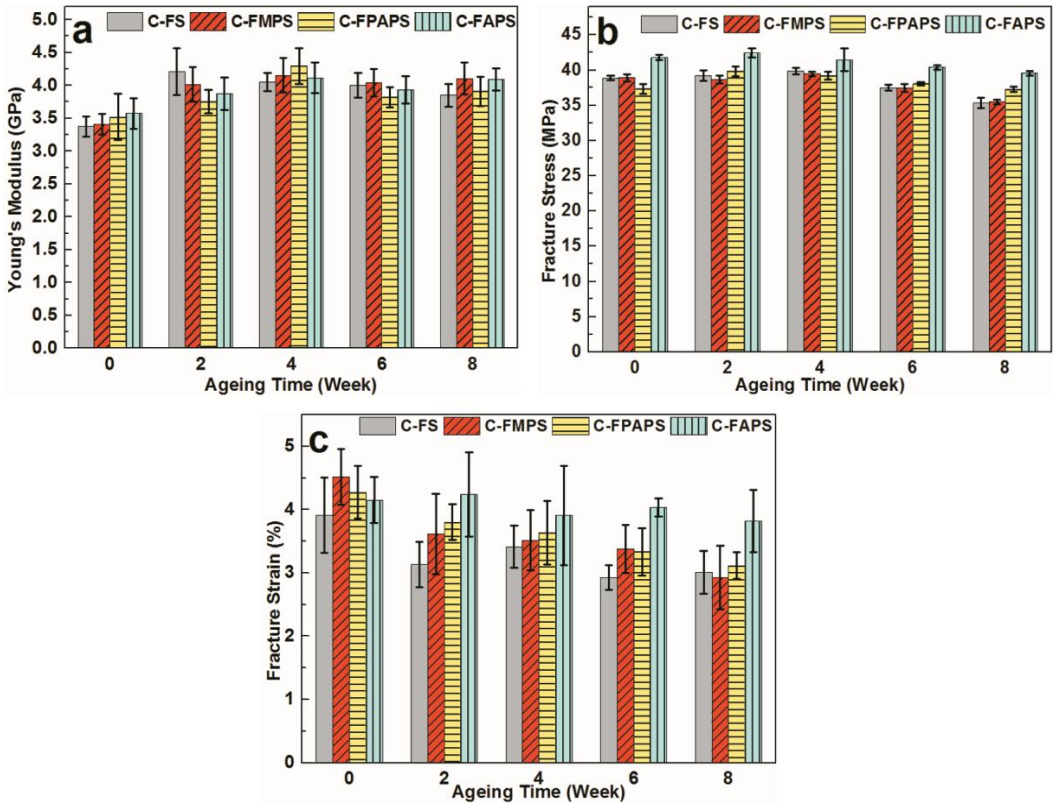


Fig. 6-22 Propriétés mécaniques des composites C-FS, C-PAF, C-FPAPS et C-FAP après 8 semaines de vieillissement UV: (a) Module d'Young; (b) Contrainte à la rupture; (c) déformation de rupture

La comparaison de contrainte à la rupture des composites est faite dans la figure 6-22b. On note qu'après 8 semaines de vieillissement aux UV, la contrainte à la rupture de C-FAPS a diminué de 5,3 %, celle du C-FS a diminué de 9,1 % et celle du C-FMPS a diminué de 8,8 %. En revanche, la contrainte à la rupture de C-FPAPS a augmenté d'abord de 6,8% après 2 semaines, et puis a diminué au bout de 8 semaines. Il semblait que le PAPS agit comme un anti-oxydant ce qui empêche dans un premier temps la diminution de la résistance, une fois cet effet est épuisé, les propriétés mécaniques des composites commencent à baisser.

Sur la figure 6-22c, la déformation à la rupture des composites a fortement diminué, sauf C-FAPS. Après 8 semaines, celle de C-FMPS a diminué de 35,2 %, plus

que celle du C-FS (23,0 %) et du C-FPAPS (27,1 %). En revanche, C-FAPS présente la plus faible baisse de 8,0 %.

Compte tenu des résultats obtenus par essais de traction, lorsque les composites sont vieillis par UV, le traitement par silane a une influence considérable sur la résistance à la diminution des propriétés en traction. Pour le C-FAPS, l'effet du vieillissement aux UV est le moins important parmi ces quatre composites.

*6.4.2.2. Spectres d'UV/visible des agents de silane*

La figure 6-23 montre les spectres d'UV/visible des trois agents de silanes: MPS, APS et PAPS. L'analyse se fait avec une solution de 5 % en Wt. On note que le PAPS a un large pic d'absorption, variant de 245 à 330 nm. Ce pic correspond à la π-π * transition de l'anneau benzénique dans le monomère d'aniline de PAPS. Après la modification des fibers, le PAPS, se situant sur la surface des fibres de C-FPAPS, peut absorber la majeure partie du rayonnement UV. Cela pourrait expliquer pourquoi la contrainte à la rupture de C-FPAPS est presque inchangée après 8 semaines du vieillissement aux UV, même si sa surface semblait plus dégradée que les autres composites.

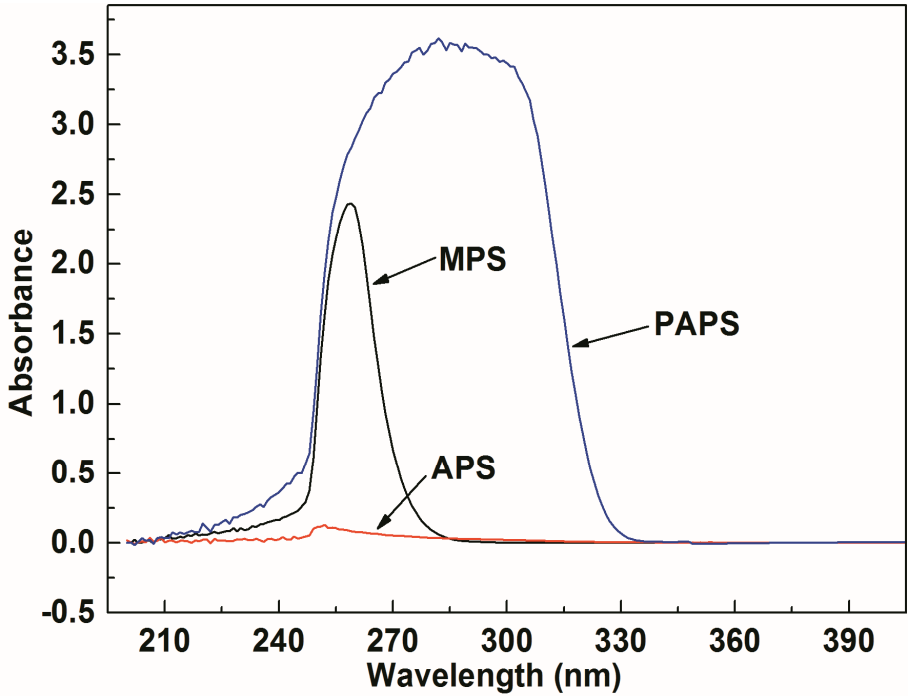


Fig. 6-23 Spectres d'UV/visible des agents de silane MPS, APS et PAPS

Dans la figure 6-23, il est clair que l'APS absorbe très peu de rayonnement UV. Cependant, selon l'analyse précédente, le groupe amino primaire -$NH_2$ d'APS peut réagir avec l'anhydride maléique attaché au PP pour former un groupe de succinimide dans le composite C-FAPS [20]. A cause de cette bonne adhérence d'interface, les propriétés mécaniques du C-FAPS sont meilleures que les trois autres composites non vieillis. Il semble que la bonne adhérence à l'interface est également favorable au retardement du vieillissement aux UV, ce qui empêche la formation de fissures dans la zone d'interface. Parmi les trois modifications (MPS, APS et PAPS), l'effet de vieillissement aux UV sur les propriétés en traction est moins important pour le composite C-FAPS.

La MPS montre un pic d'absorption à 256 nm signifiant que le rayonnement UV peut provoquer la dégradation de MPS. Les groupes radicaux générés accélèrent la dégradation à l'interface, des fibres et du PP autour. En outre, avant vieillissement aux UV, en présence des groupes d'esters et de vinyliques de MPS, la déformation à la rupture du C-FMPS est supérieure aux trois autres composites (C-FS, C-FPAPS et

C-FAPS). Pour ces raisons, la dégradation du MPS entraîne la diminution de la déformation à la rupture du C-FMPS de façon considérable que les trois autres composites.

## *6.5. Conclusions & perspectives*

Étant donné l'importance et les intérêts de recherche en cours dans ce domaine, cette thèse est principalement axée sur le traitement chimique des fibres de chanvre et sur des effets de ces traitements sur les propriétés mécaniques des composites PP renforcés.

1) Le traitement par l'alcali peut supprimer en partie l'hémicellulose et la lignine. Le traitement par l'eau élimine efficacement les polysaccharides existants sur la surface des fibres, sans endommager leur structure. En raison de la surface lisse et d'une structure intacte des fibres après le traitement par l'eau, les propriétés mécaniques des composites renforcés par ces fibres sont nettement améliorées. En revanche, nous n'avons pas remarqué le même effet pour les composites renforcés par des fibres non traitées et traitées par alcali.

2) La modification par l'agent de silane a une grande influence sur les propriétés mécaniques des composites dépendant de la structure du groupe fonctionnel du silane. Comme l'amine primaire d'APS peut réagir avec l'anhydride maléique et former une liaison covalente, la contrainte à la rupture du composite renforcée par des fibers modifié par APS est améliorée par rapport à d'autres matériaux composites. Par contre, la modification des fibers par PAPS a une incompatibilité entre l'aniline et le propylène, cette modification diminue donc la contrainte à la rupture des composites. L'existence des groupes esters et vinyliques de MPS peut provoquer l'augmentation de la déformation à la rupture des composites.

3) Pour le vieillissement à humidité, les propriétés mécaniques des composites ont augmenté dès le début du vieillissement à cause de la pression d'interface due au gonflement des fibres. Cependant, l'eau absorbée provoque la dégradation tant sur l'interface que sur la structure des fibres, ce qui a pour effet de diminuer les propriétés

mécaniques des composites. La forte adhérence d'interface permet de retarder efficacement la diminution des propriétés mécaniques par l'inhibition de l'absorption d'eau des composites. L'ajout de PP-g-MAH empêche plus la pénétration d'eau dans les composites. Le traitement des fibres par l'eau, l'alcali et le silane peut retarder efficacement la dégradation des propriétés mécaniques et améliorer la stabilité dimensionnelle des composites.

4) Pour le vieillissement en température, l'effet de température sur les propriétés mécaniques des composites est similaire à celui de l'humidité, mais moins important par rapport au vieillissement à humidité.

5) Pour le vieillissement aux UV, le blanchiment et les micros fissures se produisent d'abord sur la surface de composites autour des fibres. La présence de fibres accélère la dégradation de PP autour d'elles, mais empêche plus ou moins la dégradation à l'intérieur du composite. L'utilisation d'eau ou d'alcali pour traiter les fibres pourrait retarder la dégradation des composites. Cependant, ces traitements n'ont pas de l'effet évident sur la résistance en traction.

6) L'agent de silane a des effets importants sur la résistance à la dégradation par UV grâce à sa structure et à sa compatibilité avec la matrice de polymère. Dans l'ensemble, grâce à la bonne cohésion à l'interface, les composites renforcés par les fibres modifiées par APS montrent une dégradation plus lente que celui renforcé par des fibres modifiées par MPS ou PAPS. Le monomère d'aniline dans PAPS absorbe fortement le rayonnement UV, ce qui est favorable à la protection des composites. De ce fait, la dégradation à l'interface des composites est limitée et la contrainte à la rupture reste inchangée après 8 semaines de vieillissement aux UV. Les composites renforcés par les fibres modifiées par MPS ont une plus grande diminution de la déformation à la rupture à cause de la dégradation de MPS par l'UV.

Dans cette thèse, nous avons utilisé de l'eau, de l'alcali et trois agents de silane pour traiter les fibres de chanvre. Les effets de ces traitements sur les fibres et les

composites renforcés ont été étudiés. A court et à long terme, de nombreux travaux peuvent être effectués:

1. La cristallisation à l'interface des composites après le traitement des fibres par eau, alcali et silane doit être étudiée. En particulier pour le traitement de l'APS, la réaction de l'APS avec l'anhydride maléique de PP-g-MAH doit également donner plus d'informations sur la cristallisation d'interface du composite C-TAPS.

2. Pour calculer le gonflement des composites renforcés par les fibres végétales, il est nécessaire de développer un modèle soit analytique soit numérique selon la mécanique de l'interface.

3. Pour la dégradation par l'UV, nos études ne sont focalisées que sur la surface des composites. La dégradation à différentes profondeurs devrait être étudiée sur différents composites.

4. Le mécanisme de la dégradation des composites par l'UV devrait être étudié de façon approfondie. Par exemple, la dégradation par l'UV se produit d'abord dans la fibre ou dans la matrice ? Quels sont les effets de l'absorption d'eau dans les composites lors du vieillissement aux UV ? L'agent d'anti-UV ou le stabilisant doit agir sur les fibres ou sur matrice polymère ?

5. Le caractère hydrophile des fibres végétales est l'un des grands inconvénients pour ces composites. Pour améliorer cela, il est nécessaire de développer les autres traitements des fibres plus efficaces et plus écologiques, surtout sans dégradation de la structure physique des fibres.

## *Références*

[1] P. Wambua, J. Ivens, I. Verpoest. Natural fibres: can they replace glass in fibre reinforced plastics? *Composites Science and Technology,* 63:1259-1264, 2003.

[2] H. Hargitai, I. Rácz, R.D. Anandjiwala. Development of HEMP Fiber Reinforced Polypropylene Composites. *Journal of Thermoplastic Composite Materials,* 21:165-174, 2008.

[3] O. Faruk, A.K. Bledzki, H.-P. Fink, M. Sain. Biocomposites reinforced with natural fibers: 2000–2010. *Progress in Polymer Science,* 37:1552-1596, 2012.

[4] J.W. Kaczmar, J. Pach, C. Burgstaller. The chemically treated hemp fibres to reinforce polymers. *Polimery,* 56:817-822, 2011.

[5] Sangappa, B.L. Rao, S. Asha, R. Somashekar, in: A.K. Chauhan, C. Murli, S.C. Gadkari (Eds.), Solid State Physics, Vol 57, Amer Inst Physics, Melville, 2013, pp. 586-587.

[6] N. Lu, S.M. Bhogaiah, I. Ferguson, in: J.L. Bu, Z.Y. Jiang, S. Jiao (Eds.), Advanced Materials, Pts 1-3, Trans Tech Publications Ltd, Stafa-Zurich, 2012, pp. 666-670.

[7] Sangappa, B.L. Rao, S. Asha, R.M. Kumar, R. Somashekar. Physical, chemical, and surface properties of alkali-treated Indian hemp fibers. *Composite Interfaces,* 21:153-159, 2014.

[8] M.S. Islam, K.L. Pickering, N.J. Foreman. Influence of alkali treatment on the interfacial and physico-mechanical properties of industrial hemp fibre reinforced polylactic acid composites. *Composites Part a-Applied Science and Manufacturing,* 41:596-603, 2010.

[9] H.L. Liu, L.L. You, H.B. Jin, W.D. Yu. Influence of alkali treatment on the structure and properties of hemp fibers. *Fibers and Polymers,* 14:389-395, 2013.

[10] M.M. Kabir, H. Wang, K.T. Lau, F. Cardona. Chemical treatments on plant-based natural fibre reinforced polymer composites: An overview. *Composites Part B: Engineering,* 43:2883-2892, 2012.

[11] L.Y. Mwaikambo, M.P. Ansell. Mechanical properties of alkali treated plant fibres and their potential as reinforcement materials. I. hemp fibres. *Journal of Materials Science,* 41:2483-2496, 2006.

[12] M.M. Kabir, H. Wang, K.T. Lau, F. Cardona. Effects of chemical treatments on hemp fibre structure. *Applied Surface Science,* 276:13-23, 2013.

[13] M. Le Troedec, D. Sedan, C. Peyratout, J.P. Bonnet, A. Smith, R. Guinebretiere, V. Gloaguen, P. Krausz. Influence of various chemical treatments on the composition and structure of hemp fibres. *Composites Part A: Applied Science and Manufacturing,* 39:514-522, 2008.

[14] J.W. Kaczmar, J. Pach, C. Burgstaller. The chemically treated hemp fibres to reinforce polymers. *Polimery/Polymers,* 56:817-822, 2011.

[15] N. Nosbi, H.M. Akil, Z.A.M. Ishak, A.A. Bakar. Effect of water absorption on the mechanical properties of pultruded Kenaf fibre reinforced polyester composites. *Advanced Composites Letters,* 20:21-26, 2011.

[16] N.M. Stark. Effect of weathering cycle and manufacturing method on performance of wood flour and high-density polyethylene composites. *Journal of Applied Polymer Science,* 100:3131-3140, 2006.

[17] B. George, E. Suttie, A. Merlin, X. Deglise. Photodegradation and photostabilisation of wood – the state of the art. *Polymer Degradation and Stability,* 88:268-274, 2005.

[18] M.I. Popa, S. Pernevan, C. Sirghie, I. Spiridon, D. Chambre, D.M. Copolovici, N. Popa. Mechanical Properties and Weathering Behavior of Polypropylene-Hemp Shives Composites. *Journal of Chemistry,* 2013:8, 2013.

[19] L.Y. Mwaikambo, M.P. Ansell. Chemical modification of hemp, sisal, jute, and kapok fibers by alkalization. *Journal of Applied Polymer Science,* 84:2222-2234, 2002.

[20] H.C. Han, X.L. Gong, Effect of fiber surface modification with different functional groups silane agents on mechanical properties of hemps/polypropylene composites, Beijing, 2014, 23-26.

# References

# References

[1] Wambua P, Ivens J, Verpoest I. Natural fibres: can they replace glass in fibre reinforced plastics? Compos Sci Technol. 2003;63:1259-64.

[2] Duval A, Bourmaud A, Augier L, Baley C. Influence of the sampling area of the stem on the mechanical properties of hemp fibers. Mater Lett. 2011;65:797-800.

[3] Hargitai H, Rácz I, Anandjiwala RD. Development of HEMP Fiber Reinforced Polypropylene Composites. J Thermoplast Compos Mater. 2008;21:165-74.

[4] Kraessig H. Cellulose chemistry and its applications, T. P. Nevell and S. H. Zeronian, Eds., Halsted Press, John Wiley, New York, 1985, 552 pp. Journal of Polymer Science Part C: Polymer Letters. 1987;25:87-8.

[5] Guido DB, Vincenzo F, Antonino V. Natural fiber-reinforced composites. Fiber-Reinforced Composites: Nova Science Publishers, Inc.; 2012. p. 57-89.

[6] Thomas S, Paul SA, Pothan LA, Deepa B. Natural Fibres: Structure, Properties and Applications. In: Kalia S, Kaith BS, Kaur I, editors. Cellulose Fibers: Bio- and Nano-Polymer Composites: Springer Berlin Heidelberg; 2011. p. 3-42.

[7] Rong MZ, Zhang MQ, Liu Y, Yang GC, Zeng HM. The effect of fiber treatment on the mechanical properties of unidirectional sisal-reinforced epoxy composites. Compos Sci Technol. 2001;61:1437-47.

[8] Kabir MM, Wang H, Lau KT, Cardona F. Effects of chemical treatments on hemp fibre structure. Appl Surf Sci. 2013;276:13-23.

[9] Monteiro S, Lopes F, Barbosa A, Bevitori A, Silva I, Costa L. Natural Lignocellulosic Fibers as Engineering Materials—An Overview. MMTA. 2011;42:2963-74.

[10] Genet M, Stokes A, Salin F, Mickovski S, Fourcaud T, Dumail J-F, et al. The influence of cellulose content on tensile strength in tree roots. In: Stokes A, Spanos I, Norris J, Cammeraat E, editors. Eco-and Ground Bio-Engineering: The Use of Vegetation to Improve Slope Stability: Springer Netherlands; 2007. p. 3-11.

[11] Shelat BR, Radhakrishnan T, Iyer BV. The Relation between Crystallite Orientation and Mechanical Properties of Mercerized Cottons. Textile Research Journal. 1960;30:836-42.

[12] Dai D, Fan M, Huang B, Chen X, Tang L, Li S. Investigation of the effect mechanism of dislocations on natural fibres mechanical properties. Transactions of the Chinese Society of Agricultural Engineering. 2011;27:180-5.

[13] Tripathy AC. Effect of drying methods on the Physical and structural changes in Oil-Seed Flax Fiber. SAE Int J Commer Veh. 2010;3:284-97.

[14] Mukhopadhyay S, Fangueiro R. Physical modification of natural fibers and thermoplastic films for composites - A review. J Thermoplast Compos Mater. 2009;22:135-62.

[15] Moghe VV, Nabar PS. Bio scouring: An ecological way of scouring. Colourage. 2006;53:95-6.

[16] Montane D, Farriol X, Salvadó J, Jollez P, Chornet E. Application of steam explosion to the fractionation and rapid vapor-phase alkaline pulping of wheat straw. Biomass Bioenergy. 1998;14:261-76.

[17] Focher B, Marzetti A, Beltrame PL, Avella M. Steam exploded biomass for the preparation of conventional and advanced biopolymer-based materials. Biomass Bioenergy. 1998;14:187-94.

[18] Zhang Y, Xie J, Jiang Y. Study on division of natural bamboo fibers by steam explosion. 3rd International Conference on Manufacturing Science and Engineering, ICMSE 2012. Xiamen2012. p. 1873-6.

[19] Law KN, Valade JL, Yang KC. Fibre development in thermomechanical pulping: Comparison between black spruce and jack pine. J Pulp Pap Sci. 1998;24:73-6.

[20] Bledzki AK, Faruk O, Specht K. Influence of separation and processing systems on morphology and mechanical properties of hemp and wood fibre reinforced polypropylene composites. J Nat Fibers. 2007;4:37-56.

[21] Kato K, Vasilets VN, Fursa MN, Meguro M, Ikada Y, Nakamae K. Surface Oxidation of Cellulose Fibers by Vacuum Ultraviolet Irradiation. J Polym Sci Part A. 1999;37:357-61.

[22] Rahman GMS, Mamun MAA, Khan MA. Effect of γ (Gamma)-radiation on the physico-mechanical properties of grafted jute fabric reinforced polypropylene (PP) composites. Fibers and Polymers. 2014;15:340-6.

[23] Khan MA, Haque N, Al-Kafi A, Alam MN, Abedin MZ. Jute reinforced polymer composite by gamma radiation: Effect of surface treatment with UV radiation. Polym Plast Technol Eng. 2006;45:607-13.

[24] Wang Q, Fan XR, Cui L, Wang P, Wu J, Chen J. Plasma-aided cotton bioscouring: Dielectric barrier discharge versus low-pressure oxygen plasma. Plasma Chem Plasma Process. 2009;29:399-409.

[25] Korkmaz S, Oksuz L, Helhel S. Results of dielectric barrier discharge (DBD) on wool and cotton. AIChE Annual Meeting, Conference Proceedings2004. p. 1643.

[26] Borcia G, Anderson CA, Brown NMD. Surface treatment of natural and synthetic textiles using a dielectric barrier discharge. Surf Coat Technol. 2006;201:3074-81.

[27] Botaro VR, Dos Santos CG, Arantes Júnior G, Da Costa AR. Chemical modification of lignocellulosic materials by irradiation with Nd-YAG pulsed laser. Appl Surf Sci. 2001;183:120-5.

[28] Bahners T, Kesting W, Schollmeyer E. Designing surface properties of textile fibers by UV-laser irradiation. Appl Surf Sci. 1993;69:12-5.

[29] Rechmann P, Sadegh HM, Goldin DS, Hennig T. Surface changes of implants after laser irradiation. Proc SPIE Int Soc Opt Eng. 1999;3593:102-9.

[30] Kalia S, Kaith BS, Kaur I. Pretreatments of natural fibers and their application as reinforcing material in polymer composites-a review. Polym Eng Sci. 2009;49:1253-72.

[31] Ragoubi M, Bienaimé D, Molina S, George B, Merlin A. Impact of corona treated hemp fibres onto mechanical properties of polypropylene composites made thereof. Industrial Crops and Products. 2010;31:344-9.

[32] Belgacem MN, Bataille P, Sapieha S. Effect of corona modification on the mechanical properties of polypropylene/cellulose composites. J Appl Polym Sci. 1994;53:379-85.

[33] Sawatari A, Nakamura H. Analysis of the Functional Groups Formed on the Corona-Treated Cellulose Fibre Sheet Surface by Means of Chemical Modification in Liquid Phase-ESCA Technique. Sen'i Gakkaishi. 1993;49:279-86.

[34] Sahin HT, Manolache S, Young RA, Denes F. Surface fluorination of paper in CF4-RF plasma environments. Cellu. 2002;9:171-81.

[35] Zhou Z, Liu X, Hu B, Wang J, Xin D, Wang Z, et al. Hydrophobic surface modification of ramie fibers with ethanol pretreatment and atmospheric pressure plasma treatment. Surf Coat Technol. 2011;205:4205-10.

[36] Gassan J, Gutowski VS. Effects of corona discharge and UV treatment on the properties of jute-fibre expoxy composites. Compos Sci Technol. 2000;60:2857-63.

[37] Uehara T, Sakata I. Effect of corona discharge treatment on cellulose prepared from beech wood. J Appl Polym Sci. 1990;41:1695-706.

[38] Kabir MM, Wang H, Lau KT, Cardona F. Chemical treatments on plant-based natural fibre reinforced polymer composites: An overview. Composites Part B: Engineering. 2012;43:2883-92.

[39] Kaczmar JW, Pach J, Burgstaller C. The chemically treated hemp fibres to reinforce polymers. Polimery. 2011;56:817-22.

[40] Le Troedec M, Sedan D, Peyratout C, Bonnet JP, Smith A, Guinebretiere R, et al. Influence of various chemical treatments on the composition and structure of hemp fibres. Composites Part A. 2008;39:514-22.

[41] Belgacem MN, Gandini A. The surface modification of cellulose fibres for use as reinforcing elements in composite materials. Compos Interfaces. 2005;12:41-75.

[42] Gassan J, Bledzki AK. Alkali treatment of jute fibers: Relationship between structure and mechanical properties. J Appl Polym Sci. 1999;71:623-9.

[43] Mwaikambo LY, Ansell MP. Chemical modification of hemp, sisal, jute, and kapok fibers by alkalization. J Appl Polym Sci. 2002;84:2222-34.

[44] Huang WY, Zhao M, Zhu HZ, Zhou X. Structure of ramie treated by liquid ammonia. J Donghua Univ. 2006;23:103-7.

[45] Pejic BM, Kostic MM, Skundric PD, Praskalo JZ. The effects of hemicelluloses and lignin removal on water uptake behavior of hemp fibers. Bioresour Technol. 2008;99:7152-9.

[46] Muensri P, Kunanopparat T, Menut P, Siriwattanayotin S. Effect of lignin removal on the properties of coconut coir fiber/wheat gluten biocomposite. Composites Part A. 2011;42:173-9.

[47] Khan MA, Hassan MM, Taslima R, Mustafa AI. Role of pretreatment with potassium permanganate and urea on mechanical and degradable properties of photocured coir (cocos nucifera) fiber with 1,6-hexanediol diacrylate. J Appl Polym Sci. 2006;100:4361-8.

[48] Xie Y, Hill CaS, Xiao Z, Militz H, Mai C. Silane coupling agents used for natural fiber/polymer composites: A review. Composites Part A. 2010;41:806-19.

[49] Bledzki AK, Mamun AA, Lucka-Gabor M, Gutowski VS. The effects of acetylation on properties of flax fibre and its polypropylene composites. Express Polymer Letters. 2008;2:413-22.

[50] Tserki V, Zafeiropoulos NE, Simon F, Panayiotou C. A study of the effect of acetylation and propionylation surface treatments on natural fibres. Compos Part A Appl Sci Manuf. 2005;36:1110-8.

[51] Bledzki AK, Gassan J. Composites reinforced with cellulose based fibres. Prog Polym Sci (Oxford). 1999;24:221-74.

[52] Khalil HPSA, Ismail H, Rozman HD, Ahmad MN. Effect of acetylation on interfacial shear strength between plant fibres and various matrices. Eur Polym J. 2001;37:1037-45.

[53] Singha AS, Rana AK. Kinetics of graft copolymerization of acrylic acid onto cannabis indica fibre. Iran Polym J Eng Ed. 2011;20:913-29.

[54] Xiao C, Wu L, Ren S. Studies on graft copolymerization of acrylic acid onto ramie fibers with chromic acid initiation system. Wuhan Univ J Nat Sci. 1998;3:359-65.

[55] Gironès J, Pimenta MTB, Vilaseca F, de Carvalho AJF, Mutjé P, Curvelo AAS. Blocked isocyanates as coupling agents for cellulose-based composites. Carbohydr Polym. 2007;68:537-43.

[56] Tonoli GHD, Mendes RF, Siqueira G, Bras J, Belgacem MN, Savastano Jr H. Isocyanate-treated cellulose pulp and its effect on the alkali resistance and performance of fiber cement composites. Holz. 2013;67:853-61.

[57] Karmarkar A, Chauhan SS, Modak JM, Chanda M. Mechanical properties of wood-fiber reinforced polypropylene composites: Effect of a novel compatibilizer with isocyanate functional group. Composites Part A. 2007;38:227-33.

[58] Kiattipanich N, Kreua-ongarjnukool N, Pongpayoon T, Phalakornkule C. Properties of polypropylene composites reinforced with stearic acid treated sugarcane fiber. J Polym Eng. 2007;27:411-28.

[59] Torres FG, Cubillas ML. Study of the interfacial properties of natural fibre reinforced polyethylene. Polym Test. 2005;24:694-8.

[60] Zhang Q, Shi L, Nie J, Wang H, Yang D. Study on poly(lactic acid)/natural fibers composites. J Appl Polym Sci. 2012;125:E526-E33.

[61] Corrales F, Vilaseca F, Llop M, Gironès J, Méndez JA, Mutjè P. Chemical modification of jute fibers for the production of green-composites. J Hazard Mater. 2007;144:730-5.

[62] Kalia S, Kaushik VK, Sharma RK. Effect of benzoylation and graft copolymerization on morphology, thermal stability, and crystallinity of sisal fibers. J Nat Fibers. 2011;8:27-38.

[63] Thiruchitrambalam M, Shanmugam D. Influence of pre-treatments on the mechanical properties of palmyra palm leaf stalk fiber-polyester composites. J Reinf Plast Compos. 2012;31:1400-14.

[64] Ghasemi I, Farsi M. Interfacial behaviour of wood plastic composite: Effect of chemical treatment on wood fibres. Iran Polym J Eng Ed. 2010;19:811-8.

[65] Manaila E, Stelescu MD, Craciun G, Surdu L. Effects of benzoyl peroxide on some properties of composites based on hemp and natural rubber. Polym Bull. 2014;71:2001-22.

[66] Lopattananon N, Panawarangkul K, Sahakaro K, Ellis B. Performance of pineapple leaf fiber-natural rubber composites: The effect of fiber surface treatments. J Appl Polym Sci. 2006;102:1974-84.

[67] Wang B, Panigrahi S, Tabil L, Crerar W. Pre-treatment of flax fibers for use in rotationally molded biocomposites. J Reinf Plast Compos. 2007;26:447-63.

[68] Mishra S, Naik JB, Patil YP. Compatibilizing effect of maleic anhydride on swelling and mechanical properties of plant-fiber-reinforced novolac composites. Compos Sci Technol. 2000;60:1729-35.

[69] López Manchado MA, Arroyo M, Biagiotti J, Kenny JM. Enhancement of Mechanical Properties and Interfacial Adhesion of PP/EPDM/Flax Fiber Composites Using Maleic Anhydride as a Compatibilizer. J Appl Polym Sci. 2003;90:2170-8.

[70] Naik JB, Mishra S. Esterification effect of maleic anhydride on swelling properties of natural fiber/high density polyethylene composites. J Appl Polym Sci. 2007;106:2571-4.

[71] Fuqua MA, Ulven CA. Characterization of polypropylene/corn fiber composites with maleic anhydride grafted polypropylene. Journal of Biobased Materials and Bioenergy. 2008;2:258-63.

[72] Sombatsompop N, Yotinwattanakumtorn C, Thongpin C. Influence of type and concentration of maleic anhydride grafted polypropylene and impact modifiers on mechanical properties of PP/wood sawdust composites. J Appl Polym Sci. 2005;97:475-84.

[73] Park JM, Quang ST, Hwang BS, DeVries KL. Interfacial evaluation of modified Jute and Hemp fibers/polypropylene (PP)-maleic anhydride polypropylene copolymers (PP-MAPP) composites using micromechanical technique and nondestructive acoustic emission. Compos Sci Technol. 2006;66:2686-99.

[74] Pothan LA, Bellman C, Kailas L, Thomas S. Influence of chemical treatments on the electrokinetic properties of cellulose fibres. J Adhes Sci Technol. 2002;16:157-78.

[75] Gulati D, Sain M. Fungal-modification of natural fibers: A novel method of treating natural fibers for composite reinforcement. J Polym Environ. 2006;14:347-52.

[76] Pickerinq KL, Li Y, Farrell RL. Fungal and alkali interfacial modification of hemp fibre reinforced composites. Key Eng Mater2007. p. 493-6.

[77] Kalia S, Sheoran R. Modification of ramie fibers using microwaveassisted grafting and cellulase enzyme-assisted biopolishing: A comparative study of morphology, thermal stability, and crystallinity. Int J Polym Anal Charact. 2011;16:307-18.

[78] Kalia S, Sheoran R, Mittal H, Kumar A. Surface modification of ramie fibers using microwave assisted graft copolymerization followed by brevibacillus parabrevis pretreatment. Adv Mater Lett. 2013;4:742-8.

[79] Montazer M, Ghayem Asghari MS, Pakdel E. Electrical conductivity of single walled and multiwalled carbon nanotube containing wool fibers. J Appl Polym Sci. 2011;121:3353-8.

[80] Xue P, Park KH, Tao XM, Chen W, Cheng XY. Electrically conductive yarns based on PVA/carbon nanotubes. Compos Struct. 2007;78:271-7.

[81] Johnston JH, Kelly FM, Moraes J, Borrmann T, Flynn D. Conducting polymer composites with cellulose and protein fibres. CAP. 2006;6:587-90.

[82] Rubacha M. Magnetically active composite cellulose fibers. J Appl Polym Sci. 2006;101:1529-34.

[83] Jonoobi M, Harun J, Tahir PM, Shakeri A, SaifulAzry S, Makinejad MD. Physicochemical characterization of pulp and nanofibers from kenaf stem. Mater Lett. 2011;65:1098-100.

[84] Jonoobi M, Niska KO, Harun J, Misra M. Chemical composition, crystallinity, and thermal degradation of bleached and unbleached kenaf bast (Hibiscus cannabinus) pulp and nanofibers. BioResources. 2009;4:626-39.

[85] Han G, Qu L, Guo X. Characterization of hemp fiber using microwave-assisted extraction(MAE) pretreatment. 2010 International Conference on Advances in Materials and Manufacturing Processes, ICAMMP 2010. Shenzhen2011. p. 1594-9.

[86] Hermanutz F, Ingildeev D, Buchmeiser MR. Cellulosic fibres with new properties based on ionic liquid technology. 2012 Spring Conference of the Fiber Society. St. Gallen: Fiber Society; 2012.

[87] Meng Z, Zheng X, Tang K, Liu J, Qin S. Dissolution of natural polymers in ionic liquids: A review. E-Polymers. 2012.

[88] Haverhals LM, Foley MP, Brown EK, Fox DM, De Long HC, Trulove PC. Natural fiber welding: Ionic liquid facilitated biopolymer mobilization and reorganization. ACS Symp Ser: American Chemical Society; 2012. p. 145-66.

[89] Rahatekar SS, Rasheed A, Jain R, Zammarano M, Koziol KK, Windle AH, et al. Processing of natural fibers nanocomposites using ionic liquids. Molten Salts and Ionic Liquids 16 - 214th ECS Meeting. 49 ed. Honolulu, HI2008. p. 119-27.

[90] Haris MY, Laila D, Zainudin ES, Mustapha F, Zahari R, Halim Z. Preliminary review of biocomposites materials for aircraft radome application. 8th International Conference on Composite Science and Technology, ICCST8. Kuala Lumpur2011. p. 563-7.

[91] Huber T, Müssig J, Curnow O, Pang S, Bickerton S, Staiger MP. A critical review of all-cellulose composites. JMatS. 2012;47:1171-86.

[92] Soykeabkaew N, Sian C, Gea S, Nishino T, Peijs T. All-cellulose nanocomposites by surface selective dissolution of bacterial cellulose. Cellu. 2009;16:435-44.

[93] Haq M, Burgueño R, Mohanty AK, Misra M. Hybrid bio-based composites from blends of unsaturated polyester and soybean oil reinforced with nanoclay and natural fibers. Compos Sci Technol. 2008;68:3344-51.

[94] Kumar V, Kumar R. Improved mechanical and thermal properties of bamboo-epoxy nanocomposites. Polym Compos. 2012;33:362-70.

[95] Rajini N, Jappes JTW, Rajakarunakaran S, Jeyaraj P. Mechanical and free vibration properties of montmorillonite clay dispersed with naturally woven coconut sheath composite. J Reinf Plast Compos. 2012;31:1364-76.

[96] Kaiser MR, Anuar H, Razak SBA. Improvement in thermomechanical properties of injection molded nano-modified hybrid biocomposite. J Thermoplast Compos Mater. 2014;27:992-1009.

[97] Burgueño R, Haq M, Mohanty AK, Misra M. Hybrid bio-based composites from nano-reinforced bio-petro polymer blends and natural fibers. 7th Annual

Automotive Composites Conference and Exhibition, ACCE 2007 - Driving Performance and Productivity. Troy, MI2007. p. 32-40.

[98] Da Silva LJ, Panzera TH, Velloso VR, Christoforo AL, Scarpa F. Hybrid polymeric composites reinforced with sisal fibres and silica microparticles. Composites Part B: Engineering. 2012;43:3436-44.

[99] Hapuarachchi TD, Peijs T. Multiwalled carbon nanotubes and sepiolite nanoclays as flame retardants for polylactide and its natural fibre reinforced composites. Composites Part A. 2010;41:954-63.

[100] Chen CZ, Li Y, Xu J. Creep and dynamic mechanical behavior of natural fiber/functionalized carbon nanotubes modified epoxy composites. 18th International Conference on Composites Materials, ICCM 2011. Jeju2011.

[101] Ayub M, Nor M, Fouladi M, Zulkifli R, Amin N. A practical acoustical absorption analysis of coir fiber based on rigid frame modeling. APhy. 2012;58:246-55.

[102] Nor MJM, Jamaludin N, Tamiri FM. A preliminary study of sound absorption using multi-layer coconut coir fibers. Electronic Journal Technical Acoustics. 2004;3:1-8.

[103] Zulkifh R, Nor MM, Tahir MM, Ismail A, Nuawi M. Acoustic properties of multi-layer coir fibres sound absorption panel. J Appl Sci. 2008;8:3709-14.

[104] Manfredi LB, Rodríguez E, Wladyka-Przybylak M, Vázquez A. Thermal Properties and Fire Resistance of Jute-Reinforced Composites. Compos Interfaces. 2010;17:663-75.

[105] Manfredi LB, Rodríguez ES, Wladyka-Przybylak M, Vázquez A. Thermal degradation and fire resistance of unsaturated polyester, modified acrylic resins and their composites with natural fibres. Polym Degrad Stab. 2006;91:255-61.

[106] Naughton A, Fan M, Bregulla J. Fire resistance characterisation of hemp fibre reinforced polyester composites for use in the construction industry. Composites Part B: Engineering. 2014;60:546-54.

[107] Zawawi NA, Ismail A, Abdan K, Mahdi MA. Investigation on the microwave properties of kenaf and rice-husk fiber reinforced pla composite utilizing one-port coaxial transmission line reflection method. 8th International Conference on Composite Science and Technology, ICCST8. Kuala Lumpur2011. p. 868-73.

[108] Law TT, Ishak ZAM. Water absorption and dimensional stability of short kenaf fiber-filled polypropylene composites treated with maleated polypropylene. J Appl Polym Sci. 2011;120:563-72.

[109] Ku H, Wang H, Pattarachaiyakoop N, Trada M. A review on the tensile properties of natural fiber reinforced polymer composites. Composites Part B: Engineering. 2011;42:856-73.

[110] Nosbi N, Akil HM, Ishak ZAM, Bakar AA. Effect of water absorption on the mechanical properties of pultruded Kenaf fibre reinforced polyester composites. AdvCompos Lett. 2011;20:21-6.

[111] Pflug G, Koine A. Preparation of heat stabilized and strengthened cellulose fibers by hot pressing, lamination, and injection molding, useful for polyolefin matrix composites. Google Patents; 2001.

[112] Sawpan MA, Pickering KL, Fernyhough A. Effect of various chemical treatments on the fibre structure and tensile properties of industrial hemp fibres. Composites Part A. 2011;42:888-95.

[113] Fang H, Zhang Y, Deng J, Rodrigue D. Effect of fiber treatment on the water absorption and mechanical properties of hemp fiber/polyethylene composites. J Appl Polym Sci. 2013;127:942-9.

[114] Mohd Nazarudin Z, Mohd Ariff J, Masitah AK, Othman NS, Maizatulnisa O, Syaidatul Hazira MN, et al. The effect of alkaline treatment on water absorption and tensile properties of non-woven kenaf polyester composite. Advanced Materials Research. 2013;812:258-62.

[115] Sangappa, Rao BL, Asha S, Somashekar R. Effect of Alkali Treatment on the Physical and Surface Properties of Indian hemp Fibers. In: Chauhan AK, Murli C, Gadkari SC, editors. Solid State Physics, Vol 57. Melville: Amer Inst Physics; 2013. p. 586-7.

[116] George B, Suttie E, Merlin A, Deglise X. Photodegradation and photostabilisation of wood – the state of the art. Polym Degrad Stab. 2005;88:268-74.

[117] Joseph PV, Rabello MS, Mattoso LHC, Joseph K, Thomas S. Environmental effects on the degradation behaviour of sisal fibre reinforced polypropylene composites. Compos Sci Technol. 2002;62:1357-72.

[118] Zhou M, Li Y, He C, Jin T, Wang K, Fu Q. Interfacial crystallization enhanced interfacial interaction of Poly (butylene succinate)/ramie fiber biocomposites using dopamine as a modifier. Compos Sci Technol. 2014;91:22-9.

[119] Jiang H, Kamdem DP. Development of poly(vinyl chloride)/wood composites. A literature review. Journal of Vinyl and Additive Technology. 2004;10:59-69.

[120] Matuana LM, Kamdem DP, Zhang J. Photoaging and stabilization of rigid PVC/wood-fiber composites. J Appl Polym Sci. 2001;80:1943-50.

[121] Anisimov AM, Lobanova LA, Anisimova OM, Krichevsky GE. Spatial distribution, light resistance and light stabilization of dyestuff molecules in polymeric matrices. Int J Polymer Mater. 1993;19:127-36.

[122] García M, Hidalgo J, Garmendia I, García-Jaca J. Wood–plastics composites with better fire retardancy and durability performance. Composites Part A. 2009;40:1772-6.

[123] Nerurkar M, Vaidyanathan J, Adivarekar RV, Bhathena Z. Dyeing of natural fibres with a red pigment produced by Streptomyces coelicolor. J Text Assoc. 2012;72:377-80.

[124] Dai JF, Wang XY. Research on modification of wool fiber and its dyeing property dyed with pomegranate husk pigment. Wool Text J. 2012;40:28-32.

[125] El-Gaoudy H, Kourkoumelis N, Varella E, Kovala-Demertzi D. The effect of thermal aging and color pigments on the Egyptian linen properties evaluated by physicochemical methods. Applied Physics A: Materials Science and Processing. 2011;105:497-507.

[126] Zhang LG, Wu ZM, Zhang C. Research on dyeing effect of wool fiber with natural pigment in supercritical carbon dioxide. Wool Text J. 2007:5-7.

[127] Matuana LM, Jin S, Stark NM. Ultraviolet weathering of HDPE/wood-flour composites coextruded with a clear HDPE cap layer. Polym Degrad Stab. 2011;96:97-106.

[128] Lu N, Bhogaiah SM, Ferguson I. Effect of Alkali and Silane Treatment on the Thermal Stability of Hemp Fibers as Reinforcement in Composite Structures. In: Bu JL, Jiang ZY, Jiao S, editors. Advanced Materials, Pts 1-3. Stafa-Zurich: Trans Tech Publications Ltd; 2012. p. 666-70.

[129] Sangappa, Rao BL, Asha S, Kumar RM, Somashekar R. Physical, chemical, and surface properties of alkali-treated Indian hemp fibers. Compos Interfaces. 2014;21:153-9.

[130] Islam MS, Pickering KL, Foreman NJ. Influence of alkali treatment on the interfacial and physico-mechanical properties of industrial hemp fibre reinforced polylactic acid composites. Composites Part A. 2010;41:596-603.

[131] Liu HL, You LL, Jin HB, Yu WD. Influence of alkali treatment on the structure and properties of hemp fibers. Fiber Polym. 2013;14:389-95.

[132] Mwaikambo LY, Ansell MP. Mechanical properties of alkali treated plant fibres and their potential as reinforcement materials. I. hemp fibres. JMatS. 2006;41:2483-96.

[133] Kaczmar JW, Pach J, Burgstaller C. The chemically treated hemp fibres to reinforce polymers. Polimery/Polymers. 2011;56:817-22.

[134] Rachini A, Le Troedec M, Peyratout C, Smith A. Comparison of the Thermal Degradation of Natural, Alkali-Treated and Silane-Treated Hemp Fibers Under Air and an Inert Atmosphere. J Appl Polym Sci. 2009;112:226-34.

[135] Mulinari DR, Voorwald HJC, Cioffi MOH, da Silva MLCP, Luz SM. Preparation and properties of HDPE/sugarcane bagasse cellulose composites obtained for thermokinetic mixer. Carbohydr Polym. 2009;75:317-21.

[136] Jonoobi M, Harun J, Tahir PM, Zaini LH, SaifulAzry S, Makinejad MD. Characteristics of nanofibers extracted from kenaf core. BioResources. 2010;5:2556-66.

[137] Rachini A, Le Troedec M, Peyratout C, Smith A. Chemical modification of hemp fibers by silane coupling agents. J Appl Polym Sci. 2012;123:601-10.

[138] Kalaitzidou K, Fukushima H, Askeland P, Drzal LT. The nucleating effect of exfoliated graphite nanoplatelets and their influence on the crystal structure and electrical conductivity of polypropylene nanocomposites. JMatS. 2008;43:2895-907.

[139] Favaro MM, Branciforti MC, Bretas RES. A X-ray study of β-phase and molecular orientation in nucleated and non-nucleated injection molded polypropylene resins. Materials Research. 2009;12:455-64.

[140] Razak NIA, Ibrahim NA, Zainuddin N, Rayung M, Saad WZ. The influence of chemical surface modification of kenaf fiber using hydrogen peroxide on the mechanical properties of biodegradable kenaf fiber/poly(Lactic Acid) composites. Molecules. 2014;19:2957-68.

[141] Li X, He L, Zhou H, Li W, Zha W. Influence of silicone oil modification on properties of ramie fiber reinforced polypropylene composites. Carbohydr Polym. 2012;87:2000-4.

[142] Pracella M, Chionna D, Anguillesi I, Kulinski Z, Piorkowska E. Functionalization, compatibilization and properties of polypropylene composites with Hemp fibres. Compos Sci Technol. 2006;66:2218-30.

[143] Hu GH, Lindt JT. Amidification of poly(styrene-co-maleic anhydride) with amines in tetrahydrofuran solution: A kinetic study. Polym Bull. 1992;29:357-63.

[144] Dhakal HN, Zhang ZY, Richardson MOW. Effect of water absorption on the mechanical properties of hemp fibre reinforced unsaturated polyester composites. Compos Sci Technol. 2007;67:1674-83.

[145] BALEY C. Fibres naturelles de renfort pour matériaux composites. Textiles à usage technique / Référence 42534210. 2005;N2220.

[146] Lutz W, Herrmann J, Kockelmann M, Hosseini HS, Jäckel A, Schmauder S, et al. Damage development in short-fiber reinforced injection molded composites. Comput Mater Sci. 2009;45:698-708.

[147] Jin S, Gong X. Study of mechanical properties and performance of aging hemp fibers. World Journal of Engineering. 2011;8:325-30.

[148] Jin S. Etude de vieillissement du comportement mécanique des agro-matériaux à base de fibres de chanvre 2013.

[149] Hong W, Zhao X, Zhou J, Suo Z. A theory of coupled diffusion and large deformation in polymeric gels. J Mech Phys Solids. 2008;56:1779-93.

[150] Jagur-Grodzinski J. Polymers for tissue engineering, medical devices, and regenerative medicine. Concise general review of recent studies. Polym Adv Technol. 2006;17:395-418.

[151] Cowin SC. Bone poroelasticity. JBiom. 1999;32:217-38.

[152] Tsai H, Pence T, Kirkinis E. Swelling Induced Finite Strain Flexure in a Rectangular Block of an Isotropic Elastic Material. JElas. 2004;75:69-89.

[153] Dolbow J, Fried E, Ji H. Chemically induced swelling of hydrogels. J Mech Phys Solids. 2004;52:51-84.

[154] Durning CJ, Morman KN. Nonlinear swelling of polymer gels. J Chem Phys. 1993;98:4275-93.

[155] Bouklas N, Huang R. Swelling kinetics of polymer gels: comparison of linear and nonlinear theories. Soft Matter. 2012;8:8194-203.

[156] Cai SQ, Lou YC, Ganguly P, Robisson A, Suo ZG. Force generated by a swelling elastomer subject to constraint. J Appl Phys. 2010;107:-.

[157] Flory PJ. Thermodynamics of High Polymer Solutions. J Chem Phys. 1942;10:51-61.

[158] Klemm D, Heublein B, Fink HP, Bohn A. Cellulose: fascinating biopolymer and sustainable raw material. Angew Chem Int Ed Engl. 2005;44:3358-93.

[159] Xu F. Chapter 2 - Structure, Ultrastructure, and Chemical Composition. In: Sun R-C, editor. Cereal Straw as a Resource for Sustainable Biomaterials and Biofuels. Amsterdam: Elsevier; 2010. p. 9-47.

[160] Yang Y, Ota T, Morii T, Hamada H. Mechanical property and hydrothermal aging of injection molded jute/polypropylene composites. JMatS. 2011;46:2678-84.

[161] Stark NM, Matuana LM. Influence of photostabilizers on wood flour-HDPE composites exposed to xenon-arc radiation with and without water spray. Polym Degrad Stab. 2006;91:3048-56.

[162] Beg MDH, Pickering KL. Accelerated weathering of unbleached and bleached Kraft wood fibre reinforced polypropylene composites. Polym Degrad Stab. 2008;93:1939-46.

[163] Fechine GJM, Demarquette NR. Cracking formation on the surface of extruded photodegraded polypropylene plates. Polym Eng Sci. 2008;48:365-72.

[164] Rabello MS, White JR. The role of physical structure and morphology in the photodegradation behaviour of polypropylene. Polym Degrad Stab. 1997;56:55-73.

[165] Rabello MS, White JR. Photodegradation of polypropylene mouldings containing weld lines: Mechanical properties and surface cracking. Plastics, Rubber and Composites Processing and Applications. 1996;25:237-48.

[166] Yakimets I, Lai D, Guigon M. Effect of photo-oxidation cracks on behaviour of thick polypropylene samples. Polym Degrad Stab. 2004;86:59-67.

[167] Schoolenberg GE. A fracture mechanics approach to the effects of UV-degradation on polypropylene. JMatS. 1988;23:1580-90.

[168] Girois S, Delprat P, Audouin L, Verdu J. Oxidation thickness profiles during photooxidation of non-photostabilized polypropylene. Polym Degrad Stab. 1997;56:169-77.

[169] Li T, White JR. Photo-oxidation of thermoplastics in bending and in uniaxial compression. Polym Degrad Stab. 1996;53:381-96.

[170] Ndiaye D, Fanton E, Morlat-Therias S, Vidal Lc, Tidjani A, Gardette J-L. Durability of wood polymer composites: Part 1. Influence of wood on the photochemical properties. Compos Sci Technol. 2008;68:2779-84.

[171] Ogier L, Rabello MS, White JR. Influence of morphology and surface preparation on the weatherability of polypropylene. JMatS. 1995;30:2364-76.

[172] Stark NM. Effect of weathering cycle and manufacturing method on performance of wood flour and high-density polyethylene composites. J Appl Polym Sci. 2006;100:3131-40.

[173] Popa MI, Pernevan S, Sirghie C, Spiridon I, Chambre D, Copolovici DM, et al. Mechanical Properties and Weathering Behavior of Polypropylene-Hemp Shives Composites. Journal of Chemistry. 2013;2013:8.

[174] Islam MS, Pickering KL, Foreman NJ. Influence of accelerated ageing on the physico-mechanical properties of alkali-treated industrial hemp fibre reinforced poly(lactic acid) (PLA) composites. Polym Degrad Stab. 2010;95:59-65.

[175] Han HC, Gong XL. Effect of fiber surface modification with different functional groups silane agents on mechanical properties of hemps/polypropylene composites. Beijing2014. p. 23-6.

# Hongchang HAN

## Doctorat : Systèmes Mécaniques et Matériaux

Année 2015


## Étude des agro-composites chanvre/polypropylène: Traitement des fibres, caractérisation morphologique et mécanique


L'utilisation des fibres végétales dans les polymères composites suscite de nombreuses investigations. Avant de mélanger les fibres végétales dans le polymère, un traitement chimique peut être effectué permettant de réduire l'hydrophilicité des fibres et d'améliorer l'adhérence à l'interface fibre/matrice. Dans cette thèse, l'eau et l'alcali sont utilisés d'abord pour traiter les fibres de chanvre, puis trois agents silane : 3-(triméthoxysilyl)propyl méthacrylate (MPS), N-[3- (triméthoxysilyl)propyl] aniline (PAPS) et (3-Aminopropyl)-triéthoxysilane (APS), sont utilisés pour modifier plus ou moins la surface des fibres de chanvre. Ces fibres traitées ou modifiées sont ensuite mélangées avec le polypropylène (PP) pour la fabrication des composites. Les effets de ces différents traitements sur la structure, les composants et l'hydrophilicité des fibres, et les propriétés mécaniques de ces composites sont mis en évidence. Nous avons étudié ensuite l'effet de vieillissement sur leurs comportements mécaniques, notamment l'humidité, la température et le rayonnement ultraviolet. Les résultats ont montré que le traitement de fibres par l'eau et l'alcali a des effets considérables sur la structure de fibres, les propriétés mécaniques et la durabilité des composites renforcés. La modification par l'agent de silane a une influence moins importante sur la structure des fibres, pourtant son groupe fonctionnel a une influence significative sur les propriétés mécaniques et la résistance au vieillissement des composites renforcés.



Mots clés : fibres végétales - matières plastiques renforcées avec des fibres - traitements de surface – matériaux, détérioration – matériaux, propriétés mécaniques.


## Study of Agro-composite Hemp/Polypropylene: Treatment of Fibers, Morphological and Mechanical Characterization


Using agro fiber as reinforcement of polymer composites attracts numerous investigations due to the good mechanical properties and environmental benefits. Prior to blend agro fiber with polymer, chemical treatment can be employed to treat agro fiber for the purpose of reducing the hydrophilicity of fiber and improving the interfacial adhesion fiber/polymer matrix. In this thesis, water and alkali are utilized to treat hemp fiber firstly and then three silane agent as 3-(Trimethoxysilyl)propyl methacrylate (MPS), N-[3-(Trimethoxysilyl)propyl]aniline (PAPS) and (3-Aminopropyl)-triethoxysilane (APS) are employed to modify the hemp fiber surface. These treated or modified fibers are blended respectively with polypropylene (PP) to fabricate the hemp fiber/PP composites. The effects of these different treatments on the structure, components and hydrophilicity of fiber, and the mechanical properties of the reinforced PP composites are studied. Moreover, the accelerated ageing experiments including humidity, temperature and ultraviolet of the reinforced PP composites are conducted. The results showed that the fiber treatment of water and alkali has a considerable effect on fiber structure, mechanical properties and durability of the reinforced composites. The silane agent modification of fiber has less influence on the fiber structure but its functional group has great influence on the mechanical properties and ageing resistance of the reinforced composites.



Keywords: plant fibers - fiber reinforced plastics - surface preparation - materials, deterioration - materials, mechanical properties.


**Thèse réalisée en partenariat entre :**


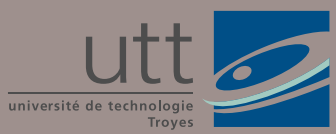


**Ecole Doctorale** "Sciences et Technologies"